A mi familia

Acknowledgments

The accomplishment of this work would not have been possible without the participation and assistance of so many people whose names may not be all listed. I would like to extend my most sincere thanks to all of them. However, I would like to express my gratitude particularly to the following:

First of all, I would like to thank my supervisor, Aitzol Lamikiz, for his guidance and support throughout this time. Without his help, this work would not have been possible.

I would also like to express my special thanks to my colleagues at the Mechanical Workshop of the University of the Basque Country (UPV/EHU) for making my daily life more bearable and, above all, fun. Nevertheless, I am especially grateful to my colleagues in the Laser Team, whose contribution to this work at both the human and technical level is invaluable. Working with you is always a pleasure.

My deepest appreciation belongs to my family, who have never doubted my abilities and have supported and encouraged me in everything I have set out to do. In the same way, these acknowledgments would not be complete without mentioning Iñaki, with whom I believe I share this work. Thank you for your ideas and motivation, but thank you also for your patience, understanding and good humor.

eman ta zabal zazu
Universidad del País Vasco
Euskal Herriko Unibertsitatea
FACULTY OF ENGINEERING BILBAO
UNIVERSITY OF THE BASQUE COUNTRY

PhD Thesis

A Methodology for the Application of Hybrid Additive and Subtractive Machines for the Coating and Repair of Hot Stamping Tools

Presented by
Magdalena Cortina Burón

At the
Department of Mechanical Engineering

Of the
University of the Basque Country (UPV/EHU)

For obtaining the degree of
International PhD in Mechanical Engineering

Supervised by
Aitzol Lamikiz Mentxaka

April 2020

Summary

This research work is focused on the study of the application of the Laser Metal Deposition (LMD) technology to hot stamping tools. Throughout it, several topics have been dealt with, ranging from the characterization of materials for their correct deposition to their application in the generation of coatings or geometries. In addition, thermal and mechanical analyses have been performed in order to determine the capabilities and potential benefits that the use of LMD can offer compared to conventional manufacturing techniques.

In order to determine a methodology to be followed for the LMD of the material under study, in this case, AISI H13, this material has been firstly characterized. On the basis of this characterization, and on the interest aroused by hybrid machines that combine additive and subtractive processes, the implications of performing LMD on surfaces with residual cutting fluid have been analyzed. To that end, two different materials have been investigated, i.e., Inconel®718 and AISI H13. As a result, the conditions under which successful depositions are attained have been determined. Nevertheless, it is worth noting that different conclusions have been reached for each material studied. Thus, although the most frequent defect when processing Inconel®718 is the formation of voids and pores, for AISI H13 it is cracking.

Regarding the application of LMD to hot stamping tools, research efforts have been focused on enhancing the heat transfer between the blank and the tools. The present work has dealt with the increase of the thermal conductivity of the tools, as well as the boost of their cooling system:

The enhancement of the cooling system has been addressed through the study of conformal cooling channels manufactured via LMD. To this end, once they were fabricated, their performance was analyzed and compared with conventional straight channels manufactured via drilling, obtaining satisfactory results. In addition, the impact of implementing conformal cooling on the hot stamping process has been analyzed via thermal simulations, in which the thermal field of a stamped blank and the reduction in cycle time attained for a B-pillar part geometry have been determined. The results show that conformal cooling channels manufactured by LMD meet the mechanical requirements demanded by the hot stamping process. Moreover, the employment of conformal cooling channels leads to a more homogeneous temperature distribution within the tool and the stamped part, as well as the reduction of the process cycle times, thus increasing productivity.

In hot stamping, the temperature distribution of the tools and the blank are related to the thermo-physical properties of the employed materials, which change with temperature. In

addition, any enhancement in the thermal conductivity of the tools leads to an increase in the heat transfer between the tools and the blank. In this research work, the suitability of employing LMD technology to generate bimetallic hot stamping tools has been studied. For this purpose, the enhancement of the surface properties of inexpensive, high thermal conductivity steels by coating with highly alloyed steels has been investigated. In this case, AISI 1045 medium-carbon steel has been coated with AISI H13 tool steel, thus increasing the thermal conductivity of the tool compared to one manufactured exclusively with AISI H13. This way, and for the studied tool geometry, the cycle time was reduced by 44.5% compared with conventional tools made of AISI H13. In order to accurately know the thermal conductivity of the laser-deposited AISI H13, its effective thermal diffusivity has been experimentally determined and compared with cast AISI H13. Results showed that the thermal conductivity of LMD AISI H13 was significantly lower than that of cast AISI H13. This is an issue that directly affects the thermal conductivity of the bimetallic tools and has been taken into account in order to determine the cycle-time reduction that their use in hot stamping processes involves.

To sum up, this work presents an investigation of the improvement of the hot stamping process, both in terms of productivity and performance, through the application of LMD. The obtained results intend to demonstrate the suitability of this technology in order to process high-added-value components, such as hot stamping tools.

Main Index

Figures Index

Tables Index

Nomenclature

AAGR	Average Annual Growth Rate
AISI	American Iron and Steel Institute
AM	Additive Manufacturing
ASTM	American Society for Testing and Materials
CAD	Computer-Aided Design
CAGR	Compound Annual Growth Rate
CAM	Computer-Aided Manufacturing
CHTC	Convective Heat Transfer Coefficient
CNC	Computer Numerical Control
CMM	Coordinate Measuring Machine
DED	Directed Energy Deposition
DIN	Deutsches Institut für Normung (German Institute for Standardization)
DMD	Direct Metal Deposition
EBM	Electron Beam Melting
EDX	Energy Dispersive X-ray
EMO	Machine Tool World Exposition
EoL	End of Life
FEM	Finite Elements Method
FGM	Functionally Graded Materials
GTAW	Gas Tungsten Arc Welding
HAZ	Heat-Affected Zone
HIP	Hot Isostatic Pressing

IHTC	Interfacial Heat Transfer Coefficient
IMTS	International Manufacturing Technology Show
ISO	International Organization for Standardization
JIMTOF	Japan International Machine Tool Fair
LAM	Laser Additive Manufacturing
LENS	Laser Engineered Net Shaping
LMD	Laser Metal Deposition
MCDA	Multi-Criteria Decision Analysis
MQL	Minimum Quantity Lubrication
MRO	Maintenance, Repair and Overhaul
OEM	Original Equipment Manufacturer
PBF	Powder Bed Fusion
PTAW	Plasma Transferred Arc Welding
R&D	Research and Development
SEM	Scanning Electron Microscope
SLM	Selective Laser Melting
TEM	Transverse Electromagnetic Mode
TIG	Tungsten Inert Gas
WAAM	Wire Arc Additive Manufacturing

Symbols

Symbol	Units	Description
Δr_1	[mm]	Distance between cooling ducts
Δr_2	[mm]	Distance from cooling duct center to the surface
BPP	[mm·mrad]	Beam Parameter Product
c_p	[J·kg^{-1}·K^{-1}]	Material specific heat
CHTC	[W·m^{-2}·K^{-1}]	Convective Heat Transfer Coefficient
d	[mm]	The diameter of the laser beam at the focus position
D	[mm]	The diameter of the cooling channel
ED	[J·mm^{-2}]	Energy Density
f	[Hz]	Modulation frequency
F	[-]	Friction factor
IHTC	[W·m^{-2}·K^{-1}]	Interfacial Heat Transfer Coefficient
k	[W·m^{-1}·K^{-1}]	Thermal conductivity
L	[mm]	Length of the cooling ducts
M^2	[-]	Beam quality factor
Nu	[-]	Nusselt number
P	[W]	Laser power
PD	[W·mm^{-2}]	Power Density
Pr	[-]	Prandtl number
Re	[-]	Reynolds number
s	[mm]	Plate thickness
T	[°C]	Temperature

t	[s]	Time
t_p	[s]	Time pulse
V	[m·s^{-1}]	Mean velocity of the fluid
V_f	[mm·min^{-1}]	Scan velocity
υ	[-]	Volume fraction
w_0	[mm]	Beam radius measured at the beam waist
α	[mm^2·s^{-1}]	Thermal diffusivity
$\alpha_{\parallel}$	[mm^2·s^{-1}]	In-plane thermal diffusivity
$\alpha_{\perp}$	[mm^2·s^{-1}]	Through thickness thermal diffusivity
ε	[µm]	Surface roughness
θ_0	[mrad]	Far-field full divergence angle
μ	[kg·m^{-1}·s^{-1}]	Dynamic viscosity
ρ	[kg·m^{-3}]	Material density

Chapter I. Introduction

Chapter I. Introduction

In this chapter, the research work carried out within the framework of this thesis is introduced. First, the background and motivation of this work are presented. To that end, the manufacturing process under study and the industrial application which is dealt with, that is Laser Metal Deposition and hot stamping, are detailed. Then, the main objectives pursued are identified. Last, the structure of the memory and the chapters it is comprised of are explained in detail.

I.1. Background and motivation

The present document discloses the results obtained after the realization of a research work focused on the study of the Laser Metal Deposition (LMD) process aimed at the manufacturing, refurbishment, and modification of hot stamping tools. The work has been carried out at the Department of Mechanical Engineering of the University of the Basque Country (UPV/EHU) and its objective is to establish a methodology of application of LMD in high-added-value components of the hot stamping industry. For this purpose, the advantages that the use of LMD entails, as well as the new manufacturing possibilities it offers are highlighted. The final aim of this work is to demonstrate the feasibility of the LMD process as a new manufacturing approach applicable to the die and mold industry, overcoming the challenges and fulfilling the requirements inherent to this sector.

As reported by Optech Consulting, a market research and consulting firm serving the laser and photonics industry, the global market for laser systems for materials processing rose by 34.1% in 2017, thus achieving a record volume of $16.9 billion [Optech, 2018]. The market for additive manufacturing methods has been also growing at a fast pace for years [Trumpf, 2017]. According to the *Wohlers Report 2018*, the annual report on the state of the industry of Additive Manufacturing (AM) and three-dimensional (3D) printing published by Wohlers Associates Inc., the AM industry grew by 21% in worldwide revenues in 2017, as the industry expanded by more than $1.25 billion [Wohlers, 2018]. One of the fastest-growing segments is metal AM systems. According to this report, there has been an increase of nearly 80% on the number of metal AM systems sold, rising from 983 units in 2016 to 1768 in 2017, see Figure I. 1. As a consequence, AM materials development and consumption experienced record growth in 2018.

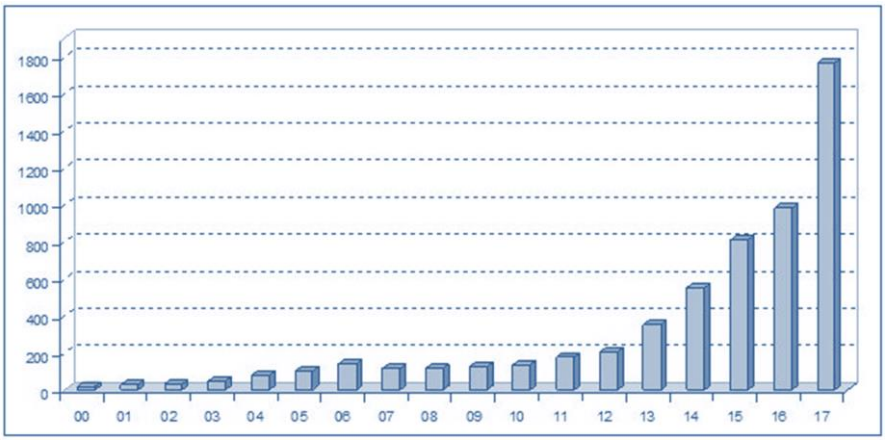

Figure I. 1 Rise in the number of metal AM system sales [Wohlers, 2018].

This rise in metal AM purchases is due to the improvement of the reliability of 3D printing, making important advances on issues, such as process monitoring and quality assurance. The AM industry is, therefore, advancing beyond prototyping towards industrial production. In fact, the total AM market size is forecasted to reach nearly $26.2 billion by 2022, from which approximately 20-25% is metal AM [Oerlikon, 2017].

Among the metal additive manufacturing technologies, Laser Metal Deposition (LMD) has lately gained attention as a manufacturing method able to add features to pre-existing components or repair them. This technology enables one to build free-form parts with almost no geometrical restriction and high-quality metallurgy. The process is based on the generation of a melt pool on the surface of the substrate, whereas filler material is simultaneously added in the form of powder or wire. Line by line, coating layers are generated and, by means of overlapping the subsequent layers, the desired final geometry is obtained [Poprawe, 2011]. The application of LMD focuses on the manufacturing or repair of high-added-value functional parts. Therefore, it has a wide spectrum of industrial applications, ranging from space and aircraft sectors to automotive or biomedical among others [Klocke, 2017]. Moreover, in the last years, the LMD process has been integrated into 5-axis machining centers, giving rise to the so-called hybrid manufacturing systems.

Regarding the automotive industry, increasing demand for high strength and lightweight components has led to the promotion and development of hot stamping (also known as press hardening) processes [Steinbeiss, 2007]. Through this technique, a boron steel blank is heated until austenitization at temperatures between 900 ˚C and 950 ˚C and then transferred to an internally cooled stamping set, where it is simultaneously stamped, quenched and formed. Hot stamping tools are required to withstand high thermomechanical loads and have wear and

tempering resistance. Hence, they are normally made of hot working tool steels, which exhibit good tempering resistance and toughness.

Under this framework, Laser Additive Manufacturing (LAM) processes are already becoming an effective production tool, able to enhance the performance of hot work tool steels. In addition, LMD is especially appropriate for the manufacturing and repair of large parts, such as dies and molds, enabling the improvement of their thermomechanical properties and their lifespan extension. In this way, LMD could be used for manufacturing tools of hot work tool steels used in hot stamping, which allows the production of ultra-high-strength automotive body components.

Metal additive manufacturing and more specifically LMD applied to H-type tool steels processing are currently under research. Many authors have worked in the fields of surface properties enhancement by developing thick metallic coatings [Ley, 2018] or surface alloying [Norhafzan, 2016]. Others have concentrated their research on the manufacturing of near-net-shape components or have studied the effects of process parameters on the resulting metallurgical structures and properties of the deposited parts [Zadi-Maad, 2018; Bohlen, 2018]. However, further R&D efforts focused on validating, standardizing and demonstrating this technology are necessary in order to overcome the challenges still ahead, increasing the reliability of this new manufacturing approach and opening doors for new tool designs and applications.

The present work is focused on the suitability of LMD for processing hot work tool steels aimed at the hot stamping industry and the enhancement of the hot stamping tools. To that end, two main issues are analyzed. On the one hand, the manufacturing of new components by realizing novel tool designs or coatings that improve the performance of the tools. On the other hand, the repair of components that have been already in use or need to undergo a last-minute modification due to either manufacturing errors or changes of design.

I.2. Objectives

The main objective of the present research work is the study of the application of LMD to the manufacturing, modification, and repair of hot stamping tools. This study aims to provide a better understanding of the LMD process applied to hot work tool steels.

The objectives of this thesis are stated in detail below:

- ✓ Identification of an optimum parameter window for processing hot work tool steels so that defect-free layers are deposited.

- ✓ Further the understanding of the interactions between machining and LMD in hybrid machines combining both technologies.
- ✓ Determination of the influence of the use of cutting fluid on the LMD process in hybrid machines combining additive and subtractive processes.
- ✓ Development of a methodology for the coating and repair of hot stamping tools, attaining a good bonding between the substrate and the deposited material, as well as the required hardness.
- ✓ Prove the advantages of LMD regarding the fabrication of designs impossible to accomplish using traditional manufacturing methods. In addition, these new designs will be aligned with improved tool properties for the hot stamping process.
- ✓ Analyze the impact of the LMD process on hot stamping tools, giving special attention to hardness evolution, heat transfer coefficient and wear resistance, among others.

By the fulfillment of the aforementioned objectives, the present work intends to provide a broader knowledge and better understanding of the LMD process and its application to high-added-value industrial components that could not be processed easily by traditional techniques.

I.3. Memory organization

The present document is organized in a series of chapters described below:

Chapter I is an introductory section, in which the background and motivation of the present research work are briefly described. For that purpose, the growing relevance of the laser market, and more specifically the additive manufacturing industry and its industrial applications are highlighted. In addition, the main objectives of the thesis and the organization of the present document are also described.

In **Chapter II**, a review of the state of the art of Laser Metal Deposition and the latest developments is conducted. To that end, both the lasers and the LMD process are first introduced. Afterward, a subchapter is dedicated to the concept of hybrid manufacturing, indicating its strong and weak points, as well as the latest emerging hybrid solutions. Last, industrial applications are described, special attention being given to the die & mold industry and more specifically to the hot stamping process.

Chapter III deals with the characterization of the Laser Metal Deposition of AISI H13 hot work tool steel. In addition, special focus is placed on its processing in hybrid machines and the issues arisen from the use of cutting fluids affecting the LMD process, to which a subchapter is

dedicated. In this regard, the effect of different oil concentrations in the LMD of AISI H13 and Inconel® 718 is investigated.

Chapter IV is focused on the application of the LMD technology to new hot stamping tool designs and, more specifically, to the manufacturing of conformal cooling channels. First, in addition to analyzing the technical feasibility of manufacturing these ducts using LMD, their mechanical and thermal behavior in comparison with conventional ducts are also evaluated. In the following subchapter, the implementation of this new design for manufacturing a B-pillar part is addressed via thermal simulations, including an analysis of the temperature distribution within the tool-blank set, as well as an estimation of the reduction in cycle time.

In **Chapter V**, the suitability of employing the LMD technology to generate cost-effective bimetallic hot stamping tools is analyzed. The technical feasibility of coating an AISI 1045 core with AISI H13 in terms of bonding quality and mechanical properties is first addressed. In a second step, the cycle-time reduction achieved is estimated by means of thermal simulations. At the end of the chapter, an investigation on the effective thermal diffusivity of laser metal deposited AISI H13 is also presented.

Last, in **Chapter VI**, the main contributions of the present thesis and its prospective lines are detailed.

Chapter II. The Laser Metal Deposition process and its application to the Die & Mold industry

Chapter II. The Laser Metal Deposition process and its application to the Die & Mold industry

In this second chapter, a summary of the State of the Art of the Laser Metal Deposition process and its application to the Die & Mold industry is presented. First, an introduction to the lasers and metal additive manufacturing is performed, where the Laser Metal Deposition process is explained in detail. Then, the concept of hybrid manufacturing and the emergent hybrid machine tools with additive and subtractive capabilities are dealt with, giving an insight into the current advances and pending tasks of hybrid machines both from an academic and industrial perspective. Afterward, the industrial application fields of Additive Manufacturing and Laser Metal Deposition are discussed, then analyzing the Die & Mold industry and the Hot Stamping process in greater depth.

II.1. Introduction to the lasers

Lasers are regarded as one of the greatest inventions of the mid-twentieth century. The first working laser consisted of an electronic flash tube coiled around a ruby crystal and was invented by Theodore H. Maiman in 1960 [Maiman, 1960]. The word LASER is an acronym that stands for **Light Amplification by Stimulated Emission of Radiation**, which describes its working principle. A laser emits an electromagnetic beam generated by an active medium, which is monochromatic, collimated and coherent [Thomas, 2011]. These characteristics allow lasers to be focused on a tiny spot, thus concentrating energy on that spot without affecting the surrounding area.

Due to their exceptional properties, lasers have found a multitude of application fields, including industry, medicine, communications, defense and science and technology [Gupta, 2018]. According to Strategies Unlimited, a market research firm with expertise in lasers, total laser sales in 2017 reached $12.3 billion, while the biggest segments were communication and materials processing, see Figure II. 1a [Strategies Unlimited, 2017].

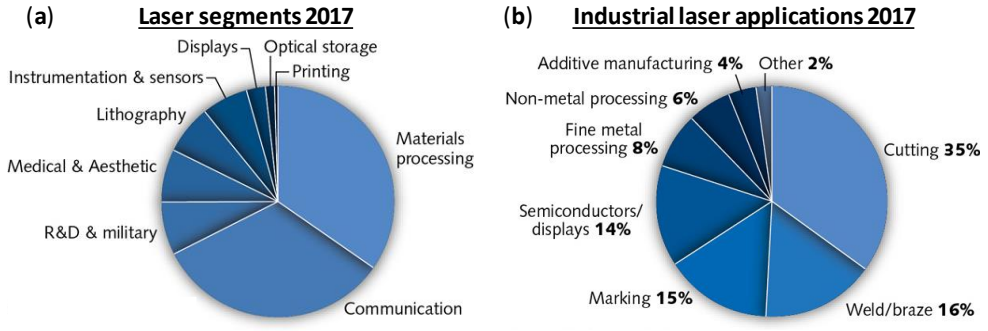

Figure II. 1 (a) Laser segments and (b) industrial laser applications in 2017 [Strategies Unlimited, 2017].

As far as their industrial use is concerned (see Figure II. 1b), lasers are being employed as a manufacturing tool in diverse sectors because of the outstanding properties they have over other materials processing tools:

- *Contactless tool*: Due to their nature, lasers are non-contact tools and, hence, no forces take place in laser processing. As a result, there is no tool wear and they enable processing, for instance, very hard or brittle materials.
- *Low thermal input*: Lasers concentrate high energy density in a localized spot on the workpiece, thus resulting in a low heat-affected zone (HAZ).
- *High speed and positioning accuracy*: The fact that lasers have no inertia enables one to guide them by means of mirrors with almost no acceleration limit and great accuracy.
- *High repeatability*: Where accuracies below 0.1 mm are easily achieved.
- *Easy automation:* As it is CNC programmable, it can be easily integrated into conventional manufacturing systems. In addition, it enables the processing of a wide variety of materials.
- *Clean process*: As laser material processing does not need any coolant or produce any noise, it can be considered as a clean process.

Laser-based manufacturing is increasing and the processes involved are usually classified into two categories, macro, and micro, according to the scale in which the processed material is affected. In this way, macro processes cover cutting, welding, cladding, alloying, drilling, and brazing, whereas micro-processes include micro-texturing, marking, polishing, micromachining, micro-drilling or micro engraving, among others [Padmanabham, 2018].

II.1.1. Basic principles of lasers

Lasers consist of three main elements: the active medium, the excitation system or “pump” and the optical resonator [Haley, 2017].

1. *Active medium*: Element that, once it is excited or “pumped”, generates a laser beam. It may be solid, liquid or gas and determines the wavelength of the generated laser. Depending on the active medium, different excitation systems are used.
2. *Excitation system or “pump”*: It supplies energy to the laser-active medium and may be optical, electrical or chemical.
3. *Optical resonator*: Its function is amplifying the laser beam until a stable beam is attained. The classical resonator consists of two parallel mirrors containing the laser-active medium, hence causing the photons to pass back and forth and resulting in

amplification by stimulation. One of the mirrors is partially transparent (R<100), thus allowing some of the photons to exit and form the laser beam. New laser types use different resonator designs but based on the same principle.

A laser beam is generated by transferring energy to the laser-active medium, hence raising its energy level and reaching an excited state. At this point, if one of the "high-energy" particles returns to a lower energy level, then a photon is released as a consequence of the energy difference between both states. This photon may then be reflected inside the resonator, passing back and forth the laser-active medium and stimulating another "high-energy" particle to pass to a lower energy level. As a result, a second photon with the same characteristics of the first one is emitted. This process is repeated once and again, generating monochromatic, coherent and collimated radiation. Eventually, some of the photons inside the resonator are allowed to exit and therefore form a laser beam, which is directed onto the workpiece, as illustrated in Figure II. 2 [Rofin, 2004].

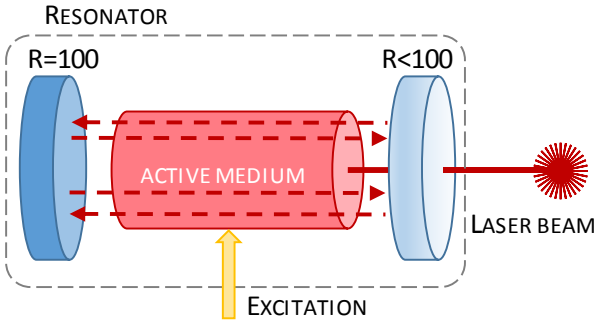

Figure II. 2 Working principle of lasers.

As materials processing involves the use of powerful lasers, the main lasers that are employed in this application are CO_2, solid-state and diode lasers [Steen, 2010].

II.1.2. Main parameters of the laser-based processes

There are several laser process parameters that define the characteristics of the generated beam and are therefore of paramount importance in materials processing. Laser process parameters must be adapted for each application, material and laser type, resulting in different energy inputs into the workpiece, as well as interaction time. Some of the most relevant laser parameters are here explained:

Laser power: It represents the output power of the laser in watts and is limited by the maximum power of the laser source employed. This parameter is modified depending on the application and material to be processed. Nevertheless, also other power-related parameters offer a clearer understanding of the process:

Power Density (PD): Specific parameter that represents the laser power per unit area of the laser beam and is calculated according to equation (Eq. II. 1), where *P* represents the power and *d* the diameter of the laser beam at the focus position.

$$PD = \frac{P}{\pi \cdot d^2/4} \quad \textbf{(Eq. II. 1)}$$

Energy Density (ED): It represents the energy per unit area of the laser beam and, hence, it considers the interaction time between the laser beam and the workpiece. Its calculation is different depending on the kind of process, continuous wave (CW) (Eq. II. 2) or pulsed (Eq. II. 3), taking place, where V_f represents the scan velocity and t_p the time pulse.

$$ED_{CW} = \frac{P}{D \cdot V_f} \quad \textbf{(Eq. II. 2)}$$

$$ED_{pulsed} = \frac{P \cdot t_p}{\pi \cdot d^2/4} \quad \textbf{(Eq. II. 3)}$$

Transverse Electromagnetic Mode (TEM): The power distribution of the laser beam is not uniform and the quality of the laser beam depends on it. After the resonance of the laser beam in the resonator, specific electromagnetic field distributions are produced. Each field distribution has a specific shape that is named after the term "Transverse Electromagnetic Mode" or TEM. Transverse modes are defined by TEM_{mn} for cartesian coordinates, where the subscripts m and n indicate the number of nodes of zeros of intensity transverse to the beam axis in vertical and horizontal directions, respectively. Alternatively, in cylindrical coordinates the modes are designated by TEM_{pl}, representing the number of radial *p* and angular *l* nodes (see Figure II. 3) [Koechner, 2006].

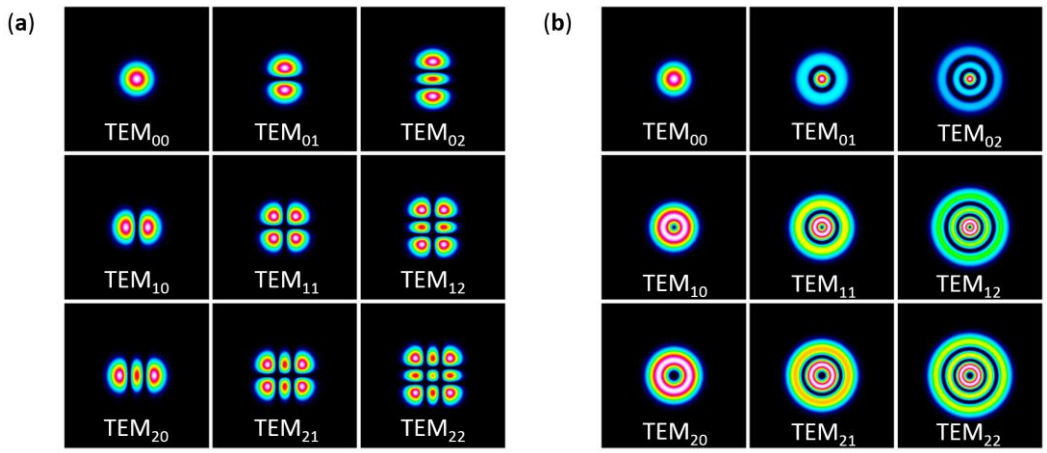

Figure II. 3 Arrays of subplots containing various (a) Hermite-Gaussian and (b) Laguerre-Gaussian modes [DataRay, 2018].

The first mode is the TEM_{00} or fundamental mode, which is the fundamental mode and represents the shape of a Gaussian energy distribution over the laser-beam spot area. The fundamental mode is able to generate the tiniest spot with low divergence. It is considered as the theoretically perfect laser beam and is the reference for determining the quality of a laser beam.

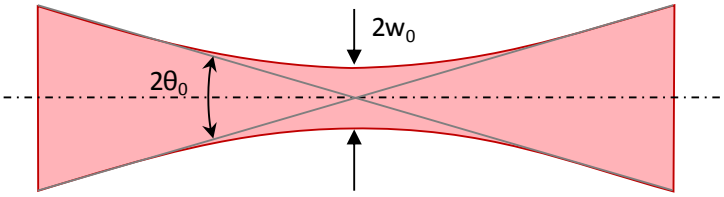

Figure II. 4 Definition of parameters for the Beam Parameter Product (BPP) formula.

Beam Parameter Product (BPP): It represents the quality of the laser beam, that is, the ability to focus the beam on a very small spot, and is calculated by equation (Eq. II. 4), where w_0 represents the beam radius measured at the beam waist and θ_0 the far-field full divergence angle, as shown in Figure II. 4 The lower the BPP, the higher the beam quality regardless the beam is Gaussian or not.

$$BPP = w_0 \cdot \theta_0 \qquad \textbf{(Eq. II. 4)}$$

Nevertheless, the beam quality can be also represented by K and M^2 factors, which are directly related to BPP, as shown in equation (Eq. II. 5), where λ represents the laser wavelength. In the case of M^2, also called beam quality factor, it describes how close to "perfect-Gaussian" a laser beam is. In that case, $M^2=1$, while for a non-perfect Gaussian, $M^2>1$.

$$K = \frac{1}{M^2} = \frac{\lambda}{\pi} \cdot \frac{1}{BPP} \qquad \textbf{(Eq. II. 5)}$$

II.1.3. Industrial lasers market

The materials processing market has available a range of industrial lasers, each of which offers its own particular advantages and processing characteristics. Among them, the following selection of lasers can be found according to their laser-active medium:

1. CO_2 lasers

CO_2 or carbon dioxide lasers are the most common type of lasers in the industry, where the laser-active medium is constituted by CO_2 molecules that are excited by an electrical gas discharge. The emitted laser beam has a wavelength of 10.6 µm, making this kind of lasers especially well suited for processing organic materials, such as wood or rubber, but limiting their

application to metals. This limitation can be compensated with the high output laser power they can reach, which is up to ≈20 kW, with an excellent beam quality of M^2<1.2 [Woods, 2009]. A disadvantage of this kind of lasers is that they cannot be transmitted through optical fibers, but by means of a set of mirrors under careful alignment and constant maintenance. Another drawback of CO_2 lasers is their low efficiency, which is below 20% for most of the systems.

2. Solid-state lasers

Solid-state lasers are constructed by doping a host material with ions. The most common solid-state lasers are the Nd:YAG and the Yb:YAG, where Neodymium (Nd) and Ytterbium (Yb) ions are used as dopants of the laser-active medium, respectively. However, Nd:YAG laser is the most widely used solid-state laser for materials processing. Optical excitation systems, lamps or laser diodes, are used for pumping the active medium. The generated laser can operate in both CW and pulsed mode and, depending on the dopant, it has a wavelength of 1.064 µm and 1.030 µm for Nd and Yb, respectively [Mans, 2011]. These near-infrared wavelengths make them ideally suited for absorption in most metals, even those reflective, to the detriment of many other materials (e.g. plastics, fabrics, wood, etc.). Contrarily to CO_2 lasers, solid-state lasers can be transmitted by means of optical fibers, avoiding the problematic mirrors system.

There are different types of solid-state lasers according to the geometry of the active medium. Beginning with a rod geometry, researchers have been continuously looking for solutions with a higher surface-to-volume ratio so that a uniform and efficient heat absorption is procured and better working performance is attained. In this way, the disk, and the fiber lasers arose, whose active mediums are a crystal disk and a coiled fiber, respectively, obtaining higher quality beams. For instance, disk lasers are claimed to reach output powers of around 16 kW with a beam quality of BPP<3.4 mm·mrad, while fiber lasers operate with average powers as high as 3 kW and BPP<0.5 mm·mrad [Mans, 2011]. In addition, fiber lasers are susceptible to achieve even higher power output values (>100 kW [IPG, 2018]) by means of coupling several fibers. The efficiency of solid-state lasers is between 20-40% depending on the laser type.

3. High-Power Diode Lasers

High-power diode lasers, also known as semi-conductor lasers, are pumped by an electrical current, generating a laser beam with wavelengths between 0.790 and 1.080 µm [Mans, 2011], thus being able to process metals. Their power output ranges from 10's of Watts to ≈10 kW and the laser beam can be delivered to the part directly or through an optical fiber. In addition, as shown in Figure II. 5, diode lasers are the option that offers the highest energy efficiency and

therefore lowest energy costs. However, the beam quality of these lasers is far below that of solid-state ones, being therefore usually employed for welding or heat treatment applications.

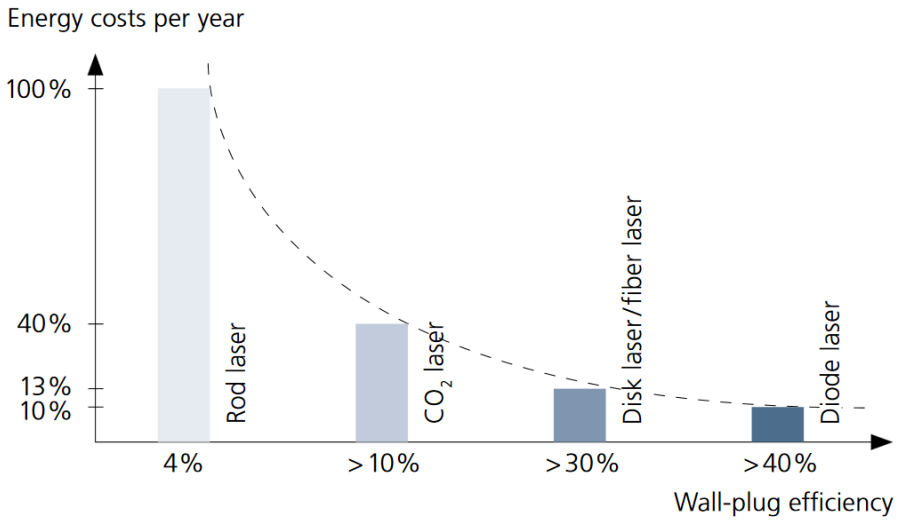

Figure II. 5 Comparison of different kinds of lasers of the same power [Trumpf, 2018].

As described before, there are many laser applications in the market. However, solid-state lasers and, in some cases, high-power diode lasers (HPDL) are most commonly used in the LMD process [Toyserkani, 2005; Trumpf, 2018; IPG, 2018].

II.2. Introduction to metal additive manufacturing

The ISO/ASTM 52900 International Standard Terminology for Additive Manufacturing (AM) Technologies defines AM as the "process of joining materials to make parts from 3D model data, usually layer upon layer, as opposed to subtractive manufacturing and formative manufacturing methodologies" [ISO/ASTM, 2018]. This technology is being successfully applied through diverse additive processes to different materials, such as polymers, ceramics, composites, and metals [Bourell, 2017]. The implementation of AM is, therefore, affecting the industrial panorama, gaining attention from the aeronautical, automotive, medical or tooling sectors, among others [Al-Makky, 2014].

As far as the different additive manufacturing technologies are concerned and according to the standard, they are divided into seven groups. Figure II. 6 includes the process categories and their definitions as stated by ISO/ASTM.

Binder Jetting	a liquid bonding agent is selectively deposited to join powder materials
Directed Energy Deposition	focused thermal energy is used to fuse materials by melting as they are being deposited
Material Extrusion	material is selectively dispensed through a nozzle or orifice
Material Jetting	droplets of build material are selectively deposited
Powder Bed Fusion	thermal energy selectively fuses regions of a powder bed
Sheet Lamination	sheets of material are bonded to form a part
Vat Photopolymerization	liquid photopolymer in a vat is selectively cured by light-activated polymerization

Figure II. 6 Additive Manufacturing process categories and definitions [ISO/ASTM, 2018].

Nevertheless, only Binder Jetting, Directed Energy Deposition, Powder Bed Fusion and Sheet Lamination are used for processing metallic components [Gonzalez-Gutierrez, 2018], giving rise to metal additive manufacturing processes. However, the industry has predominantly opted for Directed Energy Deposition (DED) and Powder Bed Fusion (PBF) for manufacturing quality metal parts [Fatemi, 2017], in which the energy sources employed are usually a laser, electron beam or plasma arc. Almost any weldable metal can be processed with any of these two techniques. Both technologies are comprised of different specific processes: Selective Laser Melting (SLM) and Electron Beam Melting (EBM) or Laser Metal Deposition (LMD) and Wire Arc Additive Manufacturing (WAAM) are some examples of PBF and DED approaches, respectively, depending on the energy source used.

When higher deposition rates are to be achieved, the WAAM process is gaining wider acceptance in the industrial manufacturing sector. This process is a wire-based DED technique that uses an arc-based energy source, which melts the substrate, while the wire is used as feedstock material [McAndrew, 2018]. The components manufactured by this technique are built layer by layer, thus being the deposition procedure similar to that of LMD [Hejripour, 2018]. Nevertheless, WAAM presents some advantages such as high deposition rates (up to 10 $kg \cdot h^{-1}$), low equipment cost and high material utilization. However, high levels of heat input are also inherent to this process, hence inducing residual stresses and high distortion in the built

components [Cunningham, 2018]. As a result, part accuracy and surface finish are lower than in other additive approaches, and more complex post-processing, usually carried out by subtractive operations, is required. The variety of materials processed by WAAM ranges from nickel alloys and steels to titanium or aluminum [Wu, 2018]. Its main application field is the manufacture of medium-large size parts of medium geometrical complexity with high mechanical requirements, for instance, aircraft structural components [Tabernero, 2018].

Nevertheless, in metal additive manufacturing lasers play an important role, as they are considered as efficient heat sources, capable of transferring concentrated energy to the base material without any transfer medium, thus generating a localized melt pool [Lee, 2017]. The advantageous characteristics of lasers make laser additive manufacturing one of the most relevant technologies employed for processing metals.

II.2.1. Laser Additive Manufacturing

Additive Manufacturing (AM), commonly referred to as 3D printing, has experienced substantial growth over the past decades, taking it from a promising technology from the early 1980s to a market size of $6063 billion in 2016, from which 10-15% is metal AM [Wohlers, 2017]. The AM industry is leaving behind its prototyping past and advancing towards industrial production applications, being increasingly used for spare parts, small series production, and tooling. Focusing on metal AM, most industries have adopted laser technologies, giving rise to Laser Additive Manufacturing (LAM) [Pinkerton, 2016; Klocke, 2017].

In this regard, the industry has focused on Powder Bed Fusion (PBF) and Directed Energy Deposition (DED) processes [Flynn, 2016]. On the one hand, **Powder Bed Fusion (PBF)** processes are based on the selective melting of determined regions of a pre-deposited powder bed by one or more thermal sources (typically lasers), thus generating a thin layer of solid material. In order to guarantee uniform distribution of the powder, a leveling system or recoater blade is used. This process is repeated layer by layer until the desired solid is built (see Figure II. 7). Once the process is completed and the part finished, the metal powder that has not been melted can be sieved and reused [Herzog, 2016].

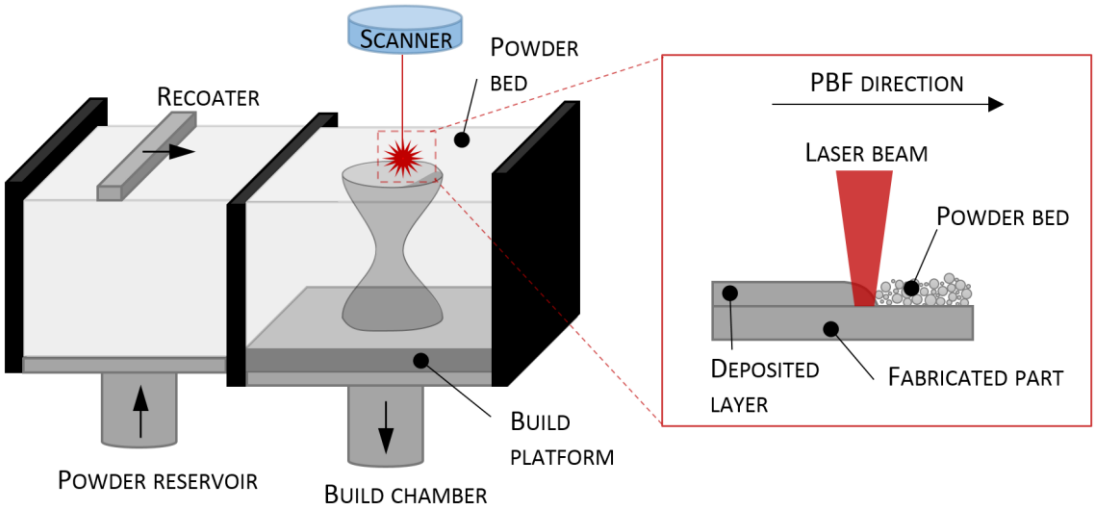

Figure II. 7 Powder Bed Fusion working principle.

PBF processes are performed on a build platform inside an enclosed build chamber, which in the case of SLM is filled with inert gas, and often require support structures in order to keep the part from excessive warping [Bobbio, 2017]. As a result, both the orientation of the part together with the location of the supports are key factors when setting up a build. Additionally to support structures, the pre-heating of the build platform can also be used for reducing residual stresses.

Due to the nature of PBF technologies, a broad range of materials, including polymers, ceramics, metals, and composites can be processed, where the main application is the manufacture of full 3D parts with high-complexity geometries. Besides, good accuracy and resolution are attained for metals. For those reasons, metal PBF processes are becoming increasingly popular for aerospace and biomedical applications, due to their ability to fabricate complex geometries with a wide range of materials and their excellent properties compared to traditional metal manufacturing techniques [Gibson, 2016]. Some examples of the application of PBF processes for the production of functional parts are dental and bone implants [Wally, 2019; Ataee, 2018], airfoils, or turbine blades with embedded cooling channels [Liu, 2017a], thus being able to give service to the aerospace, energy, and medical industries, among others.

Compared to DED technologies, PBF processes have a relatively slow build rate, but higher complexity geometries and better surface finish can be achieved. However, the size of the build chamber remains as a limitation on the part size. In addition, when the PBF manufacturing process is finished, the obtained part must be post-processed in order to be separated from the build platform inherent to this technique and remove the supports [Morgan, 2017].

On the other hand, **Directed Energy Deposition (DED)** consists on building up a part by means of focusing thermal energy (e.g. laser, plasma arc or electron beam) that simultaneously heats

and melts a substrate while filler material is injected into the melt pool [Terrassa, 2018], as shown in Figure II. 8.

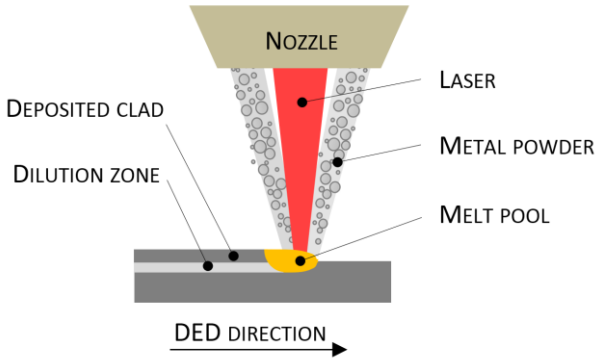

Figure II. 8 Directed Energy Deposition working principle.

Deposition can be done using 3-axis systems, but also with 4- or 5-axis, where complex parts can be built up with the help of rotatory tables or tilting deposition heads. Despite this approach can process several materials, including polymers, ceramics, and metal matrix composites, it is predominantly used for metal powders. DED processes are employed for generating new geometries, as well as for repairing, joining or applying coatings to pre-existing components. In addition, some companies have started to integrate DED heads into milling machines, enabling additive plus subtractive capabilities within a single platform and giving rise to the so-called hybrid machines [Fujishima, 2017]. This configuration is very advantageous for overhaul and repair. DED processes are capable of manufacturing fully dense components with controllable microstructure, produce functionally graded parts with material composition variations and apply corrosion and wear-resistant coatings. Nevertheless, the DED manufactured components have poor resolution and surface finish [Bonaiti, 2017]. In order to overcome these limitations, they typically require a post-processing that involves machining. Moreover, heat treatments may be also necessary in order to relieve residual stresses inherent to the deposition process [Oyelola, 2018].

Among the different existing DED approaches, Laser Metal Deposition (LMD) is gaining increasing attention by both academia and industry due to the versatile repairing and manufacturing possibilities it offers.

II.2.2. Laser Metal Deposition fundamentals

Laser Metal Deposition (LMD), also known as laser cladding, Laser Engineered Net Shape (LENS) or Direct Metal Deposition (DMD), is an Additive Manufacturing (AM) technique that enables

the buildup of fully dense coatings and functional parts with almost no geometrical restriction and high-quality metallurgy [Toyserkani, 2005].

The process is based on the generation of a melt pool on the surface of a substrate by a laser beam, while filler material in the form of powder or wire is injected simultaneously through a nozzle [Arrizubieta, 2017a], which is also responsible for generating a protective atmosphere that avoids material oxidation [Thompson, 2015]. In the case of powder LMD, this is realized by means of carrier gas, usually argon or helium, which also acts as shielding gas, being the typical powder grain sizes range between 20 and 100 µm. The filler material is molten by the laser beam and bonded to the substrate, forming clads and subsequent layers until the required geometry is obtained [Gasser, 2011].

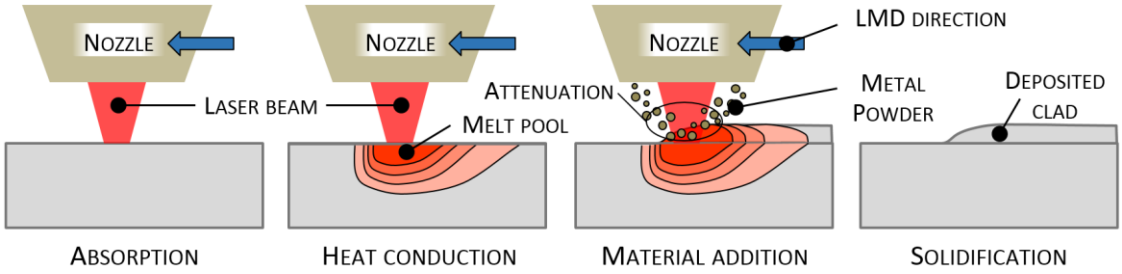

Figure II. 9 Laser Metal Deposition process [Arrizubieta, 2017c].

The total amount of energy introduced by the LMD technology into the substrate material is very low when compared to other conventional metal joining techniques, such as arc welding or plasma spraying, which leads to minimum distortion of the workpiece [Caiazzo, 2018]. This creates a fine microstructure, with low levels of dilution between layers and low distortion [Toyserkani, 2005]. All these characteristics give rise to final parts with good mechanical properties and minimal imperfections.

The suitability of the LMD process is proved for a high diversity of materials common in a wide spectrum of industries, ranging from the aerospace sector, to automotive or biomedical, among others [Torims, 2013]. To that end, many researchers have worked on the experimental determination of the optimal process parameters for the different materials. Some of them are tool steels [Bohlen, 2018], stainless steels [Kono, 2018], nickel alloys [Richter, 2004], titanium alloys [Kong, 2010] and copper alloys [Shamsaei, 2015]. In addition, LMD is also suitable for adapting the material properties of certain regions of the part to its final requirements and processing materials with different structure and composition along their total volume, known as Functionally Graded Materials (FGM) [Lima, 2017; Hwang, 2018]. Besides, LMD enables the production of near-net-shape parts, which reduces the material wastage and results in a cleaner and more environmentally friendly process [Priarone, 2017]. For instance, typical buy-to-fly

material ratios of 4:1 (input material to final component) are common in traditional 5-axis milling processes, with some components having a ratio as high as 20:1 [Allen, 2006]. Nevertheless, LMD is capable of improving these buy-to-fly ratios up to values below 1.5:1 [Caiazzo, 2017].

This additive manufacturing process is proved to be effective in the remanufacturing, coating, and repair of existing parts [Ruiz, 2018], as well as to open new possibilities in the design of innovative geometries [Abdulrahman, 2018; Leino, 2016]. Therefore, it has a wide spectrum of industrial applications. For instance, LMD is used for the manufacture and repair applications of critical aerospace engine components [Wilson 2014; Kumar, 2017], dies and molds [Jhavar, 2013] and coatings [Mazumder, 1996], among others.

However, LMD technology also has limiting factors that make the post-processing of the manufactured parts necessary in order to attain the required final properties. Some examples of the process limitations are the relatively low accuracy of the parts manufactured via LMD and the fact that the resultant surface roughness does not usually match the final requirements [Flynn, 2016]. In addition, the anisotropic behavior of the material properties and the generation of residual stresses can lead to geometrical distortions and even cracking of the material [Fayazfar, 2018]. Consequently, continuous corrective measurements during the LMD process are necessary in order to manufacture near-net-shape functional parts with close tolerances and acceptable residual stress [Mazumder, 2017].

Considering all this, despite the numerous benefits of additive manufacturing, the resulting parts often require additional machining, regardless of the additive approach [Klocke, 2014]. The combination of additive with subtractive operations helps to overcome the low accuracy, precision and high roughness usually related to additive manufacturing, hence enabling the production of components that were previously unattainable.

II.3. Hybrid manufacturing

Manufacturing industries demand efficient processes that provide a reduction in manufacturing costs and the required time in order to gain competitiveness while meeting high-quality standards [Lorenz, 2015]. As reported by Transparency Market Research, the global hybrid manufacturing machines market achieved a volume of $1.2 billion in 2017 and is expected to expand at a compound annual growth rate (CAGR) of 21.69%, thus reaching $6.7 billion by 2026 [Transparency Market Research, 2018]. Hence, hybrid-manufacturing systems are becoming an industrial solution for the manufacture and repair of high-complexity parts aimed at various sectors [El-Hofy, 2005]. The objective of developing hybrid processes is to enhance their

individual advantages while minimizing their limitations [Karunakaran, 2010]. Therefore, they enable to manufacture components that are not cost-effective or even impossible to manufacture by a single process [Zhu, 2013].

The concept of hybrid machines that combine various processes is not new. In 2011, Nassehi proposed a technology-based classification for the different technologies that could be integrated into a hybrid machine [Nassehi, 2011]. These processes are joining, dividing, subtractive, transformative and additive. Nevertheless, due to their irruption, the present section focusses on hybrid processes that combine subtractive and additive technologies.

In view of the market possibilities ahead, many machine tool builders have opted for this solution and started to develop different hybrid machines that combine additive and subtractive operations. In this way, hybrid machines have allowed overcoming the main drawbacks associated with additive manufacturing such as low accuracy and high surface roughness [Merklein, 2016]. The combination of both technologies in a single machine is therefore advantageous, as it enables one to build ready-to-use products within an all-in-one hybrid machine [Merklein, 2016; Du, 2016], which maximizes the strong points of each technology [Flynn, 2016]. In this way, complex components that are originally not possible to be machined due to accessibility constraints are now approachable [Chen, 2018].

Among the different metal additive manufacturing technologies available, the hybrid-manufacturing industry has predominantly opted for Powder Bed Fusion (PBF) and Directed Energy Deposition (DED) processes [Flynn, 2016]. Nevertheless, the vast majority of hybrid systems integrate DED, and more specifically LMD, which is faster than SLM and does not need any process chamber nor supporting structures [Yamazaki, 2016; Hansel, 2016]. For instance, in LMD, typical deposition rate values of 5-30 $g \cdot min^{-1}$ are obtained, whereas the SLM process presents typical values of 2-3 $g \cdot min^{-1}$ [Sciaky, 2017]. In addition, this approach is adaptable to existing conventional machine tools. Hence, hybrid machines give rise to new opportunities in the manufacturing of high-added-value parts, enabling the high-efficiency production of near-net-shape geometries, as well as the repair and coating of existing components [Thompson, 2015]. Besides, the capability to switch between laser and machining operations during the manufacturing process enables the finishing by machining of regions that are not reachable once the part is finished. In Figure II. 10, the main additive and subtractive process combinations are shown. They are divided into two groups according to the additive approach they are based on. It is worth mentioning that while PBF-based processes are mainly directed to produce complex whole parts, DED processes are more focused on the generation

of coatings or new features onto existing parts. Due to its process principle and easy integration into a machining center, DED-based additive processes can be combined with a wider range of subtractive processes.

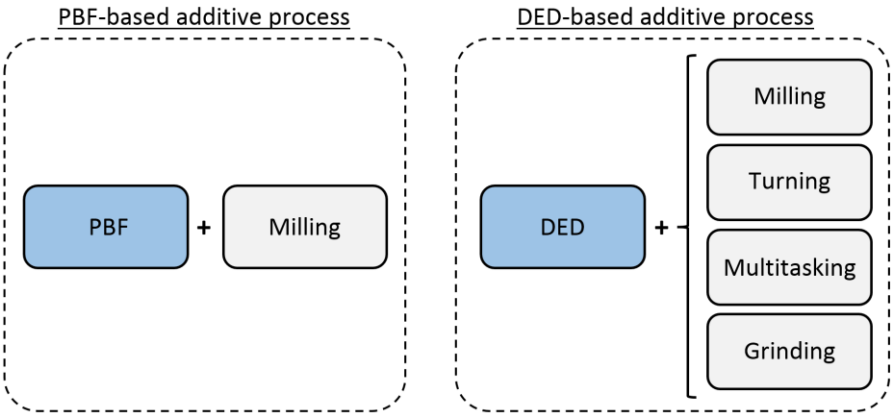

Figure II. 10 Different process combinations in existing hybrid machines.

The combination of additive and subtractive processes in a single hybrid machine is especially well suited for the manufacture of low machinability materials, such as heat resistant alloys and high hardness materials, which are widely used in various industries, including aerospace & defense, automotive, medical, and oil & gas, among others [Yamazaki, 2016]. In fact, this hybrid manufacturing approach has already been used for remanufacturing existing high-added-value components, such as turbine blades [Wilson, 2014], integrally bladed rotors [Ruiz, 2018], gas turbine burner tips [Navrotsky, 2015] or dies & molds [Ren, 2006]. Nevertheless, the full integration of both processes is a complex task that must still overcome many difficulties. Both laser-based additive processes and machining processes need to overcome challenges on their own in order to improve their performance and enhance the quality of the manufactured parts.

II.3.1. Configuration of the hybrid machines

In this section, the particularities in terms of configuration resulting from the integration of both additive and subtractive processes in a single platform are addressed. From a general point of view and regarding the hybrid machine tools architecture and typology, the same considerations as for conventional machine tools are usually valid. However, the implementation of some specific systems such as powder feeders, laser heads or optics involves some extra issues that need to be addressed.

1. Kinematic configurations

Aiming at the manufacturing of high-complexity parts, the kinematics of hybrid machines plays an important role in both the accessibility during the process and the resulting accuracy. In

Figure II. 11, the kinematic chains usually employed in hybrid machines are shown. From left to right they are classified according to their suitability for the manufacture of bigger and therefore, heavier parts. Despite 3-axis machines can be also used for hybrid machines, DED processes usually require the deposition of the material normal to the substrate. On the other hand, DED processes are usually applied to parts with very complex shapes. Thus, most of the hybrid machines that combine additive and subtractive processes are based on 5-axis machine configurations in order to enable performing both deposition and machining of high-complexity parts.

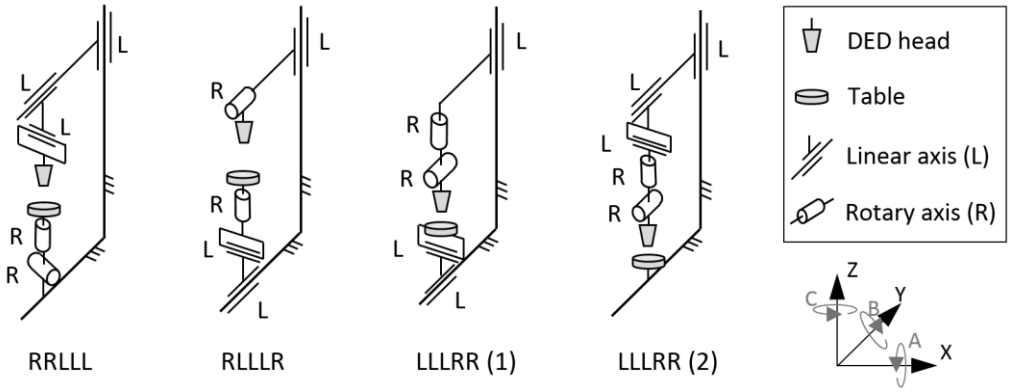

Figure II. 11 Most common kinematic schemes of hybrid machines.

On the one hand, most hybrid machines are currently based on an RLLLR kinematic chain, where the DED head includes a tilting movement (usually B-axis) and the table includes a rotary table or a universal clamping system (A or C-axis). These types of machines offer high flexibility together with an elevated stiffness. Moreover, most machine builders have already developed multitasking machines combining turning and milling, where the RLLLR is the most widely used kinematic chain. Therefore, the development of a 5-axis hybrid machine does not imply much design change from the point of view of kinematics, although many changes are required in terms of safety and machine protection.

On the other hand, if the machine is focused on the production of small and complex parts, the use of tilting-table machines, RRLLL kinematic chain, is extended. On the contrary, the biggest parts are manufactured in LLLRR (2) type machines, where the part to be manufactured is fixed and all moving axes are situated in the DED head.

2. Nozzles and Strategy Restrictions

In order to obtain a stable process, simultaneously to the generation of the melt pool on the surface of the substrate, filler material needs to be directed and injected using a specific nozzle. There are different types of nozzles for powder-based DED processes and based on their

geometry and depending on the powder injection system, three nozzle types can be distinguished: off-axis, coaxial discrete, and coaxial continuous [Zekovic, 2007]. The design of the nozzle is a key factor that has a direct influence on the powder mass distribution at the nozzle exit and therefore determines its efficiency. In addition, the design type also determines the kind of application of the nozzle, restricting the operations in which it is suitable: off-axis nozzles are usually employed for coatings, while coaxial nozzles are used for building 3D parts.

The off-axis nozzles are the simplest and most economical, where a single powder stream is fed laterally into the laser beam. However, as their powder feed is dependent on the direction, their use is restricted to a unidirectional deposition strategy, mainly to the coating of rotary parts, being unable to build 3D parts. Therefore, their use in hybrid machines is residual.

As an evolution of the off-axis, coaxial discrete nozzles have been developed (see Figure II. 12a), which enable multidirectional deposition at an intermediate price. Their working principle is based on a number of discrete injectors that are positioned around the axis of the nozzle and powder particles are fed coaxially to the laser beam. Depending on the design, three or four injectors may be positioned, whose powder flow can be regulated independently. However, due to its working principle, the powder distribution obtained from overlapping the lateral powder flows of the injectors is not uniform. The configuration of the coaxial discrete nozzles enables the tilting of the DED head up to 180° without altering the powder stream focus, thus allowing 5-axis deposition [Weisheit, 2001].

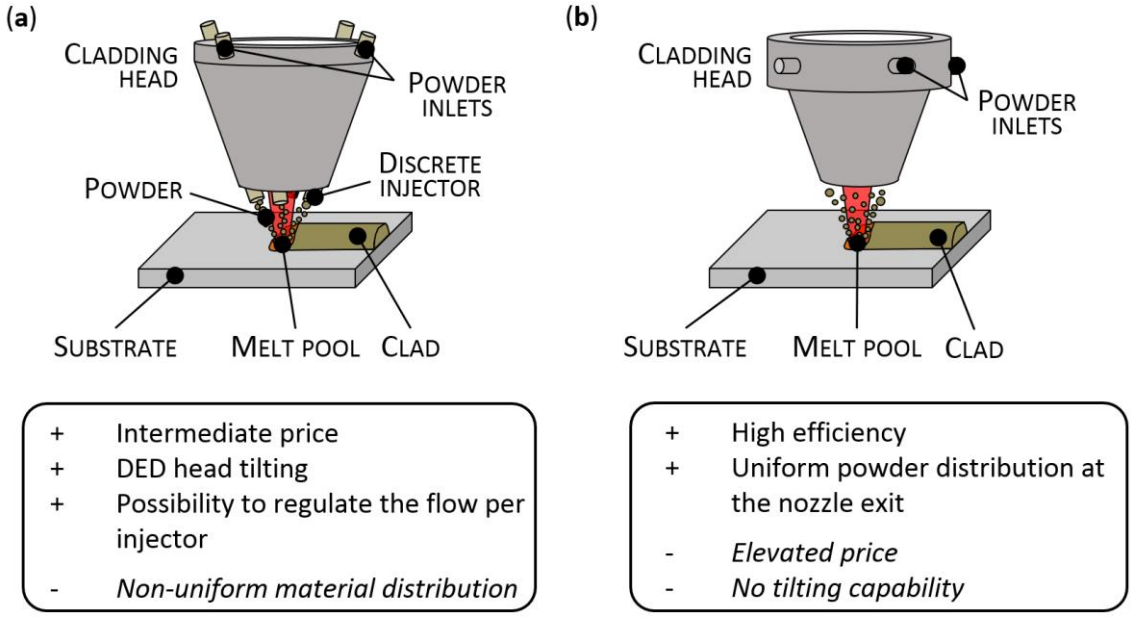

Figure II. 12 Different nozzles used in powder-based DED: (a) Discrete and (b) Continuous coaxial nozzles [Arrizubieta, 2017b].

Conversely, coaxial continuous nozzles have also arisen (see Figure II. 12b), generating an axisymmetric flow of powder at the nozzle exit that encloses the laser beam, thus being able to build 3D parts. In this case, greater nozzle efficiency can be achieved, as the diameter of the powder stream can be adapted to the size of the laser beam on the workpiece [Nagulin, 2018]. In addition, the powder distribution is ensured to be uniform and homogeneous at the nozzle exit. However, due to their complexity, these kinds of nozzles are expensive. Besides, their tilting is restricted due to the effect of gravity on the powder cone. Experiments show that this system can work satisfactorily with a maximum tilt angle of 20° [Weisheit, 2001].

3. Other Features

The introduction of powder particles in the working envelope of the hybrid machine in order to perform additive operations forces to make some considerations in order to preserve the integrity of the moving elements. Thus, machine tool builders have started to take measures to address this issue. For instance, some manufacturers (e.g. Mitsui Seiki, Okuma) have incorporated the same features as in their machining centers aimed at the machining of graphite, during which graphite dust is generated. That is, the machines include a fully enclosed guard that completely seals powder particles from other machine elements and then extracts them by means of an exhaust system. In addition, kinematic protections are also implemented in order to protect the moving elements (e.g. guideways, ball screws or nuts) from metal powder [Zelinski, 2016; Zelinski, 2018]. Furthermore, another kind of safeguard to be taken is that against sparks due to static discharges.

The combination of additive and subtractive technologies also has certain implications to be considered so that one process does not affect the other negatively. One example of it is the cutting fluid–laser tandem. In order to remove the excessive cutting fluid from the part to be processed additively, some manufacturers are opting for blowing it off the part [Gorman, 2016]. However, this is not an advisable practice when metal powder is present, as it poses fire and explosion risks [Skarzynski, 2018]. Other manufacturers use the laser beam to vaporize the residual cutting fluid before the additive process [Hybrid, 2019].

II.3.2. Study of the real capabilities of Hybrid Machines

The combination of additive and subtractive technologies in a single hybrid machine brings unquestionable advantages for the production of complex parts. However, not only are there positive aspects. Hence, in this section, a critical analysis of the capabilities of hybrid machines is performed, including their potentials, as well as the challenges still to be faced.

1. Potentials of Hybrid Machines

The development of hybrid machines has enabled us to unite the advantages of multiple processes using a single machine for the whole manufacturing of metallic parts with the subsequent benefits that it brings (pre and post-process operations that require other machines or working stations might still be necessary: heat treatments, painting operations, etc.). The most relevant strong points derived from the use of hybrid machines are presented in Figure II. 13 and expanded upon in the subsequent list.

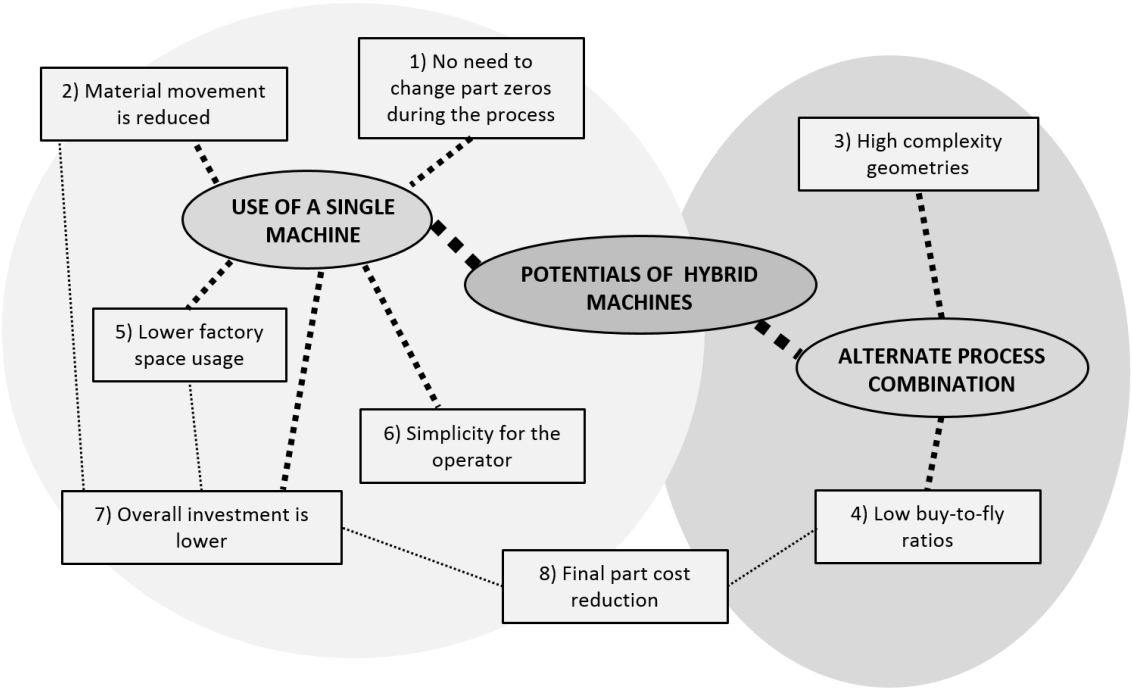

Figure II. 13 Potentials of the hybrid machines.

1. There is no need to change part zeros during the manufacturing process. A single setup is used for both additive and subtractive operations [Manogharan, 2015]. Therefore, the part-positioning error is minimized, which results in higher final accuracy. Furthermore, as there is only the need for a single zero-setup per part or set of parts, non-productive time due to zero making is reduced to minimum values.
2. The material movement inside the factory is reduced. Hybrid machines enable one to manufacture whole parts in the same machine, without the necessity to move the part to other machines for finishing operations [Li, 2018]. Hence, intermediate warehouses are eliminated from the factory, which results in better use of the available space. Besides, as the movement of the material is minimized, on the one hand, the workload of the equipment for material handling is reduced and, on the other hand, the chances for collisions and accidents are lowered, which results in an increase of the employees´ safety.

3. Manufacture of higher complexity geometries. The hybrid machine can switch between additive and machining operations seamlessly during the manufacturing of a single part [Soshi, 2017]. Therefore, it is feasible to machine areas that are no longer accessible once the part is finished. This results in higher freedom and flexibility when designing the optimum geometry of the part. Besides, this point is directly related with the previously introduced issues 1 and 2, because when the manufacturing process switches between additive and subtractive operations, there is no material movement inside the factory, nor precision lost due to zero changes between different manufacturing platforms.
4. Low buy-to-fly ratios. The possibility to generate near-net-shape components by using additive manufacturing leads to a reduction of material waste, as well as the economic costs related to material recycling and waste treatment. Buy-to-fly ratios as low as 1.5:1 are achieved thanks to hybrid machines [Allen, 2006]. Consequently, the ecological footprint resulting from the process is reduced. Combining additive and subtractive operations enables one to take advantage of the potential of both processes and therefore, material-efficiencies up to 97% can be achieved [Allwood, 2012; Achillas, 2015].
5. Lower factory space is used. Thanks to the use of hybrid machines additive and subtractive operations can be carried out within the same machine, the number of required machines for the manufacture of a certain part is reduced. Therefore, occupied space in the workshop is also reduced.
6. Simplicity for the operator. The integration of both processes in a single machine under a unique interface means that the operator must only deal with one working station, which simplifies training as well as daily work.
7. The overall investment is lower. Hybrid machines are more expensive than simple additive or milling machines. However, the integration of both technologies in a hybrid machine involves sharing common elements (e.g. guideways, machine tool structure, CNC control, user interface). Hence, the total investment required for the acquisition of a hybrid platform is considerably lower than buying two separate machines.
8. Reduction of the costs of the final part. Additive manufacturing enables the realization of high-performance coatings over ordinary or “cheap” materials, thus achieving a final part with enhanced properties, but at a cheaper cost. In addition, the capability of combining different materials and apply Functionally Graded Materials is also introduced by hybrid machines.

2. Challenges of Hybrid Machines

Despite the numerous potentials of the hybrid machines, many issues still need to be solved when combining additive and subtractive processes. In Figure II. 14, the most relevant challenges to be faced before their complete implementation are shown and their connections are highlighted.

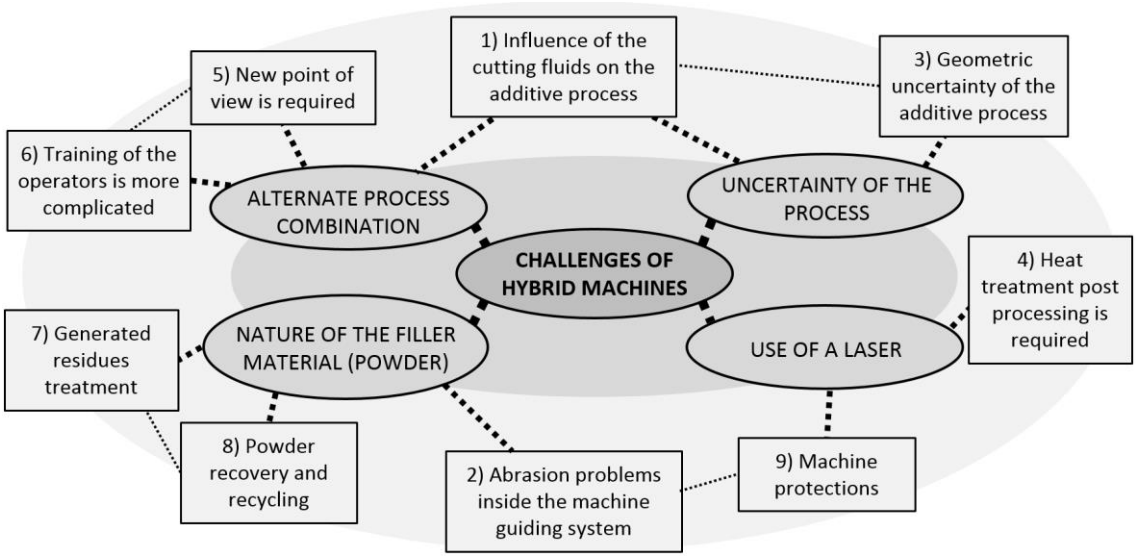

Figure II. 14 Challenges of hybrid machines.

1. Influence of the cutting fluids on the additive process. The remains of the cutting fluids from the machining process can influence the subsequent additive process [Yan, 2018]. As a result, ensuring the cleanliness of the substrate is of great importance in order to guarantee a good bonding between the deposited and base materials, and therefore perform a high-quality additive operation [Mahamood, 2013]. This means that, as far as hybrid machines are concerned, an intermediate cleaning stage between machining and the subsequent additive operation might be necessary. However, there is no agreement in either industry or academia on how to proceed with regard to this issue and only a few studies can be found [Yan, 2018].

   Problems with cutting fluids are even more critical when PBF processes and milling are combined. In this case, no cutting fluids can be used in the subtractive operation, as their mixture with the powder bed would be detrimental for the whole process, which results in lower feed rate, lower plunging depths, higher tool wear, etc. when machining.

2. Abrasion problems inside the guiding system of the machine. Hybrid machines require special protection that preserves the guiding system from the powder used in the additive operation [Zelinski, 2016; Zelinski, 2018]. The powder particles used in DED and PBF processes have diameters ranging between 45–150 µm and 10–40 µm, respectively.

Therefore, if the machine is not properly sealed, powder particles might intrude and interfere with the smooth movement of the guiding system, as well as with the encoders used for determining the position in the machine.

3. Geometric uncertainty of the additive process. Due to the uncertainty that additive manufacturing suffers as a consequence of the state of the art and lack of maturity of the technology, the additive stage is the weakest link within hybrid machines. For example, it is well known that additive manufacturing can produce complex internal features, but there is a lack of knowledge regarding how those features should be inspected [Zelinski, 2015]. Regarding the accuracy of the additive process, especially in DED operations, it is lower than that of machining. In Table II. 1, a comparison between PBF and DED technologies in terms of dimensional accuracy and surface roughness is presented [Gu, 2015]. As can be seen, DED is a less accurate process than PBF. However, in both cases, a post-processing stage is necessary depending on the final requirements of the part.

Table II. 1 Comparison between PBF and DED technologies

Dimensional	Dimensional accuracy	Surface Roughness	References
PBF	±0.05 mm	9-16 µm	[Zhu, 2003], [Mumtaz, 2009]
DED	±0.13 mm	≈40 µm	[Milewski, 1998], [Mazumder, 2000]

The material deposition rate in the additive process is extremely sensitive to the feed rate of the machine, the volume of the substrate, the geometry of the region where the material is being deposited, the surface finish, etc., which may generate differences between the originally designed and finally manufactured part [Arrizubieta, 2018]. Besides, the internal stresses generated during the additive stage due to the thermal nature of the process may generate considerable geometrical distortions. Therefore, in the subsequent machining operation, the tool may encounter material over-accumulations and different geometries from those expected, which may lead to the breakage of the cutting tool.

4. The requirement of a post-processing heat treatment. During the additive process, the material is subjected to heating and cooling thermal cycles, which leads to the generation of residual stresses that might be released during the subsequent machining operations. This results in distortions of the part geometry and hence the machining tool may encounter different plunging depths to those programmed [Heigel, 2018]. Besides, the mechanical properties of the deposited material, for instance, ductility, are very sensitive to the presence of internal defects and porosity [Bermingham, 2018].

In order to reduce internal stresses and solve these issues, additively manufactured parts usually require post-processing heat treatment [Oyelola, 2018]. For example, Kobryn and Semiating studied the influence of a post-processing stage on a Ti-6Al4V part produced by Laser Engineered Net Shaping (LENS) and concluded that a Hot Isostatic Pressing (HIP) operation can increase ductility from 0.8% to values of almost 12% [Kobryn, 2001]. Besides, authors like Åsberg et al. studied the influence of HIP on the yield strength of an AISI H13 tool steel and a 30% improvement was obtained with regard to the as-deposited material, reaching an average value of 1502 MPa [Åsberg, 2019].

Therefore, in case the hybrid machine is not prepared for providing the required heat treatment, material movement to an external furnace is mandatory, which eliminates one of the main advantages of using a hybrid machine.

5. The necessity of a paradigm shift. Design engineers need to learn not only each process independently (additive and subtractive) but also the possibilities that have arisen thanks to their combination, which may result in a change of the whole concept of designing parts. For instance, Salonitis and Zarban proposed a methodology for redesigning the geometry of a part to be additively manufactured based on a Multi-Criteria Decision Analysis (MCDA) for assisting in decision-making [Salonitis, 2015]. However, there is no standard methodology or process planning aimed at hybrid machines.

   Besides, Hällgren et al. stated that additive manufacturing could be approached from two points of view: design-driven and process-driven [Hällgren, 2016]. The first one focuses on improving the geometry of the manufactured part, but without considering the optimization of the manufacturing process itself, whereas the second one works the other way. However, if satisfying results are to be obtained and the full potential of hybrid manufacturing is to be exploited, a new point of view that combines both ideas is required.

6. The training of operators is more complicated. Operators require wider background knowledge to master in both processes; hence, this is directly translated into a longer training period. Moreover, due to the extensive freedom of additive manufacturing, hybrid machines usually require the use of computational frameworks in order to optimize both processes [Jared, 2017]. Besides, operators must be trained in safety issues, especially with regard to powder handling and laser operating [Stavropoulos, 2018].

7. Complex waste treatment. Thanks to the capability of additive manufacturing to generate near-net-shape geometries, hybrid machines reduce the amount of generated waste material by as much as 90% [Markillie, 2013]. However, their treatment may be far more complicated, from a logistical point of view, and economically expensive. Special attention must be paid to powder handling, recycling of the liquid wastes (e.g. lubrication oils used

for the movement of the axes, cutting fluids employed in machining). Depending on the composition of the powder particles, the residues might be extremely hazardous to human health. Especially, powder with a high content of nickel or cobalt is carcinogenic to human health. All this obliges the company to install special protective measures, as well as a proper protocol for treating the residues [Walter, 2018]. Moreover, despite the latest advances, there is a lack of knowledge and studies related to the toxicity and harmful effects related to the powder particles [Drizo, 2006].

8. Powder recovery and recycling. In laser metal additive processes, only a fraction of the fed powder is melted by the laser and added to the substrate, whereas the rest is lost. Industrial powder-based DED systems have an efficiency ranging between 5 and 70% [Carroll, 2006], while in wire-based DED and PBF much higher efficiencies are obtained, reaching values of virtually 100%. However, this powder has interacted with the laser beam and, consequently, the shape and composition of the particles may have changed, which is detrimental for its reuse. Carroll et al. concluded that the reused powder reduces the hardness of the deposited material and increases the surface roughness [Carroll, 2006]. Besides, it may have been exposed to other substances, such as oil, dust, other composition powders, etc., negatively affecting the process. In order to highlight the discrepancies between the different authors and the existing uncertainty in this field, some authors conclude that Inconel® 718 powder can be reused twice [Renderos, 2017], whereas others increase this number up to 10 reuses without major changes in the results for the Inconel® 625 powder [Carroll, 2006].
9. Machine protections. Besides protecting the machine operator from collisions, the guarding of the hybrid machines needs to be capable of retaining the high-intensity light generated by the laser inside the machine and withstanding the heat generated during the additive process. Reflections of the laser beam when highly reflective materials are being processed (e.g. aluminum, copper) may result in the melting of specific areas of the guarding or other sensitive elements and, therefore, proper protection must be arranged. In this direction, some machines are provided with sensors in the guarding that detect these reflections and trigger the emergency stop when there is a danger of piercing.

II.3.3. Latest developments from an industrial perspective

Despite the potential of additive manufacturing, its application also has some limitations, such as accessing difficult to reach areas inside complex parts. This issue is one of the main reasons

why many machine tool builders have opted for offering hybrid systems that combine additive and subtractive processes.

Many manufacturers are successfully operating in the market of additive manufacturing using both DED and PBF technologies. However, when it comes to hybrid systems, the available offer of machines based on DED technology is noticeably wider than those integrating PBF processes. Some of the underlying reasons for this situation are the much higher deposition rate offered by the DED, as well as the possibility of adding material on existing parts. Moreover, thanks to the feasibility of depositing material while the five axes of the machine are simultaneously interpolated, complex geometries can be built without any support structure. In addition, the integration of DED technology into a conventional machine tool is much simpler than incorporating PBF systems.

In this section, the latest hybrid machines developed by the market-leading machine tool builders are detailed with the aim of providing readers a broad vision of the market situation and the latest launches.

1. DMG Mori

The German-Japanese company DMG Mori is one of the global leaders of machine tool manufacturers, which has also been successfully operating in the market of additive manufacturing using powder-based DED and PBF technologies. However, with regard to additive technologies to be integrated into hybrid platforms, DMG Mori has strongly invested in DED processes rather than in PBF, giving rise to the LASERTEC 3D hybrid series. In this way, DMG Mori focuses on the production of relatively large components in finished part quality and aims to gain access to the aerospace, energy, and die & mold industries.

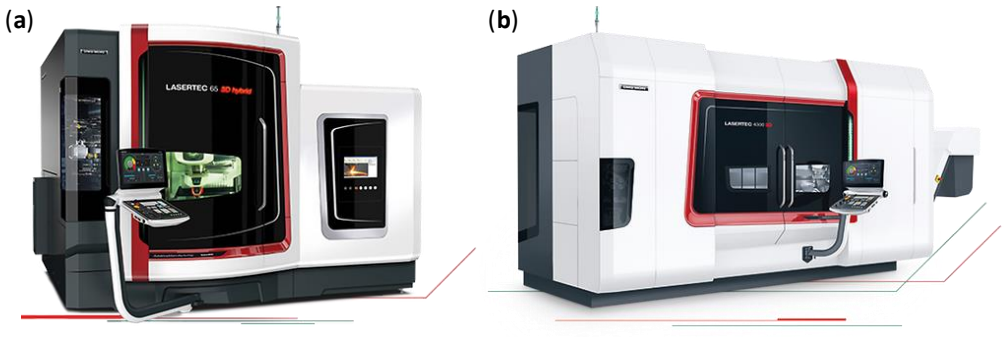

Figure II. 15 (a) *LASERTEC 65 3D*; (b) *LASERTEC 4300 3D* hybrid machines [DMG Mori, 2017].

DMG Mori launched in 2014 its first hybrid machine, the *LASERTEC 65 3D hybrid*, which is based on an RRLLL kinematic chain and includes a tilting table, thus combining the flexibility of LMD

with the precision of five-axis milling in one single machine, see Figure II. 15a [DMG Mori, 2019a]. The flexible changeover between laser and milling operations enables the manufacture of complex parts, as well as intermediate machining operations between additive stages in a single setup. Moreover, DMG Mori offers assistance during the complete process chain, including a hybrid CAD/CAM module for additive and subtractive programming, technology parameters coming from a material database and process monitoring. With regard to the latter, *LASERTEC 65 3D hybrid* includes in-process regulation, as well as analysis and control systems, based on closed-loop systems. This technology consists of real-time tracking of the melt pool size and temperature together with laser power and argon gas flow, among other parameters.

In 2016, DMG Mori expanded its hybrid machines offer with the *LASERTEC 4300 3D hybrid*, which includes a B-axis tilting movement in the head and an RLLLR kinematic chain, thus integrating six-axis LMD and five-axis turning/milling operations. This configuration allows working with components up to 660 mm in diameter and 1500 mm height, see Figure II. 15b [DMG Mori, 2019b]. In addition, this machine is equipped with up to five nozzles of different sizes and an automatic laser head changer, attaining homogeneous powder distribution within the nozzle independently from the direction of laser deposition. Regarding process monitoring and control, *LASERTEC 4300 3D hybrid* has a two-color coaxial pyrometer and a closed-loop control that automatically regulates laser power so that a constant temperature in the melt pool is ensured. Furthermore, an additional titanium-processing package can be purchased, enabling the safe additive manufacturing of highly-reactive materials, such as titanium powder.

Additive manufacturing and hybrid machines are hot topics for DMG Mori, which has already established itself as a full-liner in additive manufacturing and is setting the benchmarks in the production of complex parts [DMG Mori, 2017]. In addition, it has expanded its hybrid series portfolio with the larger *LASERTEC 125 3D hybrid*, which is aimed at the manufacturing, maintenance, and repair of large parts, has been launched to the market at Formnext 2019.

2. Yamazaki Mazak

The Japanese Mazak has established itself as a leading global company in the development of advanced machine tools and automation systems. Based on its extensive expertise in building multitasking machine centers, Mazak has also made inroads into the hybrid machine's market with five DED-based hybrid machines.

The *INTEGREX i-400 AM* [Mazak, 2019a], launched in 2014, is the company´s first hybrid multitasking machine with additive capabilities. The machine is addressed to the production of

small lots, as well as the manufacture of low-machinability materials by combining 5-axis machining and LMD. It has an RLLLR kinematic configuration, where the turning spindle offers a full A-axis contouring capability, whereas the milling spindle includes a -30/+120° B-axis tilting movement, together with the A-axis rotation.

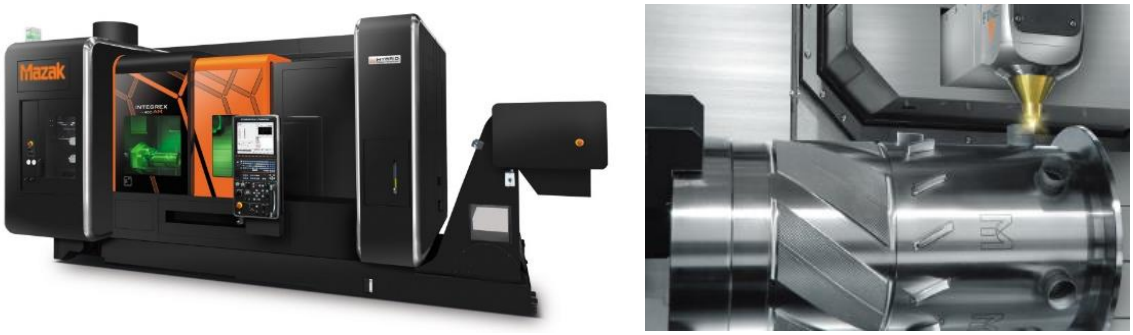

Figure II. 16 *INTEGREX i-400AM* hybrid machine and sample workpiece [Mazak, 2019a].

The machine can switch between two different laser processing heads that are loaded into the milling spindle by a standard tool changer, aiming high speed or high accuracy deposition and enabling the adjustment of the deposited clad size depending on the process requirements and employed material. The former has a more efficient deposition rate, while the latter is more focused on the generation of complex geometries.

Two years later, in 2016, the *VC-500 AM* hybrid multitasking machine was presented [Mazak, 2019b]. This machine, which is only available in the US market, features 5-axis milling and LMD additive technology. Alike the *INTEGREX i-400AM*, the *VC-500 AM* is based on an RRLLL kinematic chain, which includes a tilting-table, A and C axes, and the translation movements are situated in the LMD head. Besides, the machine is provided with the Mazak *MAZATROL SmoothX* CNC technology [Mazak, 2018], which eases the generation of programs for manufacturing complex parts.

Both *INTEGREX i-400 AM* and *VC-500 AM* hybrid machines were equipped with multiple Ambit™ laser processing heads, developed by Hybrid Manufacturing Technologies [Hybrid, 2019]. The Ambit™ system is a series of laser heads and docking systems that, after being integrated into a machine tool, enables the automatic changeover between LMD and machining.

The *INTEGREX i-200S AM* was introduced at JIMTOF 2016 [Mazak, 2016]. This hybrid machine tool uses an RLLLR kinematic chain; including two turning spindles, a milling spindle and a Gantry AM head (Figure II. 17a), and integrates Multi-Laser Metal Deposition with milling/turning. Multi-Laser Metal Deposition is a process in which multiple laser beams are used to melt metal

powder fed through the center of a laser head, attaining a stable metal powder flow even when tilting the laser head and provides very high accuracy (Figure II. 17b).

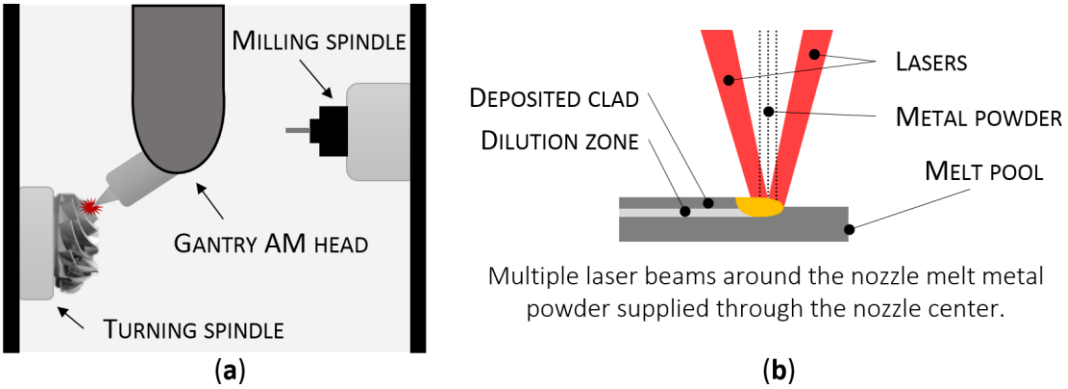

Figure II. 17 (a) Gantry AM head used in the *INTEGREX i-200S AM*; (b) Multi-Laser Deposition process [Mazak, 2014].

The *INTEGREX i-200S AM* is especially well suited for the production of mid-size complex parts. The gantry AM head is independent of the milling spindle, enabling the processing of larger areas. Moreover, it is stored away during machining operations in order to avoid any contamination originated by the cutting fluids or machining chips. The evolution of this machine, the *INTEGREX i-300S AM*, was also launched and presented at the Machine Tool World Exposition (EMO) 2017.

However, the latest machines launched by Mazak incorporate own developed laser heads and no Ambit™ laser processing heads are employed, which claim to have much higher efficiency than the Ambit™ series. In the last International Manufacturing Technology Show (IMTS) 2018 held in Chicago, the *INTEGREX i-400s AM* was presented, which includes in-house developed nozzles, as well as a complete redesign of the LMD head. In addition, opposite to the vast majority of commercial laser processing heads, in these new nozzles, the metal powder is fed through the center while shielding gas is externally supplied.

The *VARIAXIS j-600/5X AM* [Mazak, 2017], launched in 2016, is based on a vertical 5-axis machining center combined with WAAM. It is based on an RRLLL kinematic chain, where a tilting table is used and the additive manufacturing head includes linear movements. This machine is equipped with a wire-arc welding head mounted on the machine's headstock, which enables the speeding of the additive process as well as the production of higher volume parts. At EMO 2017, a variant of this machine was also presented, incorporating LMD technology instead of WAAM as additive process.

3. OKUMA

Okuma is a global leader machine tool manufacturer headquartered in Japan. It offers a wide variety of machine tools, including lathes, grinding machines, machining centers, and multitasking machines. In order to provide better control of the process, Okuma has also developed its own CNC control system and software, ranging from virtual simulators to CAM postprocessors. Since 2016, Okuma has also broken into the hybrid market by including the LASER EX series within its portfolio. This machine series, developed in collaboration with Trumpf, combine subtractive and additive functionalities, including also hardening and coating capabilities in a single platform.

Figure II. 18 *MU-6300V LASER EX* hybrid machine applications [OKUMA, 2019a].

On the one hand, the *MU-V LASER EX* [OKUMA, 2019a] machines are 5-axis vertical machining centers provided with laser processing capabilities. All MU-V machines are based on an RRLLL kinematic chain, where the tilting table includes the X linear axis and the Y and Z are included in the DED/milling head. On the other hand, the *MULTUS U LASER EX* [OKUMA, 2019b] series are based on a 5-axis horizontal multitasking machine. However, unlike the vertical centers, these horizontal centers include an RLLLR kinematic chain, together with a B-axis tilting head.

Currently, there are three models available for each series, which have the same characteristics, but different workspace size. Both MU-V and MULTUS machine series are capable of milling, turning, grinding, LMD, as well as applying laser heat treatments. The reliability and stability of the additive manufacturing processes are ensured by Okuma's OSP intelligent control, which was previously developed for subtractive operations and is now adapted for LMD. Okuma's intelligent technology deals with thermal deformation compensation, collision, and vibration avoidance, as well as the measurement of geometric errors in process. In addition, all hybrid

machines include especial guarding, similar to that of machine tools designed for machining graphite.

4. WFL Millturn Technologies

The worldwide manufacturer WFL, who concentrates uniquely on the production of multifunctional complete machining centers, has integrated laser-based additive technologies into a MILLTURN multi-task machining center. In this way, fully integrated laser solutions, such as laser cladding, laser welding, and laser hardening, are possible on the *M80 MILLTURN* [WFL, 2019], which is also provided with turning, boring, and milling functionalities. The machine is specially designed for the manufacture of long cylindrical parts, such as shafts, where the additive process enables the generation of additional features on it, as well as corrosion and wear-resistant coatings. The machine's kinematic chain is based on an RLLLR configuration, where the DED/milling head includes a B-axis tilting movement. In this case, as the processed parts can be up to 6 m long, a high deposition rate LMD system is included, which is based on a high-power diode laser.

5. IBARMIA

The Basque machine tool builder has a wide experience in the design and manufacture of subtractive machining centers and has also decided to start incorporating laser cladding functionalities in its 5-axis multitasking machines, giving rise to the ADD+PROCESS series and the *ZVH 45/L1600 ADD+PROCESS* machine. This machine is based on a moving column architecture with a B-axis tilting head, RLLLR kinematic chain, and combines DED with precision milling and turning. As a result, the machine is provided with high versatility to manufacture parts with complex geometries, as well as to combine different materials within the same component. In addition, the automatic change between the additive and subtractive heads enables an easy switch between both processes, allowing the finishing of additively manufactured parts with high accuracy and precision. Besides, the laser spot size can be modified in order to attain high productivity or fine geometries by DED [Ibarmia, 2015].

6. MITSUI SEIKI

Mitsui Seiki also launched to the market in 2016 the hybrid machine *Vertex 55X-H*, which integrates a spindle-adapted laser DED system into a traditional high precision machine tool [Scott, 2016]. The machine is based on an RRLLL kinematic chain with a tilting table and a gantry-type structure and aims particularly at the manufacture of complex parts for the aerospace industry. The company Hybrid Manufacturing Technologies has also contributed to

the development of this machine and therefore, it includes Ambit™ S7 cladding heads that maximize productivity [Hybrid, 2017] and enable to switch between LMD and milling.

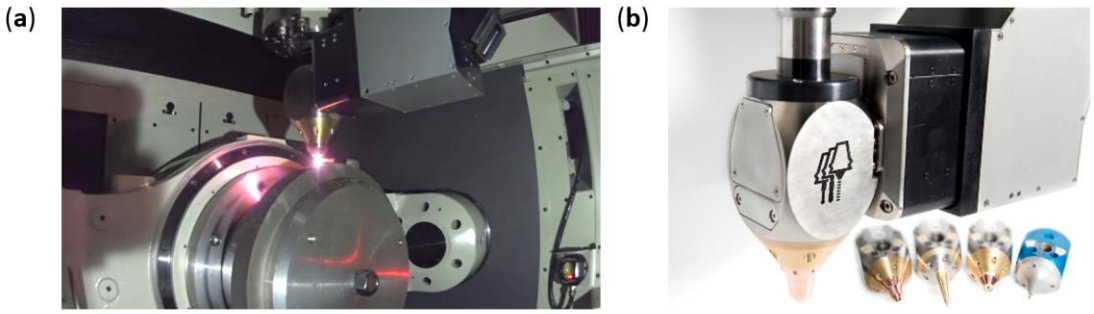

Figure II. 19 (a) Vertex 55X-H hybrid machine during additive operation; (b) Ambit™ S7 cladding heads [Hybrid, 2017].

Especially notable are the measures this company has taken in order to face the problems arisen due to the combination of additive and subtractive operations. On the one hand, the machine includes an air blow-off operation that removes much of the volume of coolant still on the part, followed by a laser cleaning stage prior to the additive operation [Zelinski, 2016]. On the other hand, in order to avoid problems in the ball screws and guideway systems, the machine has especial guarding and other kinematic protections that the company has adapted from other milling machines that are specifically designed for working with graphite.

7. Elb-Schliff Werkzeugmaschinen

Despite traditionally integrating machining operations, the hybrid manufacturing and hybrid machine tool concept are also open to other alternatives. One example of this is the *millGrind* hybrid machine developed by Elb-Schliff WZM GmbH, which combines DED and grinding technologies, offering, according to the company, 0.1 µm accuracy [TCT Magazine, 2015].

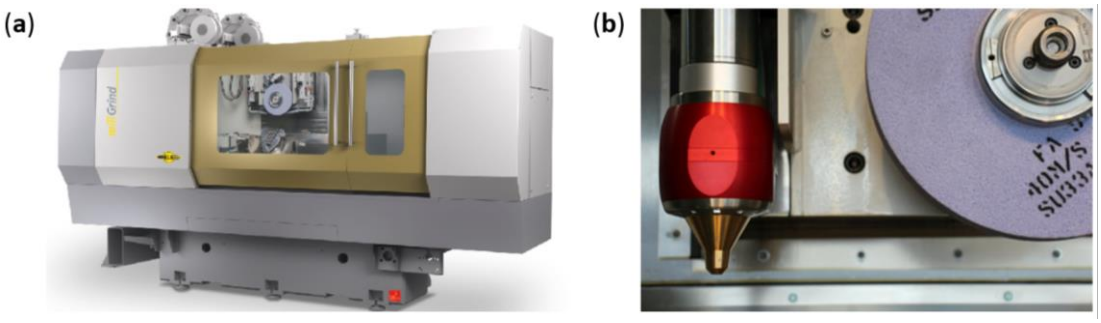

Figure II. 20 (a) millGrind hybrid machine; (b) Ambit™ cladding head and grinding wheel [Hybrid, 2017].

The hybrid machine is equipped with Ambit™ laser cladding heads for the additive process. Its main advantage is that it offers a new standard for precision by integrating grinding and DED in a single setup [Elb Schliff, 2019].

8. SODICK

Sodick is a world leader in the manufacturing of Electrical Discharge Machining (EDM) and high-speed milling center machines, which has also broken into the additive market. Sodick's new OPM series, comprised of *OPM250L* [Sodick, 2019a] and *OPM350L* [Sodick, 2019b], perform both SLM and high-speed milling. Each layer is milled as soon as it is built so that a high-quality accuracy and precision are attained, even on cavities or inner features that are not reachable once the part is finished. Therefore, these hybrid machines are specially designed for the manufacture of small mold inserts with cooling channels.

9. MATSUURA

The high-speed machining centers manufacturer Matsuura has developed, since 2003, Metal Laser Sintering Hybrid Milling Machines under the name LUMEX Series [Matsuura, 2019a]. This series consists of two different machines that differ in the size of their working area, which is 250 x 250 mm^2 for the *Lumex Avance 25* [Maquinser, 2019a] and 600 x 600 mm^2 for the *Lumex Avance 60* [Maquinser, 2019b]. In both models and depending on the layer thickness to be attained, a 500 W or a 1000 W maximum power Ytterbium fiber laser can be installed and the milling operation is performed by default after every 10 layers are processed, as seen in Figure II. 21 [Matsuura, 2019c]. For the milling operation, the machines include an in-house developed BT20 Maxia spindle with a 45,000 rpm maximum rotation speed and, for the proper integration of both processes, Matsuura offers the LUMEX CAM solution for the path generation.

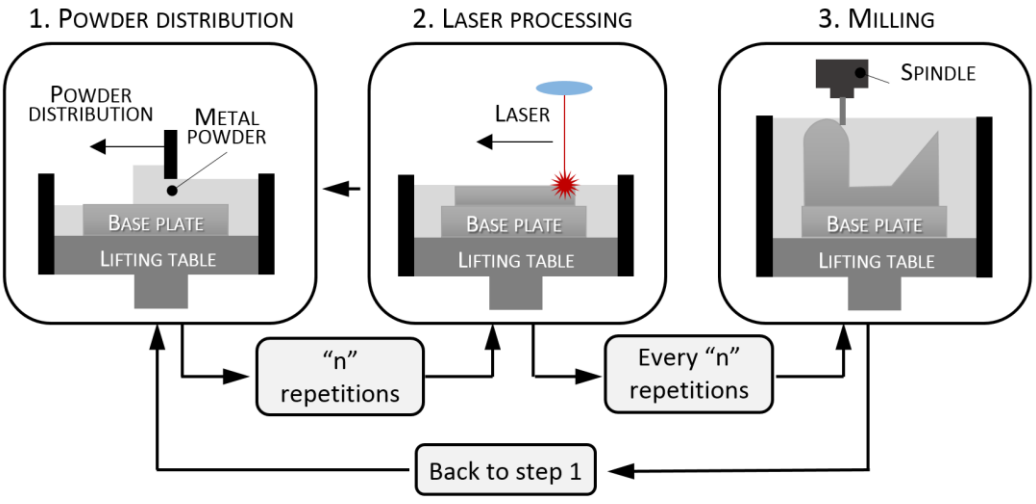

Figure II. 21 Additive and subtractive operation combination proposed by Matsuura. [Matsuura, 2019a]

According to the numbers shown by Matsuura, thanks to the combination of Metal Laser Sintering and milling, the total time required for an easy mold construction is reduced by 65% and the cost up to the 49% [Matsuura, 2019b]. In this way, the use of hybrid machines in the

manufacturing of molds is justified. Besides, the developed machines are capable of generating porous regions previously defined by the design engineer, allowing the gases trapped inside the mold to exit during the injection process and thus reducing the defects inside the part.

10. GF Machining Solutions

Finally, yet importantly, GF Machining Solutions has collaborated with different additive manufacturers and now is developing joint solutions with the US company 3D Systems in order to develop the *DMP Factory 500* [GF, 2018; GF, 2019]. The machine is grounded on a Direct Metal Printing-based additive manufacturing platform, in which a *System3R tooling system* has been incorporated (Figure II. 22) [PR Newswire, 2018]. This tooling system enables one to switch the part between the different additive and subtractive machines. A similar solution was previously presented at EMO 2017 in collaboration with the German company EOS.

Figure II. 22 An example of a System 3R tooling system used for keeping a fixed reference during the whole process.

Therefore, the proposal of GF and 3D Systems is not a hybrid machine itself, but a special tooling system that claims to reduce the setup time to a few minutes and to guarantee precision and accuracy during the entire manufacturing process chain. In this way, they compare their process to that performed in a hybrid machine.

II.3.4. Current situation and future perspectives

The development of hybrid machines combining additive and subtractive processes opens doors to a new concept in terms of both design and manufacturing, enabling the construction of new components previously beyond reach. Nevertheless, the consideration of both technologies in holistic terms is a pressing need in order to perform their full integration within a single platform as a comprehensive manufacturing approach. This necessity gives rise to a new vision of the process, conscious of the requirements and restrictions of each technology and leveraging their potentials. In order to grasp its importance, the most relevant advances made in this direction are addressed in terms of process planning, monitoring and inspection, and CAM software developments.

1. Process Planning

An integral view of hybrid processes combining additive and subtractive operations is required in order to optimize the interaction of both technologies during the production of a component. Hybrid manufacturing is especially interesting for the manufacture and repair of high-added-value parts. Depending on whether a new geometry is to be manufactured or a damaged existing part needs to be repaired, a different approach is adopted, as shown in Figure II. 23. The manufacture of a new geometry starts with the addition of material followed by a finishing operation, usually by machining, so that the requirements of the final part are met. By contrast, the process sequence required in a repair or coating context may involve alternating additive and subtractive operations. In this case, the interaction between both processes becomes especially important.

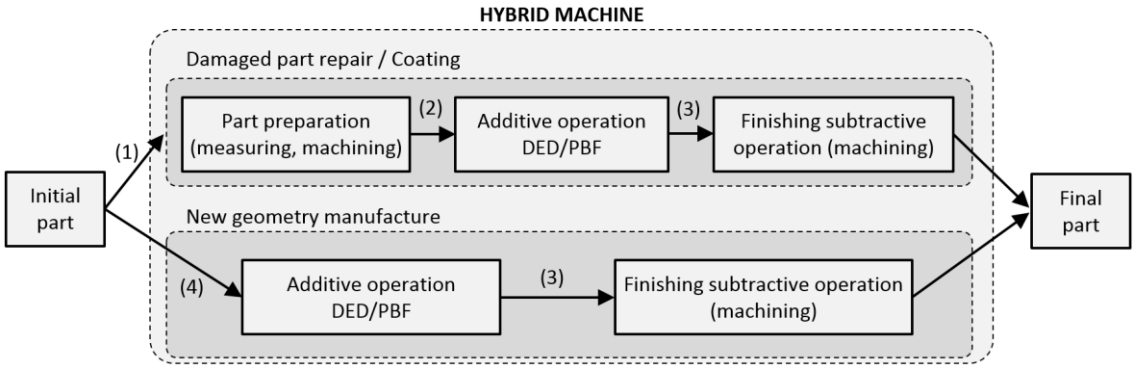

Figure II. 23 Process interactions within a hybrid machine.

Nevertheless, some considerations to be taken are represented in the figure. On the one hand, when repairing a component, (**1**) the initial part needs to be measured and characterized before any operation is performed. Then, (**2**) an intermediate cleaning stage between the subtractive and additive operations is required in order to remove the cutting fluid remnants from the area to be additively processed. In addition, after performing any additive approach, (**3**) the resulting component needs to be measured so that the outcome of the additive operation is checked, and the subsequent machining tool paths are defined. On the other hand, when a new geometry is to be built, (**4**) the initial part or substrate needs to be inspected and subsequently clean in order to ensure a good quality of the deposited material. Similar to the previous case, the dimensional characterization of the additively built-up part (**3**) is crucial in order to proceed with the finishing operation. Nevertheless, the difference lies in the fact that, for repair/coating of a damaged part, a preparatory machining operation is required before any additive approach, due to the use of cutting fluids. As explained in section II.3.2, cutting fluid remnants on the part may negatively affect the additive process. Therefore, this sequence of operations introduces

contaminants such as cutting fluids or machining chips that may involve the appearance of undesired effects at the additive stage. In this scenario, cleaning steps should be considered. In any case, few works in literature study the influence of machining contaminants on the LMD process [Yan, 2018; Cortina, 2018a]. On the contrary, for the manufacture of a new geometry, the substrate material can be just visually inspected and preliminarily cleaned (e.g. manually) before being introduced into the hybrid machine.

So far, few researchers have focused their efforts on process planning for combined additive and subtractive manufacturing technologies. Ren et al. [Ren, 2006] defined a process planning procedure for repairing dies by DED and machining. For that purpose, the authors identified the following sequence of operations: (1) determining the features to be repaired, (2) machining the damaged features, (3) additive operation to repair the feature and (4) finishing of the deposited material by machining. Nevertheless, problems that may arise from the geometrical distortions generated during the additive process are not considered. On the other hand, Kerbrat et al. [Kerbrat, 2011] proposed a methodology based on manufacturability indexes to identify features that can be manufactured by additive processes during the product design stage. Besides, Le et al. [Le, 2017; Le,2018] generated a manufacturing process sequence aimed at reincarnating end-of-life (EoL) or existing components into final parts with new functionalities. In a first step, the authors identified machining and additive manufacturing features by comparing the CAD models of the existing and the objective geometries and considering the restrictions of each technology. Then, the process plan is designed by respecting relationships between features, rules based on manufacturing precedence constraints and tool accessibility. However, process factors, such as the importance of maintaining a constant processing velocity during the DED process and the influence of the coolant used in previous machining stages, are not considered. More recently, Behandish et al. [Behandish, 2018] developed an early approach for automatic evaluation of manufacturability and generation of process plans for hybrid manufacturing via computer-aided process planning. Thus, process planning is moving towards combining additive and subtractive operations from a holistic perspective and not only machining as a preparatory or finishing operation.

2. Monitoring and Inspection

The implementation of in situ monitoring and inspection systems enables the attainment of immediate information from the manufacturing process and early detection of defects or anomalies. In this way, the quality of both the final part and the process is enhanced, while the number of rejections and amount of scrap are reduced. To that end, process parameters need

to be controlled instantaneously depending on external variables and many authors have focused their efforts on monitoring the process during the last decade [Tapia, 2014; Purtonen, 2014; Everton, 2016; Kim, 2018].

As far as DED processes are concerned, temperature monitoring is of major importance, as the melt pool temperature is a relevant parameter that affects both the metallurgical quality and geometry accuracy of the manufactured component [Yang Chua, 2017]. Melt pool size is also a key parameter that is monitored, especially the melt pool width since it defines the deposited clad geometry. In addition, the height of the layers deposited by this technique does not stay constant throughout the process, which makes the subsequent inspection of the produced part crucial. Literature shows that researchers have made efforts in monitoring the size and temperature of the melt pool. For instance, some authors suggest the integration of imaging sensors into the nozzle, aiming to control the width of the melt pool and, consequently, the quality of the deposition [Colodrón, 2011; Araújo, 2012]. Hofman et al. developed a feedback control algorithm that enables one to adjust process parameters in situ in order to control the melt pool size [Hofman, 2012] and measure the clad height in real time [Donadello, 2019; Mozaffari, 2013]. Furthermore, aiming to control the microstructure of the deposited material, Farshidianfar et al. processed thermal information in real time [Farshidianfar, 2017]. Aware of the growing interest aroused by monitoring and control, Siemens is currently looking for cooperation with additive manufacturing OEMs to develop and implement process monitoring into different additive manufacturing processes [Yang, 2017]. Nevertheless, these monitoring systems are only capable of acting on the process once they have detected a deviation from the set values. Therefore, in order to obtain higher quality parts and avoid waste, a look-ahead monitoring system should be developed, which not only acts on the process variables according to the instantaneous measurements, but that can also predict what will happen in the following steps and act accordingly.

Moreover, due to the relatively low dimensional accuracy of the additive processes and the related uncertainty, in many cases, it is necessary to measure the additively manufactured part before the subtractive stage. For instance, Campbell et al. implemented a 3D visualization algorithm based on AutoCAD software that evaluates the surface roughness, compares the geometry with the theoretical, and detects any potentially problematic areas [Campbell, 2002]. Similarly, Mandić et al. proposed an ATOS GOM 3D scanner for measuring the external geometry of the additively manufactured part [Mandić, 2016], whereas with the aim of obtaining a more accurate measurement of specific areas, Newton et al. proposed using focus variation microscopy for measuring the roughness resulting from the PBF additive process [Newton,

2018]. On the other hand, Townsend et al. employed an X-ray computed tomography system for detecting internal defects [Townsend, 2018]. Nevertheless, in order to take maximum advantage of the potentials that hybrid machines offer, the geometric evaluation of the part needs to be performed inside the machine.

Besides, sometimes the geometry of the substrate must be accurately defined before determining the DED strategies for the additive process [Liu, 2015]. In this direction, Liu et al. developed a set of algorithms and numerical methods to generate the most suitable tool paths and enable DED process automation. If the distance between the nozzle and the substrate departs from its optimal value, the powder–laser interaction is altered, resulting in process growth variations and, consequently, reduced deposition quality and geometric inaccuracies [Pinkerton, 2004; Zhu, 2012]. In addition, Siemens has also made inroads into part inspection by integrating computer-aided inspection tools in an NX environment. In this way, the software enables validation of the quality of printed parts by Coordinate Measuring Machine (CMM) inspection programming together with the visualization and analysis of the data so that both theoretical CAD and real geometries can be easily compared [Siemens, 2018a].

3. CAM Software Developments

In metal additive manufacturing, the built parts are usually finished by means of subtractive technologies. However, the combination of both processes in a unified software solution allowing a holistic process planning remains a challenge and thus a matter of research.

As far as the additive operation is concerned and regarding the LMD process, which is the most extended technology in hybrid machines, the main applications are focused on the generation of coatings and the repair of high-added-value components. However, the fact that the manufactured parts may have complex geometries and the LMD process orientation must be kept normal to the substrate requires one to interpolate the five axes of the machine simultaneously in order to obtain the desired part.

The trajectory generation for the subtractive processes is relatively well solved because it is mainly a geometric problem. However, the additive process is more sensitive and the resulting geometry depends on many more factors, such as the size of the part, the duration of the additive operation, and the complexity of the trajectory to be followed.

In order to solve this issue, the Fraunhofer Institute for Laser Technology (ILT) has developed a tool called LaCam3D that enables both programmers and end-users to generate tool paths and translate them into the CNC machine code. Furthermore, it allows simulating the process and

identification of possible collisions [ILT, 2013]. In addition, some researchers are also working on the development of Application Programming Interfaces (APIs) implemented on commercial software, aiming to offer full solutions for hybrid processes [Elser, 2018]. Siemens is also collaborating with DMG Mori [Siemens, 2015] on the development of the PLM software NX Hybrid Additive Manufacturing, having both additive and subtractive manufacturing functions in a single software. This module is considered as a specific section within the global CAM solution of Siemens NX. Despite its use is still limited to DMG Mori systems, Siemens claims to open this module for any DED system [Siemens, 2018b]. As can be seen in Figure II. 24, the in-process workpiece designed in the NX CAD module can undergo both additive and subtractive operation in any order.

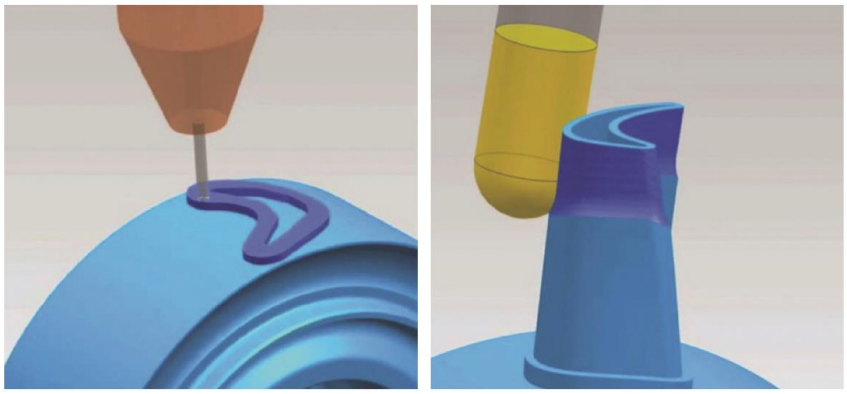

Figure II. 24 In-process workpiece and verification work for both additive and subtractive modes [Siemens, 2018c].

This is the first commercial solution that allows CAD/CAM additive operations and was presented in Milan at the EMO in 2015. The developed *NX Hybrid Additive Manufacturing* module is currently specifically configured for the *LASERTEC 65 3D* from DMG Mori and the Siemens Sinumerik 840D CNC control system.

However, the additive process is extremely sensitive to the feed rate of the machine and the thermal field of the substrate and, therefore, the tool paths calculation is not a trivial task as in the case of the machining operations. Thermal simulations may be a solution to the problem because they enable calculation of the thermal field as well as the clad height, but due to their extremely high computational cost, a combination of CAD/CAM and experimentally-based databases seems to be the best solution.

II.4. Industrial applications of the LMD process

Metal additive manufacturing has declared itself as a technology with great potential for industrial application and is reaching the industrialization stage, thus becoming an object of

interest for several sectors. During the last years, consumer products and electronics have been the leading sector incorporating AM technologies. However, the panorama has recently changed, as represented in Figure II. 25, where the industries using AM and approximate revenues in 2016 are shown.

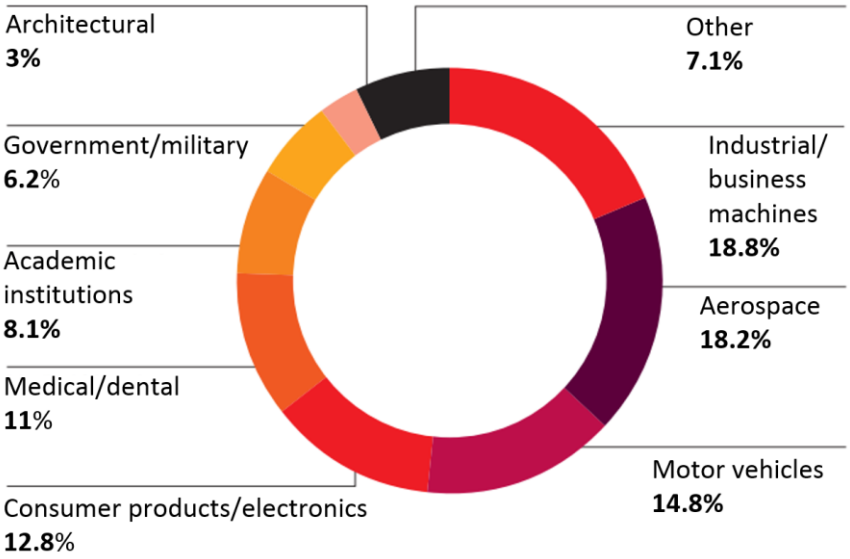

Figure II. 25 Industries using AM and approximate revenues in percentage in 2016 [Oerlikon, 2017].

As it can be observed, industrial/business machines lead the way, followed closely by aerospace and motor vehicles. Additive manufacturing is primarily suitable for producing low volumes of products, especially when complex geometries are to be attained [Guo, 2013]. In fact, it has already found application in the manufacture and repair of high-added-value functional components aimed at diverse industrial sectors, some of which are briefly introduced below.

II.4.1. Aerospace Industry

Air passenger traffic increased at a CAGR of 5.1% over the last decade [Deloitte, 2018], while it is expected to continue growing over the next 20 years at an average annual growth rate (AAGR) of 4.7% [Boeing, 2018], thus contributing to the expansion of the aircraft manufacturing industry.

Typical aerospace components are usually complex parts with a high buy-to-fly ratio made of advanced materials that are expensive and difficult to manufacture. Nowadays, the aerospace industry is focused on improving the performance and efficiency of the aircraft in order to guarantee better service-life and reduce fuel consumption. In addition, the repairing operations aimed at damaged components also have great importance, as it involves extending the lifespan of the part, with the economic savings it implies.

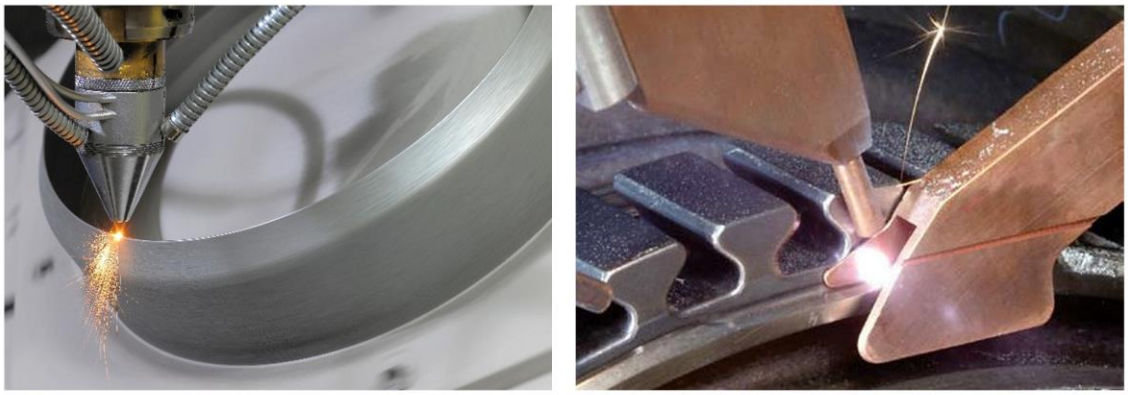

(a) (b)

Figure II. 26 (a) Manufacturing of a helicopter combustion chamber. Courtesy of TWI Ltd.; (b) Repair of a front rotor of a jet engine. Courtesy of Fraunhofer-ILT.

Metal AM technologies enable processing a wide range of low-machinability materials commonly used in the aeronautics industry, such as titanium, nickel-based alloys, special steels or ultrahigh-temperature ceramics [Guo, 2013]. Moreover, complex lightweight geometries can be also attained through this technique, which is of major interest in order to reduce fuel consumption. While Original Equipment Manufacturers (OEMs) are considering using AM to produce new parts, its application in the aerospace industry is not only restricted to the manufacture of new features or components with complex geometries and reduced weight, but is also extended to coating and repair, which is perfectly suited to Maintenance, Repair and Overhaul (MRO) applications. Despite being able to manufacture full parts, DED processes are the AM technologies specifically used in repairing aircraft engine parts [Bahnini, 2018]. In fact, LMD has been successfully adopted for both the manufacturing and repair of high-added-value aerospace components, such as blades [Gasser, 2012], blisks [Kelbassa, 2004], engine combustion chambers [Gradl, 2018] and airfoils with embedded cooling channels [Xue, 2004], among others.

II.4.2. Automotive Industry

The automotive industry is another big sector in which AM has also found its place. The advances of AM open doors for newer designs, cleaner, lighter and safer products, shorter lead times and lower costs [Giffi, 2014]. The automotive industry is currently using AM mainly for rapid prototyping and tooling purposes. Current uses of automotive AM also include the production of diverse components belonging to the fluid handling or exhaust systems. A brief scheme detailing some of the components that are presently manufactured via AM and those that will be potentially manufactured in the future is shown in Figure II. 27.

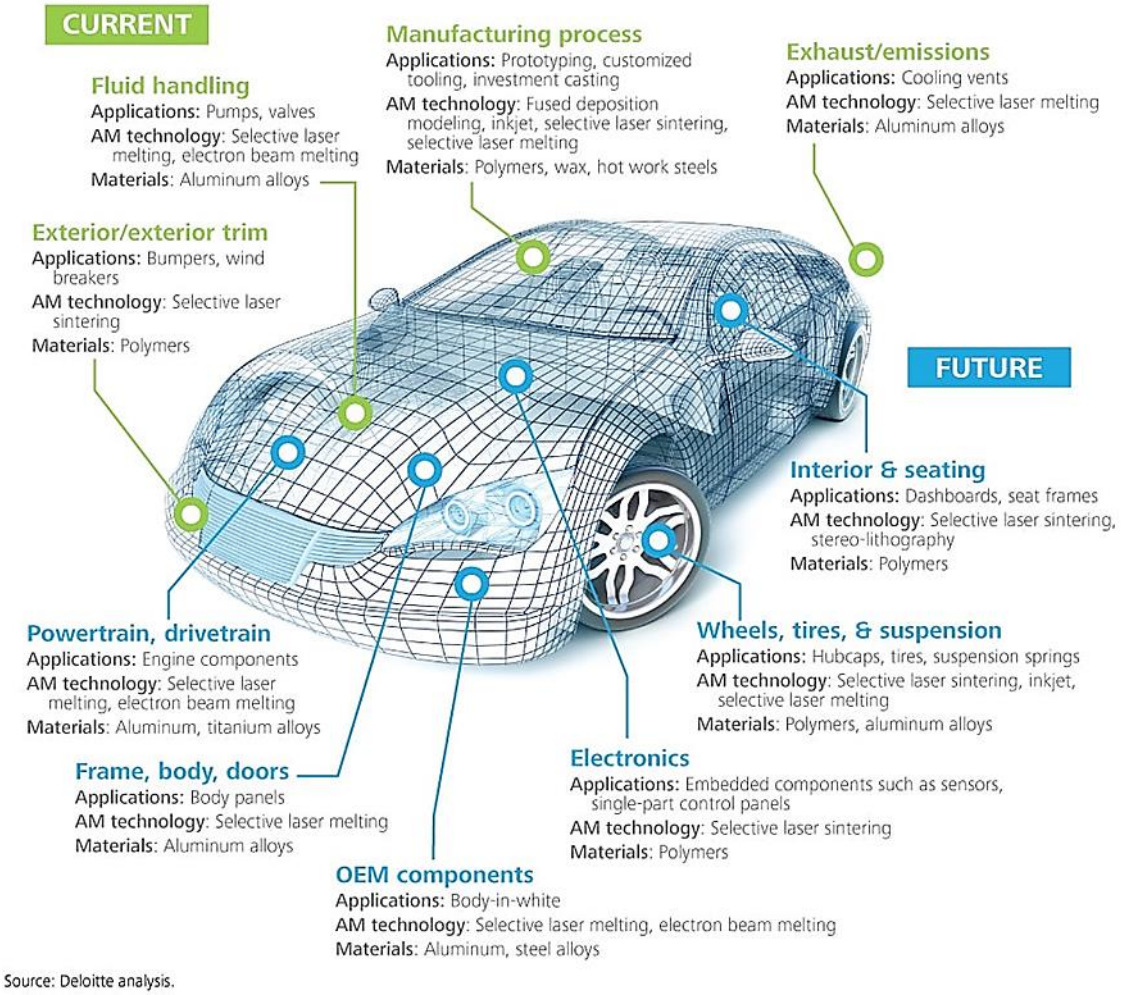

Figure II. 27 Illustrative applications of AM in an automobile [Deloitte, 2014].

Nevertheless, AM also has other potentials still to be exploited, such as the production of lighter components, leading to vehicles with lower fuel consumption and therefore meeting the intensifying environmental requirements the industry is subjected to. In addition, AM enables the integration of several parts into one only component that is manufactured at once, thus simplifying the process chain and reducing costs. As far as the aftermarket is concerned, LMD technology is once again outlined as a suitable solution for performing maintenance and repair operations on certain automobile parts, thus extending their lifetime and avoiding the expense of replacement when worn out.

II.4.3. Energy Industry

Despite being at an early stage of adoption, AM technologies are also revolutionizing the world of energy generation industries. Their key benefits are the ability to generate highly complex geometries together with the manufacturing of expensive and low-volume components, thus enabling the production of spare parts and the performance of faster repairs. The possibility to

work with corrosion-resistant superalloys allows the production of components that can operate in harsh environments. Conscious of the advantages, leading companies such as General Electric and Siemens have already opened PBF-based additive manufacturing lines, thus manufacturing gas turbine components, repairing burner tips and even producing spare parts on demand [Harvey, 2017].

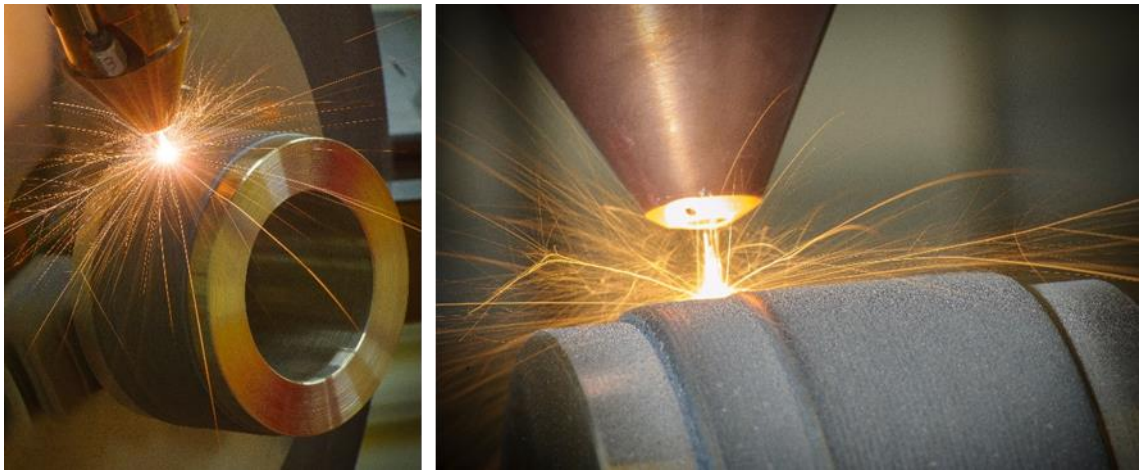

Figure II. 28 Application of wear-resistant coatings using the LMD process. Courtesy of TWI Ltd.

As far as DED technologies are concerned, LMD has been used for applying coatings, see Figure II. 28, onto steam and gas turbine shafts [Laser Systems, 2016], thus combatting wear and corrosion, as well as for repairing blades [Hauser, 2015] or surfacing oil and gas drilling components [Locke, 2010]. Considering the fact that the energy sector is an industry that operates in some remote locations and demanding environments, AM could be the key for the in-situ production of spare parts. In this way, the component could be manufactured from a certified file, thus avoiding unnecessary stock and transport and reducing lead times [Griffiths, 2015].

II.4.4. Medical Industry

Advances in AM techniques, together with the latest developments in biomaterials and biomedicine have led to the application of AM technologies to the biomedical field. Consequently, new possibilities for the manufacturing of medical devices, such as implants, prosthetics, medical training models and other medical instrumentation are beginning to emerge. Due to its great potential for customization, AM enables the personalization of implants in order to match each patient's individual needs, hence avoiding standard products and trying to offer the optimal treatment.

In spite of PBF processes being the most employed for these kinds of products, DED processes have been also successfully applied to the medical market. For instance, LMD has been employed for the manufacturing of porous structures [Ahsan, 2011], titanium hip stems with designed porosity [Bandyopadhyay, 2009] or the application of coatings on biomedical implants [Ganjali, 2018; Pou, 2018].

II.4.5. Tooling Industry

Since tooling and manufacturing are highly interdependent, the global tooling industry is essential to any industrial manufacturing sector. The term tooling includes diverse kinds of products, such as jigs and fixtures; molds used to form or dies employed for stamping or forging. No matter the application, tools are present in the design and manufacturing of diverse products, ranging from aerospace and automotive sectors to electronics, household, and equipment goods [Henriques, 2012]. All this places the tooling industry at the core of the production system.

Tooling often have complex geometries that are produced in small batches, as they are specific to a particular product. Thus, AM adapts perfectly to the needs of this industry, reducing lead times and costs, while being able to improve part functionality and performance through free design. AM's ability to produce tooling with previously unattainable geometries has been already demonstrated applied to the die & mold industry. The manufacturing of injection molds with conformal cooling channels is an example of it. Thanks to the redesign of the cooling system, a more homogeneous heat transfer within the mold can be attained, therefore improving the performance of the tooling and the subsequent quality of the produced component [Jahan, 2017]. Additively manufactured conformal cooling channels have proved beneficial not only for injection molding, but also for die casting [Brotan, 2016], hot extrusion dies [Hölker, 2015] and, to a lesser extent, hot stamping dies [He, 2016]. In addition, DED technologies, such as LMD, are useful processes in order to repair end-of-life components or perform last-minute modifications due to either manufacturing errors or changes of design.

II.5. Die & Mold Industry

The die & mold industry plays a significant role in the manufacturing world [Jhavar, 2013]. This is due to the fact that nearly all mass-produced parts are manufactured employing processes that include dies and molds, directly affecting not only the efficiency of the process but also the quality of the product [Altan, 2001]. In fact, the geometry and surface quality of the manufactured part are determined by the dies and molds, whose production is time-consuming,

technically difficult and expensive, requiring specialized materials, labor and manufacturing techniques [Chen, 2014a].

The die & mold industry, traditionally characterized by single and small batch production is currently facing new challenges as the global economy advances towards decreasing lead times and increasing diversity of products [Schuh, 2017]. In such a competitive scenario, the optimization of these tools and their use, together with extending their lifespan are of great importance. Dies and molds are normally exposed to severe working conditions, such as high loads under elevated temperatures, thermal cycling, corrosive environments and cyclic loading conditions [Morrow, 2007]. As a result, they have a limited service life and must either be replaced or undergo repair, with the consequent economic cost. Moreover, due to design changes during product development, dies and molds may also require modifications. Dies and molds are complex, costly components usually made of difficult-to-manufacture materials that require high accuracy and precision, which makes their repair highly desirable. Regardless they become obsolete or fail in service, remanufacturing in order to extend the lifespan of components that would be otherwise discarded by bringing them to their perfect working condition has recently gained attention due to its economic and environmental advantages. In fact, this practice has been already implemented by several industries, such as automotive [Ikeda, 2017], aerospace and industrial machinery [Eguren, 2018].

Among the different manufacturing processes in which dies and molds are present, stamping, hot forging, die casting and injection are the most predominant ones [Chen, 2014a]. Failure modes of dies and molds are directly related to the type of process they take part in. Major failure mechanisms are summarized below:

- Thermal cracking or heat checking: This phenomenon is due to the large thermal gradients to which the surface of dies and molds is subjected. Alternate heating and cooling put the surface in compression when heating and tension when cooling, leading to surface cracks, also known as heat checks [Srivastava, 2003]. This is a typical failure mode for hot working dies and molds.

- Wear: It is the progressive removal of material caused by cyclic loads to which dies and molds are exposed, thus deteriorating the element and losing tolerances [Chen, 2014a].

- Plastic deformation: This mode of failure is equally experienced by hot and cold working tools due to contact pressure exceeding the yield stress of the material. Hence, certain regions that are subjected to extreme pressure and temperatures, as well as long contact times, such as

corners, sharp edges and thin protuberances, tend to show this kind of failure mechanism [Choi, 2012].

- Soldering and corrosion: They are due to chemical interactions between tool and workpiece, resulting in regions of the workpiece soldering to the tool or corroding.

- Catastrophic failure: This kind of failure occurs due to thermal shock and heating of the tool, causing instability of mechanical properties and subsequent malfunction [Klobčar, 2008].

The selection of the die and mold materials is of paramount importance in order to attain good properties that lead to an acceptable lifespan at a reasonable cost. Due to their characteristics, tool steels are the most commonly used die and mold materials. In these steels, alloying elements are added to plain carbon steel in order to attain determinate properties such as higher wear resistance, toughness, strength or hardenability. In addition, these elements are different for cold or hot forming applications. According to the AISI standards, the most commonly used tool steels can be classified into the following groups: hot work (H series), cold work (D series), plastic mold (P series), special purpose (L series), shock resisting (S series) and water hardening (W series) [Roberts, 1998]. The material choice depends on the requirements of the specific process for which the tools will be used. However, tool steels are costly materials that are often not easy to process, which makes their remanufacture extremely attractive.

Manual welding is the most popular repair technique for cracked or worn out dies and molds. In addition, it can be also used for repairing chipped or worn out cutting edges, as well as for correcting machining errors or last-minute design changes [Uddeholm, 2017]. Welding is not easy though, as tool steels usually employed in dies and molds are highly alloyed, and this, together with the high temperatures reached in the welding process, can lead to local hardening and subsequent cracking. Nevertheless, the advances in manufacturing technologies make the remanufacturing of dies and molds highly feasible. Among the different welding methods available, Gas Tungsten Arc Welding (GTAW or TIG welding) and Plasma Transferred Arc Welding (PTAW) are traditional repair processes, while laser-based material deposition has recently emerged as an attractive alternative. The last one is characterized by a very accurate material deposition and low heat input, leading to a small HAZ and least changes in the substrate material, which makes it stand out among the others. In addition, it is easy to automate and control, while GTAW and PTAW are performed manually, thus requiring highly skilled operators [Thompson, 1999].

Laser-based metal deposition not only opens doors to high-quality repairs but also to manufacture complex geometries that are not workable by conventional processes and to the development of high-performance coatings. Much research has been devoted to the modification and repair of dies and molds taking part in different manufacturing processes. However, academia has focused more on die casting and injection tools, rather than stamping or hot forging dies [Chen, 2014]. Besides, laser-based material deposition applied to hot work tool steels is currently under research. For instance, surface coatings that have good resistance to corrosion, soldering, wear or thermal fatigue have been already developed through this technique. Fazarinc et al. studied the suitability of FGM in applications subjected to thermal fatigue by laser deposition of two materials with different silicon content on AISI H13 tool steel. They found that a higher content of silicon of the deposited material led to better thermal fatigue resistance, thus contributing to extend the lifespan of die casting tools [Fazarinc, 2011]. Aiming at the forging industry, Ley et al. explored the result of laser coating of a tool steel die head with a Cr-Mo-Ta-W-Zr complex concentrated alloy. Results showed that, for a laser fluence of 23.3 $J \cdot mm^{-2}$, a sound bonding between coating and substrate was achieved, also attaining a higher hardness than that of the substrate [Ley, 2018]. Thermal fatigue resistance of AISI H13 tool steel was also enhanced by laser surface remelting and alloying with cobalt-based and iron-based powders [Cong, 2014]. Results indicate that, in this way, thermal cracks on the surface of the tool steel can be repaired.

The manufacturing of near-net-shape components [Zadi-Maad, 2018] or the analysis of the influence of laser process parameters on the resulting metallurgical structures and properties of the deposited parts [Bohlen, 2018] are also topics of research. However, further R&D efforts focused on validating, standardizing and demonstrating this technology are necessary in order to overcome the challenges still ahead, thus increasing the reliability of this new manufacturing approach and opening doors for new designs and applications.

II.6. Hot Stamping process

Growing demand in the automotive industry for high strength and lightweight components has driven to the promotion and development of hot stamping (also known as press hardening) processes [Steinbeiss, 2007]. This circumstance is due to stricter CO_2 emission regulations forcing the industry to seek ways to build lightweight, more fuel-efficient cars. At the same time, car safety improvement is demanded by both customers and legislation [Belingardi, 2015]. Hot stamping enables the improvement of car safety without an increase in car weight by forming

high strength steel sheets. As a result, demand for hot stamped body parts has been growing continuously at a fast pace (see Figure II. 29).

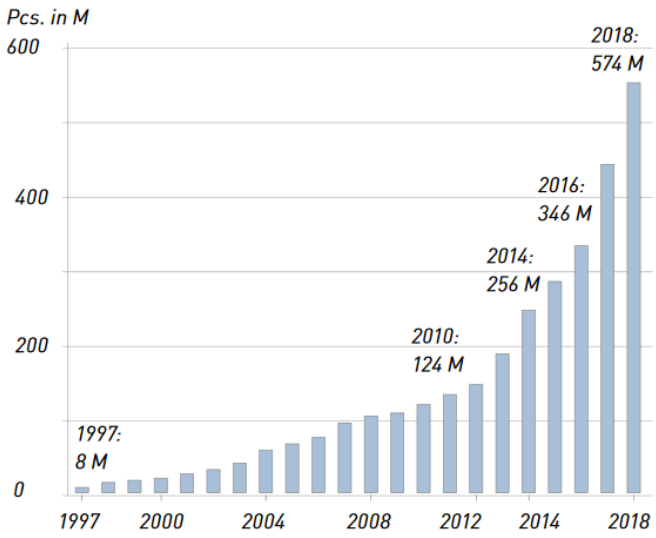

Figure II. 29 The rise in the demand for hot-stamped body parts metal [Schuler Group, 2017].

According to Arcelor Mittal, hot-stamped steel currently accounts for more than 20 percent of most vehicles total body-in-white weight [ArcelorMittal, 2018a]. This amount is increased to 40 percent by some car manufacturers, such as Volvo (see Figure II. 30).

Figure II. 30 Volvo XC60 body structure [Volvo, 2017].

Through hot stamping, a boron steel blank is heated above the austenitic temperature, between 900 °C and 950 °C, inside a furnace and then transferred to an internally cooled tool set, where it is simultaneously formed and quenched (see Figure II. 31). Due to the high formability of the blank at high temperatures, this process enables the attainment of complex geometries. The total cycle time including transfer, stamping, and quenching takes 15–25 s [Naganathan, 2012]. The transformation of austenite into martensite occurs thanks to the rapid cooling of the blank, at a temperature range of 420–280 °C, along which the tools must be actively cooled at rates above 27 $^{\circ}C \cdot s^{-1}$ [Eriksson, 2002]. As a result, a fully martensitic microstructure is achieved,

providing the final part with an ultra-high strength of up to 2000 MPa (see Figure II. 32) [Horn, 2019].

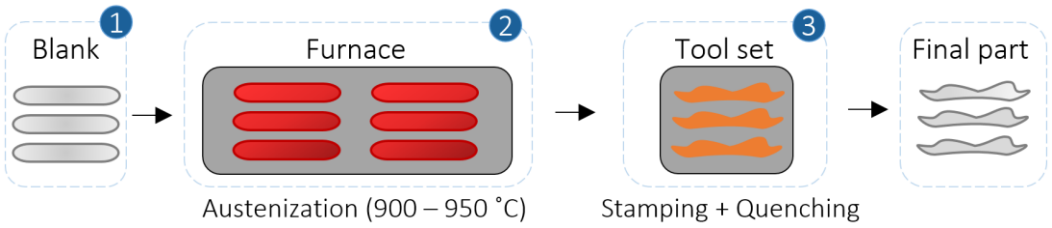

Figure II. 31 Basic hot stamping process chain.

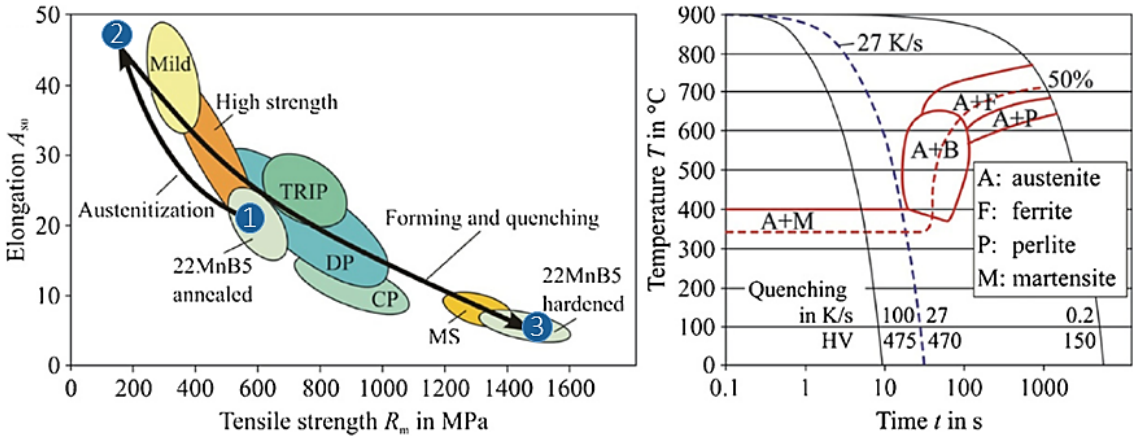

Figure II. 32 Mechanical properties of 22MnB5 and CCT diagram [García Aranda, 2002].

The formation of a martensitic structure after quenching, which depends on the cooling rate of the part, is a key factor in attaining hot formed parts with superior mechanical properties. Therefore, rapid cooling is required in order to harden the formed parts in the tool quenching [Mori, 2017]. The temperature of the hot stamping tool must be kept below 200 °C in order to ensure the cooling of the blank, achieve high strength and prolong the lifespan of the tools [Hoffmann, 2007]. Besides, the forming performance is highly influenced by the temperature distribution in the blank, which must be uniform on the surface of the tool (maximum deviation ±5 ˚C) [Naganathan, 2012]. Consequently, an inhomogeneous temperature distribution may lead to deformations in the hot-stamped part [Mori, 2017].

Because of the process characteristics, hot stamping tools are under severe working conditions in terms of both mechanical and thermal loads. The elevated temperature leads to higher friction between blank and tooling, thus increasing tool wear and reducing their service life [Ganapathy, 2017]. In order to resist wear, mechanical and thermal demands, hot stamping tools are usually made of hot work tool steels. The tool steels should exhibit high surface hardness and tensile strength, good toughness, tempering and fatigue resistance. As the final stamped product is affected by the cooling rate, the tooling material should also have high thermal

conductivity [Chen, 2014b]. Besides, high thermal conductivity not only helps to reduce the internal thermal gradients of the tool but also enhances the hot stamping process in terms of both quality and productivity, as it ensures quick heat transfer between tooling and stamped part. In this way, the cooling of the blank is much faster, reducing the risk of bainitic or pearlitic transformation and decreasing the cycle time. In this respect, the in-built cooling circuit of the hot stamping tools is also a key factor that can raise cooling performance [Escher, 2015].

Hot stamping is a process in which tooling is a key element. This is because stamping tools are high-added-value components with increased manufacturing and maintenance costs and, besides, they strongly influence the characteristics of the final product. In hot stamping, attainable productivity is closely related to the time during which the dies are held at the bottom dead center position of the press stroke until the blank undergoes the martensitic transformation. This stage is the longest one within the hot stamping process and consumes more than 30% of the total cycle time [Muvunzi, 2018]. In this regard, both the material thermal properties and the tool cooling system play a capital role. Any improvement in those elements aiming to increase heat transfer between the tools and the stamped part would lead to higher production rates.

In this direction and regarding the optimization of hot stamping tools, different research fields have been explored, such as the use of high conductivity steels [Ghiotti, 2016] or the integration of conformal channels within the stamping tools and their design optimization [He, 2016].

II.6.1. Factors influencing the IHTC in hot stamping

Research efforts have been focused on improving the performance of hot stamping through the enhancement of the quenching process of the blank. To that end, the factors influencing the Interfacial Heat Transfer Coefficient (IHTC) between blank and tool have been studied. The IHTC is a thermo-physical parameter indicating heat transferability between the interfaces of the hot blank and the cold die. This parameter has a strong influence on the temperature distribution in the blank, therefore affecting the final characteristics of the hot-stamped part. Some of the factors influencing the IHTC are the topography at the interface, the contact pressure, the temperature of blank and tool and the materials thermo-physical properties [Chang, 2016]. Here are some of the factors that most influence the IHTC:

- Topography at the interface: Actually, the contact between the tool and blank only occurs in some discrete points of their surfaces, with the heat being transmitted by conduction through them as shown in Figure II. 33. Other factors such as contact pressure and surface roughness of

tool and blank can alter the topography of the surfaces in contact and, consequently, the value of the IHTC, which varies over time.

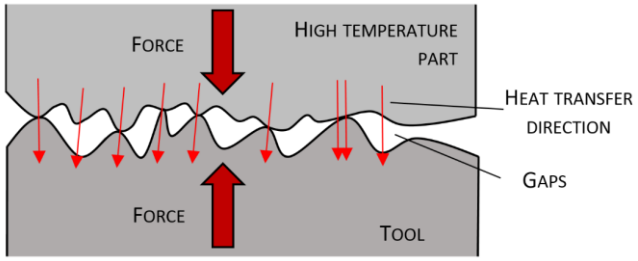

Figure II. 33 Diagram of the topography in the die and sheet metal contact.

- Contact pressure: This factor has an important influence on the IHTC. A higher contact pressure causes the deformation of the topography of the surfaces in contact, so that the actual contact area is enlarged, resulting in an increase in the heat transfer coefficient and consequent decrease in the cooling time of the stamped part. This factor has aroused great interest due to the possibility of adjusting its value by the force applied by the stamping press during the process. In addition, it is one of the few variables that can be monitored and controlled in an industrial environment [Muro, 2018a].

- Material thermo-physical properties: The temperature fields of the tools and blank are related to the thermo-physical properties of the materials used, which vary with temperature. Therefore, the material employed to manufacture the tool has a direct impact on the value of the IHTC coefficient, so that the higher the thermal diffusivity, the higher the value of the IHTC.

- Anti-oxidation coating of stamping steel: When stamping a hot boron steel blank and quenching it, the surface of the blank is oxidized, increasing the heat resistance of the contact and thus reducing the heat transfer coefficient. In addition, greater friction between the blank and the tool is generated, thus affecting the lifespan of the latter [Hu, 2013]. That is why the blanks are coated with a layer of Al-Si or oil to prevent the phenomenon of oxidation. In this sense, Chang et al. show that this coating reduces the IHTC value significantly, being the effect greater for thicker coatings [Chang, 2016].

II.6.2. Use of high thermal conductivity steels

Once good contact between the blank and the tool is guaranteed, and the water flow through the cooling system is turbulent enough, the thermo-physical properties of the tool material determine the heat transfer between the blank and the tool [Valls, 2010]. The temperature fields of both the tools and the blank are related to the thermo-physical properties of the employed

materials, which change with temperature. In fact, thermal conductivity and specific heat capacity are found to be the primary thermo-physical properties influencing the IHTC [Chang, 2016], also affecting the cooling rate and temperature distribution on blank and tool. Thermal conductivity (k) and specific heat capacity (c_p) are related by thermal diffusivity (α), which is used to express the capacity of temperature tending to balance and is defined in equation (Eq. II. 6), where ρ represents the material density.

$$\alpha = \frac{k}{\rho \cdot c_p} \qquad \textbf{(Eq. II. 6)}$$

The materials the stamping tools are manufactured with have a direct impact on the IHTC so that higher thermal diffusivity leads to a higher IHTC value. When selecting tool materials, it is necessary that there is a trade-off between good wear resistance over a wide temperature range and good thermal conductivity [Hein, 2008]. In this regard, most hot stamping tools are made of hot work steels with hardness over 44 HRC [Paar, 2007]. More concretely, AISI H13 or AISI H11 have been generally used for manufacturing hot stamping tools. Their excellent mechanical properties at high temperatures make them stand out among other materials; however, they have moderate thermal conductivity values that remain between 25-30 $W \cdot m^{-1} \cdot K^{-1}$.

Several authors have studied the influence of tool material on the IHTC. Chang et al. investigated the use of AISI 1045 steel and AISI H13 tool steel for stamping 22MnB5 blanks at different contact pressures, as shown in Figure II. 34. They found that the higher thermal conductivity and specific heat capacity of AISI 1045 contributed to higher IHTC values than AISI H13 [Chang, 2016].

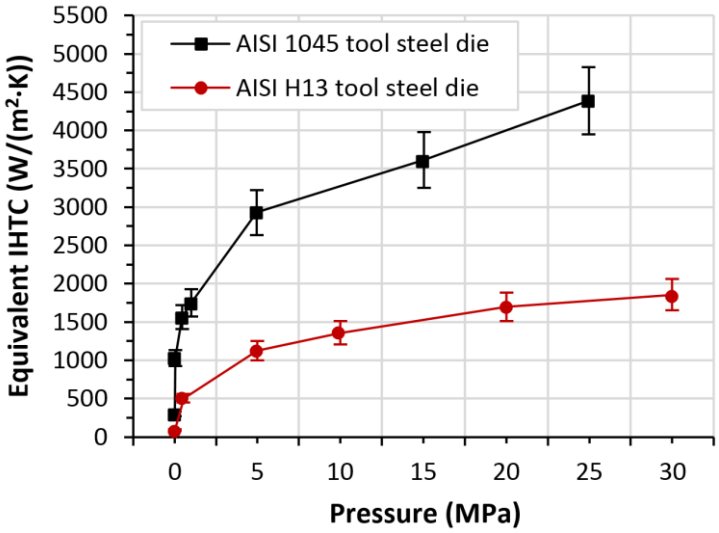

Figure II. 34 Equivalent IHTC between 22MnB5 blank and AISI H13 and AISI 1045 tested versus contact pressure, adapted from [Chang, 2016].

The same conclusion was reached by Luan et al. [Luan, 2016] and Liu et al. [Liu, 2017b], who compared different tool materials under the same contact pressure conditions and concluded that, although following a similar trend, materials with higher thermal conductivity lead to higher peak IHTC values. In this way, higher IHTC values are attained for significantly lower contact pressure values, thus reducing the requirements of the stamping press and extending the tool life.

In order to take advantage of this issue, tool steel grades with high surface hardness and improved thermal conductivity have been developed, reaching values of up to 60 $W \cdot m^{-1} \cdot K^{-1}$, which is more than twice the thermal conductivity of conventional hot work tool steels. In this way, a cycle-time reduction of 35-45% is achieved [Valls, 2017; Escher, 2015]. The benefit is twofold: on the one hand, a reduction in the time required for forming and quenching the blank is obtained, while on the other hand, the temperature distribution on the stamping tool surface is kept significantly lower and more homogeneous due to higher thermal diffusivity [Valls, 2018]. This is due to the fact that, as shown in equation (Eq. II. 6), thermal diffusivity is directly proportional to thermal conductivity. As a result, the quality of the stamped parts in terms of both hardness and properties homogeneity is also improved. Ghiotti et al. analyzed the tribological behavior of two high thermal conductivity steel grades in terms of friction and wear damage, by applying thermo-mechanical cyclic loads in temperatures ranging from 600 to 800 ˚C. On the one hand, they found that higher temperatures lead to lower friction coefficients; on the other hand, both steel grades were subjected to a combination of adhesion and abrasion phenomena. When compared with AISI H11, both high thermal conductivity steel grades tested showed a lower friction coefficient and subsequent lower resistance to sliding. However, they presented larger abrasion, especially at high temperatures. Consequently, the impact of wear phenomenon on tool life may be significantly greater [Ghiotti, 2016].

Nevertheless, components made of tool steels are quite expensive due to both material and manufacturing costs. In addition, in the case of hot stamping, higher conductivities are desirable. Therefore, hot stamping is an application where it is advantageous to manufacture tools using inexpensive, easy-to-fabricate steels, with their surface properties enhanced by coating with highly alloyed steels. In this regard, laser-based additive processes have arisen as a key element for manufacturing high-performance tools at lower costs [Wang, 2006]. Some research has been conducted in this direction in the field of high-pressure die-casting. Aiming to develop higher thermal conductivity tools, Imran et al. presented an approach to replace a conventional steel die by a bimetallic die made of a copper alloy and coated with a protective AISI H13 layer using LMD technology. In this way, the interaction between copper and aluminum, which have a

strong chemical affinity, is avoided. As a result, they obtained a metallurgically sound and fully dense coating and were able to manufacture bimetallic dies with superior thermal performance, thus reducing the solidification time of aluminum by more than 30% of the time required with conventional dies [Imran, 2011]. Nevertheless, copper is a difficult material to use in laser-based additive manufacturing due to its high reflectivity index. Besides, its mechanical properties limit the range of applications of copper. For instance, with regard to hot stamping, tools need to withstand high pressures, ranging between 10-15 MPa [Muro, 2018a; Muro, 2018b], values that copper would be unable to withstand. In this direction, the German company Hermle has developed a machine especially aimed at toolmaking that, through thermal spray, enables the embedment of copper elements as heat conductors (see Figure II. 35) so that hot spots are reduced [Hermle, 2019].

Figure II. 35 Copper elements embedded in steel components [Hermle, 2019].

Hu et al. deposited CPM 10V and CPM 15V high-vanadium steel powders on AISI 1045 medium-carbon steel aimed at manufacturing cutting and stamping dies. Sound clads free of porosity and cracks were attained, with an as-clad hardness of 650 HV, which is a similar value to that of heat-treated AISI D2. Nevertheless, a final hardness of 850 HV was reached after the samples were double tempered and dipped in liquid nitrogen, which might help to prolong the lifespan of cutting dies in comparison to AISI D2. In fact, the authors claim that results could be used for cost-effective die manufacturing by replacing the expensive tool steel die blocks by ordinary structural steel [Hu, 1998]. However, no further work was carried out in that direction. In the same direction, Ocelík et al. coated AISI 1045 steel with Cr-Mo-W-V alloyed steel that shows enhanced properties, such as high wear resistance and compressive strength, good toughness, dimensional stability and tempering resistance. They attained homogeneous, defect-free coatings with good bonding to the substrate material and properties in terms of hardness, toughness and wear resistance [Ocelík, 2007]. In order to improve the wear resistance of tool steels, Navas et al. studied the application of laser cladded protective coatings to repair AISI A2 cold work tool steel, commonly used in die stamping, with AISI M2 high-speed steel and

AISI 431 stainless steel. They found that wear resistance under unlubricated conditions improved significantly with AISI M2, which shows a better performance than AISI 431, especially at high loads. This is attributed to the finer microstructure of AISI M2 and to the presence of carbides, which protect the material matrix from being worn [Navas, 2005]. With regard to repairing hot work tool steels, Kattire et al. deposited CPM 9V high-vanadium tool steel on AISI H13 aiming at die restoration applications. The generated clads showed a hardness of about four times greater than the substrate hardness and compressive residual stresses, which would prevent cracks from propagating, thus enhancing the service life of dies [Kattire, 2015]. However, none of these works is focused on the manufacturing of cost-effective tools aimed at hot stamping.

II.6.3. Integration of conformal cooling channels

In hot stamping, tools include cooling channels to treat the formed sheet and achieve higher cooling rates. If the cooling system is not adequately designed, the temperature of the tool can be increased during the production process, the quenching of the blank may not be successful and therefore, the final product would not meet requirements. Moreover, the temperature distribution within the stamping tools could be non-homogeneous, resulting in hot areas where the martensitic transformation could not be achieved. The efficiency of the cooling channels determines the characteristics and cooling time of the final part. Some authors [Hölker, 2017] relate low cooling rates and thermally induced surface defects on the stamped part to an inadequate cooling system. These consequences could be avoided by the optimization and new arrangement of the cooling ducts.

Optimizing the cooling system of hot stamping tools is, therefore, an issue that arouses interest within both industry and academia. On the one hand, any improvement in this direction involves a shortening of the process cycle, not only reducing the cooling time of the blank but also recovering the initial tool temperature in minimum time. In addition, the lower temperature of the surface of the tools leads to a reduction of wear, which is the main failure mechanism of hot stamping tools [Taha, 2014]. On the other hand, it also has an impact on the quality of the process and, consequently, on the final properties of the product.

The optimum cooling channels design of dies and molds result in homogeneous temperature distribution and uniform cooling. Optimal cooling channels design should adapt the shape of the cooling system to the geometry of the tool surface. In addition, the lower the distance between the cooling channel and tool surface, the better the cooling efficiency. Nevertheless, that

distance needs to be big enough for the tool to withstand the process working conditions and avoid failure. Thus, a tradeoff is required for reaching an optimal solution with high cooling efficiency. However, the cooling ducts are conventionally manufactured by drilling, attaining straight channels unable to follow the geometry of the tool and often leading to a not uniform heat transfer [Venkatesh, 2017]. This may lead to longer cycle times and unequal cooling [Shinde, 2017]. Thus, the employment of traditional techniques for the manufacture of the inner cooling conducts of the stamping tools leads to restrictions on the final geometry of the parts.

Researchers have carried out some work with regard to the design and optimization of the cooling system. For instance, Steinbeiss et al. studied the influence of the diameter of the ducts on the effectiveness of the cooling system in hot stamping tools by developing a methodology of optimization [Steinbeiss, 2007]. However, no experimental validation is presented. Hu et al. performed an analysis of several cooling system designs such as straight, longitudinal, transversal, parallel and serpentine conformal cooling channels and found that longitudinal ones present the best cooling performance [Hu, 2016]. He et al. developed a technique aimed at optimizing the layout of longitudinal conformal cooling channels within hot stamping tools. The radius of the channels, their distance to the tool work surface and the ratio of each channel center were considered as the design variables. They found that the maximum work surface's temperature was reduced by using conformal cooling. Moreover, temperature uniformity was also improved and stability was reached faster than in traditional tools, obtained results are shown in Figure II. 36 [He, 2016].

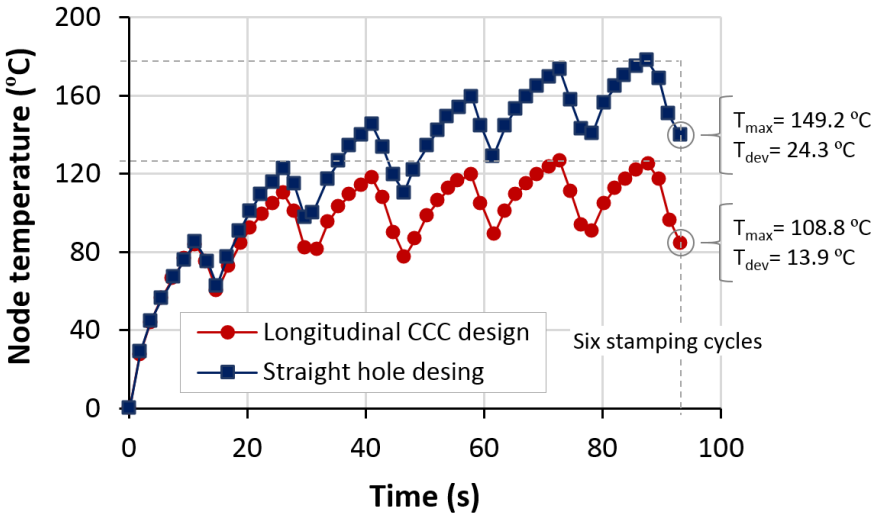

Figure II. 36 Cooling performance with the straight and conformal cooling channel design, adapted from [He, 2016].

Nevertheless, the authors mentioned above present no manufacturability evaluation of the proposed cooling channels design, neither their mechanical performance throughout the stamping cycles; the process improvement is only approached from a thermal simulation point of view.

From the literature review, it is noted that additive manufacturing technologies offer a real solution when manufacturing adaptive or conformal cooling channels with complex geometries. In this way, the heat transfer within the tooling is enhanced and the cycle time required for cooling down the part is minimized, therefore advancing towards rapid cooling [Schieck, 2011]. There are two kinds of techniques for manufacturing conformal cooling ducts in hot stamping tools: the layer-laminated method and the powder metallurgy-based additive manufacturing, belonging powder bed and powder nozzle technologies to the latter [Hölker, 2015].

On the one hand, by layer-laminated manufacturing, single layers are cut, stacked and then joined together in order to generate a final part. This technique is used for the production of plain and geometrically simple parts. For instance, Hölker et al. [Hölker, 2011] studied the design of straight holes in layered extrusion dies by joining lamellas with holes and thus creating cooling channels.

On the other hand, components are built up layer by layer by locally melting a metal powder bed or stream, implying freeform manufacturing with nearly no geometric restrictions. The application of conformal cooling in the field of injection molds was studied by Ahn et al., who manufactured molds with conformal cooling ducts by combining direct metal rapid tooling and machining. As a result, they found that the cooling time and required energy were highly reduced when compared to traditional molds [Ahn, 2010]. Huskic et al. investigated the integration of conformal cooling channels into forging dies and hot stamping tools by using SLM. In the case of forging, they used DIN 1.2709 hot work tool steel and attained a yield strength of 1800 MPa and 54 HRC hardness in the tempered condition. Results showed that the hybrid die could withstand the mechanical loads originated during forging, showing no macroscopic cracks or deformations, while the conventional die showed adhesive wear [Huskic, 2013]. Müller et al. built up inserts with conformal cooling ducts in hot stamping tools by additive manufacturing and showed that they cooled six times faster than the conventionally drilled ducts [Müller, 2013]. They also employed PBF additive technology for building adaptive cooling channels. Therefore, the size of the tools is limited by the building chamber of the used machine.

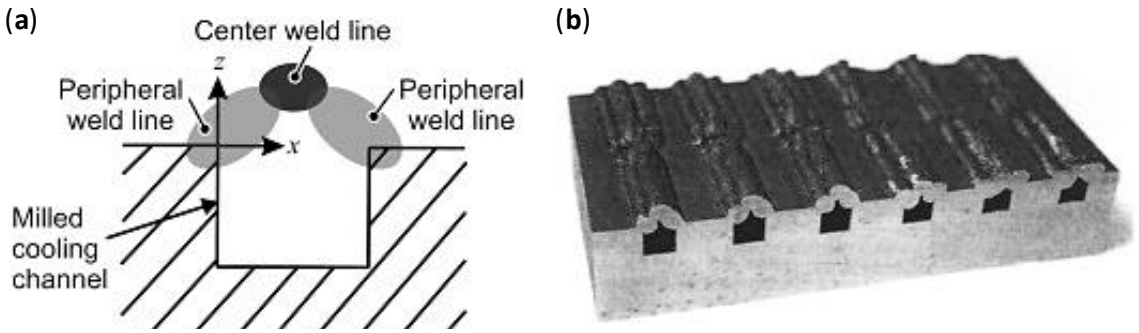

Figure II. 37 (a) Schematic of the manufacturing strategy for closing a cooling channel by powder laser deposition; (b) A die body with cooling channels (width, 6 mm) [Vollmer, 2014].

With regard to powder nozzle-based additive technologies, Vollmer et al. studied the integration and manufacturing of additively built up cooling channels for the fabrication of hot stamping tools. For this purpose, several grooves were machined and afterward closed by LMD and finished by milling [Vollmer, 2014]. However, no application of the proposed methodology to complex geometries is presented and experimental tests are only performed with AISI 316L stainless steel as filler material, which is less prone to cracking than the usually employed tool steels (AISI D2, AISI H13, etc.).

II.7. Main highlights after the analysis of the State of the Art

After performing an analysis of the state of the art of LMD technology and its suitability for the hot stamping industry, the following conclusions are drawn:

- The application of DED processes, such as LMD, is focused on generating new geometries, as well as repairing, joining or applying coatings to pre-existing components.
- With regard to hybrid machines, the full integration of additive and subtractive processes within a single platform is a complex task that must still overcome many difficulties. Therefore, it is mandatory to understand the complexity of combining both processes from a technical and environmental point of view.
- The application of AM in the manufacture and repair of high-added-value functional components has attracted considerable interest from diverse industrial sectors, including aerospace, energy and tooling industries, among others. Hence, it remains a motivation for researchers to develop AM technologies to improve the productivity of industrial processes, to facilitate new innovative tooling processes, to add value to other

components by repairing features, adding new features to an existing component and/or coating a component and increase the lifetime of the component/tool.

- Dies and molds are high-added-value parts with a limited service life, whose remanufacture or repair is highly desirable, both from an economic and environmental point of view. In this regard, laser-based metal deposition not only opens doors to high-quality repairs but also to the manufacture of complex geometries that are not feasible by conventional processes and to the development of high-performance coatings. However, further R&D efforts focused on validating, standardizing and demonstrating this technology are necessary.
- As far as the enhancement of the hot stamping process is concerned, increasing tool life and improving the heat transfer between the tool and stamped part remain pressing topics. In this respect, both the material thermal properties and the tool cooling system play a capital role and requires further study.
- Although some research has been focused on the use of high thermal conductivity steel in dies and molds, few works consider the manufacturing of bimetallic tools via LMD. In addition, none of them is aimed at hot stamping.
- With regard to the enhancement of the cooling system within tooling, this issue has been investigated by a large number of authors, dealing with topics ranging from the optimization of the size and layout of cooling channels to its manufacturability by means of additive technologies. In this regard, the application of conformal cooling to hot stamping is a relevant topic to researchers, but most works are focused on mold injection. Despite there being several studies aimed at hot stamping, this topic is mainly analyzed from a thermal simulation point of view. Therefore, no manufacturability evaluation of the resulting cooling system is performed in these works. In addition, although tools are expected to work for a high number of cycles, few studies consider the performance of the tools throughout the stamping cycles.

Chapter III. Laser Metal Deposition of AISI H13 tool steel

Chapter III. Laser Metal Deposition of AISI H13 tool steel

In this third chapter, the experimental characterization of the Laser Metal Deposition of AISI H13 tool steel in hybrid machines is dealt with. On the one hand, the equipment and methods employed for the deposition and characterization of AISI H13 are described. To that end, a metallographic analysis is performed, where the quality of the deposition is studied including both microstructural and hardness analyses. On the other hand, special attention is given to the issues arisen from the use of cutting fluids in hybrid machines and affecting the LMD process. Therefore, the influence of different oil concentrations in laser-deposited AISI H13 is analyzed in terms of dilution, and clad quality. In addition, in order to consider the possible variations that may occur when this methodology is applied to different materials, the same tests are performed on Inconel® 718.

III.1. Introduction

The modern industry is heading to the “factory in the machine” concept, where hybrid machines that combine additive and machining operations are gaining relevance thanks to the fact that they enable them to build ready to use products in a single machine [Merklein, 2016; Du, 2016]. As it has been mentioned in the previous chapter, the integration of laser-based additive and machining processes results in a combined process that strengthens both processes' advantages [Flynn, 2016] and process time reduction [Yamazaki, 2016]. Evidence of this are the hybrid machine solutions developed by the most advanced machine tool companies, such as DMG Mori, Mazak, Okuma and many other smaller but leading companies such as Ibarmia. The preparation of the substrate prior to the material deposition process is very relevant to avoid internal defects such as pores, the entrapment of impurities and ensure the proper bonding between the filler and substrate materials. Nevertheless, in hybrid machines where both machining and LMD operations are carried out without loosening the part, the elimination of the intermediate cleaning stage reduces the total manufacturing time and subsequent production costs.

AISI H13 (DIN 1.2344) is a Cr-Mo-V alloyed tool steel with a high level of resistance to thermal shock and fatigue, and good temperature strength, qualities which make this material particularly valuable for tooling [Patra Karmakar, 2019]. AISI H13 hot work tool steel is broadly applied in die & mold applications, such as casting, extrusion dies, hot forming tooling and plastic injection molds [Lu, 2019]. In this regard, dies and molds are high-added-value components,

whose manufacturing and repair via AM technologies and subsequent machining could be highly valuable.

This chapter deals with the experimental LMD characterization of the AISI H13 tool steel so that defect-free layers and good metallurgical bonding between them and the substrate are attained. To that end, the equipment used for the performance of the experimental tests is first described and the LMD process parameter window for the deposition of AISI H13 is defined, including microstructural and hardness analyses. Then, the influence of the use of cutting fluids in the LMD process is investigated. To that end, experimental tests have been performed over cutting fluid impregnated specimens. Images of the cross-sections have been analyzed and the porosity and pore size have been estimated. Then, the influence of the different oil concentrations and cleaning methods employed is evaluated in terms of porosity and clad quality. In order to determine the influence of the material on this analysis, LMD of AISI H13 and Inconel® 718 were performed.

III.2. Characterization of AISI H13 tool steel

III.2.1. Laser Metal Deposition tests of AISI H13 tool steel

The LMD experiments described in this chapter were performed on a 5-axis (three linear and two rotatory) laser-processing machine, with a work-piece size capacity of 700 x 360 x 380 mm^3. A high-power Yb:YAG fiber laser source, Rofin FL010, with a maximum power output of 1 kW and emitting wavelength of 1070 nm was employed. The laser beam was guided through an optical multi-mode fiber from the laser source to the processing machine, generating a circular laser spot of 2 mm on the surface of the workpiece, situated at a 200 mm focal distance. The powder filler material was fed by means of a Sulzer Metco Twin 10-C powder feeder and an in-house designed coaxial nozzle, EHU-Coax 2015 [Arrizubieta, 2014], using argon as both the drag and shielding gasses.

In the experimental tests, AISI H13 (DIN 1.2344) powder was used as filler material, which was supplied by Flame Spray Technologies and obtained via gas atomization, consisting of spherical particles with diameters of 53-150 µm. On the other hand, either AISI H13 or CR7V-L hot work tool steel by Kind & Co. Edelstahlwerk [CR7V-L, 2019] was used as the substrate material. CR7V-L is a special high Cr-alloyed steel commonly used in hot work applications, such as hot forming tools of structural automobile parts. Furthermore, it is characterized by excellent high-temperature strength and wear resistance, as well as good thermal fatigue resistance. CR7V-L tool steel, which does not conform to any standard, is similar to AISI H13 hot work tool

steel, but with lower silicon and higher chromium contents. The chemical composition of the employed materials is included in Table III. 1.

Table III. 1 Chemical composition (wt. %) of AISI H13 [FST, 2019] and CR7V-L [CR7V-L, 2019].

Material	C	Si	Mn	Cr	Mo	V	Fe
AISI H13	0.41	0.80	0.25	5.12	1.33	1.13	Balance
CR7V-L	0.42	0.50	0.40	6.50	1.30	0.80	Balance

Different experimental tests were performed varying the process parameters, which include power values of 400, 600 and 800 W, feed rates of 450, 600 and 750 mm·min^{-1} and powder flow rates of 1.5, 3.3 and 5 g·min^{-1}. The analysis of the results showed that the optimal parameters for depositing AISI H13 are those detailed in Table III. 2 [Cortina, 2018b], which resulted in defect-free single clads 2 mm wide and 0.4 mm high, matching with an optimum aspect ratio (ratio of height and width) of 1/5 [Steen, 2005; Candel, 2013].

Table III. 2 Process parameters employed for the deposition of AISI H13.

Process parameters	Value
Continuous-wave laser power (W)	600
Feed rate (mm·min^{-1})	450
Track offset (mm)	1
Overlap (%)	50
Powder flow rate (g·min^{-1})	3.3
Shielding gas flow rate (L·min^{-1})	14

A zigzag pattern was used to deposit the filler material, alternating longitudinal and transversal directions for the deposition of successive layers. This strategy aims to reduce the anisotropic behavior inherent to DED processes.

III.2.2. Metallographic analysis

In order to perform a metallographic analysis of the deposited AISI H13, the cross-sections of the samples were cut, polished and etched. Murakami and 4% Nital solutions were used to reveal the macro- and microstructure of both the substrate and the deposited material and then enable the identification of internal defects within the deposited material, such as pores and cracks. Micrographs were acquired with a Nikon Optiphot 100 optical microscope.

In Figure III. 1, the microstructure of the deposited AISI H13 and its bonding with the substrate can be observed. Two types of microstructures were produced during the solidification process: equiaxed grains (Figure III. 1c) within the clad zone and columnar grains (Figure III. 1d) at the boundary, that is, within the inter-diffusion zone. In the clad zone, the microstructure is dendritic, consisting of martensite, retained austenite and carbides in the inter-dendritic region [Bonek, 2006; Telasang, 2014]. In the inter-diffusion zone, columnar dendritic microstructure is found, in which the columnar grains are oriented in the direction of the maximum temperature gradient [Bonek, 2006].

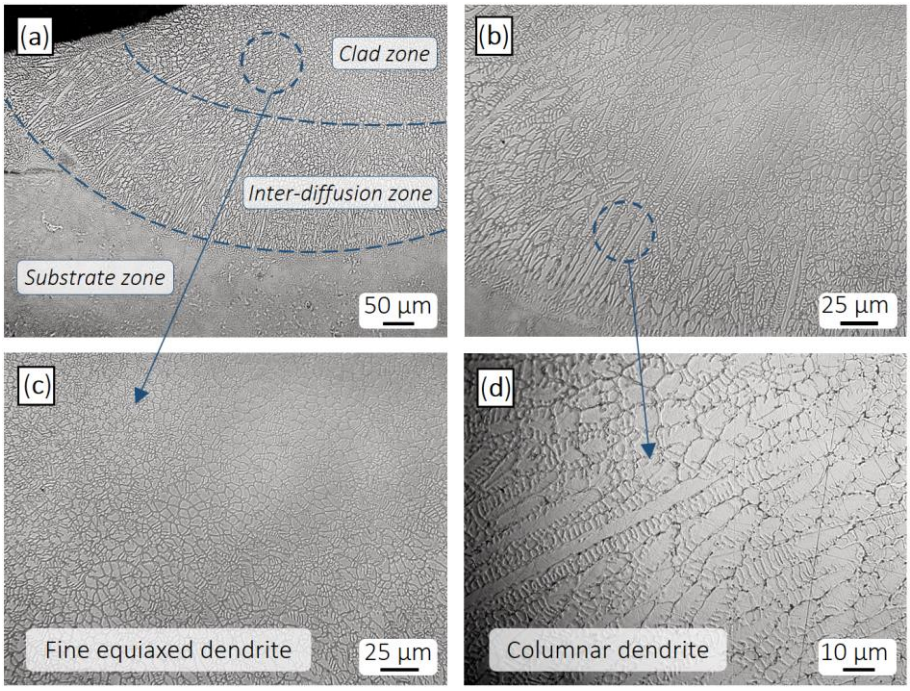

Figure III. 1 Microstructure of deposited AISI H13: (a) Bonding between deposited and substrate material; Higher magnification (b) of the bonding; (c) showing fine equiaxed dendrite; (d) showing columnar dendrite.

The difference in the morphologies is because cooling occurs primarily by conduction of heat through the substrate or previously deposited layer and partially through the adjacent solidified clad. Thus, there is a higher solidification velocity at the boundary of the clads, which is progressively decreased from the boundary to the center and top of the clads.

III.2.3. Hardness analysis

Hardness is one of the main requirements of dies and molds in order to guarantee a complete service life for manufacturing a whole series of parts before severe wear damage occurs. Reference hardness values depend on the application and material to be formed, but hardness values can vary between 42 and 65 HRC. For hot stamping tools, typical hardness values are around 50 HRC.

Micro-hardness measurements were performed along four cross-sections of an 8-mm-thick AISI H13 deposition. To that end, a Future-Tech FM-800 micro-Vickers hardness tester was used, at 2.9 N (0.3 kgf) with a dwell time of 12 s. The collected results are shown in Figure III. 2. In all sections, homogeneous hardness values are observed across the deposited layers with values above 55 HRC in all cases. In addition, both substrate and deposited material have similar values, existing no significant decrease in hardness neither in the substrate nor at the interface between the substrate and deposited material.

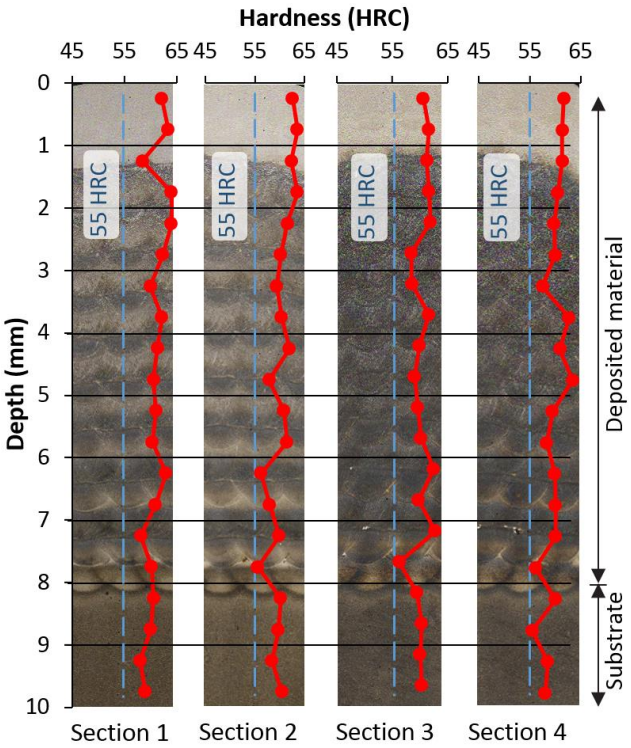

Figure III. 2 Hardness values of the deposited AISI H13 and substrate.

In view of the results, and taking into account the minimum hardness of 50 HRC required by the specification of stamping tools, the obtained hardness results are found satisfactory.

III.3. Laser Metal Deposition in hybrid machines

III.3.1. Materials and methods

In order to analyze the influence of the use of cutting fluids in the LMD of AISI H13, experimental tests were performed over cutting fluid impregnated specimens. To that end, AISI H13 metal powder and substrate material were employed, which have been previously introduced. Besides, with the aim of investigating the variability in the results introduced by the material being processed, and therefore be able to provide a full insight into the impact of the use of cutting fluids on LMD, an additional set of tests was performed. In these additional experiments,

Inconel® 718 and MetcoClad 718 metal powder were used as substrate and filler material, respectively.

On the one hand, Inconel® 718 is an age-hardenable nickel-chromium alloy that combines corrosion resistance with high strength and good creep rupture strength at high temperatures. Its application fields range from aeronautics and spacecraft to nuclear reactors and gas turbine engines. On the other hand, MetcoClad 718 by Oerlikon Metco is a gas-atomized, nickel-base superalloy powder, with a particle size distribution between 44 and 90 µm and similar in composition to Inconel® 718. It has good corrosion resistance and it also resists creep and stress rupture at elevated temperatures. Its use is indicated for the repair or buildup of nickel-base superalloys, such as turbine blades or valves. Moreover, it can be also used for the repair of steel or stainless steel parts. The chemical composition of both materials is shown in Table III. 3.

Table III. 3 Chemical composition (wt. %) of the employed materials [Oerlikon, 2019; AlloyWire, 2019].

Material	Cr	Mo	Nb	Fe	Ti	Si	Mn	C	B	Ni
MetcoClad 718	19.00	3.00	5.00	18.00	1.00	0.20	0.08	0.05	0.005	Balance
Inconel® 718	19.00	3.05	5.10	19.00	0.90	0.18	0.18	0.04	0.003	Balance

Substrate slabs of AISI H13 and Inconel® 718 were prepared and impregnated with the help of a dropper with an oil-water emulsion containing Houghton HOCUT B-750 cutting fluid so that the surface of the part was completely covered. HOCUT B-750 is a water-soluble fluid, composed of mineral oil and special emulsifiers with anti-corrosive additives. It is widely used as a coolant and lubricant in machining operations. According to the manufacturer, oil concentrations between 5% and 10% are recommended for machining [Houghton, 2019]. Therefore, concentrations of 5%, 10%, and 100% were selected for the realization of this study, simulating the last one a situation where only pure oil is supplied, such as when machining with the Minimum Quantity Lubrication (MQL) cooling technique [Shokrani, 2019]. Test tubes containing the three different oil emulsions are shown in Figure III. 3.

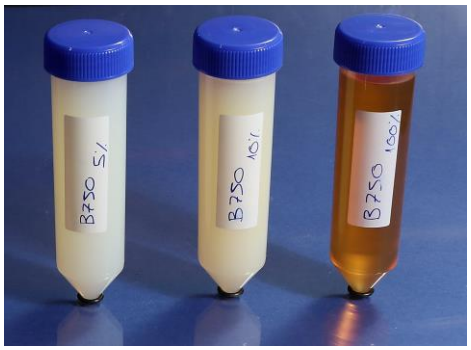

Figure III. 3 HOCUT B-750 oil-water cutting fluid emulsions with 5%, 10% and 100% oil concentration.

For each concentration and after impregnating the part with the corresponding cutting fluid, the same LMD tests were carried out, using the same process parameters. However, two different cleaning methods were performed for each case, giving rise to the list of experiments shown in Table III. 4. In addition, process parameters employed for all the tests are also detailed.

Table III. 4 List of experiments and LMD process parameters.

Test No.	**1**	**2**	**3**	**4**	**5**	**6**	**7**	**8**	**9**	**10**
Oil concentration (%)	0 No coolant	5			10			100		
Kind of test	Reference	D [1]	A [2]	L [3]	D [1]	A [2]	L [3]	D [1]	A [2]	L [3]
Material	**AISI H13**				**Inconel® 718**					
Continuous-wave laser power (W)	600				571					
Scan Velocity (mm·min^{-1})	450				525					
Track offset (mm)	1				1.036					
Overlap between tracks (%)	50				26					
Powder mass flow (g·min^{-1})	3.3				8.78					
Shielding gas flow rate (l·min^{-1})	14				14					

[1] Direct (no cleaning); [2] Air blasted; [3] Laser cleaning.

A first reference layer was deposited with no cutting fluid in order to determine clean results and establish a reference. Then, direct deposition (with no cleaning), deposition after cleaning with compressed air (air blasted) and after laser cleaning were realized. The air blasting was carried out with 7 bar air pressure, while the laser cleaning was performed at a laser power of 200 W and 100 mm focal distance. A scheme of the experimental procedure is shown in Figure III. 4, as well as the test numbers corresponding to each case.

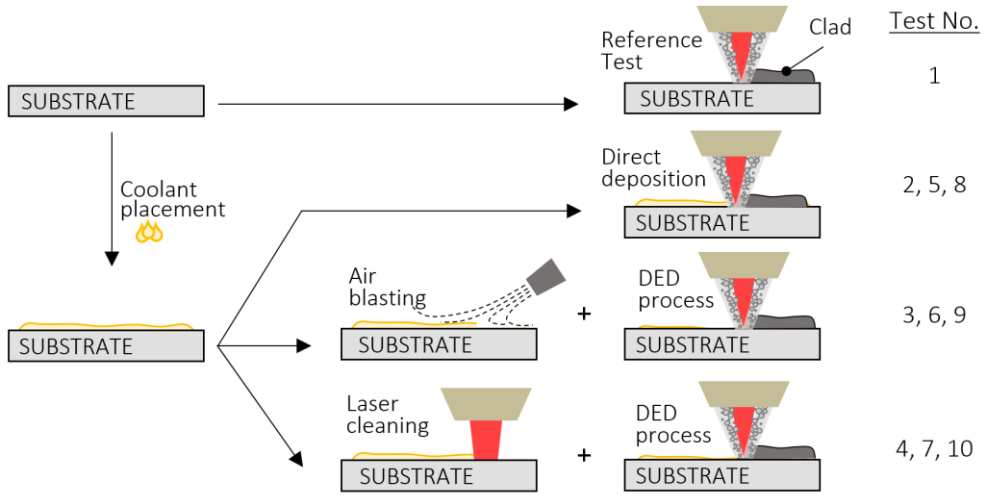

Figure III. 4 Scheme of the experimental procedure.

Once the experimental tests were finished, the samples were cross-sectioned and polished. Three different cross-sections were evaluated for each sample in order to obtain average values. To that end, images of the cross-sections were acquired by means of a Leica DCM 3D confocal microscope and a Nikon Optiphot 100 optical microscope. High-resolution images were obtained, enabling to detect pores of a minimum size of 3.0 µm. This resolution was considered appropriate, as smaller pores have a minimal influence on the mechanical properties of the resulting part.

Afterward, the images in which porosity appeared were analyzed using Matlab R2019b, software in which a program that enables the detection of the percentage and size of pores in the region of the deposited material was developed. For this purpose, in a first step, the program detects and eliminates all material belonging to the phenolic resin used for encapsulating the samples. In the second step, the material belonging to the substrate is detected and eliminated. Lastly, porosity can be evaluated in the deposited material as the number of void pores.

III.3.2. AISI H13 tool steel results

In the present section, results obtained after the evaluation of the cross-sections of the different AISI H13 test samples are detailed. In Figure III. 5, a summary of the most representative results obtained for the single-layer tests is shown. As can be seen, tests No. 2 and 5, which were performed directly on cutting fluid with 5 and 10% oil concentration, presented no defects and were comparable to the reference (test No. 1). In the same way, for 5% and 10% oil concentration tests, the application of air blasting or laser cleaning led to identical results. However, those tests realized in presence of 100% oil cracked regardless of the cleaning technique used. Besides, and taking the LMD direction into consideration, the cracked clads were found at the end of the deposition.

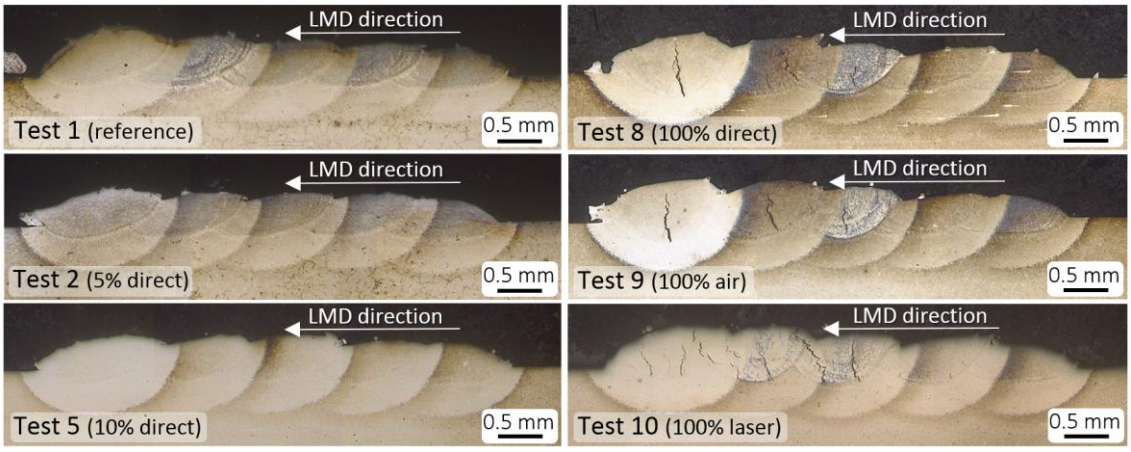

Figure III. 5 Tests No. 1, 2, 5, 8, 9 and 10 – single-layer tests results.

During the realization of the single-layer tests, it was observed that a mixture of cutting fluid and metal powder was generated. With the aim of achieving a better understanding of the phenomena that take place when LMD is performed in presence of a mixture of cutting fluid and powder, tests No. 11, 12 and 13 were realized. To this end, the process parameters detailed in Table III. 4 and the oil concentrations shown in Table III. 5 were used. A scheme that represents the experimental procedure followed for performing these tests is presented in Figure III. 6.

Table III. 5 List of the additional experiments based on preplaced powder on cutting fluid.

Test No.	11	12	13
Preplaced oil concentration in cutting fluid (%)	5	10	100

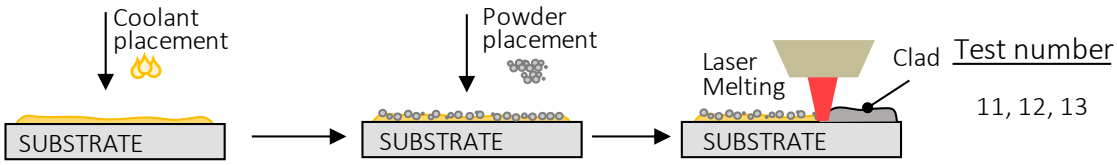

Figure III. 6 Scheme of the experimental procedure of tests No. 11, 12 and 13.

In these tests, instead of injecting the powder directly through the nozzle, a constant-thickness powder layer was preplaced on the coolant, thus generating a bed of cutting fluid and metal powder. Afterward, the laser beam swept that area using the process parameters detailed in Table III. 2, but without injecting any powder, so that the laser melted the powder previously placed. The results of these tests are shown in Figure III. 7.

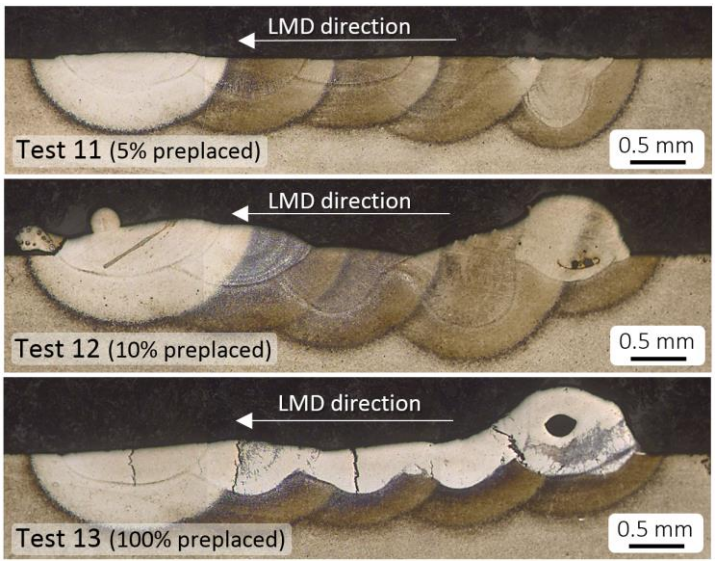

Figure III. 7 Tests No. 11, 12 and 13 – preplaced powder tests results.

In these cases, the deposition was affected by the mixture of cutting fluid and preplaced powder. In this respect, the irregular shape of the deposited clads and the heat-affected zone was

appreciated, that is, each deposited clad presents a different penetration into the substrate, which is a sign that the presence of cutting fluid reduces the repeatability of the process. The composition of the preplaced coolant has a direct influence on the resulting geometry of the clads. It was experimentally observed that, for low oil concentrations, i.e., 5%, the preplaced powder was blasted when the laser was swept over the surface, whereas this phenomenon is minimized for higher oil concentrations. Besides, tests No. 12 and 13 present some voids due to fumes trapped within the molten material. Also noteworthy are the cracks present in test No. 13, performed in presence of 100% oil, which goes in line with the previously commented results.

In order to analyze the observed cracking phenomenon in depositions of more than one layer, in each test from 1 to 10, two specimens were manufactured, one with a single layer and a second one with five layers. The results of these multi-layer tests are shown in Figure III. 8. In a similar way to the single-layer tests, tests No. 2 and 5 presented no defects and were comparable to the reference. It was, therefore, noted that, in those cases, the application of cleaning methods was not necessary. Regarding the 100% oil concentration tests, that is, test No. 8, cracks were found in the interface between the substrate and the first layer, and their propagation did not reach the top surface of the deposition.

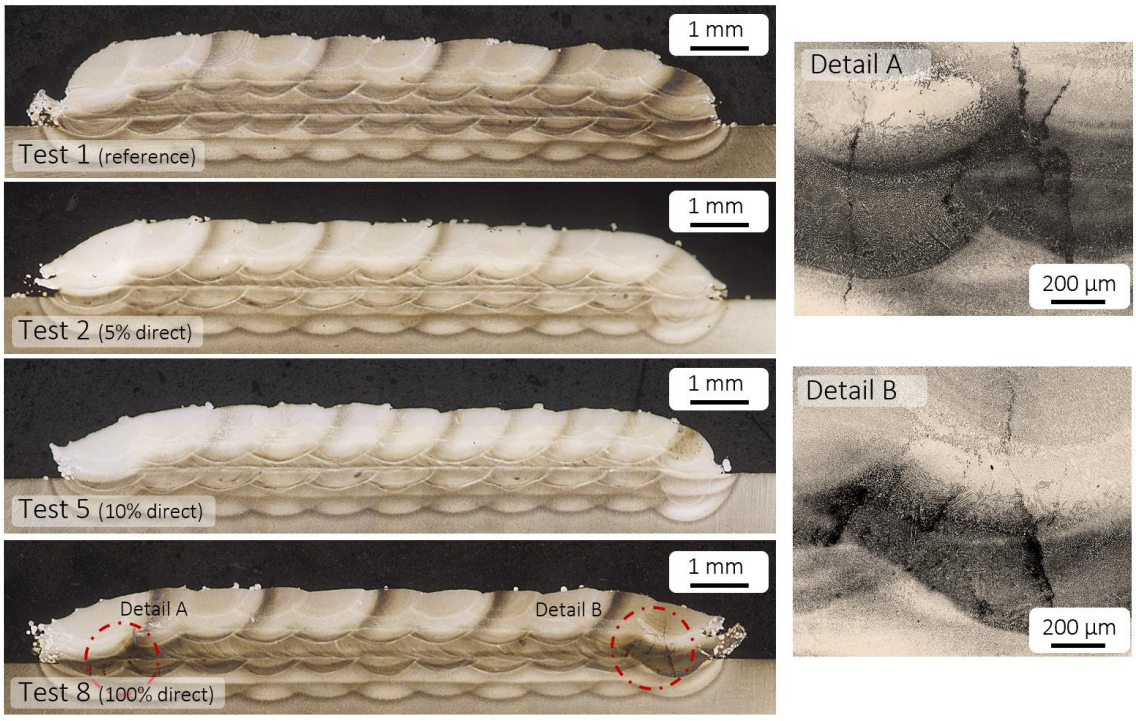

Figure III. 8 Tests No. 1, 2, 5 and 8 – multi-layer tests results.

The results obtained from the defect inspection led to a correspondence between the presence of 100% oil and the appearance of cracks both in the single-layer and multi-layer tests that

required further analysis. Besides, the cleaning techniques were found either not necessary for 5% and 10% oil concentration tests, or not effective for 100% oil concentration tests.

1. SEM analysis

Aiming to identify the origin of the cracks found in those specimens tested in presence of 100% oil concentration cutting fluid, the surrounding of the cracks were analyzed using a scanning electron microscope with tungsten filament and 3.5 nm resolution (JEOL JSM-6400) equipped with an Oxford INCA energy dispersive X-ray spectrometer (EDX) with a Pentafet Si (Li) detector. In particular, it was evaluated whether the cracks had been generated by the existence of undissolved carbides. Possible carbides were subsequently selected in the areas adjacent to the cracks and their composition was evaluated, obtaining a negative result. Therefore, the carbides were discarded as a possible reason for their initiation of the cracking phenomenon. The results of such analysis are shown in Figure III. 9.

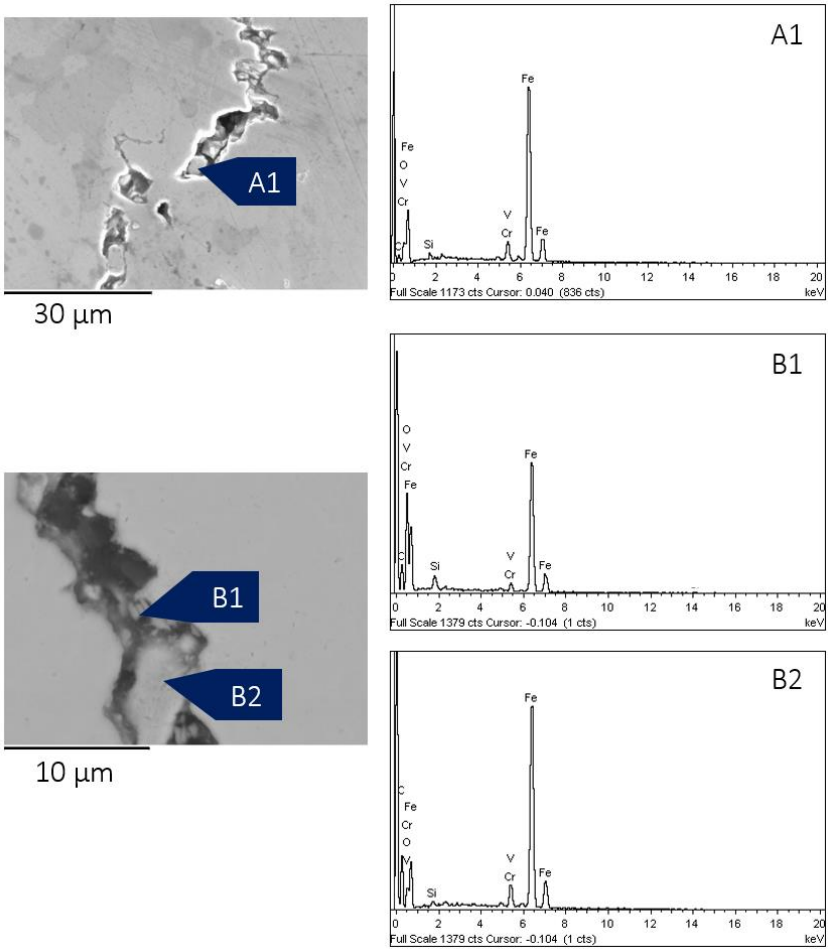

Figure III. 9 SEM micrograph of the cracks with EDX results of material composition at different spots.

As can be seen, the EDX analysis shows the presence of iron (Fe), and other alloying elements, such as vanadium (V) and chromium (Cr), which correspond to the composition of AISI H13. Therefore, no evidence of contamination or foreign elements coming from the cutting fluid was found.

2. Micro-hardness measurements

In order to evaluate the influence of the presence of cutting fluid on the mechanical properties of the deposited material, micro-hardness was measured. These measurements were taken both along the laser-fabrication length and in the build direction. In Figure III. 10, a scheme of how the measurements were taken is represented. In order to obtain representative profiles that described the variation of the hardness, an indentation was made every 0.25 mm in the single-layer tests, whereas, in the case of the multi-layer tests, measurements were taken every 0.25 mm and 0.5 mm along the build direction and the laser-fabrication length, respectively.

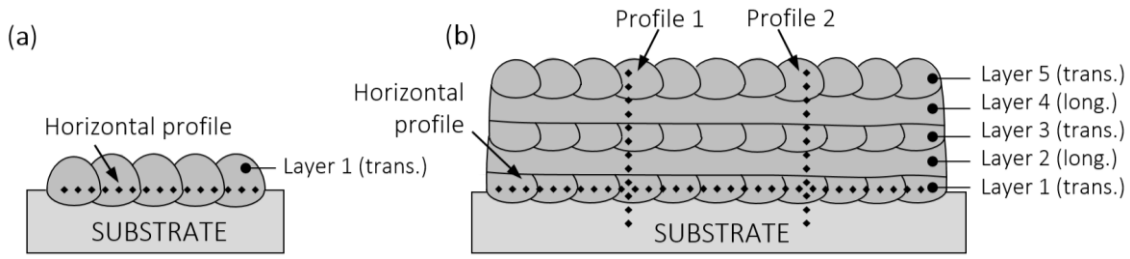

Figure III. 10 Micro-hardness measuring profiles in the (a) one-layer; (b) 5-layer specimen.

Figure III. 11a and b show the micro-hardness along the laser-fabrication length of the reference and the 100% direct single-layer tests, that is, tests No. 1 and 8, respectively. As can be observed, hardness values above 55 HRC were obtained in all cases. The highest hardness values, 62-65 HRC, are located on the last deposited clad, which consisted of fresh martensite, i.e., martensite formed during the final cooling to room temperature. In the other previously deposited clads, the measured values are lower, which was attributed to the tempering to which they are subjected when the adjacent clad is deposited. Nevertheless, when comparing the two images, Figure III. 11a and b, no significant differences were encountered.

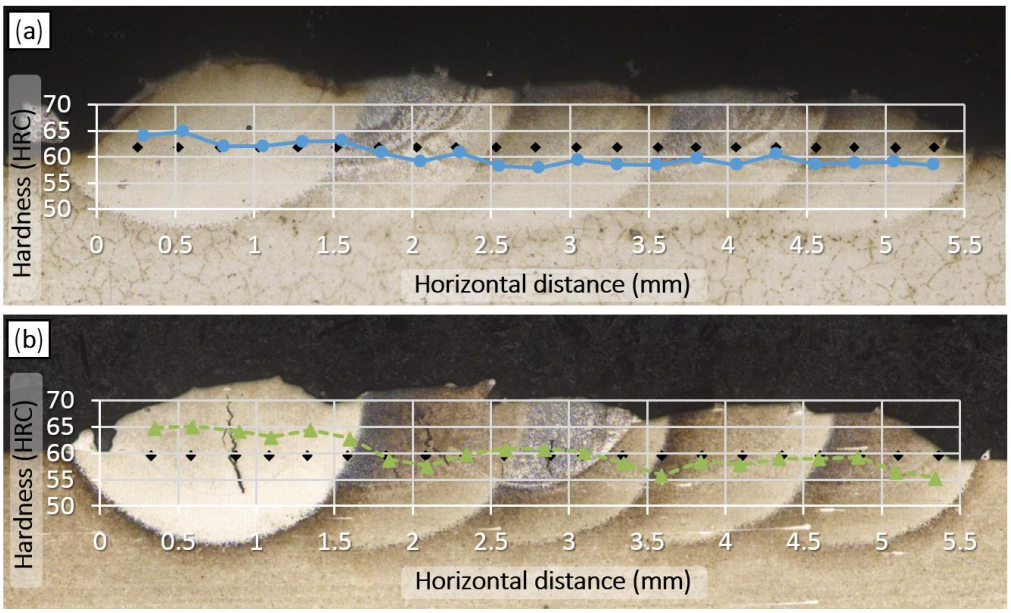

Figure III. 11 Hardness measurements along the laser-fabrication length: (a) Test No. 1 – reference; (b) Test No. 8 – 100% direct.

As far as the multi-layer tests are concerned, Figure III. 12a and b show the micro-hardness distribution in the build direction and at the substrate level along the laser-fabrication length of the reference and the 100% direct tests (tests No. 1 and 8).

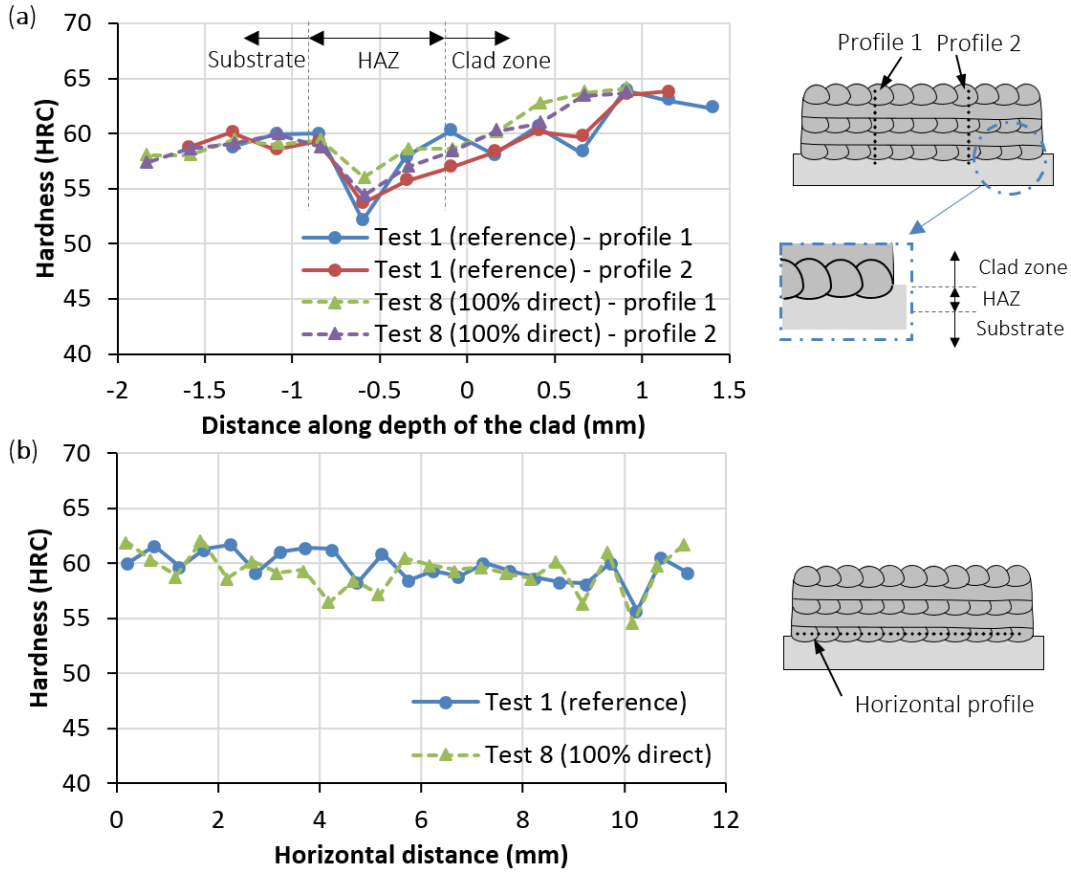

Figure III. 12 Hardness measurements (a) in the build direction; (b) along the laser-fabrication length.

From Figure III. 12a, three zones are distinguished: the substrate, the heat-affected zone (HAZ) and the clad zone. As can be seen, hardness values are significantly lower in the HAZ, which is attributed to the tempering of the substrate due to the LMD process. Then, there is a gradual increment in hardness in the clad zone, obtaining maximum values in the last deposited layer. This variation in hardness might be attributed to the effect of heating and subsequent cooling of the previously deposited layers due to the deposition of new ones. In Figure III. 12b, no significant variations are observed in the hardness values measured in the laser-fabrication length.

3. Analysis of crack mechanism

After examining the results, an analysis of the cracking mechanism of the AISI H13 specimens when processed in presence of 100% oil was performed. The results show a dominant cracking pattern taking place in the deposited clad and not in the HAZ, as shown in Figure III. 5. More specifically, cracks were observed mainly in the lower zone of the clads belonging to the first deposited layer and seem to propagate towards the top zone, as shown in Figure III. 13.

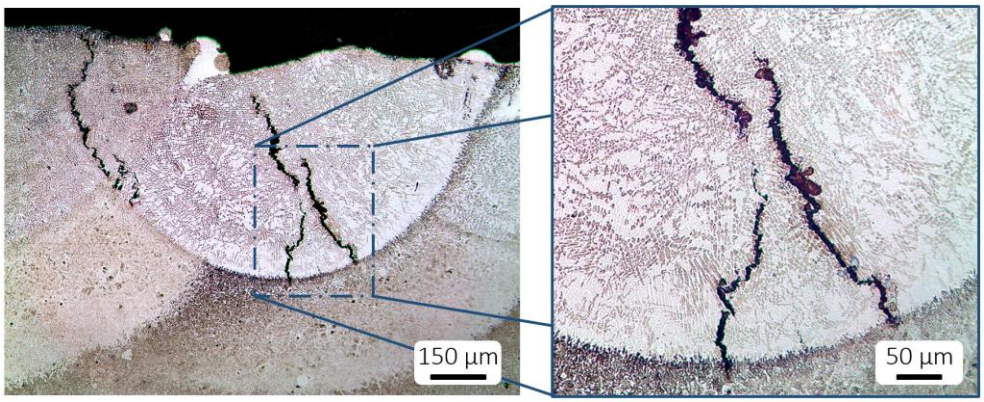

Figure III. 13 Example of crack morphology.

The only difference between cracked and intact specimens is the oil concentration with which they were processed. According to the literature, contaminants containing hydrocarbons, e.g. grease, oil or cutting fluid, are considered a major source of hydrogen during welding, which can result in a form of cracking called hydrogen-induced cracking [Bailey, 1993]. The high temperatures that occur during welding lead to the dissociation of hydrogen-bearing compounds, thus forming atomic hydrogen, which can be assimilated into the melt pool and diffuse into regions of high tensile stress and susceptible microstructure, being effectively undetectable within it. In this regard, hard microstructures (>35 HRC) are the most susceptible to hydrogen cracking, with martensite being the most susceptible [Lippold, 2014].

The happening of hydrogen-induced cracking in steels requires the interaction between a threshold level of hydrogen, a susceptible microstructure of elevated hardness, such as martensite, and tensile stress. The simultaneous fulfillment of these three conditions is required for hydrogen-induced cracking to occur. In this case, the microstructure of the laser-deposited AISI H13 is martensitic with hardness levels over 50 HRC, and tensile stress arises due to thermal contraction during rapid cooling, such as in the LMD process. Furthermore, despite being undetectable within the microstructure, there is a high level of hydrogen due to the presence of cutting oil on the surface of the substrate. As a result, it can be determined that, with a high probability, the cracking mechanism of the 100% oil concentration tests was hydrogen-induced cracking.

III.3.3. Influence of the material on the methodology

In the present section, the influence of the material deposited on the methodology employed is investigated. To that end, Inconel® 718 results obtained after the evaluation of the cross-sections of the different test samples are detailed. The quality of the clads was analyzed by comparing metallographies of the deposited material etched with Marble solution. The Matlab R2019b software was used to determine both the percentage of porosity of each cross-section in terms of surface area and pore size. The resulting image of the cross-section and porosity of the reference test is shown in Figure III. 14.

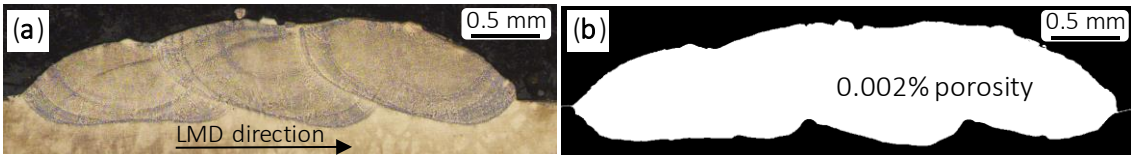

Figure III. 14 Test No. 1 — reference test (a) metallography; (b) average porosity results.

The reference test (test No. 1) is that corresponding to a clean substrate. In this test, an almost zero porosity was achieved (0.002% of the total deposited material) with an average diameter of the pores below 10 µm. Besides, both the dilution of the deposited material and the penetration of the laser beam in the substrate were qualitatively appreciated. These values were therefore considered as a reference that determines the maximum quality to be achieved with the employed equipment and process parameters.

1. Cutting fluid with 5% oil concentration

In Figure III. 15, cross-sections of the deposited material are displayed. In the case of test No. 2, a 0.019% average porosity value was found, whereas in the cases where the surface was cleaned

by means of air blasting and the laser itself, tests No. 3 and 4 respectively, porosity values comparable to those encountered in test No. 1 were found. Moreover, all pores have a size below 10 µm in diameter. This is why no porosity distribution graphs are shown regarding these 5% oil concentration cutting fluid tests.

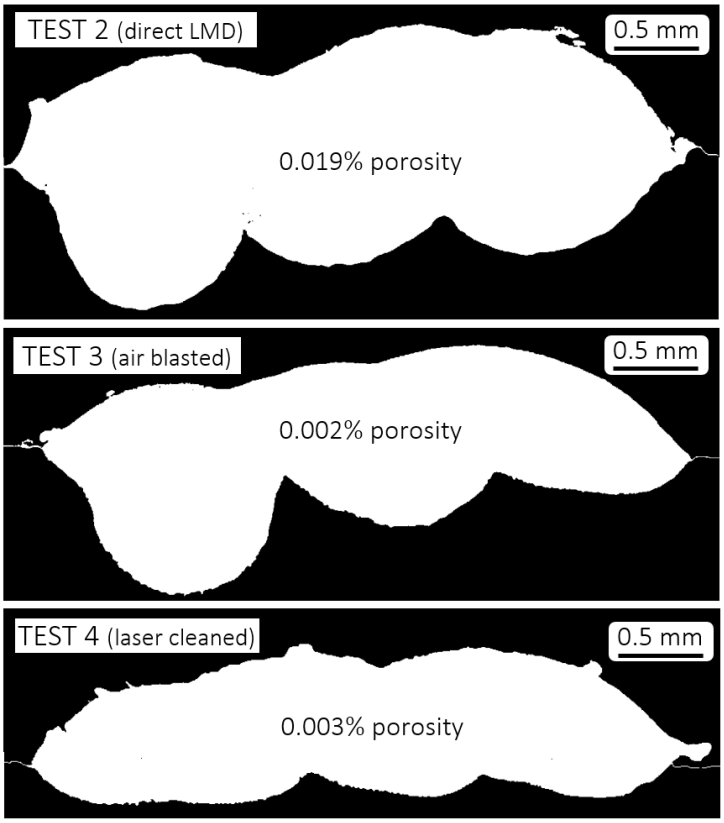

Figure III. 15 Tests No. 2, 3 and 4 — 5% concentration cutting fluid tests porosity results.

Besides, the direct LMD test (no cleaning) showed a bigger penetration of the deposited material within the substrate, which was reduced in cleaned tests (air blasted and laser cleaned). The appearance of the cross-sections of the tests is shown in Figure III. 16.

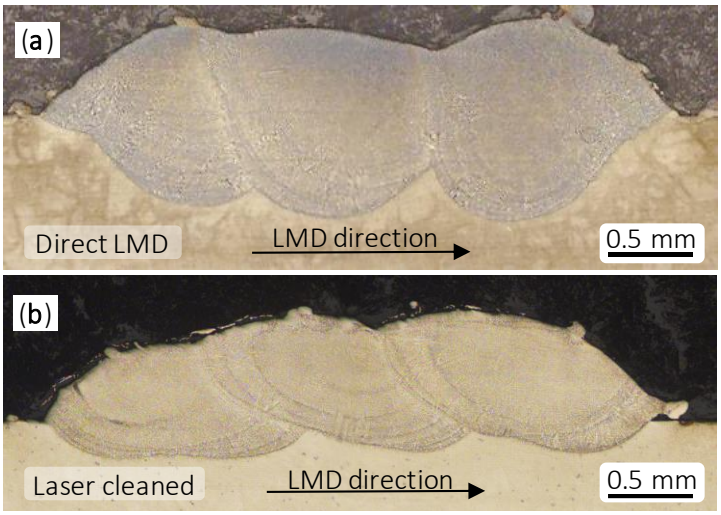

Figure III. 16 Metallographies of the 5% oil concentration tests.

Nevertheless, it was also noticed that the existence of cutting fluid on the surface of the substrate influenced the appearance and shape of the deposited material. Consequently, this fact generated variations on the resulting height of the deposited layer, which may have affected the stability of the process when depositing the following layers.

The external appearance of tests No. 2 and 3 is shown in Figure III. 17. On the one hand, it is noted that the direct test (test No. 2) looks darker and nonhomogeneous because of the slag generated in the LMD process. On the other hand, the air blasted sample (test No. 3) looks brighter and without external anomalies.

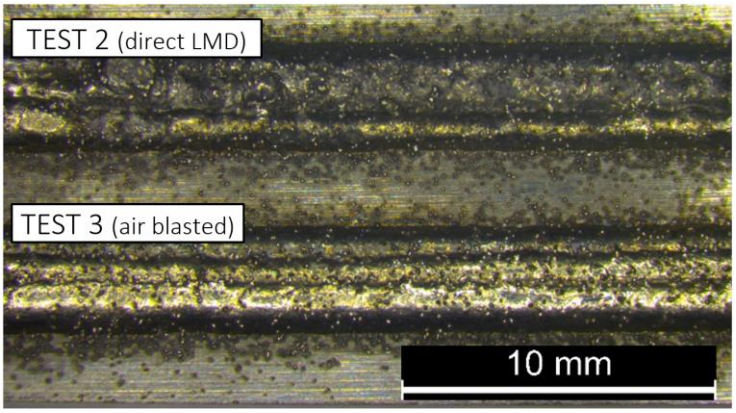

Figure III. 17 External appearance of tests No. 2 and 3.

The collected results show that, in this case, direct LMD led to an average porosity slightly higher than the reference value. However, both cleaning methods reduced the average porosity until acceptable values comparable to the reference (0.002%). Moreover, the excessive dilution present in the direct LMD test was corrected after cleaning, returning to the appearance of the reference test in the case of laser cleaning.

2. Cutting fluid with 10% oil concentration

As the content of oil in the cutting fluid is increased, the resulting porosity in the deposited material was also increased. In fact, this increase is caused by the interaction of LMD and the cutting fluid. When the cutting fluid is burnt due to LMD, the vapors generated are trapped inside the molten material because the melt pool solidifies so fast that there is not enough time for the fumes to exit.

In the case of direct deposition, that is, test No. 5, 1.876% of average porosity was measured, where pores up to 300-µm diameter were detected. Thanks to the intermediate cleaning stages,

porosity values were drastically reduced (see Figure III. 18, tests No. 6 and 7), being the lowest average value, 0.016%, achieved with laser cleaning.

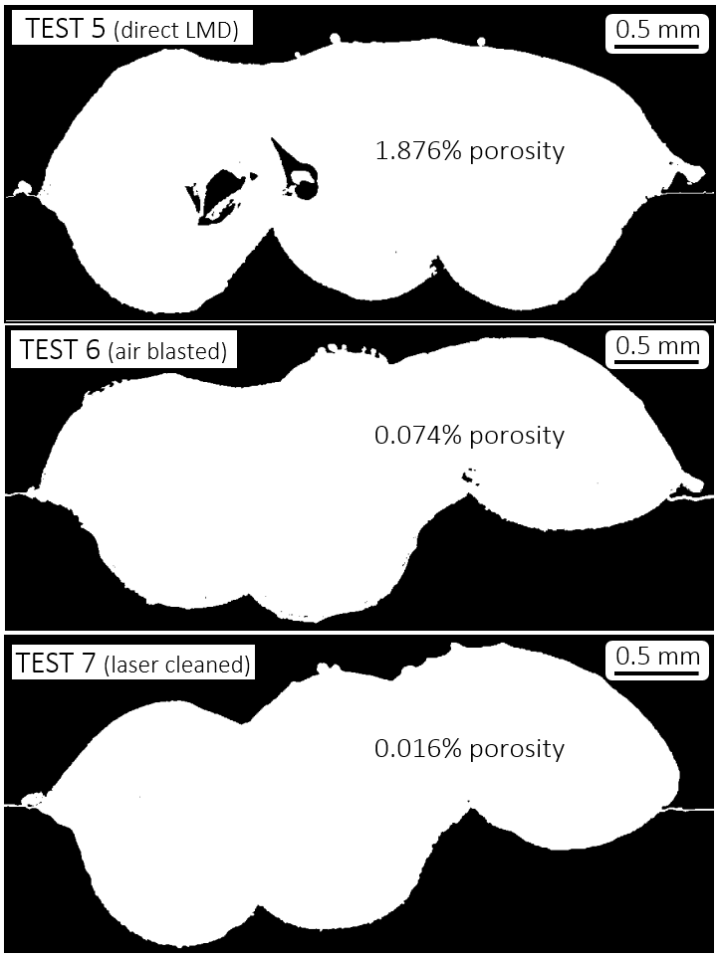

Figure III. 18 Tests No. 5, 6 and 7 — 10% concentration cutting fluid tests results.

Average porosity results were analyzed by means of graphs representing two kinds of accumulated porosity. Despite single porosity values were measured, they were connected with straight lines in order to make the obtained results more understandable. On the one hand, in Figure III. 19a, the accumulated porosity with regard to the total deposited material as a function of the diameter of the pores is shown. In all cases, pore size remains below 300-µm diameter.

On the other hand, in Figure III. 19b the accumulated relative porosity with regard to the total amount of pores of each test as a function of the size of the pores is represented. The improvement introduced by the cleaning stages is noticeable in this figure. While test No. 5 (10% Direct) results show that 60% of the pores have a size of 200–300 µm diameter, tests that include cleaning stages show a lowering of the size of the pores. For instance, the analysis of test No. 6 (10% Air) determines that all the pores remain below 100-µm diameter and, in the case of test No. 7 (10% Laser), all pores have a size below 10 µm.

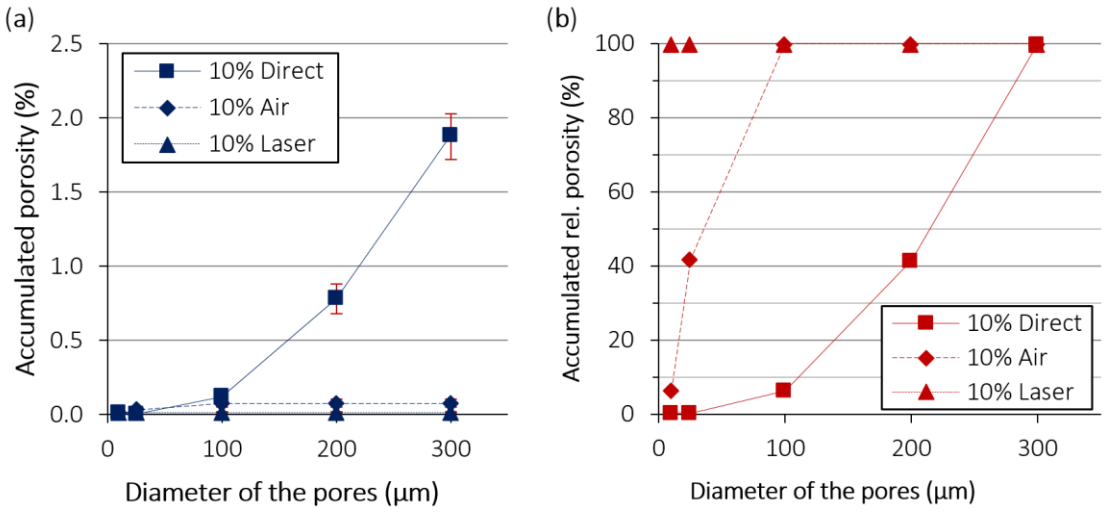

Figure III. 19 Accumulated porosity with respect to pore size in (a) total; (b) relative terms.

When comparing the obtained results, it is concluded that the cleaning process not only reduced the total amount of porosity, but also the size of the pores. In addition, best results were attained with a laser cleaning stage, achieving porosity results comparable to the reference test.

Direct LMD results appear to present bigger penetration and dilution than the reference test. Moreover, the cleaning processes did not seem to reduce them to reference values (see Figure III. 20).

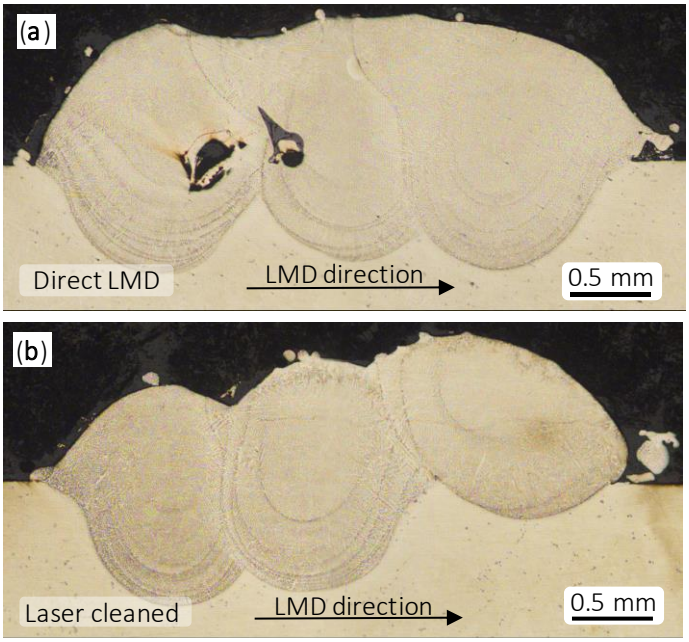

Figure III. 20 Metallographies of the 10% oil concentration tests.

Although both cleaning methods reduced the average porosity, only laser cleaning made it low enough to be considered admissible. Nevertheless, the dilution attained after the cleaning was qualitatively bigger than in the reference test.

3. Cutting fluid with 100% oil concentration

A 100% oil concentration corresponds to the situation in which only oil is supplied, such as when machining with Minimum Quantity Lubrication (MQL) cooling technique. From Figure III. 21, it is noted that obtained results are nothing like the shape of the deposited material from the previous tests. Much higher layer heights are achieved, but also higher porosity values. The increase in the layer height is induced by the generation of a mixture between the powder particles and pure oil, leading to the accumulation of powder on the surface of the substrate.

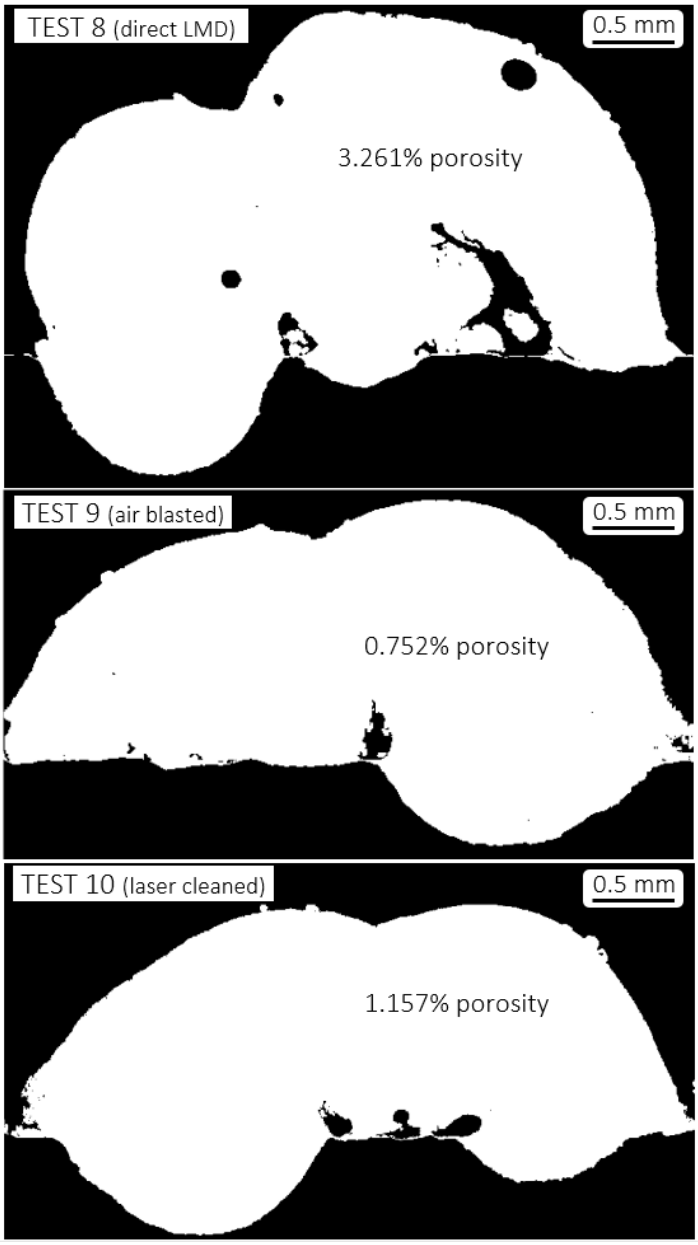

Figure III. 21 Tests No. 8, 9 and 10 — 100% concentration cutting fluid tests results.

As shown in Figure III. 22, thanks to the air blasting and laser cleaning processes, porosity values were considerably decreased. Test No. 8 (100% Direct) presents pores below 300-µm diameter,

and around 70% of them have a size below 200 µm. Air and laser cleaned tests present improved results with reduced porosity and in all cases with a size below 200-µm diameter.

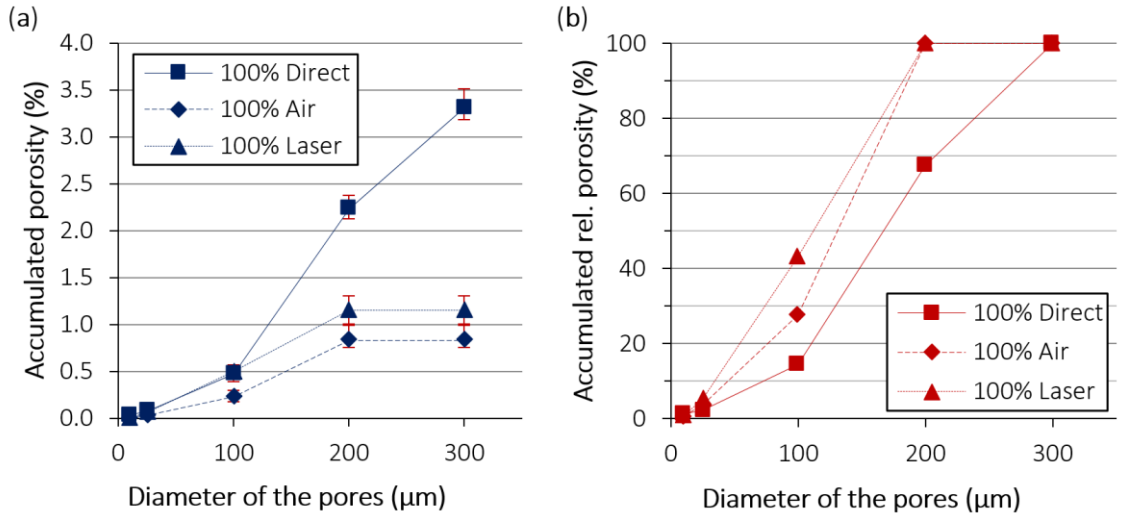

Figure III. 22 Accumulated porosity with respect to pore size in (a) total; (b) relative terms.

Thus, the size of the pores was reduced thanks to the cleaning processes, but not sufficiently to be compared to the reference test (in both cases an average porosity around 1% was obtained). Once again, the smallest pore distribution was achieved when the surface of the substrate was cleaned with the defocused laser before the LMD process.

Regarding dilution, for 100% concentration tests the penetration of the deposited material within the substrate starts to be so low that it may affect the metallurgical bonding, see Figure III. 23.

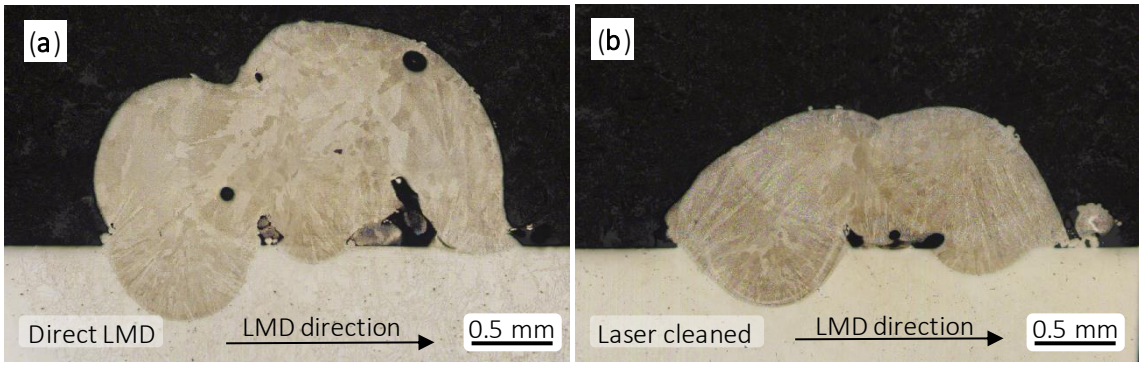

Figure III. 23 Metallographies of the 100% oil concentration tests.

The graph shown in Figure III. 24 represents the average porosity results obtained for each test realized (direct LMD, air, and laser cleaned). Besides, the dispersion of the results is indicated.

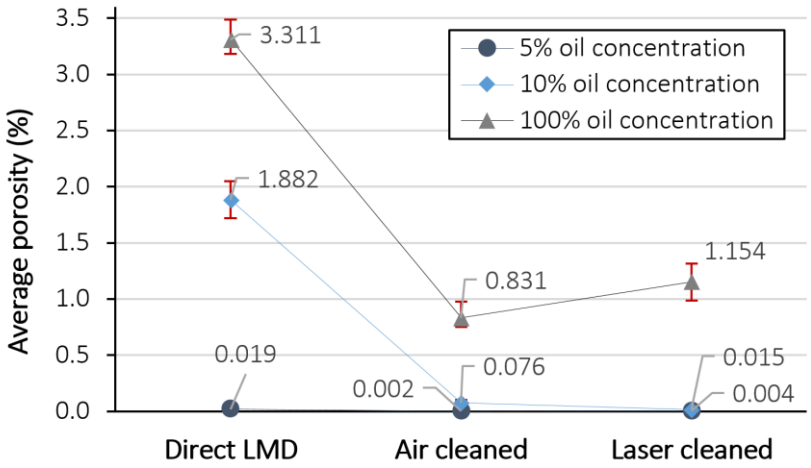

Figure III. 24 Average porosity attained for each test.

The presence of a 100% oil concentration not only increases the porosity value in the clad but also decreases the repeatability, which is detrimental to the LMD process.

III.4. Conclusions

In the present chapter, the experimental characterization of the LMD of AISI H13 tool steel and the influence of the use of cutting fluid in hybrid processes of machining and LMD have been investigated. The quality of the deposition has been evaluated for both AISI H13 and Inconel® 718. According to the attained results, the following conclusions were drawn:

- As far as the characterization of the LMD of AISI H13 is concerned, suitable process parameters were identified, so that the attained AISI H13 layers had a good metallurgical bonding and are free from defects. Besides, the hardness reached in the coatings exceeded 50 HRC, thus opening the doors to its application to stamping tools.
- Direct LMD after the machining operation in a hybrid machine was concluded to be affected by cutting fluid remnants. Besides, it should be noted that the two materials investigated, that is, Inconel® 718 and AISI H13, behaved differently under the same conditions. On the one hand and as far as the Inconel®718 tests are concerned, LMD in the presence of cutting fluid led to lower clad quality due to defects such as increased porosity, as well as a deficient metallurgical bonding with the substrate. On the other hand, AISI H13 tool steel proved to crack under the most extreme conditions.

In order to differentiate the conclusions reached with each material tested, these are presented separately as follows. On the one hand and as far as **AISI H13** is concerned, the following conclusions were drawn:

- The effect of residual cutting fluid with oil concentrations between 5 and 10% on the LMD of AISI H13 was concluded to be negligible. Therefore, the application of cleaning methods in those cases was found unnecessary.
- Nevertheless, when 100% oil was used, the deposited material showed a number of defects, e.g., irregular shape of clads and the heat-affected zone, and cracking, regardless of the cleaning technique applied.
- The mixture of coolant and preplaced powder on the surface of the substrate led to irregular clads with lower penetration of the deposited material within the substrate and porosity. Therefore, avoiding the generation of such a mixture before the laser is switched on is highly recommended in order to minimize such defects.
- The presence of remnants of cutting fluid during the LMD process had no apparent influence on the hardness of the deposited material.
- The cracks were originated in the lower zone of the clads of the first layer and propagated upwards. They were concluded to be promoted by the presence of hydrogen coming from the cutting oil, being this mechanism called hydrogen-induced cracking.
- The observed cracking phenomenon was originated during the deposition of the first layer and then propagated through the layers later deposited without reaching the surface. Thus, from an industrial perspective, these defects would remain unnoticed unless a specific inspection is performed.

On the other hand and with regard to **Inconel® 718**, the following conclusions were drawn:

- Attending to the oil concentration of the cutting fluid, the lower the concentration, the lower the number of pores. When low concentrations were employed, there was practically no need for an intermediate substrate surface cleaning step between the machining and LMD operations. However, it is highly recommended in order to obtain both porosity and dilution values comparable to the reference case and hence ensure the stability of the process. Although the performance of an intermediate cleaning step between the machining and the laser process led to the attainment of both lower porosity and dilution, for oil concentration values of 10%, and especially 100%, no results comparable to the reference test were obtained.
- With regard to the cleaning processes, if the cutting fluid was not properly removed from the surface of the substrate, a mixture between the remaining oil and the powder particles was generated. Consequently, instead of a pure LMD process, a sum of direct and preplaced powder additive process was achieved, which resulted in an increase of

the material deposition rate and higher clad heights. In that condition, the layer-by-layer process may become unstable. In addition, the best results were generally obtained after applying a laser cleaning stage. Nevertheless, the introduction of any cleaning step previous to LMD, especially the laser cleaning, involves lengthening in time the whole manufacturing process.

- The direct LMD after the machining operation in a hybrid machine was concluded to be sensible from the point of view of dilution and pore generation. For typical oil concentrations used in machining (5–10%), it was demonstrated that porosity could be completely avoided after the performance of the appropriate intermediate cleaning stage. However and with regard to dilution and clad quality, admissible results were only attained with 5% concentration (and laser cleaning), being both dilution and porosity values qualitatively comparable to those of the reference test. Hence, this work demonstrates the capability of obtaining acceptable clads in hybrid machines as far as porosity is concerned. In addition, the suggested cleaning technique does not involve any added complexity to the process, as the laser can follow the same LMD trajectory but with lower power (in order to avoid melting the surface of the substrate or damaging the microstructure). Moreover, this operation can be performed automatically and without supervision from the operator.

Chapter IV. Laser Metal Deposition process applied to new hot stamping tool designs

Chapter IV. Laser Metal Deposition process applied to new hot stamping tool designs

In this fourth chapter, the application of LMD to new hot stamping tool designs is presented. On the one hand, the technical feasibility of manufacturing conformal cooling channels via LMD is addressed, and their mechanical performance and heat transfer capability in contrast to conventional channels are evaluated. On the other hand, the implementation of this new design for manufacturing a B-pillar part is studied by means of thermal simulation. To that end, the reduction of the hot stamping cycle time is quantified and the temperature distribution within the tool-blank set is determined.

IV.1. Introduction

As previously mentioned in Chapter II, the design of the cooling system embedded within the tool plays a key role in the hot stamping process. Therefore, the optimization of the cooling design remains a topic of interest for researchers. In this regard, additive manufacturing technologies open doors to new tool cooling designs. However, the number of works focusing on the application and suitability of these technologies to hot stamping tools is very limited. In addition, there is a lack of knowledge regarding the thermal behavior of a conformal cooled tool-blank set when consecutive stamping operations are performed.

On the one hand, in the present chapter, the design and manufacturing of additively built up conformal cooling ducts have been investigated. Experimental study of LMD of AISI H13 tool steel powder on CR7V-L tool steel specimens has been carried out for the fabrication of the adaptive cooling channels. The performance of the channels has been analyzed and compared to conventional straight ducts by metallurgical, mechanical tests and thermal analysis. Finally, the suitability of this process to a 3D geometry of higher complexity has been investigated.

On the other hand, the impact of implementing conformal cooling on the hot stamping process has been analyzed from a thermal point of view. To this effect, both the thermal field of a stamped blank and the cycle-time reduction attained have been determined in the hot stamping of a B-pillar type geometry by means of transient thermal simulation. Thirty consecutive stamping operations, including the intermediate cooling stages required for the blank unloading and loading, have been simulated in order to ensure that the tools have reached a thermally stable regime. In this situation, the temperature differences in the stamping tools, as well as their influence in the cooling process of the blank have been studied.

IV.2. Methodology proposal for the Additive Manufacturing of conformal cooling channels

IV.2.1. Materials

Three different materials were used throughout the present investigation in order to generate the final part: CR7V-L, AISI H13 (DIN 1.2344) tool steel and AISI 316L (DIN 1.4404) stainless steel. The chemical composition and thermal properties of the studied materials are shown in Table IV. 1 and Table IV. 2, respectively.

Table IV. 1 Chemical composition (wt. %) of the used materials [CR7V-L, 2019; FST, 2019; Metallied, 2019].

Material	C	Si	Mn	Cr	Mo	V	Ni	P	Fe
CR7V-L	0.42	0.50	0.40	6.50	1.30	0.80	-	-	Balance
AISI H13	0.41	0.80	0.25	5.12	1.33	1.13	-	-	Balance
AISI 316L	0.0023	0.34	0.079	18.15	2.33	-	11.75	<0.001	Balance

Table IV. 2 Thermal properties of the used materials [CR7V-L, 2019; Uddeholm, 2019; AKSteel, 2019].

Material	Thermal properties	Temperature (K)		
		293	673	873
CR7V-L	Thermal conductivity ($W \cdot m^{-1} \cdot K^{-1}$)	26.7	30.8	30.8
	Coefficient of thermal expansion (10^{-6} K^{-1})	11.2	12.5	13.1
AISI H13	Thermal conductivity ($W \cdot m^{-1} \cdot K^{-1}$)	25.0	29.0	30.0
	Coefficient of thermal expansion (10^{-6} K^{-1})	-	12.6	13.2
AISI 316L	Thermal conductivity ($W \cdot m^{-1} \cdot K^{-1}$)	15.3	20.1	22.7
	Coefficient of thermal expansion (10^{-6} K^{-1})	16.0	17.5	18.5

IV.2.2. Experimental procedure

CR7V-L slabs were used as substrate and AISI H13 metallic powder as filler material so that the conformal cooling channels were closed. Both materials are compatible hot work tool steels with similar thermal properties, such as thermal conductivity and coefficient of thermal expansion. Besides, AISI 316L austenitic stainless steel was used as an intermediate layer in order to relax internal stress and improve the weldability of the materials. Otherwise, the direct deposition of AISI H13 tool steel with no intermediate layer results in the cracking of the part. The preference

of choosing AISI 316L stainless steel instead of other interface materials such as nickel alloys was due to its higher thermal conductivity and ease of LMD processing.

The present investigation was performed on a 100 × 120 × 32 mm^3 CR7V-L hot work steel slab, in which two different cooling channels of 6 mm of diameter at a depth of 10 mm below the surface were generated: one is conventionally drilled and the other additively manufactured via LMD, see Figure IV. 1.

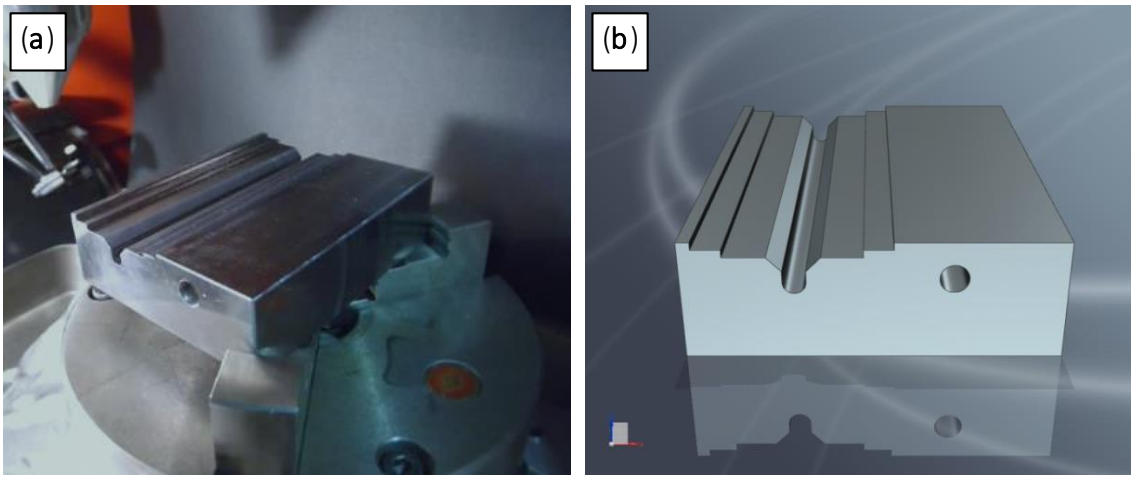

Figure IV. 1 (a) Substrate before LMD; (b) Computer-Aided Design (CAD) model to be processed.

First, the CR7V-L substrate was soft annealed by holding the specimen at 840 °C for five hours with slow cooling in a furnace in order to reduce its high hardness, 59.6 HRC, and allow its preparation by machining. This preparation consisted of directly drilling a first duct and milling a 45° V-notch for the LMD operation. Once the preparatory phase was concluded, the part was ready to be submitted to the LMD process, whose aim was to close the milled V-notch so that an additively manufactured channel comparable to the drilled one was generated. Moreover, accessibility issues and geometric restrictions were considered for verifying the suitability of the available nozzle when manufacturing the part.

Along the LMD process, two different materials were deposited: AISI 316L stainless steel as an intermediate layer and AISI H13 hot work steel for the surface coating. Different deposition strategies and process parameters were used for attaining sound clads with each material. Firstly, AISI 316L was used in order to seal the V-notch and hence generate the channel, while AISI H13 was added over it until the upper surface of the part was reached. For that purpose, the AISI 316L intermediate layer was deposited on the slopes of the milled V-notch alternately, following a longitudinal zigzag cladding strategy in which the surface of the part and the nozzle were perpendicularly orientated as shown in Figure IV. 2.

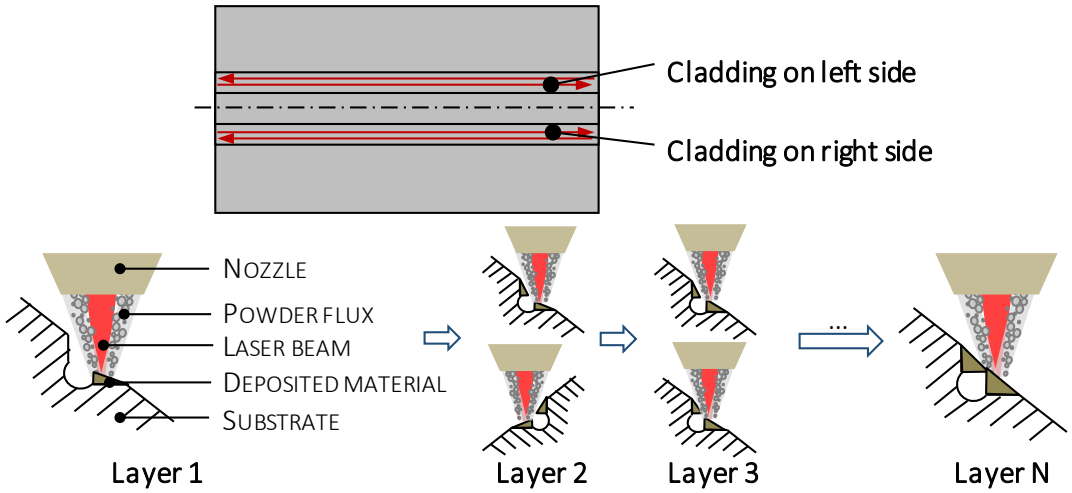

Figure IV. 2 Deposition strategy of the AISI 316L intermediate layer.

Once the channel was closed, AISI H13 was added by alternating longitudinal with transversal directions when laser cladding until the desired height is reached, as shown in Figure IV. 3. Directionality within the mechanical properties and residual stress of the deposited material that may lead to the generation of cracks are thereby avoided.

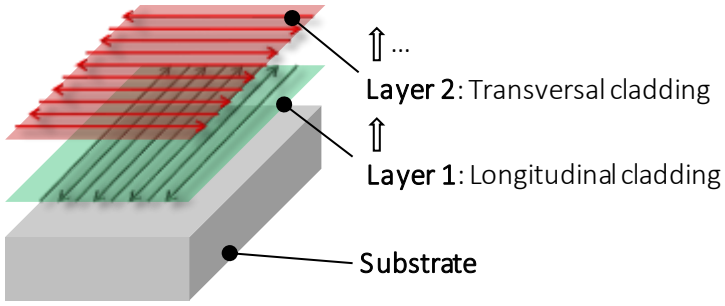

Figure IV. 3 Deposition strategy of AISI H13.

As far as the process parameters are concerned, different values were used for the deposition of each material and are presented in Table IV. 3, while the results attained when finishing the deposition of AISI 316L stainless steel and AISI H13 tool steel are shown in Figure IV. 4.

Table IV. 3. LMD process parameters regarding deposited materials.

Process parameters	AISI 316L	AISI H13
Continuous-wave laser power (W)	625	600
Feed rate (mm·min^{-1})	550	450
Track offset (mm)	1.4	1.0
Overlap (%)	30	50
Powder flow rate (g·min^{-1})	5.0	3.3
Shielding gas flow rate (L·min^{-1})	14	

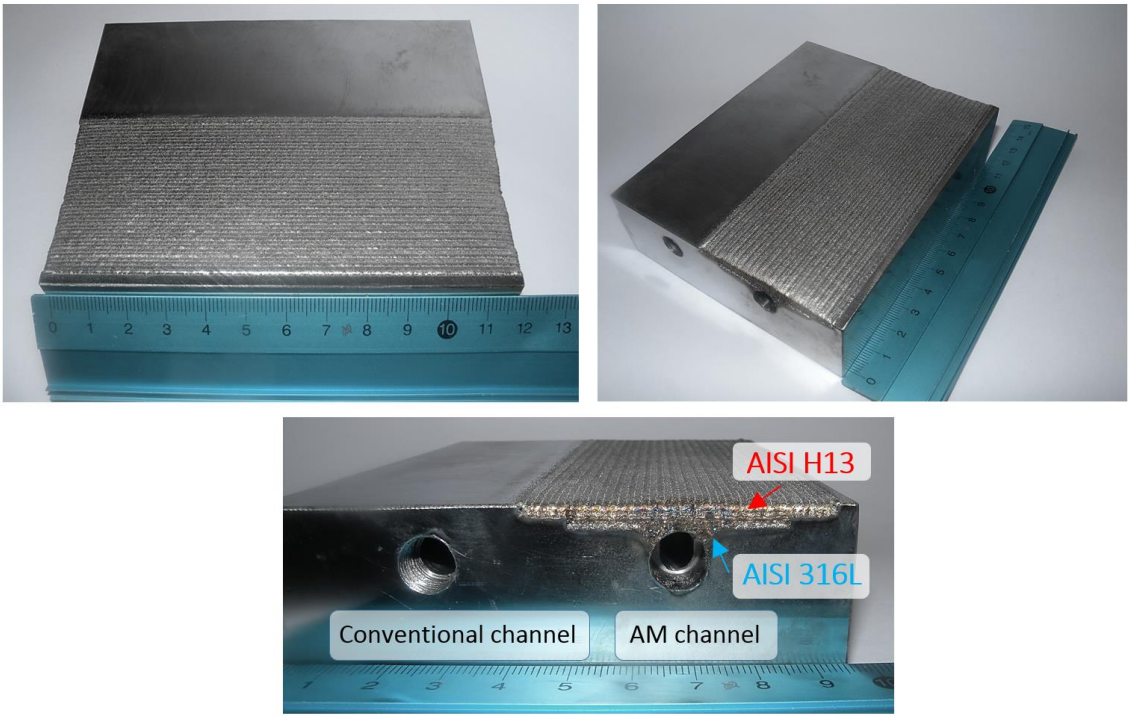

Figure IV. 4 Final part after finishing the LMD process.

Following the experiments, the part was hardened by heating at 1050 °C for 15 min and quenching in water. The component was then ground so that the desired surface quality was attained. In addition, drill holes of 10 mm length were conducted and M10 fine threaded inside the channels in order to enable the threading of push-in connectors and then proceed to the thermal and mechanical analyses.

IV.2.3. Results and discussion

1. Analysis of microstructure and internal defects

In order to analyze the macrostructure and microstructure of the deposited material and find possible internal defects, the cross-section of samples was cut, polished and etched. Marble solution was used to reveal the macrostructure and microstructure of the substrate and deposited material. Images of cross-sections are offered, where the macrostructure properties of the clads are shown. The strategy of deposition of the different layers can be appreciated in Figure IV. 5a, where the deposition directions are indicated.

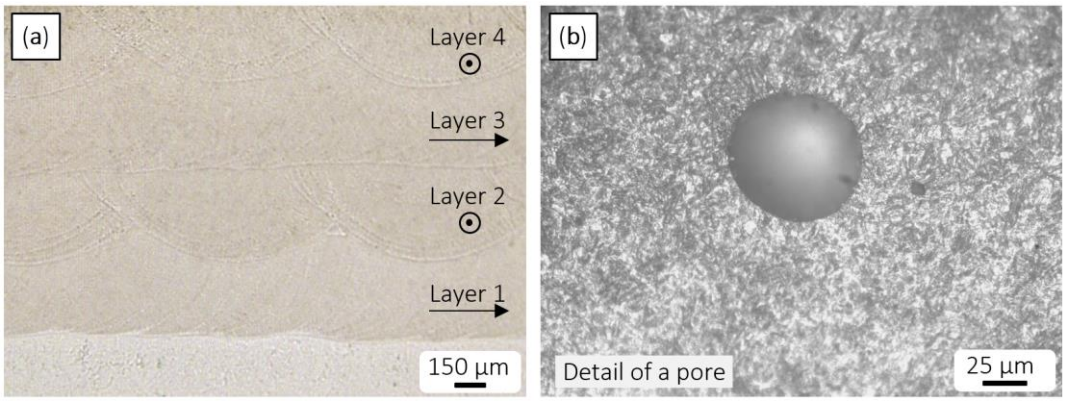

Figure IV. 5 Metallography of the (a) deposited layers; (b) detail of a pore.

As far as metallurgical quality is concerned, no cracks or other intra- or inter-layer defects were detected, except for some intralayer pores of less of 100 µm diameter. An example is shown in Figure IV. 5b, where a higher magnification of an intra-layer region is shown and a pore of approximately 75 µm diameter can be noted.

Furthermore, a detail of the microstructures of the substrate and clad is shown in Figure IV. 6. The substrate (Figure IV. 6a) presented a martensitic microstructure characteristic of tempered CR7V-L tool steel. From Figure IV. 6b, it may be noted that the morphology of the microstructure of the deposited AISI H13 was mainly martensitic, composed of retained austenite and some undissolved carbides distributed in a tempered martensite matrix.

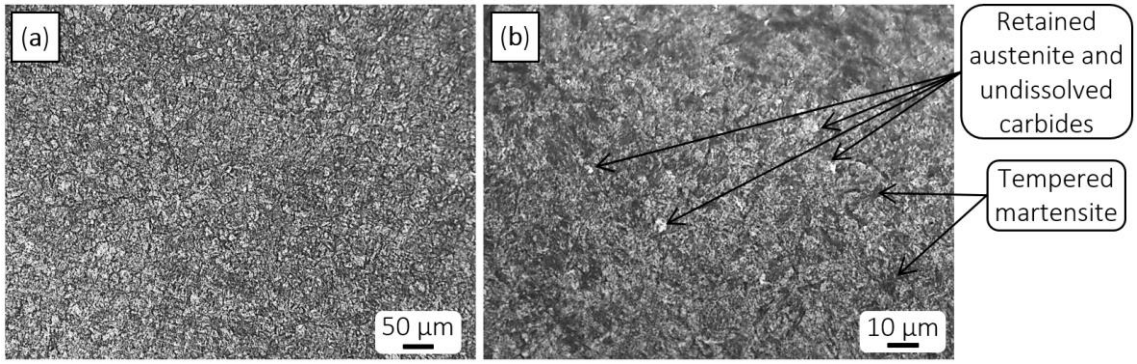

Figure IV. 6 Microstructure of (a) the substrate; (b) the deposited material.

Hence, the analysis of the microstructure and the quality of the deposited material resulted to be satisfactory and no anomalies were found.

2. Thermal comparison between conventional and AM cooling channels

Cooling capacity of the channels

In order to analyze the cooling capacity of the drilled and additively built-up channels, the specimen was monitored with an Optris PI 160 infrared camera, while the emissivity of the

material was evaluated with a type K thermocouple. For that purpose, the sample was heated by scanning the surface with the laser at 1000 W. The scanner swept a rectangular area and its thermal evolution was examined both with active and inactive water-cooling. Three points were monitored: one for each channel (LMD manufactured and drilled) and a third one for the center of the part, while a water flow of 1 $L \cdot min^{-1}$ was inserted through the connectors previously threaded.

On the one hand, the cooling capacity when the laser and the cooling are active was studied. During this test, the laser and the cooling worked simultaneously and maximum temperatures of around 60 °C were reached. Both ducts cooled the part down equally so that the part did not heat up; however, the temperature regarding the LMD channel was slightly higher, as it can be appreciated in Figure IV. 7.

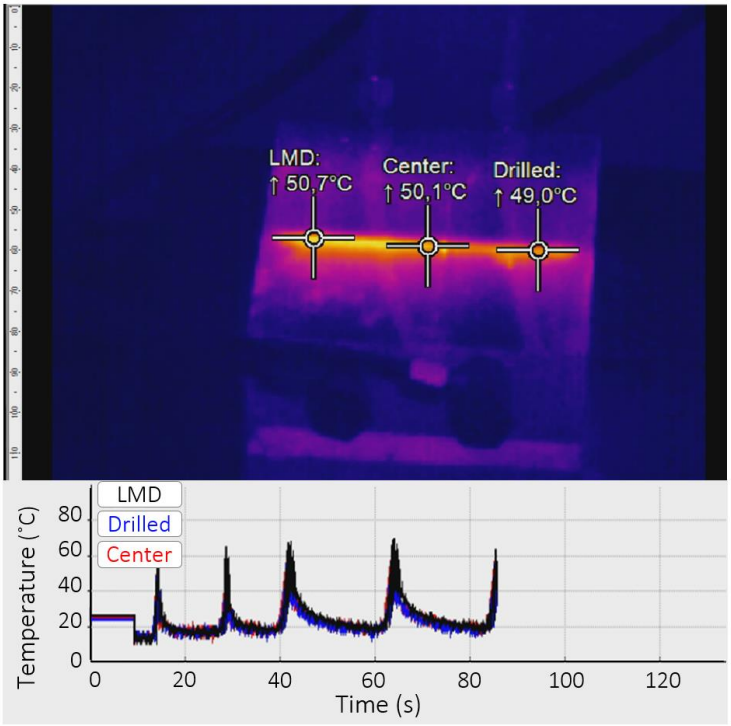

Figure IV. 7 Cooling capacity when laser and water-cooling are both active.

On the other hand, the cooling capacity after a temperature of 100 °C was reached was analyzed. In this case, the water-cooling remained inactive until a temperature value of 100 °C was accomplished. The water cooling was then activated, with the subsequent temperature descent and cooling down of the part. The temperatures obtained for both channels shared once again similar values, with a maximum difference of less than 5 °C and being slightly higher on the LMD duct, as shown in Figure IV. 8.

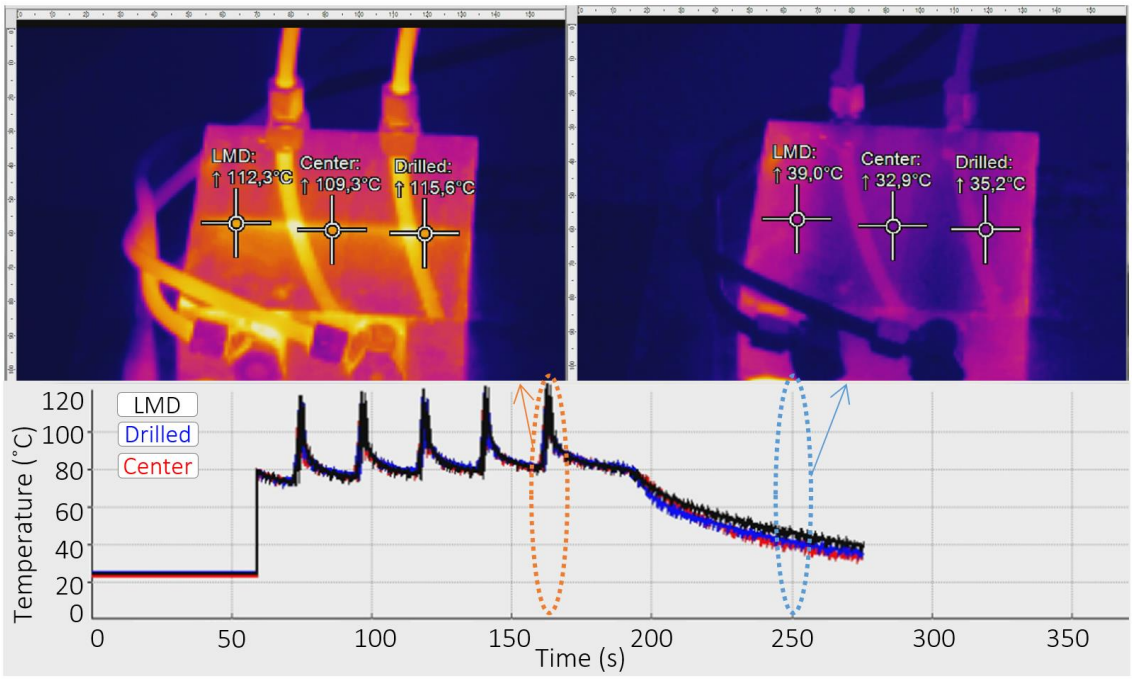

Figure IV. 8 Cooling capacity when the water-cooling is active after reaching 100 °C.

By comparing the cooling capacity of the LMD manufactured and drilled channels on both tests performed, it was concluded that both ducts work similarly during the heating and cooling cycles with a very slight difference in their temperature values. This difference could be due to the existence of the AISI 316L stainless steel intermediate layer, whose thermal conductivity is noticeably lower than the ones regarding AISI H13 and CR7V-L tool steels. The thermal effect of the stainless steel intermediate layer was therefore analyzed by means of thermal simulations.

Analysis of the thermal behavior by means of thermal simulations

The selected LMD strategy included the deposition of a stainless steel intermediate layer, whose thermal properties differ from the ones of the original part. Moreover, the surface finish of the LMD channel was coarser than the one regarding the drilled duct. Hence, the influence of the intermediate layer and the surface finish was studied by means of finite elements thermal simulations, where the effect of both issues on the thermal conductivity and cooling process of the part were analyzed.

On the one hand, the results of the thermal simulations for both drilled and LMD cooling channels along a 120 s period were shown and compared to real results in Figure IV. 9. A good correspondence was attained, as the relative error committed is below 5%, which involves the high reliability of the simulations.

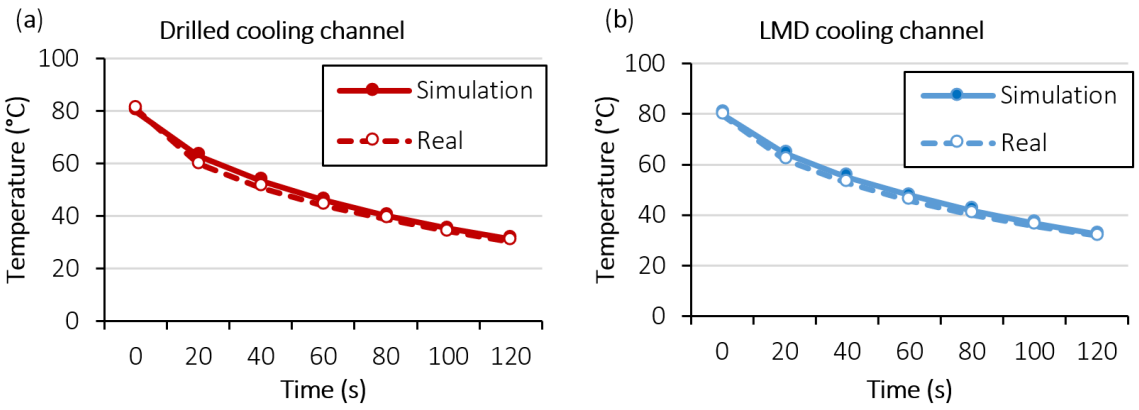

Figure IV. 9 Simulation and real results for (a) drilled; (b) LMD cooling channels.

On the other hand, a comparison between the evolutions of the temperatures of both ducts is shown in Figure IV. 10. Therefore and according to the simulations, it can be concluded that both channels worked similarly and the effect of surface finish together with the influence of the stainless steel intermediate layer was negligible.

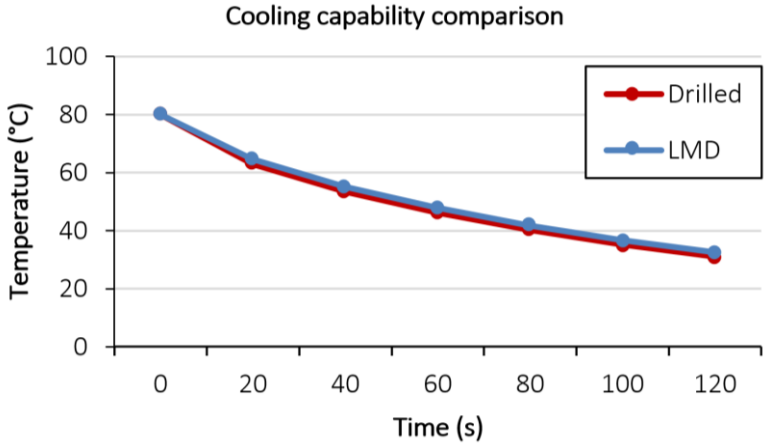

Figure IV. 10 Cooling capacity comparison between the drilled and the LMD channels.

Hence, the simulations were satisfactory and the two ducts experienced almost the same cooling. The temperature of the part was reduced from 80 °C until 30 °C in 120 s for both channels.

3. Analysis of the mechanical behavior of the cooling channels

Compression test

Once the cooling capacity of the additively built-up channel of the manufactured part was positively compared to the drilled duct, a mechanical validation of the specimen was accomplished. The service conditions of a die are limited to a maximum pressure of 12–15 MPa at a velocity of 50–80 mm·s^{-1}. However, and because of the restrictions of the available

compression machine, the tests were realized at a velocity of 40 mm·min^{-1}. The technical characteristics of the employed machine are included in Table IV. 4.

Table IV. 4 Technical characteristics of the compressive machine.

Technical Characteristics of the SDE Compressive Machine (MEM-101/SDC)	
Capacity (kN)	300
Maximum velocity (mm·min^{-1})	40
Stroke (mm)	400

Two different experiments were carried out attending to the pressure applied. On the first compression test, CT1, the force was applied on the whole surface of the specimen, while on the second compression test, CT2, the pressure was localized on the channels. For that purpose, two 10 mm width AISI 1020 rectangular bars were placed over the channels. For each compression test, two different pressures were applied: one according to the maximum pressure on service, 15 MPa, and another with a safety factor of two when possible, resulting in a pressure value of 30 MPa. Regarding the CT1-2 test, it was not possible to reach 30 MPa because the maximum force of 300 kN to be applied by the compressive machine was exceeded, therefore a pressure of 25 MPa was applied. The parameters of the compression tests performed are shown in Table IV. 5.

Table IV. 5 Realized compression tests.

Test	Applied Pressure (MPa)	Surface (mm^2)	Applied Force (kN)
CT1-1	15	11677.5	175.16
CT1-2	25	11677.5	291.94
CT2-1	15	2404	36.06
CT2-2	30	2404	72.12

The evolution of the applied force regarding the stroke of the machine on the most critical executed tests is shown in the following charts hereunder shown in Figure IV. 11. At first, the value of the force was zero because of the existing gap between the upper compressor plate and the part. Then, a minimum value of force was reached, after which a linear increasing tendency of the force with regard to the stroke of the upper plate is appreciated.

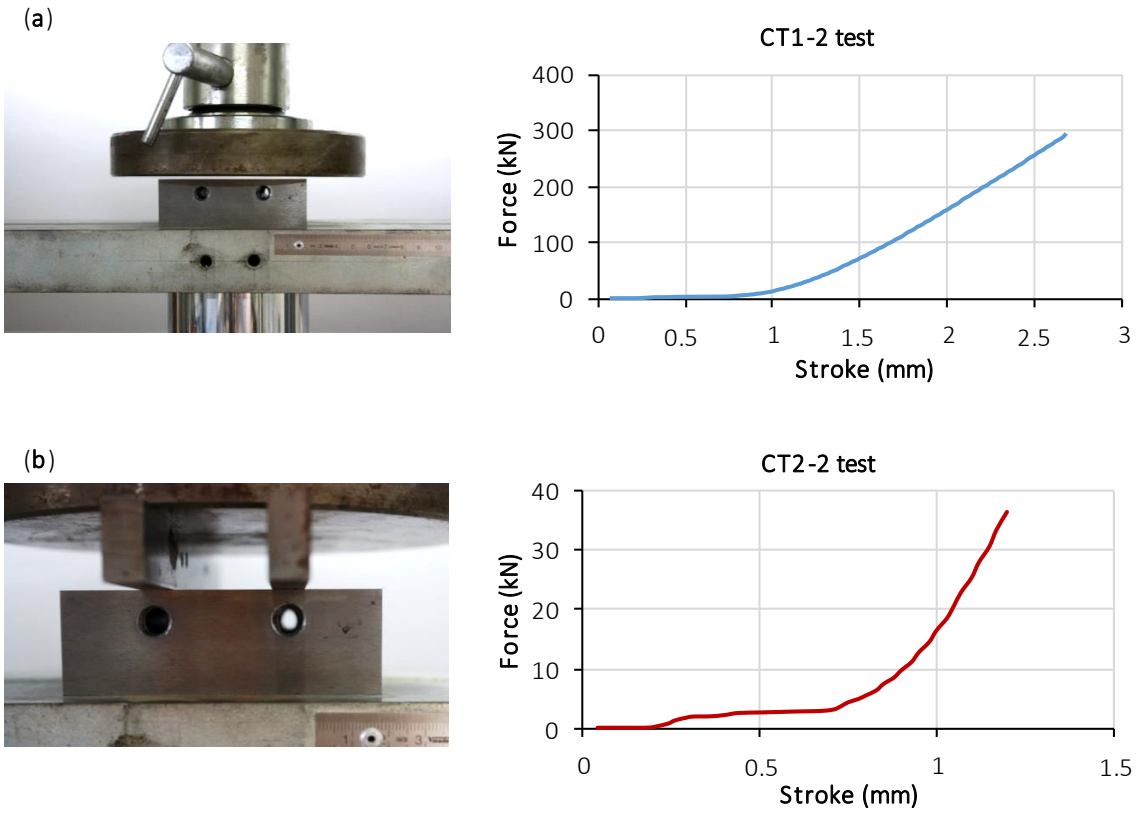

Figure IV. 11 (a) CT1-2; (b) CT2-2 set-ups and results.

The part was visually analyzed after the realization of the mechanical tests and no changes were detected. Possible cracking and deformation were inspected by means of penetrating liquids and a dial gauge, respectively. Results showed that no distortions or cracks were present in the deposited area. Thus, it is concluded that the additively built-up channel withstands the service pressure of 15 MPa, even with a safety factor of two. The manufactured specimen subsequently met the mechanical requirements necessary in hot stamping tools.

Hardness and roughness tests

Additionally, with regard to the compression tests, hardness was measured both superficially and across the different layers deposited. Surface measurements were realized at 49 N (5 kgf) with an Ernst Compumet SC hardness tester, obtaining an average hardness of 55.45 HRC, which is higher than the 50 HRC value required by the specification of the tool. The hardness measurements along the cross-section were performed at 2.9 N (0.3 kgf) using a micro Vickers hardness tester, Future-Tech FM 800, and the dwell time was 12 s. The Vickers hardness values across the different layers of material are shown in Figure IV. 12.

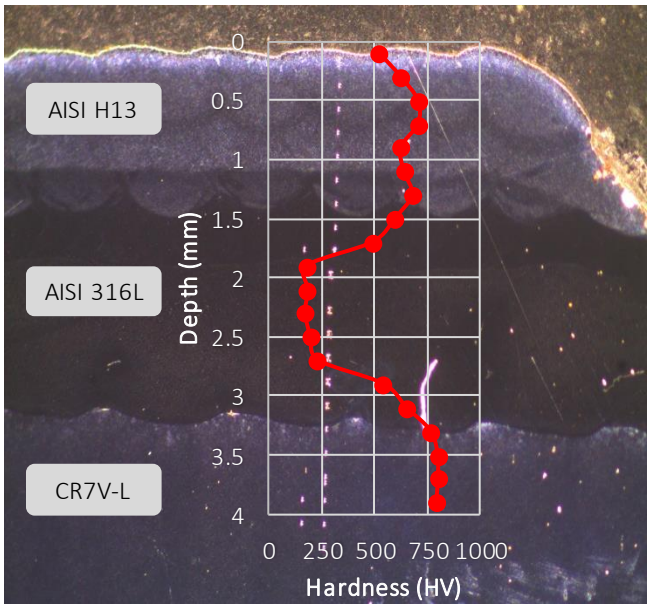

Figure IV. 12 Vickers hardness values of the deposited materials and substrate.

On the one hand, the AISI H13 upper coating generally presented similar hardness values than the CR7V-L substrate. However, the superficial area of the AISI H13 coating presented a slightly lower hardness of 523.8 HV. On the other hand, as it was expected, the hardness of the intermediate AISI 316L coating was considerably lower. This is due to the mechanical properties of the material itself, whose maximal hardness value is of 200 HV [Sandmeyer, 2014], approximately. With regard to roughness, mean roughness, Ra, was measured along the cladding direction with a profilometer, Taylor Hobson Form Talysurf Series 2, obtaining a Ra value of 3.11 µm. The hardness and roughness values of the final part were therefore satisfactory according to the materials and technology employed.

4. Methodology for the manufacturing of 3D conformal cooling channels via AM

Manufacturing strategy proposal

After verifying the use of LMD for generating suitable conformal cooling channels on hot stamping tools, the ability of the process with regard to more complex geometries was studied. For that purpose, the following geometrical challenge shown in Figure IV. 13 was proposed, where the cooling duct is adapted to the shape of the part.

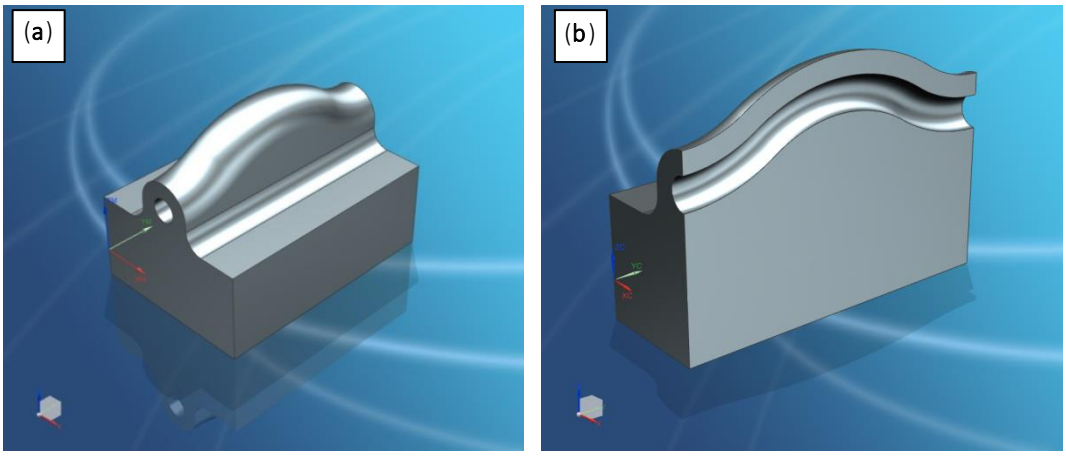

Figure IV. 13 (a) Isometric view; (b) cross-section of the 3D conformal cooling CAD model.

The experimental procedure and methodology followed in this case are analogous to those previously detailed in section IV.2.2. Experimental procedure. The 100 × 70 × 70 mm^3 CR7V-L substrate was firstly soft annealed so that the machining preliminary to the LMD process was eased, attaining hardness values of 30–35 HRC, see Figure IV. 14.

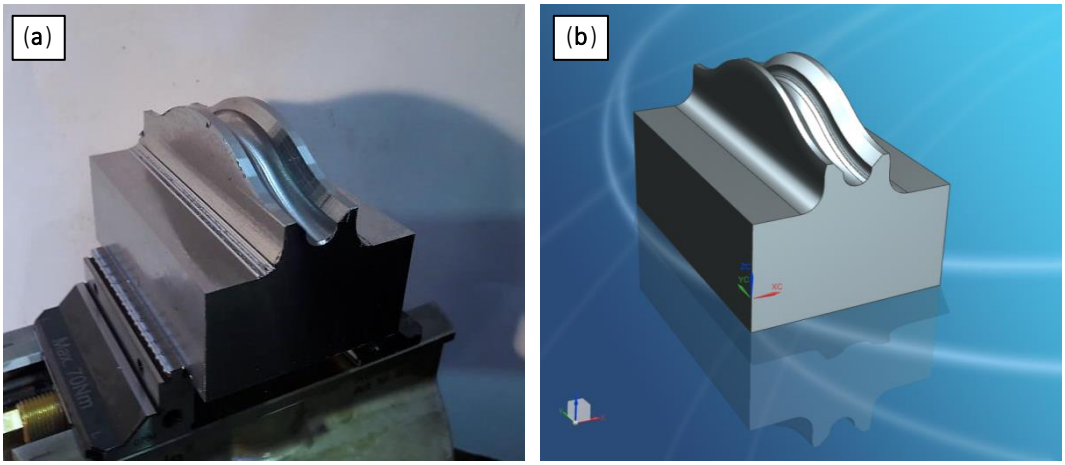

Figure IV. 14 (a) Substrate before LMD; (b) CAD model after the preparatory machining.

Once the preparatory milling stage was concluded, the additive closure of the cooling duct was conducted by the 5-axis deposition of AISI 316L and a final AISI H13 coating. In this case, a suitable building strategy was developed for the execution of the LMD process by using the CAD model data to generate the deposition paths. First, AISI 316L was used for V-notch sealing (Figure IV. 15a). The material was added following a triangle geometry so that the material added on one side of the conduct did not interfere with the material added on the other side and the conduct was subsequently closed. Afterward, AISI H13 tool steel was added until the upper surface of the desired geometry was reached. These last strategies were programmed with NX from Siemens. A zigzag strategy was followed in the added layers alternatively (Figure IV. 15c and d).

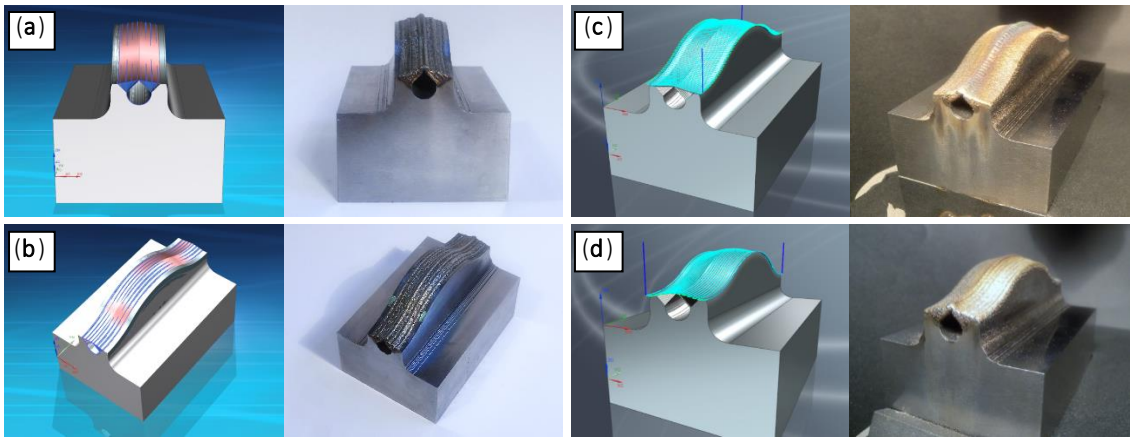

Figure IV. 15 (a) Front; (b) lateral views of the resulting part after LMD; (c) transversal LMD; (d) longitudinal LMD.

In order to obtain a near-net-shape geometry, the layer width was reduced for upper layers gradually. In this way, a semi-cylinder geometry was created and machining times were reduced because of a smaller volume of material to be machined. The resulting near-net-shape part is shown in Figure IV. 16.

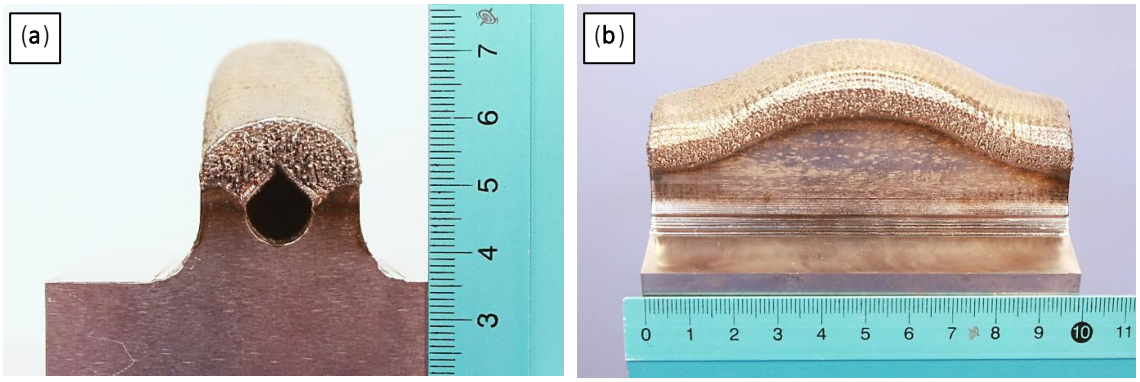

Figure IV. 16 (a) Front; (b) lateral views of the resulting part after LMD.

Because of the LMD process, residual stresses are generated. Annealing the specimen so that the residual stresses are relieved is strongly recommended. The annealing process is a conventional treatment that consists of keeping the sample at 650 °C for a holding time of two hours, slow cooling to 500 °C and free cooling in air. The part was consequently milled and hardened before the last finishing milling operation, aiming to attain a higher hardness when finished. The hardening consisted of heating the part at 1050 °C for 15 min and then quenching in water.

The final specimen was then subjected to a non-destructive test via X-ray radiography, General Electric X Cube compact 225, in order to verify its internal structure and integrity. The results are shown in Figure IV. 17b, where the geometry of the internal cooling channel can be also appreciated.

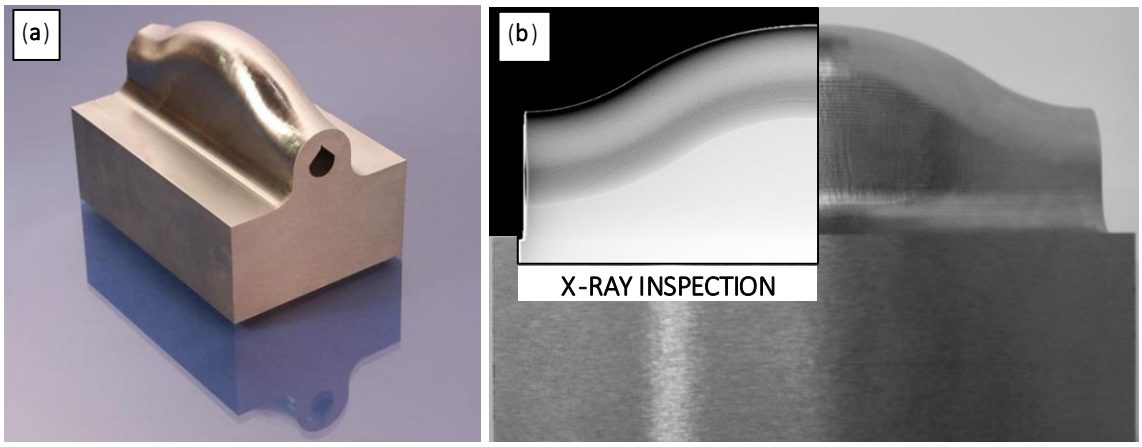

Figure IV. 17 (a) Final part; (b) X-ray inspection.

Analysis of the thermal behavior by means of thermal simulations

With the aim of demonstrating the thermal benefits of conformal cooling, a comparison between the new adaptive channel and the conventionally straight channel was realized by means of thermal simulations. An analysis of the performance of both types of cooling ducts is shown in Figure IV. 18, where the hot stamping of a sheet metal blank is simulated. This simulation was carried out with the same parameters and boundary conditions as the previously validated simulations.

At the initial time step and according to the process, the bulk temperature is 20 °C and the heated metal sheet is at 900 °C. Temperature distributions after 5 s are displayed.

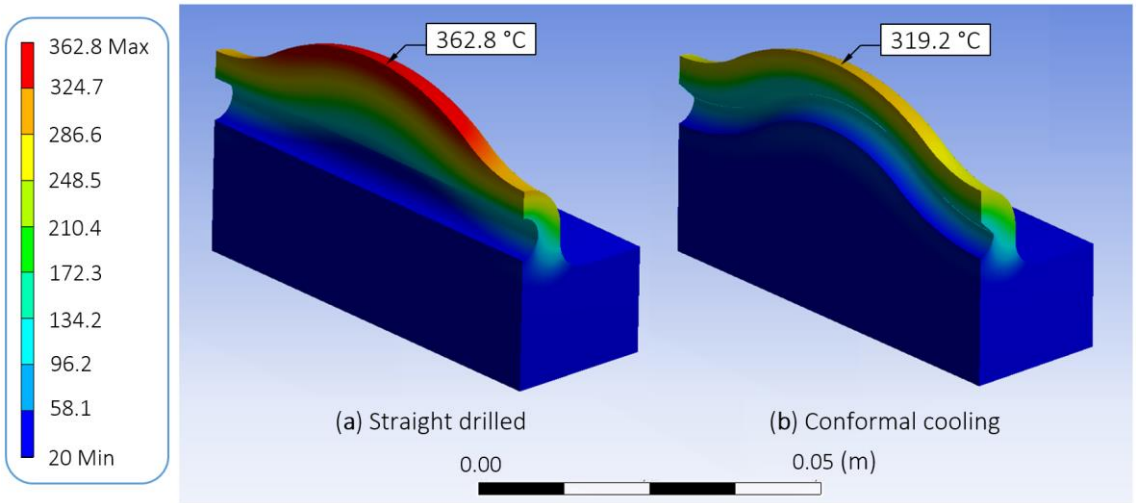

Figure IV. 18 Thermal simulation results of (a) conventional drilled vs. (b) conformal cooling.

As expected, the temperature distribution of the conformal part was more homogeneous than in the drilled specimen, following the geometry of the channel. Moreover, at the same time step, lower temperatures were reached. This may imply a higher cooling rate of the conformal

channel. Therefore, additively built up cooling channels present the same performance as drilled channels, when they have the very same geometry. However, the main benefit of conformal channels is the possibility of adapting to more complex cooling system designs and their constant distance to the die surface.

IV.3. Modeling of the cycle-time reduction in a B-Pillar hot stamping operation using conformal cooling

IV.3.1. Methodology and geometries proposed

Conformal cooling channels have been proven embeddable within hot-stamping tools using additive manufacturing. However, the cycle-time reduction that conformal cooling channels offer in comparison with those traditionally manufactured has not been studied in depth. Aiming to quantify the improvement of integrating conformal cooling in the hot-stamping process for the manufacturing of a B-Pillar type geometry, the following methodology was proposed:

1. Three case-study geometries for the cooling channels were defined: (**1**) straight, (**2**) conformal and (**3**) conformal close to surface. In order to obtain comparable results, in all cases, the number of cooling channels and water flow were kept constant, but the internal geometry was defined according to the capabilities and restrictions of each technology.
2. Heat transfer coefficients were defined for the different cases and convection coefficients based on the roughness of the channels were determined.
3. Transient thermal simulation of the hot-stamping process of a B-Pillar was performed by means of the FEM software ANSYS Workbench 19.2 and the obtained thermal field after a single blank stamping was analyzed.
4. Thirty consecutive stamping cycles were simulated to evaluate the thermal behavior of the process once a stable regime is reached.
5. Achieved results in the different case studies were compared, which provided a quantitative result of the cooling capacity improvement.

With regard to the geometries to be analyzed, in Figure IV. 19 the three proposed configurations are shown. In the first case, the cooling channels are drilled and therefore, each duct is formed by two straight drills. In the second case, the conformal cooling channels are manufactured via additive technology, with the same diameter and inlet and outlet positions as in the straight case; however, the ducts follow the shape of the surface of the tools at a constant distance. Last,

based on the fact that additive technology enables the manufacture of the cooling channels closer to the surface than conventional drilling, in the third case the same geometry considered in the second case was simulated, but displacing the cooling channels 2 mm towards the surface. The mesh employed in the three case studies consisted of over 1 million first-order tetrahedral elements, with a maximum skewness below 0.85.

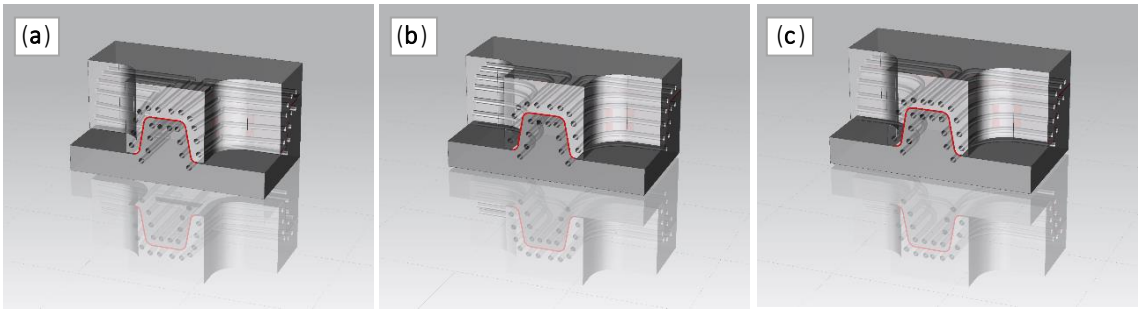

Figure IV. 19 Proposed geometries for the different case studies. (a) Case study 1: Straight cooling channels; (b) Case study 2: Conformal cooling channels; (a) Case study 3: Conformal cooling channels close to the surface.

The geometrical parameters used in the different case studies are defined in Table IV. 6. In order to ease their understanding, parameters are detailed in Figure IV. 20, where front and left views of both the stamping tools and the blank are shown.

Table IV. 6 Geometric parameters of the tooling taken as reference in the present study.

Geometric parameter	Case Study 1	Case Study 2	Case Study 3
Diameter of the cooling ducts (D)	8 mm	8 mm	8 mm
Length of the cooling ducts (L)	170-280 mm	165-275 mm	165-285 mm
Distance between cooling ducts (Δr_1)	15-20 mm	15-20 mm	18-20 mm
Distance from cooling duct center to the surface (Δr_2)	12 mm	12 mm	10 mm
Number of ducts in the upper / lower tools	12 / 10	12 / 10	12 / 10

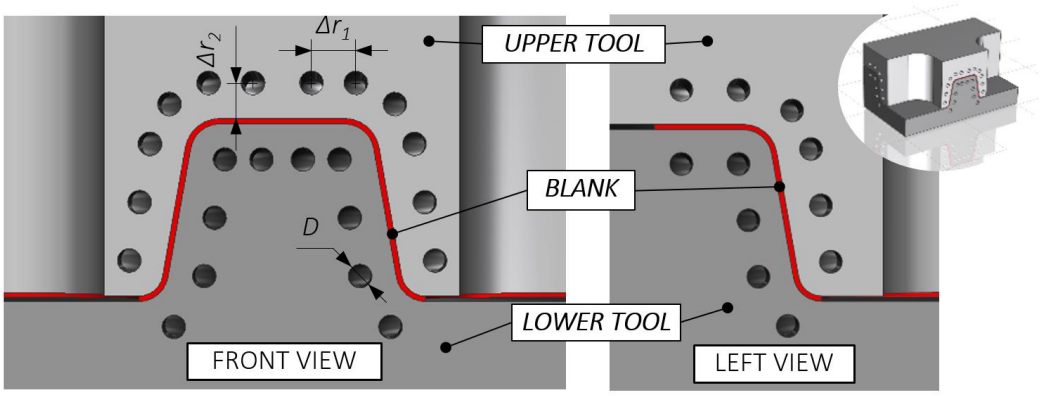

Figure IV. 20 Position of the cooling channels in the stamping tools, where the main geometrical parameters are detailed.

The material properties used within this simulation work were set according to typical conditions of hot stamping operations. On the one hand, both upper and lower tools were of AISI H13 (DIN 1.2344). On the other hand, boron alloyed steel was considered as blank material. In this case, Usibor® 1500 (22MnB5) was used, which is a boron alloyed steel well suited for the entire range of structural parts that require high resistance to anti-intrusion during crash [ArcelorMittal, 2018a]. The thermal conductivity values of both materials used in the present study are detailed in Table IV. 7.

Table IV. 7 Thermal conductivity ($W \cdot K^{-1} \cdot m^{-1}$) of AISI H13 and Usibor® 1500 [Oh, 2019; Shapiro, 2009].

Material	Temperature (°C)					
	20	200	400	600	800	1000
AISI H13	24.9	27.4	29.1	28.5	28.5	28.5
Usibor® 1500	30.7	30.0	21.7	23.6	25.6	27.6

A blank thickness value of 1.85 mm was considered [Karbasian, 2010]. The initial temperature of the tools as well as the reference temperature for the water-cooling convection was set at 20 °C, whereas the temperature of the blank after the loading operation was 810 °C [Shapiro, 2009].

IV.3.2. Process parameter definition

The hot stamping process was divided into two different stages. The first one consists of forming and quenching operations [Naganathan, 2012]. In the second one, the period from the extraction of the stamped blank until the loading of the following one is considered. In fact, if consecutive stamping operations are to be properly simulated, the cooling of the tools during the idle time, the time required for unloading-loading the blank, needs to be considered. Therefore, the convection due to the internal cooling of the tools and the heat transfer between blank and tools, as well as the heat transfer taking place during the blank change were estimated for the first and second stages, respectively.

The cooling of the stamping tools is achieved by means of forced convection of water through their internal cooling channels. This phenomenon is characterized by the Convective Heat Transfer Coefficient (CHTC) and is given by equation (Eq. IV. 1) [Çengel, 2007], where *k* is the thermal conductivity of water, *Nu* the Nusselt number, and *D* the diameter of the channel.

$$CHTC = \frac{k \cdot Nu}{D} \qquad \textbf{(Eq. IV. 1)}$$

The Nusselt number for transitional flows (2300 ≤ *Re* ≤ 10000) is given by the Gnielinski equation (Eq. IV. 2), where the friction factor, *F*, can be determined from the Colebrook equation (Eq. IV. 3). Both parameters are highly influenced by the Reynolds number, *Re*, given by equation (Eq. IV. 4) [Çengel, 2007], where *Pr* is the Prandtl number of the water, ρ is the density of the cooling water, *V* is the mean velocity of the fluid, μ is the dynamic viscosity of the cooling water and ε is the surface roughness.

$$Nu_F = \frac{(F/8)\cdot(Re-1000)\cdot Pr}{1+12.7\cdot(F/8)^{0.5}\cdot(Pr^{2/3}-1)} \quad \textbf{(Eq. IV. 2)}$$

$$\frac{1}{\sqrt{F}} = -2.0\cdot log\left(\frac{\epsilon/D}{3.7}+\frac{2.51}{Re\cdot\sqrt{F}}\right) \quad \textbf{(Eq. IV. 3)}$$

$$Re = \frac{\rho\cdot V\cdot D}{\mu} \quad \textbf{(Eq. IV. 4)}$$

Considering the geometry of the cooling ducts (Table IV. 6) and taking the properties of the water at 20 ˚C as a reference, shown in Table IV. 8, the CHTC was calculated. The geometric parameters in the present study were selected according to previous works performed by other authors [Hu, 2013; He, 2016; Fernandez, 2019].

Table IV. 8 Properties of water taken as reference in the present study [Çengel, 2006].

Properties	Value
Thermal conductivity of water at 20˚C (*k*)	0.598 $W\cdot m^{-1}\cdot K^{-1}$
Density of water at 20˚C *(ρ)*	998 $kg\cdot m^{-3}$
Dynamic viscosity of water at 20˚C *(μ)*	0.001 $kg\cdot m^{-1}\cdot s^{-1}$
Prandtl number of water at 20˚C *(Pr)*	7.01

The surface roughness (ε) needs to be estimated for the calculation of the friction coefficient, according to equation (Eq. IV. 3). This parameter depends on the manufacturing process employed. Therefore, different values were used for each case studied. For the stamping tools manufactured by additive manufacturing, the surface roughness was experimentally measured by means of a Taylor Hobson Talysurf Series 2 surface profiler, obtaining a 3.11 µm Ra value. On the other hand, in the case of conventionally manufactured tools (drilled cooling ducts), surface roughness values from the literature were taken as reference. Coldwell et al. [Coldwell, 2003] concluded in their work that the surface roughness ranges between 0.14 and 0.48 µm when drilling AISI H13 tool steel. Thus, an intermediate Ra value of 0.31 µm was considered for the present study. On that account, the value for both CHTCs was obtained, 4782.1 $W\cdot m^{-2}\cdot K^{-1}$ and 4736.7 $W\cdot m^{-2}\cdot K^{-1}$, for additively built up and conventionally manufactured tools, respectively.

The heat transfer between the blank and the tool is another factor that needs to be addressed in order to obtain more accurate and realistic results. This phenomenon is characterized by the Interfacial Heat Transfer Coefficient (IHTC), which is highly dependent on the exerted contact pressure. Many authors have experimentally correlated the heat transfer coefficient and the contact pressure in hot stamping processes, as reported by Hung et al. [Hung, 2014]. In the present study, the correlation proposed by Hu et al. [Hu, 2013] was taken as reference. Considering a 15 MPa contact pressure, the interfacial heat transfer coefficient was estimated to be around 3000 $W \cdot m^{-2} \cdot K^{-1}$ based on the aforementioned approximation.

In addition, an estimation of the time period corresponding to the quenching process was required, that is, the cooling time of the blank in the closed tools. As reported in the literature, the cooling time in closed tools is about 20 s for similar structures [Hoffmann, 2007; Naganathan, 2012; Muvunzi, 2018].

Regarding the second stage of the hot stamping operation, the heat exchange that the tools are subjected to needed to be modeled. In the present study, two heat exchange mechanisms were considered:

- The forced convection of the cooling water through the ducts.
- The natural convection that the free surfaces of the tools are exposed to.

In order to characterize the natural convection between the tools and the air, a convective heat transfer coefficient was estimated. According to Çengel [Çengel, 2007], typical values for the heat transfer coefficient in the free convection of gases ranges from 2 to 25 $W \cdot m^{-2} \cdot K^{-1}$. Hence, an intermediate value of 15 $W \cdot m^{-2} \cdot K^{-1}$ was considered for the simulations. Finally, based on the study of Caron et al. [Caron, 2014], the time required for unloading-loading the blank was estimated to be 10 s.

IV.3.3. Results and discussion

Employing different cooling system designs within the stamping tools has a direct impact on both the blank and the tools themselves. As far as the blank is concerned, conformal cooling channels help to reduce inhomogeneities in the temperature field, such as hot spots. The temperature distributions of two blanks after 30 stamping cycles, corresponding to straight and conformal cooling systems, are shown in Figure IV. 21. As can be appreciated, by incorporating conformal cooling channels, hot spots were reduced, which ensures a more homogeneous quenching and enhances the quality of the process.

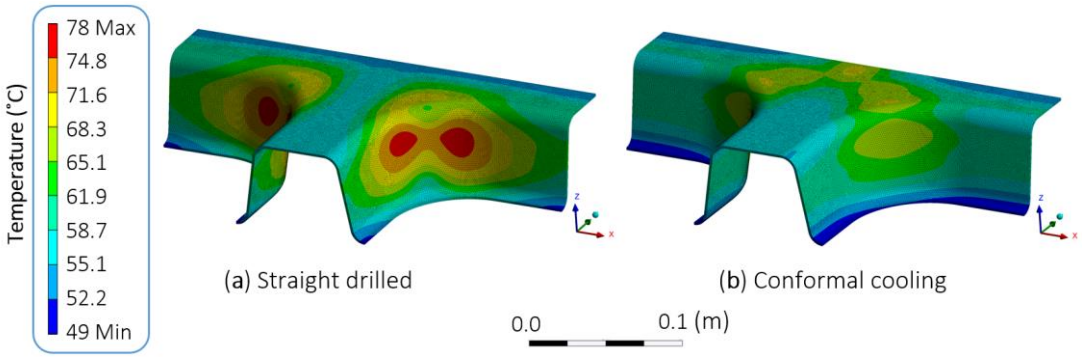

Figure IV. 21 Temperature field of the blank after the 30th consecutive stamping operation: (a) straight drilled; (b) conformal cooling channels.

With regard to the tools, and in order to evaluate the influence of the different cooling channel geometries studied, the temperature evolution of the tools after each stamping operation is shown in Figure IV. 22a. Both maximum and mean temperatures of the tools are represented, which gives information regarding the process stability, as well as the maximum temperatures of the tool, located at the contact region with the blank.

On the other hand, the differences between the highest and the lowest temperatures encountered in the stamped blank after every 20 s operation time for the different case studies are shown in Figure IV. 22b. As can be seen, the process tends to stabilize after 20 cycles approximately, and when conformal cooling is used, lower temperature differences, that is, much more homogeneous temperatures are achieved.

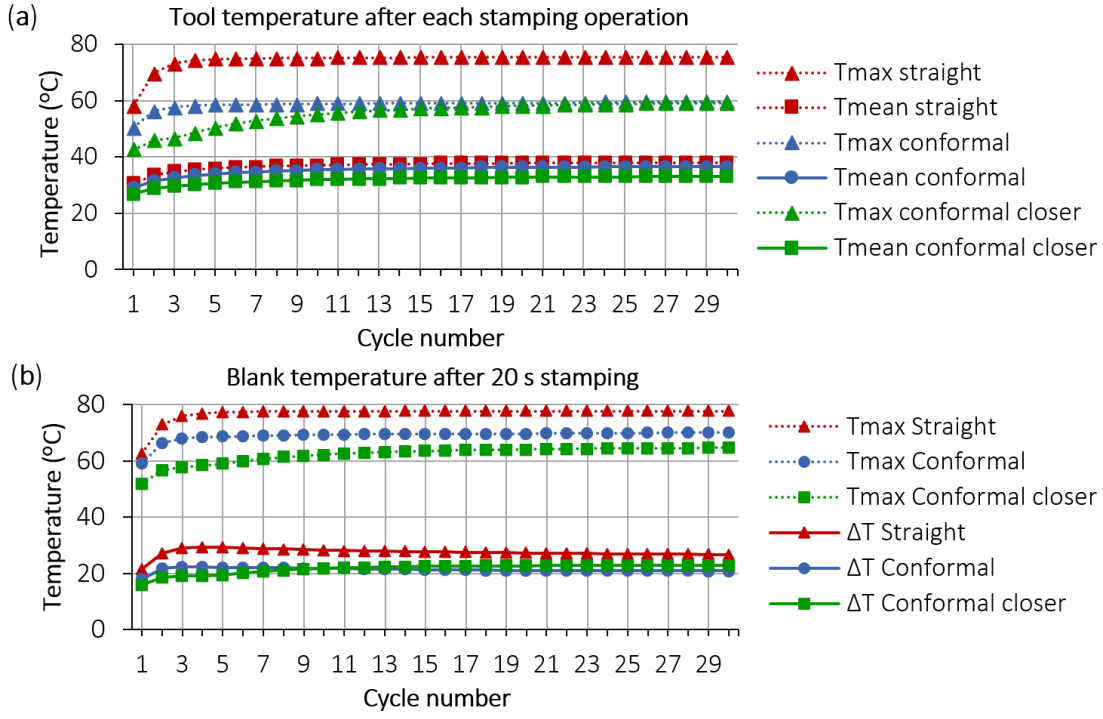

Figure IV. 22 Temperature evolution diagrams: (a) Tool temperature after each stamping operation; (b) Maximum temperature and temperature differences of the blank after 20 s stamping.

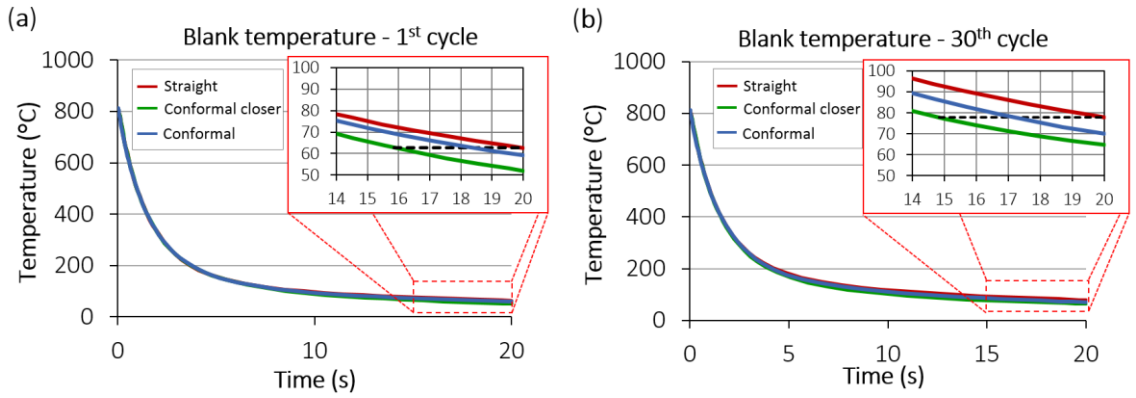

Figure IV. 23 Temperature evolution of the blank during the (a) 1st stamping; (b) 30th stamping operation.

The lower tool temperature at the beginning of every stamping operation, as well as a more homogeneous temperature distribution, results in a shorter quenching cycle time. In Figure IV. 23, the time required for the 30th stamped blank to reach a temperature below 80 ˚C is shown. As can be seen, in the case of conformal cooling, a cycle-time reduction of 3 s is obtained, whereas when the cooling channels are positioned closer to the surface a time reduction of 5 s is attained, which leads to a 25% productivity increase. In Figure IV. 24, the thermal field at the end of the 30th cycle in case study 3 is shown.

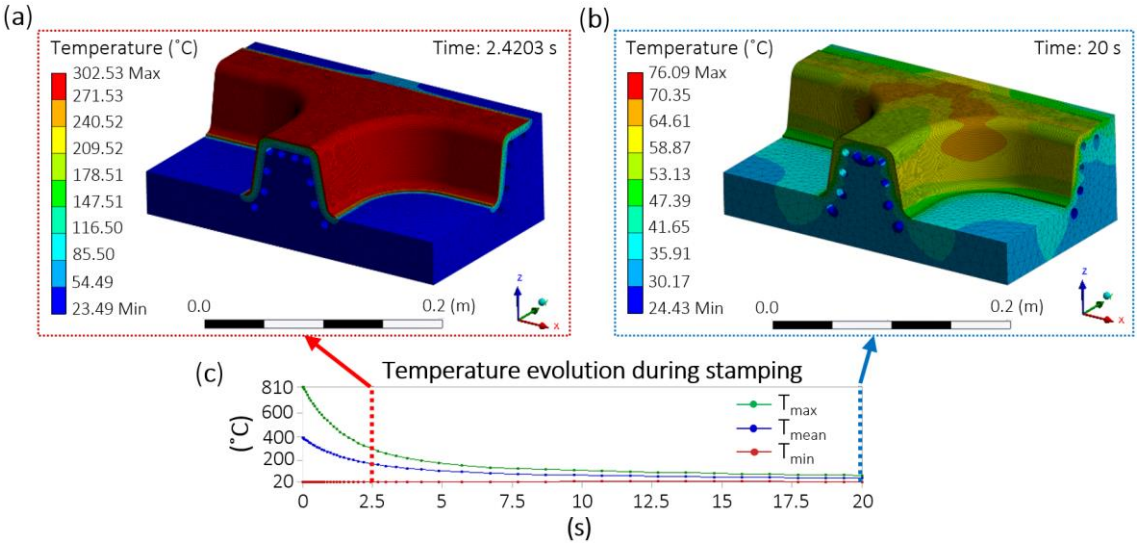

Figure IV. 24 Temperature field of case study 3 along the 30th cycle: (a) t=2.4203 s; (b) t=20 s; (c) temperature evolution during stamping.

IV.4. Conclusions

In the present chapter, the application of conformal cooling channels in hot stamping tools has been investigated. On the one hand, the manufacturability of this kind of channels by means of LMD has been studied and their mechanical performance and heat transfer capability compared to conventionally drilled ducts have been evaluated. On the other hand, the benefits that conformal cooling channels offer in terms of temperature homogeneity and cycle-time

reduction have been determined. According to the obtained results, the following conclusions were drawn:

- It can be concluded that the strategy of generating cooling channels via LMD is a viable alternative to traditional techniques in terms of metallurgical quality, mechanical behavior and thermal characteristics achieved in the manufactured tool. Previous experiments performed with this approach demonstrated the possibility of obtaining minimum channel diameters of down to 3 mm and minimum wall thicknesses of 2 mm.
- Apart from meeting the mechanical requirements demanded by the hot stamping process, the built-up channel was smooth and without projected material, leading to good internal quality. In addition, the lack of pre- and post-heating cycles during the LMD process together with the absence of inserts for the generation of the channel ease the process as far as industrialization issues are concerned.
- With regard to thermal characteristics, a more homogeneous temperature distribution within the tool and the stamped part was attained, leading to the enhancement of the dimensional accuracy and features of the produced parts. Moreover, the betterment of the temperature distribution also led to the lowering of the process cycle times in hot stamping and the subsequent improvement of the efficiency of the process and reduction of the costs.
- As far as tools temperature is concerned, the maximum temperatures were reduced by positioning the cooling channels close to the surface. Therefore, conformal cooling channels would enable to increase the service life of the tools. Nevertheless, it must be considered that if the cooling channels are too close to the surface, the temperature gradients resulting in the blank during the stamping process may increase.
- In addition, for the case analyzed, conformal cooling enables to reduce the cycle time by 3 s when compared to the straight-drilled tool, which implies a 15% time reduction. Besides, positioning the conformal cooling channels closer to the surface implies a 5 s cycle-time reduction, which involves a 25% time reduction.
- Finally, it is concluded that the performance of the hot stamping process evolves as the cycle number increases until a stable regime is obtained. Therefore, in order to evaluate the real effect of the use of conformal cooling on the stamping process, consecutive cycles must be considered.

Hence, this work demonstrated the capability of achieving good mechanical and thermal properties for additively manufactured conformal cooling hot stamping tools. Therefore, the

advances in LMD processes open doors for new designs, which may enable the generation of more complex geometries and hence innovate towards the manufacturing of new parts.

Chapter V. Bimetallic hot stamping tools

Chapter V. Bimetallic hot stamping tools

In the present chapter, a comparison between a conventionally manufactured AISI H13 hot stamping tool and a bimetallic tool is performed. The proposed bimetallic tool consists of a structural steel (AISI 1045) core and a tool steel (AISI H13) coating deposited using LMD. First, the material compatibility and quality of the deposited tool steel are analyzed. Besides, the mechanical properties are evaluated and compared with those of cast material. Special attention is given to the measurement of the effective thermal diffusivity of the deposited material. Last, the impact of effective thermal conductivity of the deposited material on the hot stamping process is analyzed with the aid of thermal simulations.

V.1. Introduction

As indicated in Chapter II, the thermo-physical properties of stamping tools greatly influence the hot stamping process. In this way, higher thermal conductivity results in increased heat transfer between blank and tool, thus reducing cooling time and subsequent cycle times. As a result, the use of highly conductive tool steels to manufacture the stamping tools contributes to the cost-effectiveness of the process.

Nevertheless, the tool steels from which hot stamping tools are manufactured are high-priced materials that lead to expensive manufacturing costs. In addition, thermal conductivity is one of the properties that must be considered along with others such as hardness or corrosion resistance. The LMD is an extensively used process for coating parts with minimum heat affection. Due to the high availability of materials that can be deposited, it is a suitable technology for coating complex components with a wide variety of components in several industries. Because of this juncture, hot stamping is an application where it is advantageous to manufacture tools using cost-effective, easy-to-fabricate steels, with their surface properties enhanced by laser cladding of highly alloyed steels.

In this chapter, the suitability of employing the LMD technology to manufacture bimetallic hot stamping tools by coating structural steels with tool steels has been analyzed. In addition, the effective thermal diffusivity of the deposited tool steel has been quantified. On the one hand and as far as the bimetallic tools are concerned, the quality of the deposited material has been first evaluated. The resulting mechanical and thermal properties have been then analyzed. Once the bimetallic tools have been studied and their correct performance has been ensured, the real advantages in terms of improved productivity have been quantified in comparison with conventional tools. On the other hand, the effective thermal diffusivity of laser metal deposited AISI H13 has been determined and compared with cast AISI H13. Besides, a case study that

illustrates the impact of considering or neglecting the effective thermal conductivity of the deposited material on the hot stamping process has been analyzed.

V.2. Methodology of analysis of bimetallic hot stamping tools

The main objective of the present research work was to evaluate the suitability of additively manufactured bimetallic hot stamping tools and determine the advantages that the material combination offers. For this purpose, the methodology shown in Figure V. 1 was employed:

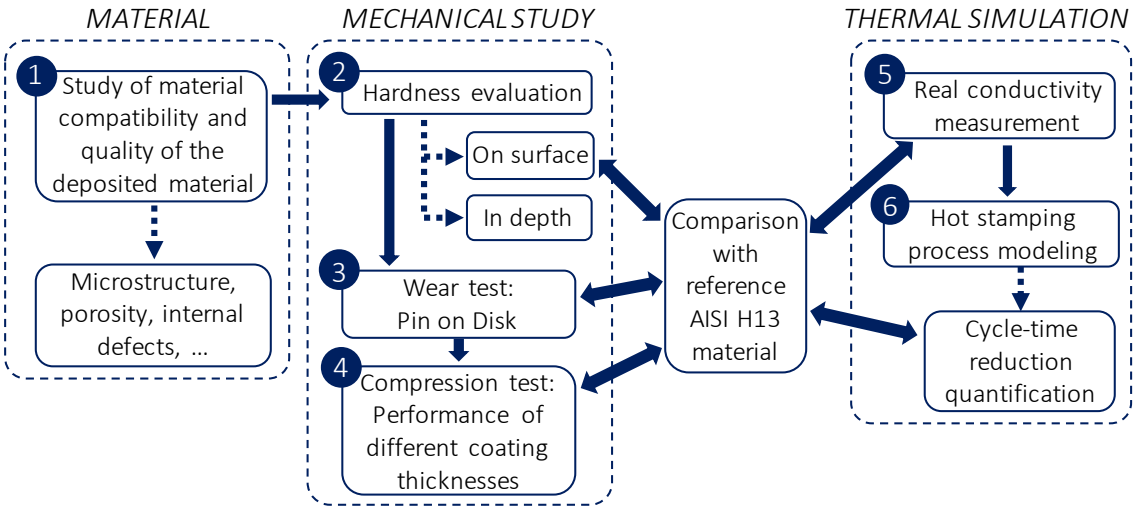

Figure V. 1 Diagram of the employed methodology for the analysis of bimetallic hot stamping tools.

1. Experimental analysis of the deposition of AISI H13 tool steel over AISI 1045 structural steel and study of the quality of the deposited material considering several aspects: dilution, proper bonding between layers, porosity generation and microstructure.

2. Hardness evaluation, measured both superficially and in the cross-section of the sample; that is, at different depths across the deposited layers, finally reaching the substrate. In this way, the variation of hardness as a function of depth could be analyzed. Obtained values were compared with reference hardness measured on a cast AISI H13 block.

3. In hot stamping, wear is the main factor affecting the service-life and maintenance needs of tools. In order to investigate the tribological behavior of the deposited AISI H13 tool steel, a pin-on-disk test was performed. The same test was conducted over a cast AISI H13 block so that a reference wear value was attained, and a comparison between results could be made. In addition, the friction coefficient was also determined.

4. Stamping tools must withstand the mechanical stress applied by the press and their subsequent contact pressures. In this regard, and in order to mechanically validate the bimetallic tool, compression tests were performed. Different AISI H13 coating

thicknesses were tested, and results were compared with those of the reference AISI H13 tool steel material.

5. In order to determine the effective thermal conductivity of the laser-deposited AISI H13, its effective thermal diffusivity was measured. The obtained results allowed the thermal model to be fed with the effective thermal conductivity value of the deposited AISI H13.

6. An analysis of the cycle-time reduction was performed by means of thermal modeling of the hot stamping process. Different AISI H13 coating thicknesses were analyzed and, additionally, the evolution of hot spots and temperature variations in the stamped blank were also evaluated.

V.3. Additive Manufacturing of bimetallic hot stamping tools

V.3.1. Materials and methods

In order to analyze the suitability of the LMD process to manufacture bimetallic tools, a series of experimental tests were performed. In the experimental tests, AISI 1045 (DIN 1.1191) and AISI H13 (DIN 1.2344) were used as the base and filler materials, respectively. AISI 1045 is a medium-carbon steel commonly used in structural parts requiring high strength and hardness, whose thermal conductivity is approximately twice that of AISI H13. Besides, AISI 1045 can be considered as a cost-effective material. The chemical compositions of the employed materials are listed in Table V. 1.

Table V. 1 Chemical composition (wt. %) of AISI 1045 [Gao, 2014] and AISI H13 [FST, 2019].

Material	C	Si	Mn	Cr	Mo	V	Fe
AISI 1045	0.45	0.24	0.8	0.16	-	0.02	Balance
AISI H13	0.41	0.80	0.25	5.12	1.33	1.13	Balance

In order to evaluate the quality of the deposition of AISI H13 over AISI 1045, coatings of approximately 7 mm thickness were deposited using the process parameters detailed in section III.2.1. The build-up strategy selected was a zigzag pattern, alternating longitudinal and transversal directions for the deposition of successive layers. The deposition direction was switched 90° between consecutive layers in order to reduce anisotropy. Following the same procedure, coatings of 1, 3 and 5 mm thick were also deposited over a 200 x 120 x 40 mm^3 substrate in order to enable performing further analyses.

V.3.2. Results and discussion

1. Metallographic analysis

First, the feasibility of depositing AISI H13 metallic powder over an AISI 1045 substrate needed to be approached. To that end, a metallographic analysis was performed, five different cross-sections were extracted, polished and etched using Marble reagent so that their macro- and microstructure were revealed. After that, they were analyzed by using the Leica DCM3D microscope. The images acquired were used both for identifying internal defects within the deposited material and for performing a porosity analysis.

The results of such analysis are presented in Figure V. 2 below. The lighter upper zone is the melted area during the deposition of the top layer. In details 1 and 2, the bonding between adjacent layers is shown. As can be witnessed, neither cracks nor lack-of-fusion regions were detected. In detail 3, the microstructure of a central region in a clad is shown, where columnar dendrites can be seen. The dendrites grow along the direction of the highest temperature gradient, usually perpendicular to the clad boundary. Last, in detail 4, the transition between the AISI 1045 substrate and the deposited AISI H13 is shown. The zone affected by the additive process is minimal, and good penetration is ensured, which guarantees a sound metallurgical bonding. The microstructure of the base material remains unaffected after the LMD process.

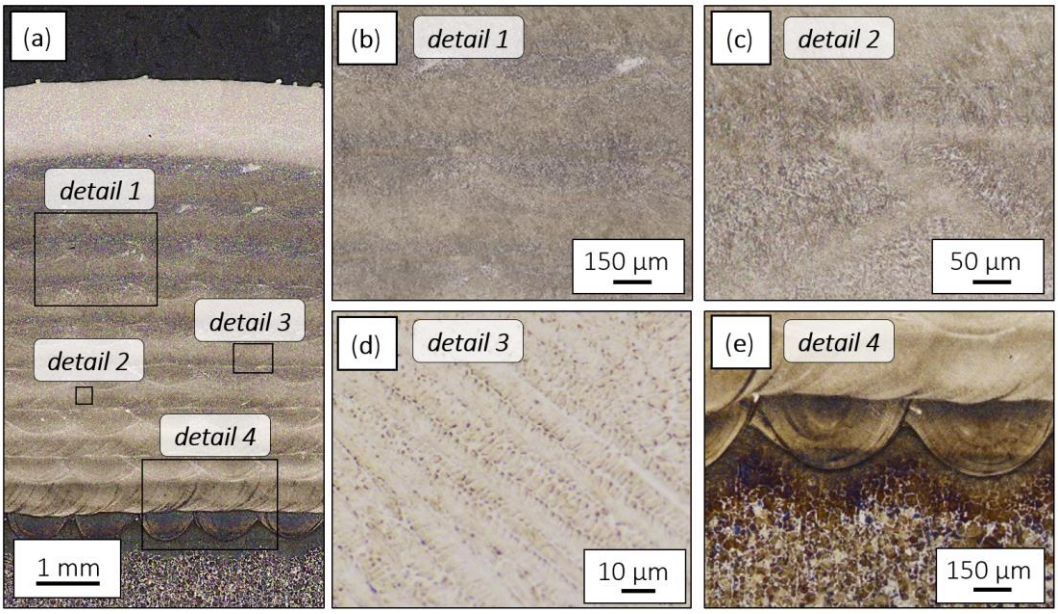

Figure V. 2 Metallographic analysis of the tests.

After that, in a second step, the porosity of the five cross-sections extracted was analyzed. In each case, an area of 5 x 8 mm^2 was studied by means of the Image Processing Toolbox from the Matlab R2019b software, so that both the percentage and size of the pores in the region of the

deposited material could be determined. Each pixel corresponded to a 12.5 x 12.5 µm^2 area, which determined the minimum size of the pores that the software could detect.

An example of the post-processed image of a cross-section is presented in Figure V. 3a, where the areas with material are displayed in white, and those with no material are represented in black. Additionally, micrographs of pores of different sizes are detailed in Figure V. 3b and c. Last, the collected results are included in the graph shown in Figure V. 3d, which represents the pore size distribution with regard to the total porosity measured. Despite single porosity values being measured, they are connected with straight lines in order to make the obtained results more understandable. In this way, blue lines correspond to the five cross-sections analyzed, and the red one is the average value. In all cases, the pore size remained below 150 µm diameter.

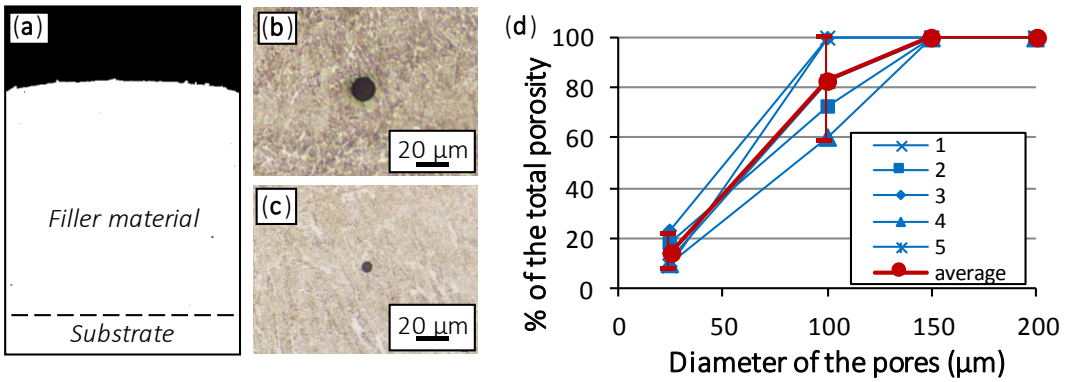

Figure V. 3 (a) Post-processed image of a cross-section; (b), (c) details of pores; (d) total porosity as a function of pore size.

The total porosity and pore-size distribution as a function of the total porosity values measured in each cross-section are detailed in Table V. 2. An average total porosity of 0.219% was obtained, which means that the deposited material was more than 99.75% dense. In terms of pore-size distribution, in all cases, the pores detected had a diameter of less than 150 µm and, on average, 83.2% of the pores had a diameter of less than 100 µm and the 14.4% of less than 25 µm.

Table V. 2 Porosity analysis results.

Test	Total porosity (%)	Pore-diameter distribution (%)			
		<25 µm	<100 µm	<150 µm	<200 µm
1	0.213	9.30	100	100	100
2	0.258	18.5	72.8	100	100
3	0.252	23.1	100	100	100
4	0.183	9.80	60.3	100	100
5	0.192	11.5	82.8	100	100
Average	**0.219**	**14.4**	**83.2**	**100**	**100**

The metallographic analysis manifested a high-quality deposition of AISI H13 tool steel over AISI 1045, free of cracks. The bonding between both the deposited material and the substrate, and that between adjacent deposited layers was sound. Besides, no lack of fusion was detected.

Thus, the metallurgical quality of the deposited material met any quality requirement for tooling, and the compatibility between both materials demonstrated satisfactory results. Therefore, the suitability of combining AISI H13 and AISI 1045 in the same part was demonstrated.

2. Hardness tests

Hardness was measured both superficially and in-depth across the deposited layers. On the one hand, average hardness values of 56.5, 53.8 and 53.2 HRC were measured for the surfaces of 1, 3 and 5-mm-thick coatings deposited, respectively. In all cases, attained hardness was higher than 50 HRC, which is the minimum hardness value required in hot stamping applications. Additional measurements were also performed on the cast AISI H13, resulting in an average hardness value of 56.0 HRC. These average values were calculated after ten measurements, as shown in Table V. 3.

Table V. 3 Hardness values for the different coating thicknesses.

Test	Hardness (HRC)			
	Cast AISI H13	Coating thickness		
		1 mm	3 mm	5 mm
1	56.0	59.1	54.1	53.2
2	55.6	55.6	52.9	52.7
3	54.9	54.7	53.1	53.2
4	55.6	56.5	54.2	52.1
5	55.6	57.0	55.9	52.9
6	56.7	57.4	51.8	54.0
7	56.2	55.8	54.1	53.6
8	56.4	55.8	54.0	53.9
9	56.9	54.8	54.9	53.6
10	55.8	58.3	53.1	52.6
Average	**56.0**	**56.5**	**53.8**	**53.2**

On the other hand, micro-hardness measurements were performed on four cross-sections of a 7-mm-thick AISI H13 deposition. The values across the different layers of material are shown in Figure V. 4. In all sections analyzed, the deposited material presented a constant hardness higher than 55 HRC across its different layers. On the contrary, this value decreased until 20-25 HRC when the AISI 1045 substrate was reached. This was expected, as the hardness of the AISI 1045 medium-carbon steel is reported to be 220-250 HV, that is, 17-28 HRC [Gao, 2014].

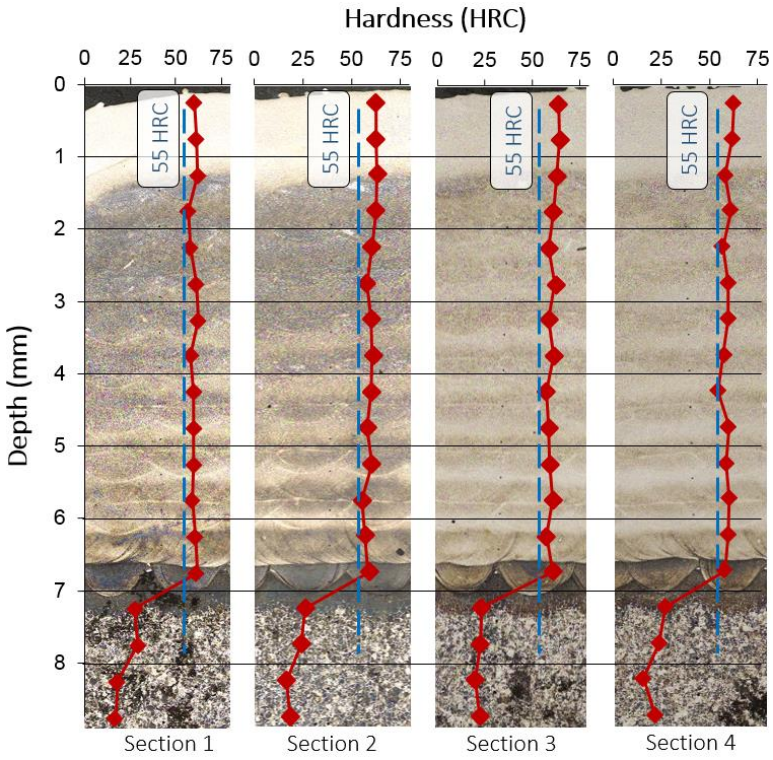

Figure V. 4 Hardness values of the deposited material and substrate.

Given the results, and considering the field of application of the present work, the hardness and micro-hardness values obtained were satisfactory in terms of the materials and technology employed. In addition, there was no need for additional heat treatment to attain the high hardness required in hot stamping tools. Moreover, hardness results maintained uniform values on the different surfaces and sections analyzed.

3. Friction and wear tests

In order to investigate the friction and wear behavior of the deposited AISI H13 coatings under sliding conditions, pin-on-disk tests were performed according to the ASTM G99 standard [ASTM, 2017] using a Microtest MT pin-on-disk tribometer, shown in Figure V. 5.

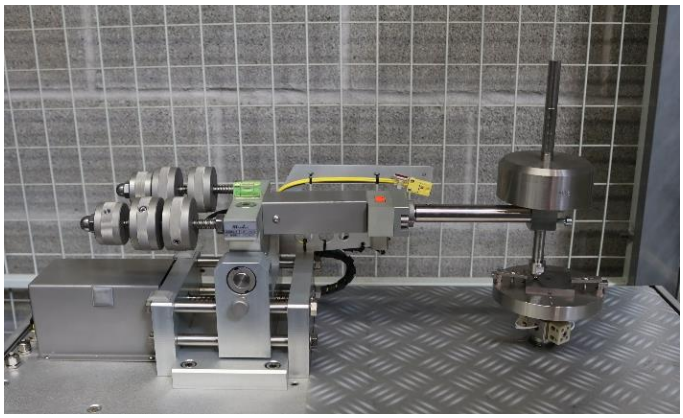

Figure V. 5 Microtest MT pin-on-disk tribometer.

A tungsten carbide spherical pin with a diameter of 6.0 ± 0.0025 mm supplied by Goodfellow was used for the tests, while the counter surface was made of AISI H13 tool steel. Tests were carried out at room temperature and the parameters were a load of 20 N, a sliding speed of 0.42 $m \cdot s^{-1}$ and a total distance of 1000 m. The specimens were ground in order to ensure their flatness and obtain an average roughness below 1 µm, the value recommended by the ASTM G99 standard [ASTM, 2017]. In each part, six measurements were performed using a Surtronic Duo Surface Roughness Tester from Taylor Hobson, three in the longitudinal grinding direction, Ra_L, and three in the transversal, Ra_T. The obtained results are shown in Table V. 4.

Table V. 4 Arithmetic average in microns of the roughness profile of the specimens before pin-on-disk tests.

Specimen	Ra_{L1}	Ra_{L2}	Ra_{L3}	Ra_{T1}	Ra_{T2}	Ra_{T3}	$Ra_{average}$
Reference AISI H13 tool	0.14	0.14	0.14	0.18	0.24	0.26	0.18
AISI H13 coating over AISI 1045 substrate	0.14	0.13	0.12	0.20	0.27	0.26	0.19

Prior to testing, and before measuring, the specimen was cleaned with acetone. After cleaning, the wear of the disk and the pin were measured using a Leica DCM3D confocal microscope. In the present case, both the disk and the pin wear were detected. Therefore, the wear suffered by the specimens was measured according to the material loss in the pin and the resulting groove on the surface of the material being tested. In the case of disk wear, the average wear-track profile was measured to obtain the track cross-section area, and multiplied by the average track length to obtain the disk wear volume. In the case of pin wear, the wear scar profile was measured in two orthogonal directions, to obtain the average profile and compare it with the original profile. In addition, the evolution of the coefficient of friction during the test was also analyzed. The results for the case of the laser-deposited AISI H13 coating are shown in Figure V. 6, in which the wear of both the coating and the pin are shown.

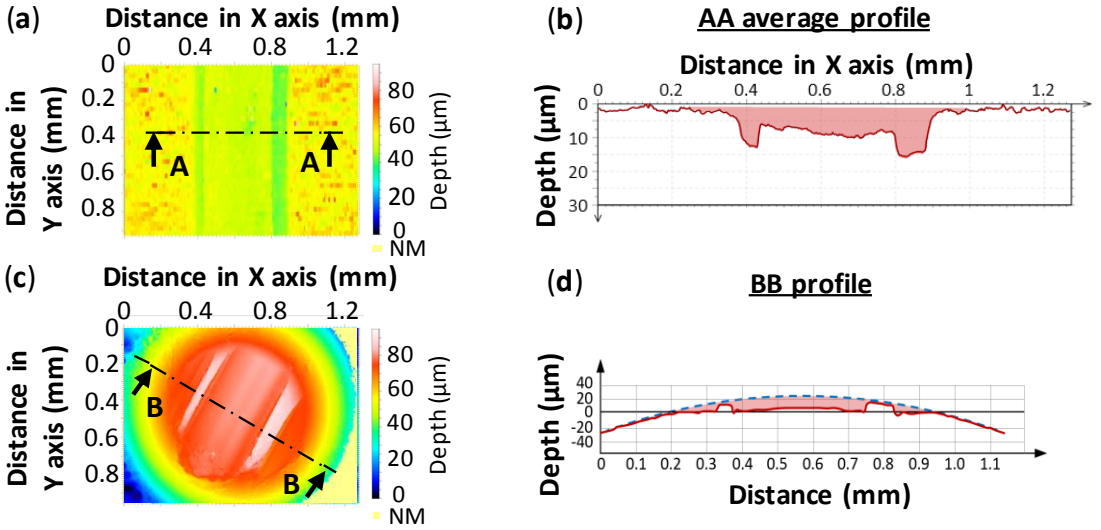

Figure V. 6 Results of the pin-on-disk tests for the (a), (b) AISI H13 coating and (c), (d) spherical pin.

Wear scar measurement was done in four representative locations of the disk surface, which were separated 90°. In each case, the 3D map of the surface was obtained by measuring multiple profiles, and the average profile was extracted as an average of 60 profiles. In each case, the width, depth, and area of the groove were measured using the Leica Map surface imaging and metrology software. Values shown in Table V. 5 represent the average of the four individual measurements. In the case of pin wear, the wear scar profile was directly extracted from the 3D map and average values were obtained, which are also detailed in Table V. 5. As can be noticed, the wear volume in both the specimen and the pin was slightly lower in the case of the laser-deposited AISI H13 coating.

Table V. 5 Pin-on-disk test results.

	Reference: Conventional AISI H13 tool	1 mm AISI H13 coating over AISI 1045 substrate	Difference (%)
Specimen wear			
Wear width (mm)	0.532	0.537	0.940
Wear depth (mm)	0.015	0.014	6.67
Area (mm^2)	$4.359 \cdot 10^{-3}$	$4.005 \cdot 10^{-3}$	8.12
Track radius (mm)	15	15	-
Wear volume (mm^3)	**0.411**	**0.377**	**8.27**
Pin wear			
Wear diameter (mm)	0.692	0.656	5.20
Pin diameter (mm)	6	6	-
Wear depth (mm)	0.018	0.017	5.55
Wear volume (mm^3)	**0.256**	**0.240**	**6.25**

The friction signals recorded during the wear test are shown in Figure V. 7. The signals present an initial metal-metal contact before stabilizing upon the formation of an interfacial layer on the pin surface due to the transfer of material from the disk, consisting of metal and oxide debris. In this way, the friction coefficient is first increased to the maximum value due to the static frictional force and then decreased in the stable stage. In comparison, the laser-deposited AISI H13 coating presented a longer starting stage (about 190 m) and a slightly lower maximum friction coefficient value (0.70) than the reference AISI H13 tool, which presented approximate values of 75 m and 0.75, respectively. After this stage, the friction coefficient of the LMD and the reference AISI H13 was lowered to average values of 0.57 and 0.55, respectively. Nevertheless, the final value for the LMD AISI H13 coating after 1000 m traveled distance was 0.61, which was slightly higher than that of the cast AISI H13 (0.58). In addition, the LMD AISI H13 signal showed more significant fluctuations than the reference AISI H13 test, which was attributed to the adhesive wear mechanism.

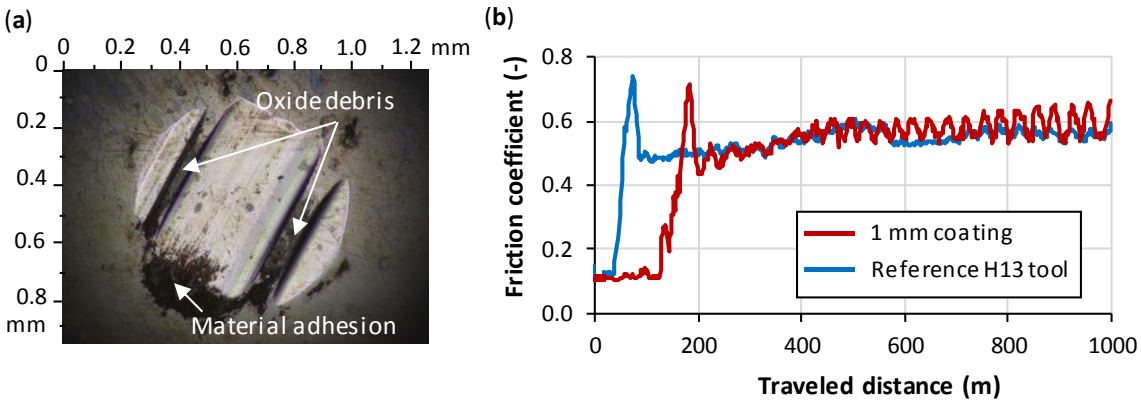

Figure V. 7 (a) Worn surface of the pin; (b) Friction coefficient results.

Therefore, it can be concluded that the friction and wear behavior of the laser-deposited AISI H13 tool steel and the AISI H13 reference were comparable.

4. Compression tests

Aiming to investigate the compression resistance of a bimetallic tool made of AISI 1045 and coated with AISI H13, three different coating thicknesses (1, 3 and 5 mm) deposited over a substrate of 200 x 120 x 40 mm^3 were subjected to compression tests. To that end, an Instron 8801 servohydraulic fatigue-testing machine was used, whose technical characteristics are detailed in Table V. 6.

Table V. 6 Technical characteristics of the Instron 8801 fatigue testing system used.

Feature	Value
Force capacity (kN)	±100
Stroke (mm)	150
Load weighing accuracy (%)	±0.002% of load cell capacity

In order to apply the desired pressures on a localized area of each coating thickness, a 12-mm-diameter stainless steel cylinder pin was used. Three different pressures were applied on each coating thickness: one according to the maximum pressure on service for hot stamping tools, 15 MPa, and another two with safety factors of two and three, thus resulting in pressure values of 30 and 45 MPa, respectively. In order to avoid any test interfering with others, each experiment was performed on a different specimen. In addition, the velocity employed was 40 $mm \cdot s^{-1}$, and the total duration of each test was 20 s, emulating hot stamping tools service conditions. The parameters of the tests are shown in Table V. 7.

Table V. 7 Performed compression tests.

Applied pressure (MPa)	Surface (mm^2)	Applied force (kN)
15	113.1	1.70
30		3.39
45		5.09

After performing the compression tests, the samples were first visually inspected and then analyzed by means of a Leica DCM3D confocal microscope, so that 3D maps of the areas subjected to the tests were generated.

The 1, 3 and 5 mm thick coatings deposited via LMD were tested and compared with the cast material. Results are presented in several graphs, where the evolution of the applied force as a function of both time and displacement on the executed tests is shown (see Figure V. 8).

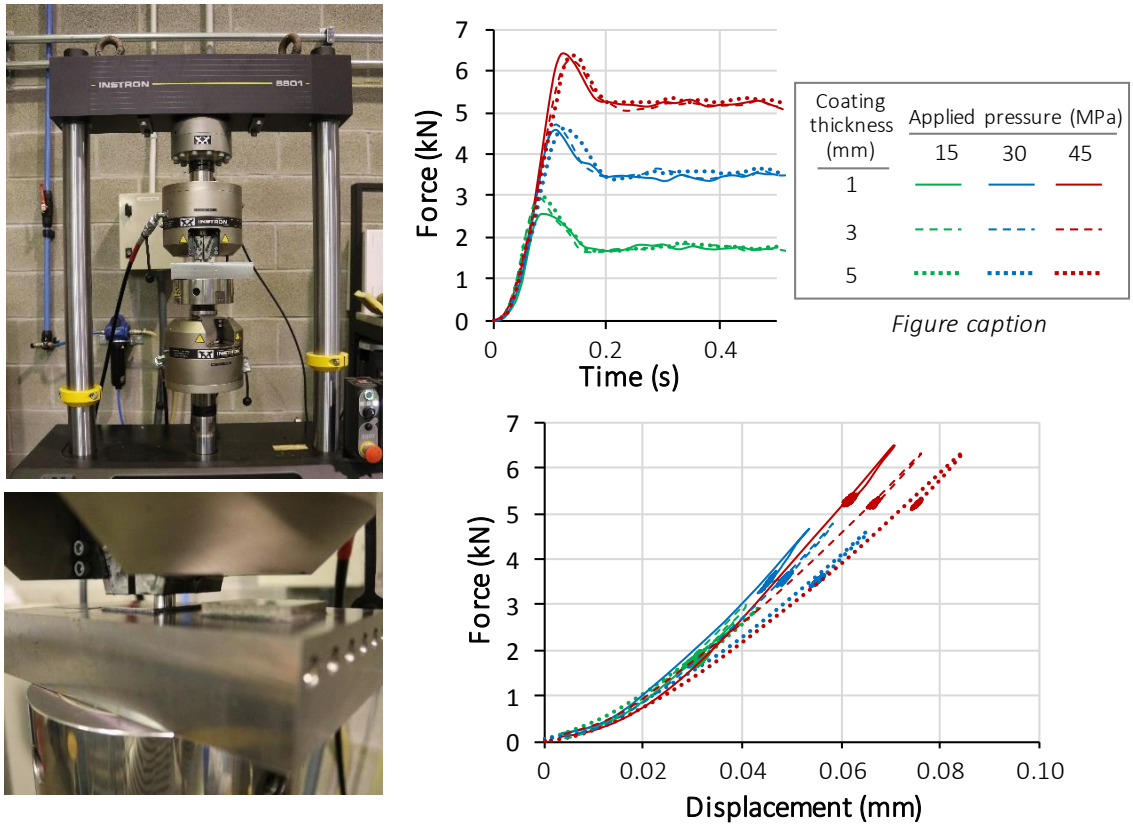

Figure V. 8 Set up (left) and results (right) of the compression tests.

On the other hand, when analyzing the graph where the force is represented as a function of displacement, other observations can be made. For each force value, each thickness behaves differently; that is, the thinner the coating, the lower is the displacement suffered to attain the desired force. In addition, each tested thickness presents a similar slope, regardless of the force applied.

In order to represent the behavior of bimetallic tools made of AISI 1045 and coated with AISI H13 versus conventional AISI H13 tools, a comparison of their performance at 30 MPa is shown in Figure V. 9a. On the one hand, 1 and 3 mm coatings behave similarly to the reference tool, which proves the suitability of bimetallic tools in these terms. On the other hand, the 5 mm coating presents a slightly higher deformation. Nevertheless, and after analyzing all the tested surfaces, both visually and by means of 3D-mapping with a Leica DCM3D confocal microscope, no changes or damage were detected on any specimen. In order to illustrate this matter, a 3D map of the 3-mm-thick coating tested under 30 MPa pressure is included in Figure V. 9b.

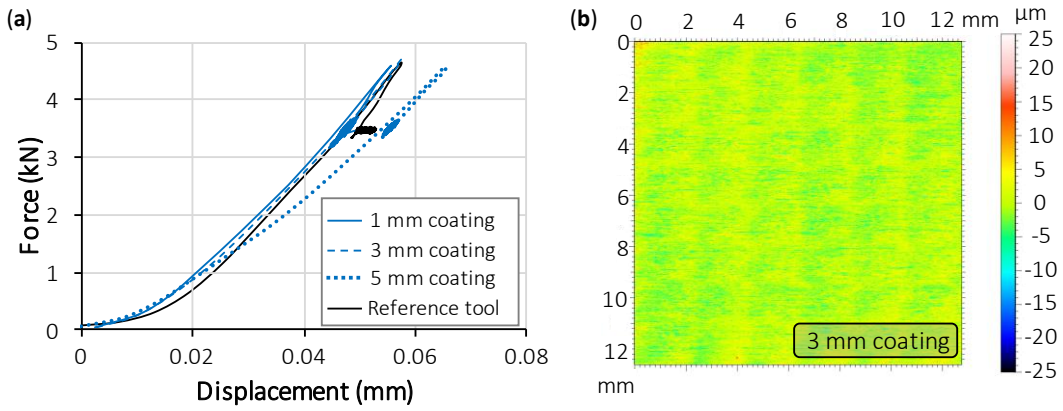

Figure V. 9 (a) Comparison with the reference tool; (b) 3D map of the 3 mm coating tested at 30 MPa.

Therefore, it was concluded that bimetallic tools coated via LMD withstood more than three times the service pressure required in hot stamping processes, which was set in 15 MPa. Nevertheless, obtained results depended on the deposited thickness, so that the best performance in terms of equivalency with the reference tool was attained with 1 and 3-mm-thick coatings.

V.4. Thermal modeling of the cooling capacity of the tools

V.4.1. 3D model geometry configuration

In order to determine the thermal behavior of the bimetallic tools, as well as the required stamping cycle-time to ensure the hardening of the stamped part, a thermal model was developed in the FEM software ANSYS Workbench 19.2 and the CFD solver Fluent was used. Aiming to determine the cooling capacity of the hot stamping tools with an AISI 1045 core and AISI H13 coating, simulations for different coating thicknesses (1, 3, 5 and 7 mm) were performed. An additional simulation for a conventionally manufactured AISI H13 tool set was also realized for further comparison with the coated specimens. The employed mesh consisted of approximately 850000 first-order elements with a maximum skewness below 0.6.

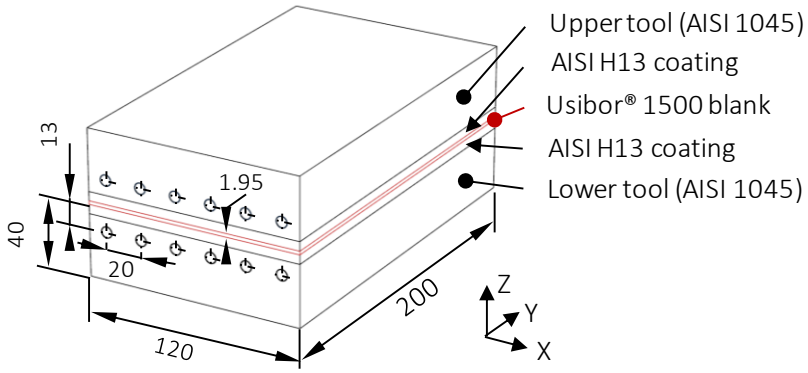

Figure V. 10 3D model geometry employed.

A 3D model comprising the upper tool, a boron steel blank, and the lower tool was developed, as shown in Figure V. 10. The total dimensions of the upper and lower tools were 200 x 120 x 40 mm^3, which included an AISI 1045 core and different AISI H13 coating thicknesses (1, 3, 5 or 7 mm) depending on each configuration to be studied. In addition, the tools were actively cooled by water; thus, each tool included six 6-mm-diameter ducts, which were located at 13 mm from the hot surface of the tools, and the distance between consecutive ducts was 20 mm. According to literature, a thickness of 1.95 mm was selected for the boron steel blank [Shapiro, 2009; Karbasian, 2010] which was made of Usibor® 1500 (22MnB5).

V.4.2. Governing equations

The commercial software ANSYS Fluent was employed to perform these simulations. A thermal transient simulation was carried out concerning the fluid-dynamic phenomena inside the cooling ducts. A turbulent flow was considered for the cooling water due to the variations in the velocity and pressure fields in both space and time, and therefore, the standard κ-ε model was employed in the simulations. The main transport equations on which the performed simulations were based are summarized below [Launder, 1972]:

$$\frac{\partial}{\partial t}(\rho k) + \frac{\partial}{\partial x_i}(\rho k u_i) = \frac{\partial}{\partial x_j}\left[\left(\mu + \frac{\mu_t}{\sigma_k}\right)\frac{\partial k}{\partial x_j}\right] + G_k + G_b - \rho\varepsilon - Y_M + S_k \quad \textbf{(Eq. V. 1)}$$

$$\frac{\partial}{\partial t}(\rho \varepsilon) + \frac{\partial}{\partial x_i}(\rho \varepsilon u_i) = \frac{\partial}{\partial x_j}\left[\left(\mu + \frac{\mu_t}{\sigma_\varepsilon}\right)\frac{\partial \varepsilon}{\partial x_j}\right] + C_{1\varepsilon}\frac{\varepsilon}{k}(G_k + C_{3\varepsilon}G_b) - C_{2\varepsilon}\rho\frac{\varepsilon^2}{k} + S_\varepsilon \quad \textbf{(Eq. V. 2)}$$

In equations (Eq. V. 1) and (Eq. V. 2), G_k represents the generation of turbulence kinetic energy due to the mean velocity gradients, G_b is the generation of turbulence kinetic energy due to buoyancy, and Y_M represents the contribution of the fluctuating dilatation in compressible turbulence due to the overall dissipation rate. Besides, σ_k and σ_ε are the turbulent Prandtl numbers for κ and ε, which are considered with the standard values of 1.0 and 1.3, respectively. $C_{1\varepsilon}$ and $C_{2\varepsilon}$ are user-defined constants, which in the present case take the values of 1.44 and 1.92, respectively. These values are the default ones proposed by Launder and Spalding [Launder, 1972], and are widely accepted. Finally, S_k and S_ε are user-defined source terms.

From the previous equations (Eq. V. 1) and (Eq. V. 2), the values of κ and ε can be obtained and, based on them, the turbulent viscosity μ_t is defined according to the following equation (Eq. V. 3), where the constant C_μ has a value of 0.09.

$$\mu_t = \rho \cdot C_\mu \frac{k^2}{\varepsilon} \quad \textbf{(Eq. V. 3)}$$

V.4.3. Material properties

The materials that took part in the present simulations are AISI 1045 medium-carbon steel, AISI H13 tool steel, Usibor® 1500 boron steel and water as a coolant of the tools. The default properties for water defined in the ANSYS Fluent materials database and shown in Table V. 8 were considered suitable. As the temperature difference between the water inlet and outlet was estimated to be below 10 ˚C [Lorenz, 2012], water properties were considered constant along the simulated process.

Table V. 8 Water properties, data from ANSYS Fluent database.

Properties	Value
Density ($kg \cdot m^{-3}$)	998.2
Specific heat ($J \cdot kg^{-1} \cdot K^{-1}$)	4182
Thermal conductivity ($W \cdot m^{-1} \cdot K^{-1}$)	0.6
Viscosity ($kg \cdot m^{-1} \cdot s^{-1}$)	$1.003 \cdot 10^{-3}$
Molecular weight ($kg \cdot kmol^{-1}$)	18.015
Standard enthalpy ($J \cdot kmol^{-1}$)	$-2.858 \cdot 10^{-8}$
Standard entropy ($J \cdot K^{-1} \cdot mol^{-1}$)	$6.990 \cdot 10^{-4}$
Surface tension ($N \cdot m^{-1}$)	$7.194 \cdot 10^{-2}$

Regarding AISI 1045, AISI H13 and Usibor® 1500, the density values for steel defined by default in ANSYS Fluent were initially set, that is, 8030 $kg \cdot m^{-3}$. Thermal properties such as the specific heat and thermal conductivity were modified to be temperature dependent, as detailed in Table V. 9.

Table V. 9 Thermal properties of AISI 1045, AISI H13 and Usibor®1500 [Gao, 2014; Oh, 2019; Shapiro, 2009].

Material	Thermal properties	Temperature (K)					
		293	473	673	873	1073	1273
AISI 1045	Specific heat ($J \cdot kg^{-1} \cdot K^{-1}$)	475	495	565	700	700	700
	Thermal conductivity ($W \cdot m^{-1} \cdot K^{-1}$)	47.6	40.4	36.2	32.0	32.0	32.0
AISI H13	Specific heat ($J \cdot kg^{-1} \cdot K^{-1}$)	461	475	519	592	592	592
	Thermal conductivity ($W \cdot m^{-1} \cdot K^{-1}$)	24.9	27.4	29.1	28.5	28.5	28.5
Usibor® 1500	Specific heat ($J \cdot kg^{-1} \cdot K^{-1}$)	444	520	563	581	590	603
	Thermal conductivity ($W \cdot m^{-1} \cdot K^{-1}$)	30.7	30.0	21.7	23.6	25.6	27.6

V.4.4. Thermal diffusivity of LMD AISI H13

The employment of thermal conductivity values obtained from the literature is an accepted customary practice when modeling the thermal behavior of the hot stamping process. Nevertheless, due to the directional nature of the LMD process and the fact that the desired geometry is obtained by overlapping successive clads and layers, the real thermal conductivity of the as-deposited material may differ from that obtained via casting. In fact, it has been reported that thermal conductivity can be decreased by volume defects, such as cracks and porosity, which lower the density of the material. In addition, a high number of dislocations and grain boundaries in the microstructure can also lead to lower thermal diffusivity values [Zhang, 2016; Marinelli, 2019].

Therefore, in order to define the thermal conductivity of the deposited AISI H13 tool steel, the thermal diffusivity was experimentally measured. The measurements were performed at different planes situated at 2, 4 and 6 mm from the surface of the substrate. Thermal conductivity, k, and thermal diffusivity, α, are related according to equation (Eq. V. 4), where ρ and c_p represent the density and specific heat of the material, respectively.

$$\alpha = \frac{k}{\rho \cdot c_p} \qquad \textbf{(Eq. V. 4)}$$

The measurement and analysis of the effective thermal diffusivity of LMD AISI H13 are presented in detail in section V.5.

V.4.5. Boundary and initialization conditions

Regarding the cooling water flow, a pressure of 0.3 MPa was defined as a boundary condition for the water inlet into the cooling ducts of the tools. This led to a water velocity in the conducts of above 1 $m \cdot s^{-1}$ so that the Reynolds number was higher than 2300 and a turbulent regime was guaranteed [Lin, 2014; Shan, 2013]. The quenching time of the stamping process was estimated to last 20 s [Naganathan, 2012]. As far as the initialization parameters are concerned, at the beginning of each stamping operation, the water in the cooling ducts was at room temperature (298 K) and the hot blank at 1200 K [Lin, 2014; Lv, 2016; Shan, 2013; Shapiro, 2009].

Regarding the temperature of the tools, two sets of initialization parameters were selected to distinguish between the hot stamping of the first blank and the following ones, and thus adjust the simulation to actual production circumstances. In this way, the stamping tools were considered to be at room temperature, 298 K (25 °C) before stamping the first blank, whereas

their temperature was increased until 348 K (75 °C) [Shapiro, 2009] to simulate a stable-regime hot stamping process.

V.4.6. Results and discussion

1. Experimental thermal conductivity measurement of the deposited AISI H13

The experimental thermal diffusivity value of the deposited AISI H13 was measured at 20 °C, attaining a value of 5.72 $mm^2 \cdot s^{-1}$. This value was slightly lower than that provided by manufacturers. The main reasons for this are the microstructure and different grain solidifying directions developed within the deposited material. These grain boundaries work as thermal barriers, thus reducing thermal diffusivity.

Based on the experimental measurement of the diffusivity performed and using equation (Eq. V. 4), the thermal conductivity value for the deposited AISI H13 tool steel was calculated, which resulted in 20.70 $W \cdot m^{-2} \cdot K^{-1}$. Since this value was 16.87% lower than the thermal conductivity of AISI H13 at 20 °C supplied by manufacturers and considered in Table V. 9, the thermal conductivity of AISI H13 deposited via LMD was subsequently modified in the simulations. In this way, the corrected thermal conductivity value for deposited AISI H13 was 83.13% of the values supplied for the cast AISI H13. Thermal conductivity values used in the simulations are detailed in Table V. 10.

Table V. 10 Experimentally determined thermal conductivity of the LMD AISI H13.

Material	Property	Temperature (K)					
		293	473	673	873	1073	1273
LMD AISI H13	Thermal conductivity ($W \cdot m^{-1} \cdot K^{-1}$)	20.7	22.8	24.2	23.7	23.7	23.7

2. Estimation of the cycle-time reduction

Two different thermal situations were simulated: on the one hand, the stamping tools were considered at room temperature (298 K) before stamping the first blank; on the other hand, a stable hot stamping process situation where the tools were initially at 348 K (75 °C). The results analysis is focused on the case where the tools are initially at 348 K (75 °C), as these are considered more restrictive and representative of long working situations. In Figure V. 11, the maximum temperature of the blank during the cooling stage is shown for the different coating thicknesses simulated in the present case.

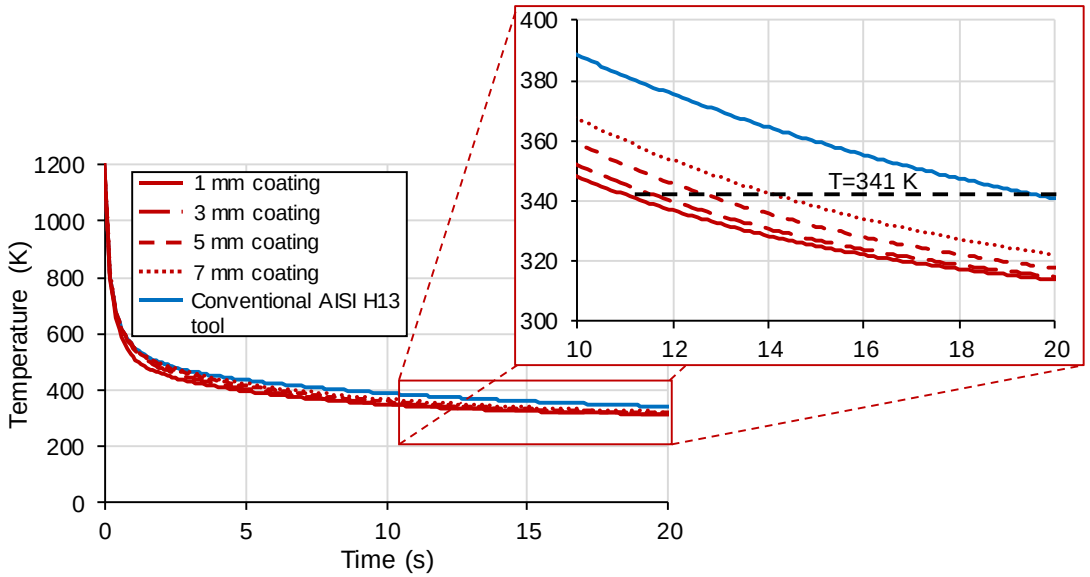

Figure V. 11 Maximum temperature of the blank (left); detail of the cycle-time reduction (right).

On the one hand, when conventional AISI H13 tools were considered, the temperature of the blank at the end of the stamping operation, that is, after 20 s of simulation, was 341 K (68 °C). This temperature has been set as a reference value for the rest of the simulations. In that way, the cooling time required to reach 341 K has been estimated for the three different coating thicknesses. On the other hand, tools composed of an AISI 1045 core and coated with AISI H13 reached the same temperature in a shorter time, thus reducing the time required for each stamping operation. These cycle-time reductions were quantified for each case, and results are shown in Table V. 11. The thinner the deposited coating, the higher the time reduction experienced, enabling a cycle-time reduction of up to 44.5% when a 1-mm-thick AISI H13 coating was considered. This was actually expected because the thermal conductivity of AISI 1045 is significantly higher than that of AISI H13.

Table V. 11 Cycle-time reduction.

Parameter	Conventional AISI H13 tool	Coating thickness			
		7 mm	5 mm	3 mm	1 mm
Time instant (s) when T=341 K	20.0 (reference)	14.2	12.8	11.7	11.1
Time reduction (s)	-	5.8	7.2	8.3	8.9
Cycle-time reduction (%)	-	29	36	41.5	44.5

Another critical point when guaranteeing homogeneous properties in the final part is the temperature distribution on the surface of the tools, as it is directly translated into unequal cooling. This may result in an unsuccessful quenching of the stamped part, thus leading to undesired material microstructures and negatively affecting its mechanical properties. To

analyze the temperature distributions of the tools-blank set, the thermal profile of the contact surface between the tool and the blank in the middle plane was extracted. Temperature distributions and results at a time instant t=2 s attained for each geometry simulated are shown in Figure V. 12.

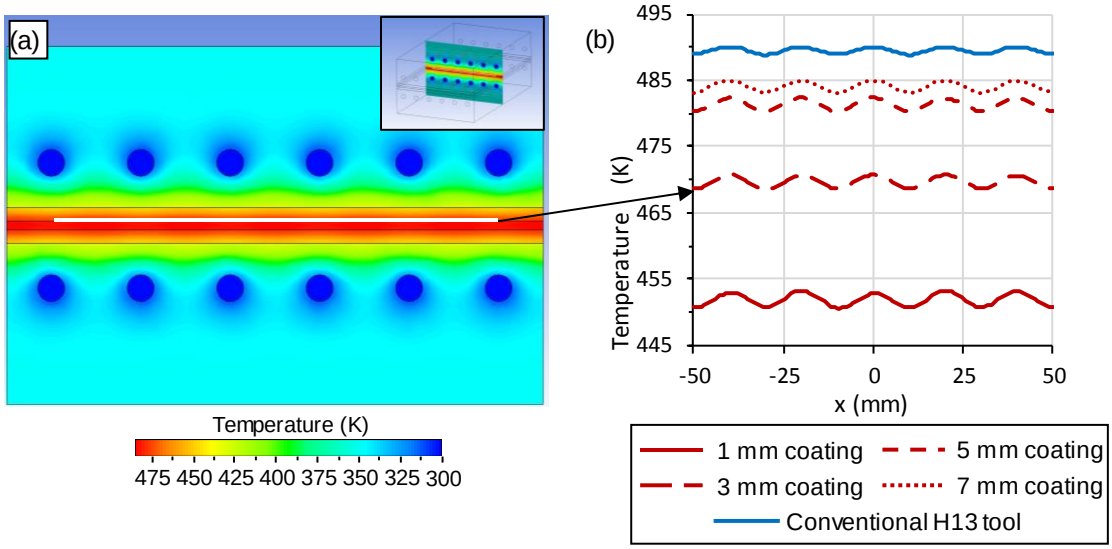

Figure V. 12 (a) Temperature distribution in the middle plane of the tool at t=2 s (3 mm AISI H13 coating); (b) Temperature profile in the tool-blank interface at t=2 s.

The maximum, minimum and mean temperatures were extracted for each case and are detailed in Table V. 12. Lower coating thicknesses led to lower mean temperatures on the surface of the tools. This was due to the higher thermal conductivity of the AISI 1045 used as the core material in these cases. Besides, it must be accounted for that a lower coating thickness also led to higher temperature variations on the surface because of higher thermal conductivity. Nevertheless, in the present case, temperature variations were kept below 3 K and, therefore, their influence on the process can be neglected.

Table V. 12 Temperature evaluation results in the surface of the tools at t=2 s.

Temperature of the contact surface	Conventional AISI H13 tool	Coating thickness			
		7 mm	5 mm	3 mm	1 mm
Maximum temperature (K)	490.09	485.01	482.37	470.73	453.24
Minimum temperature (K)	488.89	483.17	480.35	468.54	450.60
Mean temperature (K)	489.49	484.09	481.36	469.64	451.92
Temperature variation (K)	1.21	1.84	2.02	2.19	2.64

In Figure V. 13, a comparison between the thermal fields in the middle plane of the tools is presented. The three images were obtained at a 20 s time instant from the beginning of the

cooling process, which corresponded to the end of the quenching time of the stamping process. As can be seen from the figure, the heat dissipation from the blank was higher for the 1-mm-thick coating.

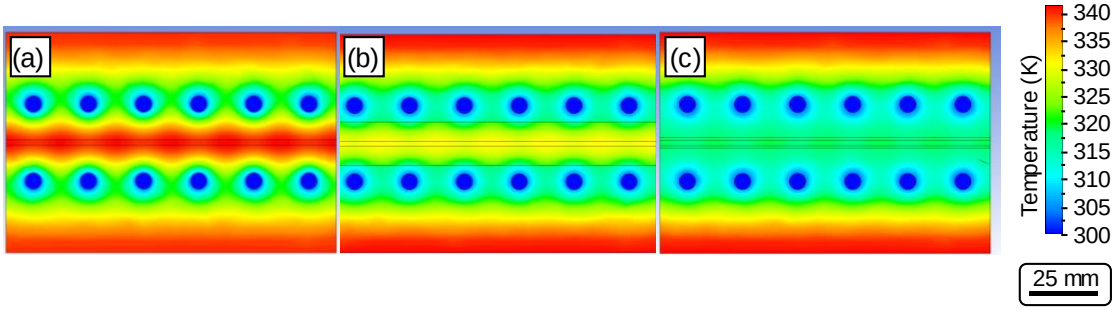

Figure V. 13 Temperature distribution in the middle plane of the tool at t=20 s for (a) conventional tool; (b) 7 mm and (c) 1 mm AISI H13 coating.

Hence, by coating AISI 1045 mild steel cores with AISI H13 tool steel, an enhanced thermal performance was obtained. In this way, an improvement was attained in the stamping process, both in terms of cycle-time reduction and temperature reduction.

V.5. Characterization of the thermal diffusivity of LMD AISI H13

V.5.1. Laser Metal Deposition tests

Two specimens of 50 x 50 x 7 mm^3 and 50 x 50 x 5 mm^3, respectively, were manufactured by adding AISI H13 over an AISI 1045 substrate via LMD. A zigzag pattern was used to deposit the filler material, alternating longitudinal and transversal directions for the deposition of successive layers, as shown in Figure V. 14a. This strategy reduces the anisotropic behavior inherent to the LMD process. Figure V. 14b shows a photograph of the manufactured specimens.

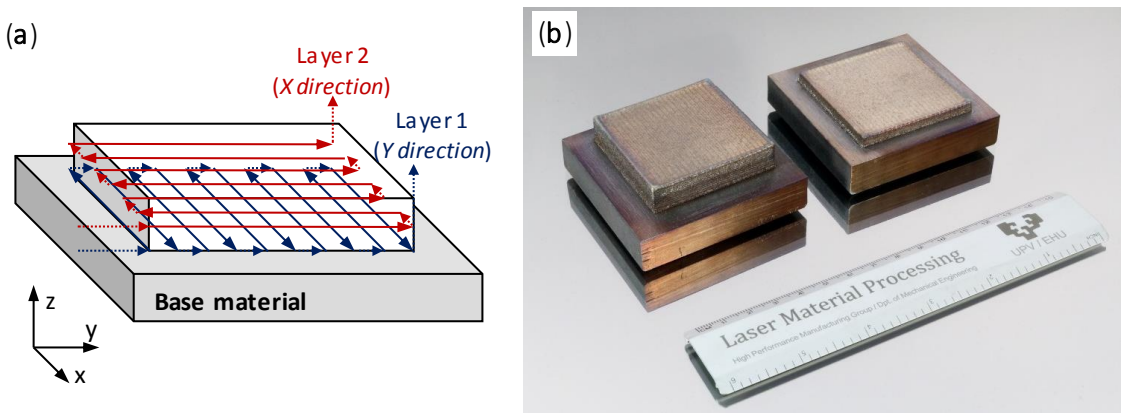

Figure V. 14 (a) Schematic of the LMD process; (b) photograph of the manufactured AISI H13 specimens.

V.5.2. Thermal diffusivity measurement

To perform thermal diffusivity measurements, three slabs, each 2 mm thick, were extracted from the deposited material at different depths, as shown in Figure V. 15. From the 7-mm-thick specimen, two plates were cut: (a) the inner plate, Sample 1, contained the deepest and earliest deposition (0 to 2 mm from the substrate); (b) the outer plate, Sample 2, contained the outermost side of the coating (4 to 6 mm from the substrate). Sample 3 was extracted from the specimen with a 3.5-mm deposition thickness, and the sample spanned the interface between the filler and substrate, from -1 to 1 mm with respect to the interface, to evaluate the influence of the LMD process on the substrate. Moreover, for comparison, a 2-mm-thick plate made of cast AISI H13 was also prepared. All samples were extracted by means of wire electrical discharge machining, and the white layer generated on the cut surfaces was removed by grinding.

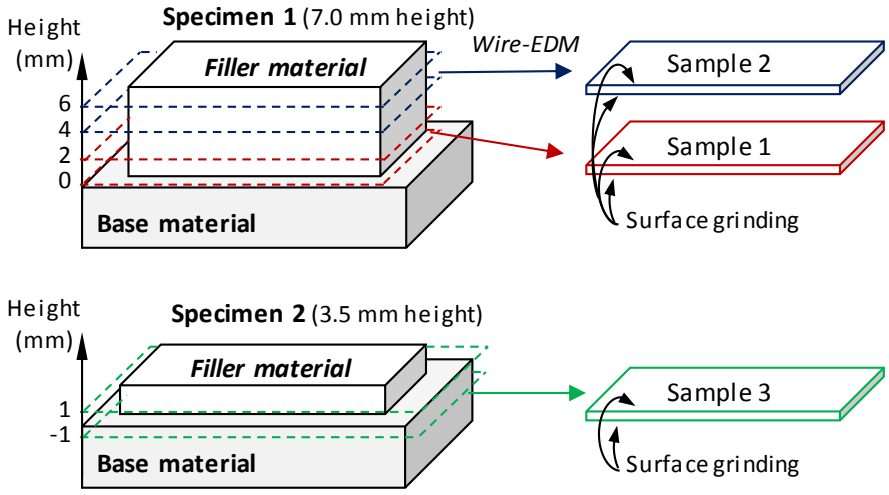

Figure V. 15 Sample extraction for thermal diffusivity measurements.

For each plate, the thermal diffusivities were measured at room temperature in two perpendicular directions: along the surface, the so-called in-plane thermal diffusivity ($\alpha_{\parallel}$), and in the direction perpendicular to the surface, the so-called through-thickness thermal diffusivity ($\alpha_{\perp}$).

To measure $\alpha_{\perp}$, a flash method was used [Parker, 1961]. In this technique, the front surface of the plate is illuminated homogeneously by the brief pulse of a flash lamp (3 kJ energy pulse, 3 ms duration) while the temperature evolution of the back-surface is recorded by a mid-infrared video camera (3-5 µm wavelength) operating at a rate of 950 frames·s^{-1}. The thermal diffusivity was obtained by measuring the time required to reach half of the maximum temperature rise

($t_{1/2}$), which is related to the thermal diffusivity through equation (Eq. V. 5), where *L* is the plate thickness.

$$t_{1/2} = 0.1388\frac{L^2}{\alpha_\perp} \quad \textbf{(Eq. V. 5)}$$

In order to enhance both the absorption to the flashlight and the infrared emissivity, the sample surfaces were covered by a thin graphite layer (≈ 3 µm thick). The influence of this layer on the accuracy of the thermal diffusivity values is less than 1% provided the sample is much thicker than the graphite layer (in the present case, 2 mm against 6 µm) [Maillet, 2000].

To measure $\alpha_\parallel$, a lock-in thermography setup with laser spot excitation was used [Heath, 1989]. This technology has been widely used for similar applications [Nolte, 2017] and enables measurements of the thermal diffusivities of the materials with high accuracy. The sample is illuminated by an intensity-modulated laser beam, tightly focused on the surface, and the oscillating component of the temperature rise is detected by an infrared video camera connected to a lock-in module. By analyzing the radial dependence of the temperature phase, the in-plane thermal diffusivity can be retrieved with ease, based on the linear relationship between the phase of the temperature and the lateral distance to the heating spot, the slope of which (m) is given by equation (Eq. V. 6), where *f* is the modulation frequency.

$$m = -\sqrt{\frac{\pi \cdot f}{\alpha_\parallel}} \quad \textbf{(Eq. V. 6)}$$

The results of the measurements of the through-thickness thermal diffusivity, $\alpha_\perp$, are summarized in the third column of Table V. 13. The statistical uncertainty was obtained by repeating each measurement five times and the uncertainty was thus found to be less than 3%.

Table V. 13 Thermal diffusivity results.

Sample	Distance from the interface (mm)	$\alpha_\perp$ (mm²·s⁻¹)	$\alpha_\parallel$ (mm²·s⁻¹)	Material
1	0	5.72±0.15	5.66±0.16	LMD AISI H13
1	2	5.72±0.17	5.88±0.17	LMD AISI H13
2	4	6.03±0.18	6.10±0.18	LMD AISI H13
2	6	6.03±0.18	6.02±0.17	LMD AISI H13
3	-1	-	12.5±0.4	Base AISI 1045
3	1	-	5.73±0.16	LMD AISI H13
Reference	-	6.75±0.20	6.42±0.19	Cast AISI H13

As shown in the table, the thermal diffusivity of the laser-deposited AISI H13 was always smaller than that of the cast sample. The thermal diffusivity of each plate was measured in two directions, i.e. from both the front (illuminated) surface and the rear (measured) surface, and the thermal diffusivities thus retrieved were the same. This homogeneity is obtained because the flash method measures the effective (or average) $\alpha_{\perp}$. Because Sample 3 included two different materials, $\alpha_{\perp}$ was not measured in that sample.

As for the in-plane thermal diffusivity measurements, $\alpha_{\parallel}$, Figure V. 16 shows the amplitude and phase thermograms of Sample 1, at the surface 0 mm from the surface, with f = 7 Hz. For each specimen, the thermal diffusivity on both sides was measured. The round shape of the isophases and isotherms in Figure V. 16 is representative of all the cases analyzed and indicates in-plane thermal isotropy. The in-plane thermal diffusivity was obtained considering the vertical profiles of the phase thermograms (the white line in Figure V. 16b), since they are free from diffraction effects, like those observed in the horizontal profile in Figure V. 16b.

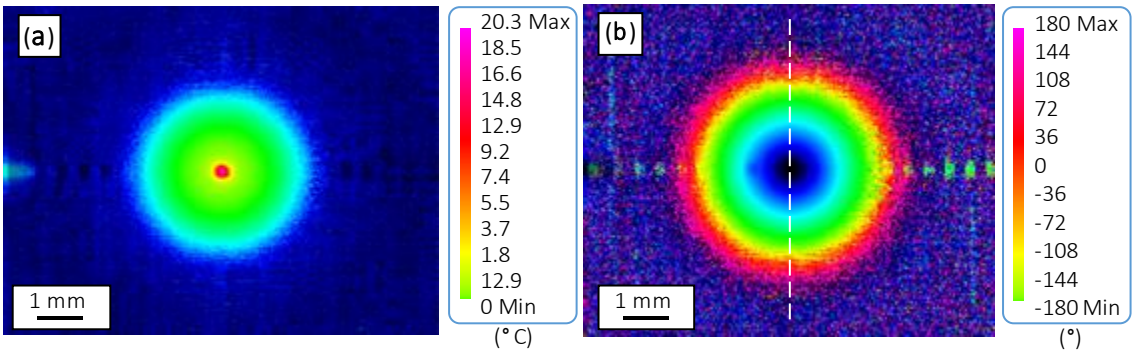

Figure V. 16 (a) Amplitude and (b) phase thermograms of Sample 1 at the surface 0 mm from the substrate, with a modulation frequency of 7 Hz. The white vertical line corresponds to the phase profile used for the thermal diffusivity measurements. The scale of the amplitude is in °C and the phase is in angular degrees.

From the slope of the vertical phase profile, the in-plane thermal diffusivity was obtained, using equation (Eq. V. 6). In order to average the local heterogeneities, the measurement was repeated at five different zones at the surface of the samples. The thermal diffusivities obtained using this method together with the uncertainty (≈3%) are summarized in the fourth column of Table V. 13. The uncertainty takes into account the standard deviation in the slope of the phase profile and the standard deviation of the five repetitions. Although the thermal diffusivity of each surface increased with the surface's height above the substrate, at all heights, the thermal diffusivity of the sample remained below the diffusivity of the reference cast material. Comparing the values of $\alpha_{\perp}$ and $\alpha_{\parallel}$, the LMD process did not introduce any thermal anisotropy.

Thermal diffusivity, α, and conductivity, k, are related by equation (Eq. V. 7), where ρ and c_p are the density and specific heat of the material, respectively.

$$\alpha = \frac{k}{\rho \cdot c_p} \quad \textbf{(Eq. V. 7)}$$

Equation (Eq. V. 7) was used to calculate the thermal conductivity of LMD AISI H13, cast AISI H13, and AISI 1045 and the results are shown in Table V. 14. The perpendicular thermal diffusivity values shown in Table V. 13 were used because the flash technique is generally acknowledged to be the most reliable method and is covered by standards [JSA, 2005; ASTM, 2013; ISO, 2013]. The density and specific heat were taken from the material specifications. In the case of LMD AISI H13, the heat capacity was calculated using the rule of mixtures given in equation (Eq. V. 8) and considering this material as a mixture of AISI H13 and air.

$$(\rho \cdot c_p)_{DED\ AISI\ H13} = \upsilon_1 \cdot (\rho \cdot c_p)_{cast\ AISI\ H13} + \upsilon_2 \cdot (\rho \cdot c_p)_{air} \quad \textbf{(Eq. V. 8)}$$

In equation (Eq. V. 8), υ_1 and υ_2 are the volume fractions of cast AISI H13 and air, respectively. Because of $\upsilon_1 > 0.995$, the same heat capacity was used for the cast reference and LMD AISI H13. This result is consistent with the fact that the heat capacity, unlike the thermal transport properties (α and k), depends only on the composition of the sample, not the microstructure. Therefore, because the LMD process does not affect the sample composition, the same heat capacity is expected for AISI H13 regardless of the production process.

Table V. 14 Thermal conductivities.

Material	Measured thermal diffusivity ($mm^2 \cdot s^{-1}$)	Effective thermal conductivity ($W \cdot m^{-1} \cdot K^{-1}$)	Reference value from literature ($W \cdot m^{-1} \cdot K^{-1}$)
LMD AISI H13 (Sample 1)	5.72	20.7	24.9 [Oh, 2019]
Cast AISI H13	6.75	24.4	
Base AISI 1045	12.5	46.7	47.6 [Gao, 2014]

In the cast AISI H13 and the base AISI 1045, the measured effective thermal diffusivities presented almost no differences compared to the reference values encountered in the literature [Oh, 2019; Gao, 2014], demonstrating the accuracy of the measurements acquired in this study. In the case of LMD AISI H13, the effective thermal conductivity was 15.3% lower than that measured for cast AISI H13. This is because the thermal conductivity of alloys depends not only on the sample composition but also on the microstructure (grain size, micro-cracks, pores, etc.). Because the metallographic analysis performed in section V.3.2 does not indicate the presence of cracks or pores, the thermal conductivity reduction was attributed primarily to the smaller

sizes of the grains produced by the fast cooling rate in LMD. The larger number of interfaces compared to the cast material reduces the electron mean free path [Berman, 1976] and consequently the thermal conductivity.

Focusing on the variation of thermal conductivity in relation to temperature, Zhang et al. studied the thermal conductivity change of multi-stacked silicon steel sheets under different pressure and temperature conditions. Their results showed that although the thermal conductivity changed under different compressive stresses, the conductivity maintained the same rate of variation in response to temperature change [Zhang, 2018]. Therefore, in this study, the thermal conductivity reduction measured at 20 °C was assumed to affect the material in proportion to the temperature, and this result was extended to the whole temperature range, as shown in Table V. 15, and applied to the case study model described in the next section.

Table V. 15 Effective thermal conductivity of the LMD AISI H13 considered in the thermal model.

Material	Thermal properties	Temperature (K)					
		293	473	673	873	1073	1273
LMD AISI H13	Specific heat ($J \cdot kg^{-1} \cdot K^{-1}$)	461	475	519	592	592	592
	Thermal conductivity ($W \cdot m^{-1} \cdot K^{-1}$)	20.7	22.8	24.2	23.7	23.7	23.7

V.5.3. Influence of the thermal conductivity on the thermal modeling of the tools

In order to quantify the influence of the effective thermal conductivity of the laser-deposited AISI H13 on a bimetallic hot stamping tool, two different cases were simulated using the same geometry, shown in Figure V. 17. The aim of the simulation was to quantify the impact of considering the real LMD AISI H13 thermal conductivity or the data from the literature.

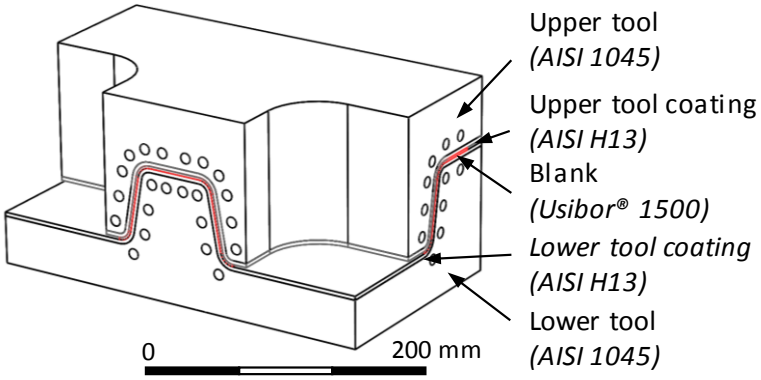

Figure V. 17 Simulated geometry of bimetallic hot stamping tool.

The simulated geometry represents a V-shaped part, which is common in hot stamping, and had a 300 x 170 x 150 mm^3 bounding box. Regarding the cooling system, the channels had an 8-mm

diameter and were positioned at a 12-mm distance from the contact face with the blank. The tool had an AISI 1045 core, which was coated with a 3-mm-thick LMD AISI H13. In Case 1, the thermal conductivity value of the cast AISI H13 was used as a reference, whereas in Case 2, the effective thermal conductivity value of the deposited AISI H13 was considered. In both cases, the stamped blank was made of Usibor® 1500 steel (22MnB5), a boron alloyed steel that is well-suited for the entire range of automotive structural parts, which require high resistance to anti-intrusion during impact [ArcelorMittal, 2018a]. The simulated geometry represents a V-shaped part, which is common in hot stamping.

The simulation was performed using the thermal transient module of the FEM software ANSYS Workbench 19.2. The employed mesh consisted of over 1 million first-order tetrahedral elements, with an average skewness of 0.246 and a maximum of 0.846. The initial temperature of the tools, as well as the reference temperature for the water-cooling convection, was set at 293 K (20 °C), whereas the temperature of the blank after the loading operation was 1083 K (810 °C) [Naganathan, 2012]. The blank was 1.85 mm thick, which is a typical thickness for an automotive sheet metal structural body part [ArcelorMittal, 2018b]. The geometric parameters of the tools are detailed in Table V. 16, and the thermal properties of the employed materials are shown in Table V. 9 in section V.4.3. The model simulated a 20 s cooling time, which is a typical value for hot stamping [Naganathan, 2012; Muvunzi, 2018].

Table V. 16 Geometric parameters of the simulated tools.

Geometric parameters	Case 1 and 2
Diameter of the cooling ducts	8 mm
Length of the cooling ducts	170-280 mm
Distance between cooling ducts	15-20 mm
Distance from cooling duct center to surface	12 mm
Number of ducts in the upper / lower tools	12 / 10
Coating thickness	3 mm

The tools are cooled by the convection of the water that is forced through the cooling channels, a parameter referred to as the Convective Heat Transfer Coefficient (CHTC). According to section IV.3.2, for mechanically drilled 8-mm-diameter ducts with an intermediate Ra value of 0.31 µm and a 20 °C cooling water, the CHTC is 4736.7 $W \cdot m^{-2} \cdot K^{-1}$.

The heat transfer between the hot blank and the tools needs to be established as an input parameter in the model. This parameter is referred to as the Interfacial Heat Transfer Coefficient

(IHTC). In the present study, the correlation proposed by Hu et al. [Hu, 2013] was taken as a reference. Considering a 15-MPa contact pressure, the IHTC was estimated to be approximately 3000 $W \cdot m^{-2} \cdot K^{-1}$, based on the aforementioned approximation.

To compare the cooling performance of the tools using either the effective thermal conductivity of LMD AISI H13 or the reference thermal conductivity, the time point at which the martensitic transformation was complete, i.e., 553 K (280 °C), was calculated. In addition, the time at which the blank was cooled to below 343 K (70 °C) was determined to define the total cycle time before the tools could be opened.

Based on the effective thermal conductivity of the laser-deposited AISI H13 tool steel, the cycle times required to lower the blank temperature below 280 and 70 °C were calculated, respectively. Figure V. 18 shows the evolution of the maximum temperature of the blank.

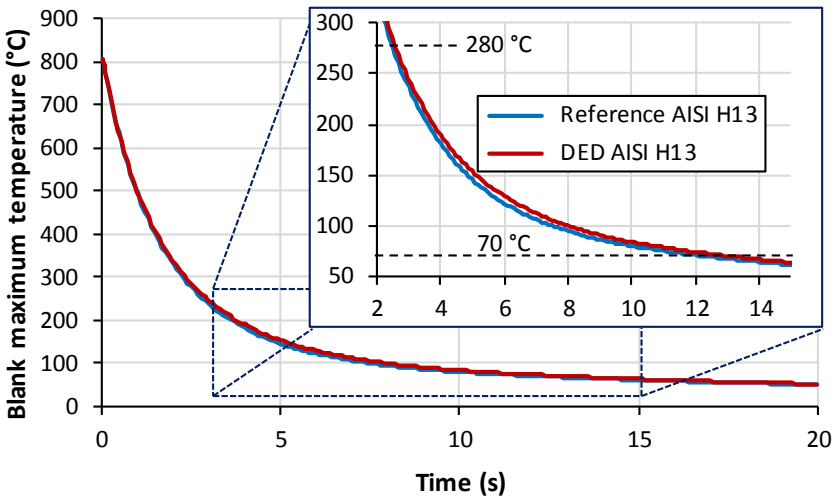

Figure V. 18 Blank maximum temperature evolution during the hot stamping process.

The lower thermal conductivity of the laser-deposited AISI H13 can be seen to reduce heat extraction from the blank, and this case thus requires a longer cooling time to achieve an equivalent thermal field. Table V. 17 presents the results of the simulated case study, as well as the error produced if the effective thermal conductivity of the laser-deposited AISI H13 is not considered in the model.

Table V. 17 Results of the simulated case study.

Blank maximum temperature	Time instant (s)		Difference (%)
	Reference AISI H13	LMD AISI H13	
280 °C	5.50	5.59	1.64
70 °C	12.10	12.89	6.53

The errors generated when calculating the thermal fields were relatively low in comparison with the differences in the thermal conductivity values. This is because the coating thickness was only 3 mm, and such low thickness values are commonly employed in bimetallic tools. Nevertheless, if fully LMD-manufactured structures are employed, much higher errors could be generated in the simulation. Nevertheless, if fully LMD-manufactured structures are simulated, much higher errors could be generated. Figure V. 19 shows the thermal field of the blank at 12.89 s in the case where the effective thermal conductivity of the LMD AISI H13 coating is considered.

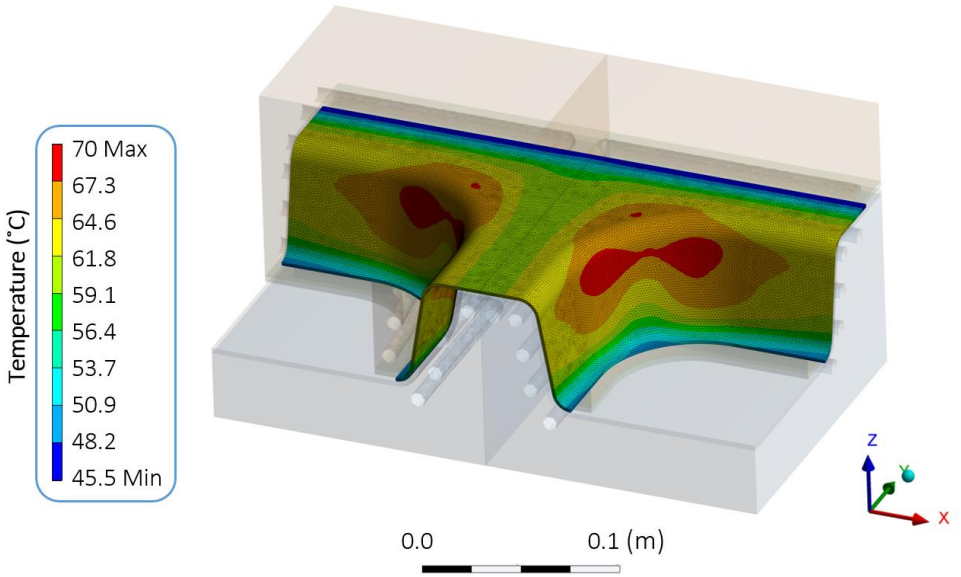

Figure V. 19 Temperature field of the blank at 12.89 s time instant, considering the effective thermal conductivity of the LMD AISI H13 coating.

V.6. Conclusions

In this chapter, an investigation on bimetallic hot stamping tools manufactured via LMD has been performed. To that end, the suitability and advantages of this novel approach have been studied in terms of both manufacturability and performance, and in comparison with conventionally manufactured tools. Besides, an investigation on the effective thermal diffusivity of laser-deposited AISI H13 tool steel has been also conducted. Based on the results obtained, the following conclusions were drawn:

- The feasibility of depositing AISI H13 tool steel over AISI 1045 steel and their subsequent metallurgical compatibility is demonstrated. Dilution, porosity, and microstructure were investigated for the material characteristics of deposited AISI H13. As a result, no cracks were found in the deposited material nor in the interface between AISI H13 and AISI 1045. In addition, obtained porosity within the deposited material was kept below

0.5%, while the average diameter of the pores was lower than 150 µm. Therefore, the quality of both deposited material and bonding with the substrate were guaranteed.

- Regarding mechanical properties, laser-deposited AISI H13 presented similar characteristics as cast AISI H13. As far as friction and wear are concerned, a friction coefficient variation of 0.03 was obtained between both materials, while the wear volume values were found similar. Hence, comparable friction and wear behavior is concluded. Hardness measurements showed that the deposited material presented a uniform hardness distribution with minimal variation and similar surface value than cast AISI H13. Slightly higher values were obtained when thin coatings were deposited. Finally, with regard to compression tests, both materials were found to present similar behavior to the reference AISI H13 tool.
- The production rate increase that bimetallic tools developed by LMD offer when compared to conventional tools is determined via thermal simulations. Maximum cycle-time reductions were obtained when an AISI 1045 core was combined with a minimum AISI H13 coating thickness. In the present case and for the studied geometry, AISI 1045 tools coated with 1 mm AISI H13 reduced cycle time in 44.5% compared with cast AISI H13.
- The effective thermal diffusivity of the laser-deposited AISI H13 tool steel is lower than that of the reference value of the cast material, which is critical for applications where the heat transfer is a key parameter. The reduction of the effective thermal diffusivity was due to the microstructure developed during the fast cooling of the deposited material, where the fine grain size reduces the heat transfer through the material.
- The microstructure that developed within the deposited material was directly related to the cooling rate, which was higher at the beginning of the LMD process. This is why the effective thermal diffusivity of Sample 1 (situated at 0-2 mm from the interface) is lower than that of Sample 2 (at 4-6 mm from the interface).
- Despite the directional nature of the LMD process, the resulting thermal properties presented very low anisotropy and it can be assumed that heat is conducted equally in all directions. Besides, the effect of the LMD process on the substrate is minimal and does not affect the thermal diffusivity of the base material at a 1 mm distance from the interface.
- To obtain reliable results in thermal simulations involving additively manufactured parts, the real thermal conductivity of the deposited material must be considered. Otherwise, the cooling capability of the LMD-manufactured tools would be overestimated.

Hence, this work demonstrated the feasibility of manufacturing bimetallic tools by coating a high thermal conductivity mild-steel core with hot work tool steel. Moreover, this approach offers a potential alternative to replace conventional tool steel dies in terms of both thermal behavior and mechanical characteristics. As a result, cost-effective tools with enhanced thermal properties can be attained. As far as the thermal diffusivity analysis is concerned, this work helps to extend current knowledge on the thermal properties of LMD materials. It is noteworthy that the thermal diffusivity and conductivity differences encountered may also affect other AM processes. Therefore, further research work is necessary to fully characterize AM parts.

Chapter VI. Contributions and future works

Chapter VI. Contributions and future works

In this last chapter, the main contributions of the present work are summarized. Besides, the future works arisen from the realization of this thesis are also detailed.

VI.1. Contributions

In this work, a research on the application of LMD to hot stamping tools has been presented. Throughout it, several topics have been dealt with, ranging from the characterization of materials for their correct deposition to their application in the generation of coatings or geometries. These topics have always been focused on improving the hot stamping process, both in terms of performance and productivity. The main contributions of the present research work are summarized below:

1. **The process parameters for laser-depositing AISI H13 hot-work tool steel have been defined, as well as a methodology for the repair and manufacturing of hot stamping tools in hybrid machines:** AISI H13 tool steel is extensively used in the die & mold industry for manufacturing high-added-value components, such as hot stamping tools. Hot stamping tools have high manufacturing and maintenance costs. Therefore, their repair in order to extend their lifespan is highly desirable. In this context, hybrid machines that combine additive and subtractive functionalities represent an attractive solution for the repair and overhaul of parts. However, the interaction between LMD and cutting fluid had not previously been addressed in the literature. In this regard, this work contributes to the deepening of knowledge regarding those interactions. It is worth highlighting that different results have been observed depending on each material tested, Inconel®718 and AISI H13, which include the formation of porosity, deficient metallurgical bonding, and cracks. In any case, since the performance of a cleaning stage does not imply any detriment to the quality of the deposition, its introduction before proceeding to LMD should be considered in order to minimize the interaction between the cutting fluid and the metal powder, thus directly affecting process planning.

2. **A new methodology for manufacturing conformal cooling channels by means of LMD has been developed:** The most critical stage in the hot stamping process is the one in which the quenching of the blank takes place. In this regard, the geometry and layout of the cooling system embedded within tools are of great importance to guarantee a homogeneous temperature distribution in them and thus achieve the complete

martensitic transformation of the blank. Through the employment of conformal cooling channels, in addition to providing a greater homogeneity of temperatures in both tool and blank, which avoids hot spots and increases the lifespan of the tools, shortens the cooling time of the blank, thus reducing the cycle time. This work contributes to demonstrating that LMD is a valid technology for the generation of conformal cooling channels, which cannot be manufactured through conventional techniques. The attained results confirm the greater homogeneity of temperatures in both tool and blank, as well as an increase in process efficiency in terms of productivity.

3. **Cost-effective hot stamping bimetallic tools with enhanced thermal conductivity manufactured by LMD have been evaluated:** The tool steels from which hot stamping tools are manufactured are high-priced materials that lead to expensive manufacturing costs. In addition, these tool steels, such as AISI H13, have moderate thermal conductivity values compared with other steels. In hot stamping, the temperature distribution of the tools and the blank are related to the thermo-physical properties of the employed materials. Any enhancement in the thermal conductivity of the tools leads to an increase in the heat transfer between the tools and the blank. In this work, the feasibility of manufacturing bimetallic tools by coating a high thermal conductivity mild-steel core with hot work tool steel has been demonstrated. This approach offers a potential alternative to replace conventional tool steel dies without any detriment in terms of thermal behavior and mechanical characteristics. As a result, cost-effective tools with enhanced thermal properties can be attained, which involves a shorter cycle time and a subsequent production rate increase.

4. **The effective thermal conductivity of laser-deposited AISI H13 has been determined:** In order to accurately determine the thermal conductivity of the laser-deposited AISI H13, its effective thermal diffusivity has been experimentally measured and compared with cast AISI H13. Results showed that the thermal conductivity of laser-deposited AISI H13 was significantly lower than that of cast AISI H13, which is attributed to the fine microstructure developed during the fast cooling of the deposited material in the LMD process. Therefore, any variation in grain size along the deposited material may result in a change in its thermal diffusivity. This work helps to broaden the current knowledge of the thermal properties of laser-deposited materials and the results obtained should be considered in order to be able to perform simulations with a higher degree of reliability.

VI.2. Future works

The contributions of the present work have served to establish new lines of research, some of which are detailed below:

- In the field of hybrid machines and the interaction between the cutting fluid and the LMD process, further research is necessary in order to determine the way it affects different materials, as well as to optimize the cleaning strategy to follow. One possible approach could be the combination of air blasting and laser cleaning techniques before proceeding to LMD.
- Development of stamping tools with varying thermal conductivities through the manufacturing of FGMs by LMD. This way, the blank is subjected to locally different heat treatments during the hot stamping operation, thus developing mechanical properties differentiated by zones. This could improve the crash performance of the part, or ease subsequent cutting operations.
- With regard to the thermal properties of laser-deposited materials, it is noteworthy that the thermal diffusivity and conductivity differences encountered in LMD may also affect other AM processes. Therefore, further research work is necessary to fully characterize AM parts.
- The development of high-performance coatings is another field in which the application of LMD can be particularly interesting. The use of LMD technology enables the manufacturing of metal-matrix composites, as well as the tuning of the microstructure of the deposited material by carefully controlling the process parameters employed. In this way, fatigue thermal resistance, hardness, tensile properties, wear behavior and adhesion resistance could be enhanced, among others. This solution could be of great value for both the repair and manufacture of components.
- Finally, the implementation of monitoring and control algorithms in the LMD process would lead to a more stable process, hence increasing the reliability of hybrid machines.

References

[Abdulrahman, 2018] K.O. Abdulrahman, *Laser metal deposition technique: sustainability and environmental impact*, Procedia Manufacturing, 21, 109-116, 2018.

[Achillas, 2015] C. Achillas, D. Aidonis, E.Iakovou, M. Thymianidis, D. Tzetzis, *A methodological framework for the inclusion of modern additive manufacturing into the production portfolio of a focused factory*, J. Manuf. Syst., 37, 328–339, 2015.

[Ahn, 2010] D.G. Ahn, H.W. Kim, S.H. Park, and H.S. Kim, *Manufacture of Mould with a High Energy Efficiency Using Rapid Manufacturing Process*, 1252, 2010.

[Ahsan, 2011] M.N. Ahsan, C.P. Paul, L.M. Kukreja, A.J. Pinkerton, *Porous structures fabrication by continuous and pulsed laser metal deposition for biomedical applications; modelling and experimental investigation*, Journal of Materials Processing Technology, 211, Issue 4, 602-609, 2011.

[AKSteel, 2019] *316/316L Stainless Steel Datasheet*, AK Steel Corporation. Available online: http://www.aksteel.com/pdf/markets_products/stainless/austenitic/316_316l_data_sheet.pdf (accessed on 20/02/2020).

[Albrecht, 2015] B. P. Albrecht, C. Hsu, *Additive manufacturing system for joining and surface overlay*, US0021379A1, 2015.

[Allen, 2006] J. Allen, *An Investigation into the Comparative Costs of Additive Manufacture vs. Machine from Solid for Aero Engine Parts*, Rolls-Royce PLC Derby, UK; 2006.

[AlloyWire, 2019] *Inconel® 718 Technical Datasheet*, AlloyWire. Available online: https://www.alloywire.com/products/inconel-718/ (accessed on 20/02/2020).

[Allwood, 2011] J.M. Allwood, M.F. Ashby, T.G. Gutowski, E. Worrell, *Material efficiency: A white paper*. Resour. Conserv. Recycl., 55, 362–381, 2011.

[Al-Makky, 2016] M. Al-Makky, D. Mahmoud, *The importance of additive manufacturing processes in industrial applications*, 2016.

[Altan, 2001] T. Altan, B. Lilly, Y.C. Yen, T Altan, *Manufacturing of Dies and Molds*, CIRP Ann., 50, 404–422, 2001.

[Araújo, 2012] J.R. Araújo, J.J. Rodríguez-Andina, J. Farina, F. Vidal, J.L. Mato, M.Á. Montealegre, *FPGA-Based Laser Cladding System with Increased Robustness to Optical Defects*, Proceedings of the 38th Annual Conference on IEEE Industrial Electronics Society, Montreal, QC, Canada, 4688–4693, 2012.

[ArcelorMittal, 2018a] *Expanding ArcelorMittal's hot stamping offer for automotive,* Arcelor Mittal. Available online: https://flateurope.arcelormittal.com/flatnews/flatarchivenews/2739/16dec/autoPHS (accessed on 20/02/2020).

[ArcelorMittal, 2018b] *Steels for hot stamping – Usibor® and Ductibor®,* Arcelor Mittal. Available online: https://automotive.arcelormittal.com/products/global_offering/PHS/usibor_ductibor/ (accessed on 20/02/2020).

[Arrizubieta, 2014] J.I. Arrizubieta, I. Tabernero, J.E. Ruiz, A. Lamikiz, S. Martinez, E. Ukar, *Continuous coaxial nozzle design for LMD based on numerical simulation,* Physcs. Proc., 56, 429–438, 2014.

[Arrizubieta, 2017a] J.I. Arrizubieta, F. Klocke, N. Klingbeil, K. Arntz, A. Lamikiz, S. Martinez, *Evaluation of efficiency and mechanical properties of Inconel 718 components built by wire and powder laser material deposition*, Rapid Prototyping Journal, 23, Issue 6, 965-972, 2017.

[Arrizubieta, 2017b] J.I. Arrizubieta, J.E. Ruiz, S. Martinez, E. Ukar, A. Lamikiz, *Intelligent nozzle design for the Laser Metal Deposition process in the Industry 4.0,* Procedia Manuf., 13, 1237–1244, 2017.

[Arrizubieta, 2017c] J.I. Arrizubieta, *Laser Metal Deposition enhancement by holistic simulation of powder mass flow and deposition into the melt pool*, Doctoral Thesis, University of the Basque Country, Bilbao, 2017.

[Arrizubieta, 2018] J.I. Arrizubieta, J.E. Ruiz, M. Cortina, E. Ukar, A. Lamikiz, *Evaluación de la sobreacumulación de material en los cambios de dirección durante el proceso de aporte por láser mediante un modelo integral*, Revista Iberoamericana de Ingeniería Mecánica, 22, 3–12,2018.

[Åsberg, 2019] M. Åsberg, G. Fredriksson, S. Hatami, W. Fredriksson, P. Krakhmalev, *Influence of post treatment on microstructure, porosity and*

mechanical properties of additive manufactured H13 tool steel, Mater. Sci. Eng. A, 742, 584–589, 2019.

[ASTM, 2013] American Society for Testing and Materials, *ASTM E1461−13: Standard Test Method for Thermal Diffusivity by the Flash Method*, ASTM International, West Conshohocken, PA, 2013.

[ASTM, 2017] American Society for Testing and Materials, *ASTM G99−17: Standard Test Method for Wear Testing with a Pin-on-Disk Apparatus*, ASTM International, West Conshohocken, PA, 2017.

[Ataee, 2018] A. Ataee, Y. Li, M. Brandt, C. Wen, *Ultrahigh-strength titanium gyroid scaffolds manufactured by selective laser melting (SLM) for bone implant applications*, Acta Materialia, 158, 354–368, 2018.

[Bahnini, 2018] I. Bahnini, M. Rivette, A. Rechia, A. Siadat, A. Elmesbahi, *Additive manufacturing technology: the status, applications, and prospects*, The International Journal of Advanced Manufacturing Technology 97, 147–161, 2018.

[Bailey, 1993] N. Bailey, F.R. Coe, T.G. Gooch, P.H.M. Hart, N. Jenkins, R.J. Pargeter, *Chapter 1: Defining the Problem*, In: Welding steels without hydrogen cracking, Woodhead Publishing, 1-16, 1993.

[Bandyopadhyay, 2009] A. Bandyopadhyay, B.V. Krishna, W. Xue, S. Bose, *Application of Laser Engineered Net Shaping (LENS) to manufacture porous and functionally graded structures for load bearing implants,* Journal of Materials Science: Materials in Medicine, 20, 1, 29-34, 2009.

[Behandish, 2018] M. Behandish, S. Nelaturi, J. de Kleer, *Automated process planning for hybrid manufacturing*, Comput.-Aided Des. 102, 115–127, 2018.

[Belingardi, 2015] G. Belingardi, A.T. Beyene, E.G. Koricho, B. Martorana. *Alternative lightweight materials and component manufacturing technologies for vehicle frontal bumper beam*, Composite Structures, 120, 483-495, 2015.

[Berman, 1976] R. Berman, *Thermal Conduction in Solids*, Oxford University Press, London, 1976.

[Bermingham, 2018] M.J. Bermingham, L. Nicastro, D. Kent, Y. Chen, M.S. Dargusch, *Optimising the mechanical properties of Ti-6Al-4V components produced by wire + arc additive manufacturing with post-process heat treatments*, J. Alloys Compd., 753, 247–255, 2018.

[Bobbio, 2017] L.D. Bobbio, S. Qin, A. Dunbar, P. Michaleris, A.M. Beese, *Characterization of the strength of support structures used in powder bed fusion additive manufacturing of Ti-6Al-4V*, Additive Manufacturing, 14, 60-68, 2017.

[Boeing, 2018] *Commercial Market Outlook 2018-2037*, Boeing. Available online: http://www.boeing.com/commercial/market/commercial-market-outlook#/downloads (accessed on 20 February 2020)

[Bohlen, 2018] A. Bohlen, H. Freiße, M. Hunkel, F. Vollertsen, *Additive manufacturing of tool steel by laser metal deposition*, Proc. CIRP, 74, 192-195, 2018.

[Bonaiti, 2017] G. Bonaiti, P. Parenti, M. Annoni, S. Kapoor, *Micro-milling Machinability of DED Additive Titanium Ti-6Al-4V*, Procedia Manufacturing, 10, 497-509, 2017.

[Bonek, 2006] M. Bonek, L.A. Dobrzański, E. Hajduczek, A. Klimpel, *Structure and properties of laser alloyed surface layers on the hot-work tool steel*, J. Mater. Process. Technol. 175, 45–54, 2006.

[Bourell, 2017] D. Bourell, J.P. Kruth, M. Leu, G. Levy, D. Rosen, A.M. Beese, A. Clare, *Materials for additive manufacturing*, CIRP Annals, 66(2), 659-681, 2017.

[Brøtan, 2016] V. Brøtan, O.Å. Berg, K. Sørby, *Additive Manufacturing for Enhanced Performance of Molds*, Proc. CIRP, 54, 186-190, 2016.

[Caiazzo, 2017] F. Caiazzo, V. Alfieri, G. Corrado, P. Argenio, G. Barbieri, F. Acerra, V. Innaro, *Laser Beam Welding of a Ti–6Al–4V Support Flange for Buy-to-Fly Reduction*, Metals, 7, 183, 2017.

[Caiazzo, 2018] F. Caiazzo, *Laser-aided Directed Metal Deposition of Ni-based superalloy powder*, Opt. Laser Technol., 103, 193-198, 2018.

[Campbell, 2002] R.I. Campbell, M. Martorelli, H.S. Lee, *Surface roughness visualisation for rapid prototyping models*, Comput.-Aided Des., 34, 717–725, 2002.

[Candel, 2013] J.J Candel, V. Amigó, J.A. Ramos, D. Busquets, *Problems in laser repair cladding a surface AISI D2 heat-treated tool steel*, Weld. Int., 27, 10-17, 2013.

[Caron, 2014] E.J.F.R. Caron, K.J. Daun, M.A. Wells, *Experimental heat transfer coefficient measurements during hot forming die quenching of*

boron steel at high temperatures, Int. J. Heat Mass Transf., 71, 396-404, 2014.

[Carroll, 2006] P.A. Carroll, P. Brown, G. Ng, R. Scudamore, A.J. Pinkerton, W. Syed, H. Sezer, L. Li, J. Allen, *The Effect of Powder Recycling in Direct Metal Laser Deposition on Powder and Manufactured Part Characteristics*, Meet. Proc. RTO-MP-AVT-139, 1–10, 2006.

[Çengel, 2006] Y.A. Çengel, *Appendix 1: Property tables and charts (SI units)*, In: Heat and Mass Transfer, 841–868, 2006.

[Çengel, 2007a] Y.A. Çengel, *Chapter 8: Internal Forced Convection*, In: Heat and Mass Transfer, 419–440, 2007.

[Çengel, 2007b] Y.A. Çengel, *Chapter 9: Natural Convection*, In: Heat and Mass Transfer, 459-514, 2007.

[Chang, 2016] Y. Chang, X. Tang, K. Zhao, P. Hu, Y. Wu, *Investigation of the factors influencing the interfacial heat transfer coefficient in hot stamping*, Journal of Materials Processing Technology, 228, 25-33, 2016.

[Chen, 2014a] C. Chen, Y. Wang, H. Ou, Y. He, X. Tang, *A review on remanufacture of dies and moulds*, J. Clean. Prod., 64, 13-23, 2014.

[Chen, 2014b] J. Chen, X. Li, X. Han, *Hot Stamping*, Comprehensive Materials Processing, 5, 351–370, 2014.

[Chen, 2018] L. Chen, K. Xu, K. Tang, *Optimized sequence planning for multi-axis hybrid machining of complex geometries*, Computers & Graphics, 70, 176-187, 2018.

[Choi, 2012] C. Choi, A. Groseclose, T. Altan, *Estimation of plastic deformation and abrasive wear in warm forging dies*, Journal of Materials Processing Technology, 212(8), 2012.

[Coldwell, 2003] H. Coldwell, R. Woods, M. Paul, P. Koshy, R. Dewes, D. Aspinwall, *Rapid machining of hardened AISI H13 and D2 moulds, dies and press tools*, J. Mater. Process. Technol., 135, 301–311, 2003.

[Colodrón, 2011] P. Colodrón, J. Fariña, J.J. Rodríguez-Andina, F. Vidal, J.L. Mato, M.Á. Montealegre, *Performance Improvement of a Laser Cladding System through FPGA-Based Control*, *IECON Proceedings (Industrial Electronics Conference)*, 2814–2819, 2011.

[Cong, 2014] D.L. Cong, G.Y. Liu, H. Zhou, L.Q. Ren, B.S. Lu, C.W. Wang, *Thermal fatigue resistance of H13 die steel repaired by partial laser surface*

remelting process, Materials Science and Technology, 30, 355–62, 2013.

[Cortina, 2018a] Cortina, M.; Arrizubieta, J.I.; Ukar, E.; Lamikiz, A. Analysis of the Influence of the Use of Cutting Fluid in Hybrid Processes of Machining and Laser Metal Deposition (LMD). Coatings 2018, 8, 61.

[Cortina, 2018b] Cortina, M.; Arrizubieta, J.I.; Calleja, A.; Ukar, E.; Alberdi, A. Case Study to Illustrate the Potential of Conformal Cooling Channels for Hot Stamping Dies Manufactured Using Hybrid Process of Laser Metal Deposition (LMD) and Milling. Metals 2018, 8(2), 102.

[CR7V-L, 2019] *CR7V-L Datasheet,* Kind & Co Edelstahlwerk. Available online: http://www.kind-co.de/en/download-centre.html?tx_kcdownloads_kcdownloads%5Bfile%5D=327&tx_kcdownloads_kcdownloads%5Baction%5D=download&tx_kcdownloads_kcdownloads%5Bcontroller%5D=Download&tx_kcdownloads_kcdownloads%5Bformat%5D=download&cHash=0c6b01daaed66bbb9ba483e32a4d5eee (accessed on 20 February 2020)

[Cunningham, 2018] C.R. Cunningham, J.M. Flynn, A. Shokrani, V. Dhokia, S.T. Newman, *Invited review article: Strategies and processes for high quality wire arc additive manufacturing*, Addit. Manuf., 22, 672-686, 2018.

[DataRay, 2018] *M^2 and other High-order Modes*, DataRay. Available online: https://www.dataray.com/blog-m2-high-order-modes.html (accessed on 20 February 2020)

[Deloitte, 2014] *3D opportunity in the automotive industry*, Deloitte. Available online: https://www2.deloitte.com/content/dam/insights/us/articles/additive-manufacturing-3d-opportunity-in-automotive/DUP_707-3D-Opportunity-Auto-Industry_MASTER.pdf (accessed on 20 February 2020)

[Deloitte, 2018] *2018 Global aerospace and defense industry outlook*, Deloitte. Available online: https://www2.deloitte.com/global/en/pages/manufacturing/articles/global-a-and-d-outlook.html (accessed on 20 February 2020)

[DMG Mori, 2019a] *Lasertec 65 3D Hybrid*, DMG Mori. Available online: https://en.dmgmori.com/products/machines/advanced-

technology/additive-manufacturing/powder-nozzle/lasertec-65-3d-hybrid (accessed on 20 February 2020)

[DMG Mori, 2019b] *Lasertec 4300 3D Hybrid*, *DMG Mori*. Available online: https://en.dmgmori.com/products/machines/advanced-technology/additive-manufacturing/powder-nozzle/lasertec-4300-3d-hybrid (accessed on 20 February 2020)

[DMG Mori, 2017] *Global full-liner for additive manufacturing*, DMG Mori. Available online: https://nl.dmgmori.com/news-and-media/technical-press-news/news/emo-2017-additive-manufacturing (accessed on 20 February 2020)

[Donadello, 2019] S. Donadello, M. Motta, A. G. Demir, and B. Previtali, *Monitoring of laser metal deposition height by means of coaxial laser triangulation*, Opt. Lasers Eng., 112, 136–144, 2019.

[Drizo, 2006] A. Drizo, J. Pegna, *Environmental impacts of rapid prototyping: An overview of research to date*, Rapid Prototyping Journal, 12(2), 64-71, 2006.

[Du, 2016] W. Du, Q. Bai, B. Zhang, *A Novel Method for Additive/Subtractive Hybrid Manufacturing of Metallic Parts*, Procedia Manuf., 5, 1018-1030, 2016.

[Eguren, 2018] J.A. Eguren, D. Justel, I. Iriarte, A. Esnaola, *Opportunities and incentives for Remanufacturing in the Basque Country*, Proc. CIRP, 73, 253–258, 2018.

[Elb Schliff, 2019] *MillGrind hybrid machine*, Elb-Schliff WZM GmbH. Available online: https://www.elb-schliff.de/product-details/alias/millGrind.html (accessed on 20 February 2020)

[El-Hofy, 2005] H. El-Hofy, *Advanced Machining Processes: Nontraditional and Hybrid Machining Processes*, McGraw-Hill, 2005.

[Elser, 2018] A. Elser, M. Königs, A. Verl, M. Servos, *On achieving accuracy and efficiency in Additive Manufacturing: Requirements on a hybrid CAM system*, Proc. CIRP, 72, 1512–1517, 2018.

[Eriksson, 2002] M. Eriksson, M. Oldenburg, M.C. Somani, L.P. Karjalainen, *Testing and Evaluation of Material Data for Analysis of Forming and Hardening of Boron Steel Components*, Model. Simul. Mater. Sci. Eng., 10, 277–294, 2002.

[Escher, 2015] C. Escher and J.J. Wilzer, *Tool steels for hot stamping of high strength automotive body parts,* Int. Conf. Stone Concr. Mach., 3, 219-228, 2015.

[Everton, 2016] S. K. Everton, M. Hirsch, P.I. Stavroulakis, R.K. Leach, A.T. Clare, *Review of in-situ process monitoring and in-situ metrology for metal additive manufacturing*, Materials and Design, 95, 431–445, 2016.

[Farshidianfar, 2017] M.H. Farshidianfar, A. Khajepouhor, A. Gerlich, *Real-time monitoring and prediction of martensite formation and hardening depth during laser heat treatment*, Surf. Coat. Technol., 315, 326-334, 2017.

[Fatemi, 2017] A. Fatemi, R. Molaei, S. Sharifimehr, N. Phan, N. Shamsaei, *Multiaxial fatigue behavior of wrought and additive manufactured Ti-6Al-4V including surface finish effect*, International Journal of Fatigue, 100(1), 347-366, 2017.

[Fayazfar, 2018] H. Fayazfar, M. Salarian, A. Rogalsky, D. Sarker, P. Russo, V. Paserin, E. Toyserkani, *A critical review of powder-based additive manufacturing of ferrous alloys: Process parameters, microstructure and mechanical properties*, Materials & Design., 144, 98-128, 2018.

[Fazarinc, 2011] M. Fazarinc, T. Muhic, A. Salej, D. Bombac, P. Fajfar, M. Tercelj, G. Kugler, *Thermal fatigue testing of bulk functionally graded materials*, Procedia Eng., 10, 692–697, 2011.

[Fernandez, 2019] B. Fernández, B. González, G. Artola, N. López de Lacalle, C. Angulo, *A Quick Cycle Time Sensitivity Analysis of Boron Steel Hot Stamping*, Metals, 9, 235, 2019.

[Flynn, 2016] J.M. Flynn, A. Shokrani, S.T. Newman, V. Dhokia, *Hybrid additive and subtractive machine tools—Research and industrial developments*, Int. J. Mach. Tools Manuf., 101, 79-101, 2016.

[FST, 2019] *AISI H13 (DIN 1.2344) Datasheet*, Flame Spray Technologies, 2019.

[Fujishima, 2017] M. Fujishima, Y. Oda, R. Ashida, K. Takezawa, M. Kondo, *Study on factors for pores and cladding shape in the deposition processes of Inconel 625 by the directed energy deposition (DED) method*, CIRP Journal of Manufacturing Science and Technology, 19, 200-204, 2017.

[Ganapathy, 2017] M. Ganapathy, N. Li, J. Lin, D. Bhattacharjee, *Investigation of a new hot stamping process with improved formability and productivity*, Procedia Engineering, 207, 771-776, 2017.

[Ganjali, 2018] M. Ganjali, A. Yazdanpanah, M. Mozafari, *Laser deposition of nano coatings on biomedical implants*, In: Micro and Nano Technologies, Emerging Applications of Nanoparticles and Architecture Nanostructures, Editor(s): A. Barhoum, A.S. Hamdy Makhlouf, Elsevier, 235-254, 2018.

[Gao, 2014] K. Gao, X. Qin, Z. Wang, H. Chen, S. Zhu, Y. Liu, Y. Song, *Numerical and experimental analysis of 3D spot induction hardening of AISI 1045 steel*, J. Mater. Process. Technol. 214, 2425–2433, 2014.

[García Aranda, 2002] L. García Aranda, Y. Chastel, J.F. Pascual, T.D. Negro, *Experiments and Simulation of Hot Stamping of Quenchable*, *Advanced Technology of Plasticity*, 1135-1140, 2002.

[Gasser, 2011] A. Gasser, *Laser Metal Deposition*, In: Tailored light 2, Editor(s): R. Poprawe, RWTH Edition: Springer, 216-224, 2011.

[Gasser, 2012] A. Gasser, I. Kelbassa, K. Wissenbach, J. Witzel, M. Göbel, *Additive Manufacturing in Turbo-Engine Applications*, AKL 2012 / EU Innovation Forum.

[GF, 2018] *GF Enters Strategic Partnership with Leading 3D Printing Manufacturer*, GF Machining Solutions. Available online: https://www.gfms.com/com/en/about-gf-machining-solutions/press-room/press-releases/2018/gf-enters-strategic-partnership-with-leading-3d-printing-manufac.html (accessed on 20 February 2020)

[GF, 2019] *GF DMP Factory 500*, GF Machining Solutions. Available online: https://www.gfms.com/content/dam/gfac/proddb/advanced-manufacturing/en/brochure-dmp-factory-500-en.pdf (accessed on 20 February 2020)

[Ghiotti, 2016] A. Ghiotti, A. Bruschi, F. Medea, A. Hamasaiid, *Tribological behavior of high thermal conductivity steels for hot stamping tools*, Tribol. Int., 97, 412–422, 2016.

[Gibson, 2016] I. Gibson, D. Rosen, B. Stucker, *Additive Manufacturing Technologies*, Springer New York, 2016.

[Giffi, 2014] C.A. Giffi, B. Gangula, P. Illinda, *3D opportunity in the automotive industry: additive manufacturing hits the road*, Deloitte Insights, 2014. Available online: https://www2.deloitte.com/insights/us/en/focus/3d-opportunity/additive-manufacturing-3d-opportunity-in-automotive.html (accessed on 20 February 2020)

[Gonzalez-Gutierrez, 2018] J. Gonzalez-Gutierrez, S. Cano, S. Schuschnigg, C. Kukla, J. Sapkota, C. Holzer, *Additive Manufacturing of Metallic and Ceramic Components by the Material Extrusion of Highly-Filled Polymers: A Review and Future Perspectives,* Materials, 11, 840, 2018.

[Gorman, 2016] L. Gorman, *New "hybrid" Additive/Subtractive Machining System Unveiled at IMTS 2016*, Lasers Today, 2016. Available online: https://www.laserstoday.com/2016/12/new-hybrid-additivesubtractive-machining-system-unveiled-at-imts-2016/ (accessed on 20 February 2020)

[Gradl, 2018] P. Gradl, S.E. Greene, C. Protz, B. Bullard, J. Buzzell, C. Garcia, J. Wood, K. Cooper, *Additive Manufacturing of Liquid Rocket Engine Combustion Devices: A Summary of Process Developments and Hot-Fire Testing Results,* 54th AIAA/SAE/ASEE Joint Propulsion Conference 2018.

[Graf, 2012] B. Graf, A. Gumenyuk, M. Rethmeier, *Laser metal deposition as repair technology for stainless steel and titanium alloys,* Physcs. Proc., 39, 376-381, 2012.

[Griffiths, 2015] L. Griffiths, *Setting the Standards in Additive Manufacturing*, TCTMagazine 2015. Available online: https://www.tctmagazine.com/3d-printing-news/setting-the-standards-additive-manufacturing/ (accessed on 20 February 2020)

[Gu, 2015] D. Gu, *Laser Additive Manufacturing (AM): Classification, Processing Philosophy, and Metallurgical Mechanisms,* In: Laser Additive Manufacturing of High-Performance Materials, Springer-Verlag: Berlin/Heidelberg, Germany, 2015.

[Guo, 2013] N. Guo, M.C. Leu, *Additive manufacturing: technology, applications and research needs*, Front. Mech. Eng., 8(3), 215–243, 2013.

[Gupta, 2018] P.K. Gupta, *Lasers for Biomedical and Material Processing Applications*, Proc. Natl. Acad. Sci., India Sect. A: Phys. Sci., 88(3), 357-358, 2018.

[Haley, 2017] D. Haley, O. Pratt, *Basic principles of lasers*, Anaesthesia & Intensive Care Medicine, 18(12), 648-650, 2017.

[Hällgren, 2016] S. Hällgren, L. Pejryd, J. Ekengren, *(Re)Design for Additive Manufacturing*, Proc. CIRP, 50, 246–251, 2016.

[Hansel, 2016] A. Hansel, M. Mori, M. Fujishima, Y. Oda, G. Hyatt, E. Lavernia, J.P. Delplanque, *Study on Consistently Optimum Deposition Conditions of Typical Metal Material Using Additive/Subtractive Hybrid Machine Tool*, Proc. CIRP, 46, 579-582, 2016.

[Harvey, 2017] A.L. Harvey. *3-D Printing: The Future of Manufacturing and Maintenance*, PowerMag, 2017. Available online: https://www.powermag.com/3-d-printing-the-future-of-manufacturing-and-maintenance/ (accessed on 20 February 2020)

[He, 2016] B. He, L. Ying, X. Li, P. Hu, *Optimal design of longitudinal conformal cooling channels in hot stamping tools*, Applied Thermal Engineering, 106, 1176-1189, 2016.

[Heath, 1989] D.M. Heath, W.P. Winfree, *Thermal Diffusivity Measurements in Carbon-Carbon Composites*, In: Review of Progress in Quantitative Nondestructive Evaluation, Editor(s): D.O. Thompson, D.E. Chimenti, Springer, Boston, MA, 1613-1619, 1989.

[Heigel, 2018] J.C. Heigel, T.Q. Phan, J.C. Fox, T.H. Gnaupel-Herold, *Experimental Investigation of Residual Stress and its Impact on Machining in Hybrid Additive/Subtractive Manufacturing*, Procedia Manuf., 26, 929–940, 2018.

[Hein, 2008] P. Hein, J. Wilsius, *Status and Innovation Trends in Hot Stamping of Usibor® 1500 P*, Steel Res. Int., 79, 85–91, 2008.

[Hejripour, 2018] F. Hejripour, D.T. Valentine, D.K. Aidun, *Study of mass transport in cold wire deposition for Wire Arc Additive Manufacturing*, Int. J. of Heat Mass Transf., 125, 471-484, 2018.

[Henriques, 2012] E. Henriques, P. Peças, *New Business Models for the Tooling Industry*, In: Advances in Business and Management, Editor(s): W.D. Nelson, Nova Science Publishers, New York, 2012.

[Hermle, 2019] *Additive Manufacturing using Hermle MPA Technology,* Hermle Maschinenbau GmbH. Available online: https://www.hermle.de/en/services/additive_manufacturing (accessed on 20 February 2020)

[Herzog, 2016] D. Herzog, V. Seyda, E. Wycisk, C. Emmelmann, *Additive manufacturing of metals*, Acta Materialia, 117, 371–392, 2016.

[Hoffmann, 2007] H. Hoffmann, H. So, H. Steinbeiss, *Design of hot stamping tools with cooling system,* CIRP Ann., 56, 269–272, 2007.

[Hofman, 2012] J. Hofman, B. Pathiraj, J. Van Dijk, D. De Lange, J. Meijer, *A Camera Based Feedback Control Strategy for the Laser Cladding Process*, J. Mater. Process. Technol., 212, 2455–2462, 2012.

[Hölker, 2011] R. Hölker, A. Jäger, N.B. Khalifa, A.E. Tekkaya, *New concepts for cooling of extrusion dies manufactured by rapid tooling*, Key Eng. Mater., 491, 223–232, 2011.

[Hölker, 2015] R. Hölker, M. Haase, N.B. Khalifa, A.E. Tekkaya, *Hot Extrusion Dies with Conformal Cooling Channels Produced by Additive Manufacturing*, Materials Today: Proceedings, 2(1), Part A, 4838-4846, 2015.

[Hölker, 2017] R. Hölker, A. Jäger, A.E Tekkaya, *Additive manufacturing of tools and dies for metal forming*, In: Laser Additive Manufacturing, Editor(s): M. Brandt, Woodhead Publishing: Cambridge, UK, 17, 439-464, 2017.

[Horn, 2019] A. Horn, M. Merklein, *Functional Optimization of Hot-Stamped Components by Local Carburization*, International Journal of Lightweight Materials and Manufacture, 2019 (*In press)*.

[Houghton, 2019] Houghton Iberica, S.A. Ficha Técnica HOCUT B-750; Houghton Iberica, S.A.: Barcelona, Spain, 2018.

[Hu, 1998] Y.P. Hu, C.W. Chen, K. Mukherjee, *Development of a new laser cladding process for manufacturing cutting and stamping dies*, J. Mater. Sci., 33(5), 1287–1292, 1998.

[Hu, 2013] P. Hu, L. Ying, Y. Li, Z. Liao, *Effect of oxide scale on temperature-dependent interfacial heat transfer in hot stamping process*, J. Mater. Process. Technol., 213, 1475-1483, 2013.

[Hu, 2016] P. Hu, B. He, L. Ying, *Numerical investigation on cooling performance on hot stamping tool with various channel designs*, Applied Thermal Engineering, 96, 338-351, 2016.

[Hung, 2014] T.H. Hung, P.W. Tsai, F.K. Chen, T. Bin Huang, W.L. Liu, *Measurement of heat transfer coefficient of boron steel in hot stamping*, Procedia Eng., 1750–1755, 2014.

[Huskic, 2013] A. Huskic, B.A. Behrens, J. Giedenbacher, A. Huskic, *Standzeituntersuchungen generative hergestellter Schmiedewerkzeuge*, Schmiede J., 9, 66–70, 2013.

[Hwang, 2018] T. Hwang, Y.Y. Woo, S.W. Han, Y.H. Moon, *Functionally graded properties in directed-energy-deposition titanium parts*, Opt. Laser Technol., 105, 80-88 2018.

[Hybrid, 2017] *Ambit™ S7 cladding heads,* Hybrid Manufacturing Technologies. Available online: http://www.hybridmanutech.com/news.html (accessed on 20 February 2020)

[Hybrid, 2019] *Ambit™ Multi-Task tools,* Hybrid Manufacturing Technologies. Available online: http://www.hybridmanutech.com/hybrid-manufacturing.html (accessed on 20 February 2020)

[Ibarmia, 2015] *ZVH 45/L1600 Add & Process—Ibarmia*, EMO 2015 Booklet. Available online: https://www.automation.siemens.com/machine-booklet/Booklet/554b7a0d3cb6e12b08e5338c/en/Machine/55d2ebeb3278301a748a9497 (accessed on 20 February 2020)

[Ikeda, 2017] A. Ikeda, *Remanufacturing of automotive parts in Japanese market,* Proc. CIRP, 61, 800 – 803, 2017.

[ILT, 2013] *New CAM system for laser material deposition*, Met. Powder Rep., 68, 36, 2013.

[IPG, 2018] *High Power CW Fiber Lasers*, IPG Photonics. Available online: https://www.ipgphotonics.com/en/products/lasers/high-power-cw-fiber-lasers (accessed on 20 February 2020)

[Imran, 2011] M.K. Imran, S.H. Masood, M. Brandt, *Bimetallic dies with direct metal-deposited steel on Moldmax for high-pressure die casting application*, Int. J. Adv. Manuf. Technol., 52, 855–863, 2011.

[ISO, 2013] British Standards Institution, ISO 13826:2013: Metallic and other inorganic coatings - Determination of thermal diffusivity of thermally sprayed ceramic coatings by laser flash method, 2013.

[ISO/ASTM, 2018] ISO/ASTM 52900. Available online: https://www.iso.org/obp/ui/#iso:std:iso-astm:52900:dis:ed-2:v1:en (accessed on 20 February 2020)

[Jahan, 2017] S.A. Jahan, T. Wu, Y. Zhang, J. Zhang, A. Tovar, H. Elmounayri, *Thermo-mechanical Design Optimization of Conformal Cooling Channels using Design of Experiments Approach*, Procedia Manufacturing, 10, 898-911, 2017.

[Jared, 2017] B.H. Jared, M.A. Aguilo, L.L. Beghini, B.L. Boyce, B.W. Clark, A. Cook, B.J. Kaehr, J. Robbins, *Additive manufacturing: Toward holistic design*, Scripta Materialia, 135, 141–147, 2017.

[Jhavar, 2013] S. Jhavar, *Causes of failure and repairing options for dies and molds: A review*, Engineering Failure Analysis, 34, 519-535, 2013.

[JSA, 2005] Japanese Standards Association, *JIS H 7801:2005: Method For Measuring Thermal Diffusivity Of Metals By The Laser Flash Method*, 2005.

[Karbasian, 2010] H. Karbasian, A.E. Tekkaya, *A review on hot stamping*, Journal of Materials Processing Technology, 210(15), 2103-2118, 2010.

[Karunakaran, 2010] K. Karunakaran, S. Suryakumar, V. Pushpa, S. Akula, *Low cost integration of additive and subtractive processes for hybrid layered manufacturing*, Robotics and Computer-Integrated Manufacturing, 26, 490-499, 2010.

[Kattire, 2015] P. Kattire, S. Paul, R. Singh, W. Yan, *Experimental characterization of laser cladding of CPM 9V on H13 tool steel for die repair applications*, J. Manuf. Process., 20, 492–499, 2015.

[Kelbassa, 2004] I. Kelbassa, A. Gasser, K. Wissenbach, *Laser cladding as a repair technique for BLISKs out of titanium and nickel base alloys used in aero engines*, Pacific International Conference on Applications of Lasers and Optics, 503, 2004.

[Kerbrat, 2011] O. Kerbrat, P. Mognol, J.Y. Hascoët, *A new DFM approach to combine machining and additive manufacturing*, Comput. Ind., 62, 684–692, 2011.

[Kim, 2018] H. Kim, Y. Lin, T.L.B. Tseng, *A review on quality control in additive manufacturing*, Rapid Prototyp. J., 24, 645–669, 2018.

[Klobčar, 2008] D. Klobčar, J. Tušek, *Thermal stresses in aluminium alloy die casting dies*, Comp. Mater. Sci., 43(4), 1147-1154, 2008.

[Klocke, 2014] F. Klocke, A. Klink, D. Veselovac, D.K. Aspinwall, S.L. Soo, M. Schmidt, J. Schilp, G. Levy, J.P. Kruth, *Turbomachinery component manufacture by application of electrochemical, electro-physical and photonic processes*, CIRP Annals-Manufacturing Technology, 63, 703–726, 2014.

[Klocke, 2017] F. Klocke, K. Arntz, M. Teli, K. Winands, M. Wegener, S. Oliari, *State of the art Laser Additive Manufacturing for Hot work Tool Steels*, Proc. CIRP, 63, 58-63, 2017.

[Kobryn, 2001] P. Kobryn, S. Semiatin, *Mechanical properties of laser-deposited Ti-6Al-4V*, Proceedings of the Solid Freeform Fabrication, Austin, TX, USA, 179–186, 2001.

[Koechner, 2006] W. Koechner, *Optical Resonator*, In: Solid-State Laser Engineering, Springer Series in Optical Sciences, 1, 210-299, Springer, New York, 2006.

[Kong, 2010] C.Y. Kong, R.J. Scudamore, J. Allen, *High-rate laser metal deposition of Inconel 718 component using low heat-input approach*, Physcs. Proc., 5, 379–386, 2010.

[Kono, 2018] D. Kono, A. Maruhashi, I. Yamaji, Y. Oda, M. Mori, *Effects of cladding path on workpiece geometry and impact toughness in Directed Energy Deposition of 316L stainless steel*, CIRP Annals, 67(1), 233-236, 2018.

[Kumar, 2017] L.J. Kumar, *Laser metal deposition repair applications for Inconel 718 alloy*, Materials Today: Proceedings, 4, 11068–11077, 2017.

[Laser Systems, 2016] *Cutting up the energy sector*, Laser Systems Europe. Available online: https://www.lasersystemseurope.com/feature/cutting-energy-sector (accessed on 20 February 2020).

[Launder, 1972] B.E. Launder, D.B. Spalding, *Lectures in mathematical models of turbulence*, London, New York, Academic Press, 1972

[Le, 2017] V.T. Le, H. Paris, G. Mandil, *Process planning for combined additive and subtractive manufacturing technologies in a remanufacturing context,* J. Manuf. Syst., 44, 243–254, 2017.

[Le, 2018] V.T. Le, H. Paris, G. Mandil, *The development of a strategy for direct part reuse using additive and subtractive manufacturing technologies*, Addit. Manuf., 22, 687–699, 2018.

[Lee, 2017] H. Lee, C.H.J. Lim, M.J. Low, N. Tham, V.M. Murukeshan, Y.J. Kim, *Lasers in Additive Manufacturing: A Review*, Int. J. Pr. Eng. Man – GT, 4, 307-322, 2017.

[Leino, 2016] M. Leino, J. Pekkarinen, R. Soukka, T*he Role of Laser Additive Manufacturing Methods of Metals in Repair, Refurbishment and Remanufacturing – Enabling Circular Economy*, Physcs. Proc., 83, 752-760, 2016.

[Leunda, 2011] J. Leunda, C. Soriano, C. Sanz, V. García Navas, *Laser Cladding of Vanadium-Carbide Tool Steels for Die Repair*, Physcs. Proc., 12, Part A, 345-352, 2011.

[Ley, 2018] N. Ley, S.S. Joshi, B. Zhang, Y.H. Ho, N.B. Dahotre, M.L. Young, *Laser coating of a CrMoTaWZr complex concentrated alloy onto a H13 tool steel die head*, Surface and Coatings Technology, 348, 150-158, 2018.

[Li, 2018] L. Li, A. Haghighi, Y. Yang, *A novel 6-axis hybrid additive-subtractive manufacturing process: Design and case studies*, J. Manuf. Process., 33, 150–160, 2018.

[Lima, 2017] D.D. Lima, S.A. Mantri, C.V. Mikler, R. Contieri, C.J. Yannetta, K.N. Campo, E.S. Lopes, M.J. Styles, T. Borkar, R. Caram, R. Banerjee, *Laser additive processing of a functionally graded internal fracture fixation plate*, Materials & Design, 130, 8-15, 2017.

[Lin, 2014] T. Lin, H.W. Song, S.H. Zhang, M. Cheng, W.J. Liu, *Cooling systems design in hot stamping tools by a thermal-fluid-mechanical coupled approach*, Adv. Mech. Eng., 2014.

[Lippold, 2014] J.C. Lippold, *Hydrogen-Induced Cracking*, In: Welding Metallurgy and Weldability, Editor: J.C. Lippold, John Wiley & Sons, 213-262, 2014.

[Liu, 2015] Y. Liu, T. Bobek, F. Klocke, *Laser path calculation method on triangulated mesh for repair process on turbine parts*, Comput.-Aided Des., 66, 73–81, 2015.

[Liu, 2017a] R. Liu, Z. Wang, T. Sparks, F. Liou, J. Newkirk, *Aerospace applications of laser additive manufacturing*, In: Laser Additive Manufacturing, Editor(s): M. Brandt, Woodhead Publishing: Sawston, UK, 2017.

[Liu, 2017b] X. Liu, K. Ji, O. El Fakir, H. Fang, M.M. Gharbi, L. Wang, *Determination of the interfacial heat transfer coefficient for a hot aluminium stamping process*, J. Mater. Process. Technol., 247, 158–170, 2017.

[Locke, 2010] D. Locke, A. Candel-Ruiz, *Laser metal deposition defined*, Industrial Lasers Solutions. Available online: https://www.industrial-lasers.com/articles/print/volume-250/issue-6/features/laser-metal-deposition.html (accessed on 20 February 2020).

[Lorenz, 2012] D. Lorenz, *Hot Stamping Process Simulation with LS-DYNA Capabilities and Benefits*, 2012. Available online: https://www.dynamore.de/en/downloads/infodays/dokumente/kalt-undwarmumformprozesse2012/hot-stamping-process/view (accessed on 20 February 2020).

[Lorenz, 2015] K.A. Lorenz, J.B. Jones, D.I. Wimpenny, M.R. Jackson, *A review of hybrid manufacturing*, Solid Freeform Fabrication Conference Proceedings, 53, 2015.

[Lu, 2019] J.Z. Lu, J. Cao, H.F. Lu, L.Y. Zhang, K.Y. Luo, *Wear properties and microstructural analyses of Fe-based coatings with various WC contents on H13 die steel by laser cladding*, Surf. Coatings Technol., 369, 228–237, 2019.

[Luan, 2016] X. Luan, X. Liu, H. Fang, K. Ji, O. El Fakir, L. Wang, *Characterization of the interfacial heat transfer coefficient for hot stamping processes*, Journal of Physics: Conference Series, 734, 2016.

[Lv, 2016] M. Lv, Z. Gu, X. Li, H. Xu, *Optimal Design for Cooling System of Hot Stamping Dies*, ISIJ Int., 56, 2250–2258, 2016.

[Tabernero, 2018] I. Tabernero, A. Paskual, P. Álvarez; A. Suárez, *Study on Arc Welding Processes for High Deposition Rate Additive Manufacturing*, Proc. CIRP, 68, 358-362, 2018.

[Telasang, 2014] G. Telasang, J. Dutta Majumdar, G. Padmanabham, M. Tak, I. Manna, *Effect of laser parameters on microstructure and hardness of laser clad and tempered AISI H13 tool steel*, Surface and Coatings Technology, 258, 1108–1118, 2014.

[Terrassa, 2018] K.L. Terrassa, J.C. Haley, B.E. MacDonald, J.M. Schoenung, *Reuse of powder feedstock for Directed Energy Deposition*, Powder Technology, 338, 819–829, 2018.

[Trumpf, 2018] *The Power of Choice*, Trumpf. https://www.trumpf.com/filestorage/TRUMPF_US/Corporate/Corporate_Brochures_and_publications/TRUMPF-laser-beam-sources-broschure-EN.pdf (accessed on 20 February 2020)

[Maeno, 2015] T.I. Maeno, K.I. Mori, M. Fujimoto, *Improvements in productivity and formability by water and die quenching in hot stamping of ultra-high strength steel parts*, CIRP Annals, 64(1), 281-284, 2015.

[Mahamood, 2013] R.M. Mahamood, E.T. Akinlabi, M. Shukla, S. Pityana, *Material efficiency of laser metal deposited Ti6Al4V: Effect of laser power*, Eng. Lett., 21, 18–22, 2013.

[Maillet, 2000] D. Maillet, C. Moyne, B. Rémy, *Effect of a thin layer on the measurement of the thermal diffusivity of a material by a flash method*, Int. J. Heat Mass Transf., 43, 4057–4060, 2000.

[Maiman, 1960] T.H. Maiman, *Stimulated optical radiation in ruby*, Nature, 187, 493-494, 1960.

[Mandić, 2016] M. Mandić, T. Galeta, P. Raos, V. Jugović, *Dimensional accuracy of camera casing models 3D printed on Mcor IRIS: A case study*, Adv. Prod. Eng. Manag., 11, 324–332, 2016.

[Manogharan, 2015] G. Manogharan, R. Wysk, O. Harrysson, R.Aman, *AIMS—A Metal Additive-Hybrid Manufacturing System: System Architecture and Attributes*, Procedia Manuf., 1, 273–286, 2015.

[Mans, 2011] T. Mans, *Laser Beam Sources*, In: Tailored light 2, Editor(s): R. Poprawe, RWTH Edition: Springer, 2011.

[Maquinser, 2019a] *Lumex Avance 25,* Maquinser. Available online: https://www.maquinser.com/en/product/lumex_avance_25/ (accessed on 20 February 2020)

[Maquinser, 2019b] *Lumex Avance 60*, Maquinser. Available online: https://www.maquinser.com/producto/lumex-avance-60/ (accessed on 20 February 2020)

[Marinelli, 2019] G. Marinelli, F. Martina, S. Ganguly, S. Williams, H. Lewtas, D. Hancock, S. Mehraban, N. Lavery, *Microstructure and thermal properties of unalloyed tungsten deposited by wire + Arc Additive Manufacturing,* J. Nucl. Mater., 522, 45–53, 2019.

[Markillie, 2013] P. Markillie, *A Third Industrial Revolution*, The Economist, 2013. Available online: http://www.economist.com/node/21552901 (accessed on 20 February 2020)

[Matsuura, 2019a] *Lumex*, Matsuura. Available online: http://www.lumex-matsuura.com/english/ (accessed on 20 February 2020)

[Matsuura, 2019b] *Hybrid Metal 3D Printer*, Matsuura. Available online: https://teknologiateollisuus.fi/sites/default/files/file_attachments/1300_matsuura.pdf (accessed on 20 February 2020)

[Matsuura, 2019c] *Lumex Series*, Matsuura. Available online: http://www.lumex-matsuura.com/english/contents/lumex03.html (accessed on 20 February 2020)

[Mazak, 2014] *Hybrid Multi-Tasking Machine—AM,* Mazak. Available online: https://www.mazakeu.co.uk/machinestechnology/technology/hybrid-multi-tasking-machine/ (accessed on 20 February 2020)

[Mazak, 2016] *Integrex i-200s AM,* Mazak. Available online: https://english.mazak.jp/news-events/press-releases/integrex-i-200s-am/ (accessed on 20 February 2020)

[Mazak, 2017] *Variaxis j-600 AM*, Mazak. Available online: https://www.mazakusa.com/news-events/news-releases/new-variaxis-j-600am-grows-the-mazak-additive-series/ (accessed on 20 February 2020)

[Mazak, 2018] *Mazatrol Smooth CNC*, Mazak. Available online: https://english.mazak.jp/machines/process/cnc-software/CNC/#high-quality (accessed on 20 February 2020)

[Mazak, 2019a] *Integrex i-400 AM*, Mazak. Available online: https://www.mazakusa.com/machines/integrex-i-400am/ (accessed on 20 February 2020)

[Mazak, 2019b] *Integrex VC-500 AM*, Mazak. Available online: https://www.mazakusa.com/machines/vc-500-am/ (accessed on 20 February 2020)

[Mazumder, 1996] J. Mazumder, *Laser assisted surface coatings*, In: Metallurgical and Ceramic Protective Coatings, Editor(s): Stern K.H., Springer, Dordrecht, 1996.

[Mazumder, 2000] J. Mazumder, D. Dutta, N. Kikuchi, *Closed loop direct metal deposition: Art to part*, Opt. Laser Eng., 34, 397–414, 2000.

[Mazumder, 2017] J. Mazumder, *Laser-aided direct metal deposition of metals and alloys*, In: Laser Additive Manufacturing, Editor(s): M. Brandt, Woodhead Publishing: Sawston, UK, 21-53, 2017.

[McAndrew, 2018] A.R. McAndrew, M. Alvarez Rosales, P.A. Colegrove, J.R. Hönnige, A. Ho, R. Fayolle, K. Eyitayo, I. Stan, P. Sukrongpang, A. Crochemore, Z. Pinter, *Interpass rolling of Ti-6Al-4V wire + arc additively manufactured features for microstructural refinement*, Addit. Manuf., 21, 340-349, 2018.

[Merklein, 2016] M. Merklein, D. Junker, A. Schaub, F. Neubauer, *Hybrid additive manufacturing technologies—An analysis regarding potentials and applications*, Physcs. Proc., 83, 549–559, 2016.

[Metallied, 2019] *Pearl® Micro 316L Datasheet*, Metallied Powder Solutions S.A., 2019.

[Milewski, 1998] J.O. Milewski, G.K. Lewis, D.J. Thoma, G.I. Keel, R.B. Nemec, R.A. Reinert, *Directed light fabrication of a solid metal hemisphere using 5-axis powder deposition*, J. Mater. Process. Technol., 75, 165-172, 1998.

[Morgan, 2017] D. Morgan, E. Agba, C. Hill, *Support Structure Development and Initial Results for Metal Powder Bed Fusion Additive Manufacturing*, Procedia Manufacturing, 10, 819 – 830, 2017.

[Mori, 2017] K. Mori, P.F. Bariani, B.-A. Behrens, A. Brosius, S. Bruschi, T. Maeno, M. Merklein, J. Yanagimoto, *Hot stamping of ultra-high strength steel parts*, CIRP Annals, 66(2), 755-777, 2017.

[Morrow, 2007] W.R. Morrow, H. Qi, I. Kim, J. Mazumder, S.J. Skerlos, *Environmental aspects of laser-based and conventional tool and die manufacturing*, J. Clean. Prod., 15, 932-943, 2007.

[Mozaffari, 2013] A. Mozaffari, A. Fathi, A. Khajepour, E. Toyserkani, *Optimal Design of Laser Solid Freeform Fabrication System and Real-Time Prediction of Melt Pool Geometry Using Intelligent Evolutionary Algorithms*, Appl. Soft Comput., 13, 1505–1519, 2013.

[Müller, 2013] B. Müller, *Konturnahe Temperierung beim Presshärten*, Fraunhofer Institut für Werkzeugmaschinen und Umformtechnik (IWU), 2013.

[Mumtaz, 2009] K. Mumtaz, N. Hopkinson, *Top surface and side roughness of Inconel 625 parts processed using selective laser melting,* Rapid Prototyp. J., 15, 96–103, 2009.

[Muro, 2018a] M. Muro, G. Artola, A. Gorriño, C. Angulo, *Effect of the Martensitic Transformation on the Stamping Force and Cycle Time of Hot Stamping Parts*, Metals, 8, 385, 2018.

[Muro, 2018b] M. Muro, G. Artola, A. Gorriño, C. Angulo, *Wear and Friction Evaluation of Different Tool Steels for Hot Stamping*, Adv. Mater. Sci. Eng., 2018, 1–11, 2018.

[Muvunzi, 2018] R. Muvunzi, D.M. Dimitrov, S. Matope, T.M. Harms, *Development of a Model for Predicting Cycle Time in Hot Stamping*, Procedia Manufacturing, 21, Pages 84-91, 2018.

[Naganathan, 2012] A. Naganathan, L. Penter, *Hot stamping,* In: Sheet Metal Forming—Processes and Applications, Editor(s): T. Altan, A. Tekkaya, ASM International, 133–142, 2012.

[Nagulin, 2018] K.Y. Nagulin, F.R. Iskhakov, A.I. Shpilev, A.K. Gilmutdinov, *Optical diagnostics and optimization of the gas-powder flow in the nozzles for laser cladding*, Opt. Laser Technol., 108, 310–320, 2018.

[Nassehi, 2011] A. Nassehi, S. Newman, V. Dhokia, Z. Zhu, R.I. Asrai, *Using formal methods to model hybrid manufacturing processes*, 4th International Conference on Changeable, Agile, Reconfigurable and Virtual Production, Montreal, Canada, 2011.

[Navas, 2005] C. Navas, A. Conde, B. J. Fernández, F. Zubiri, J. de Damborenea, *Laser coatings to improve wear resistance of mould steel*, Surf. Coatings Technol., 194(1), 136–142, 2005.

[Navrotsky, 2015] V. Navrotsky, A. Graichen, H. Brodin, *Industrialisation of 3D printing (additive manufacturing) for gas turbine components repair and manufacturing*, VGB PowerTech, 12, 48-52, 2015.

[Newton, 2018] L. Newton, C. Gomez, F. Helmli, L. Blunt, N. Senin, R. Danzl, R. Leach, *A real topography measurement of metal additive surfaces using focus variation microscopy*, Addit. Manuf., 25, 365–389, 2018.

[Nolte, 2017] P.W. Nolte, T. Malvisalo, F. Wagner, S. Schweizer, *Thermal diffusivity of metals determined by lock-in thermography*, Quant. Infrared Thermogr. J., 14, 218–225, 2017.

[Ocelík, 2007] V. Ocelík, U. De Oliveira, J.T.M. De Hosson, *Thick tool steel coatings with laser cladding*, WIT Trans. Eng. Sci., 55, 13–22, 2007.

[Oerlikon, 2017] *Additive Manufacturing Factsheet*, Oerlikon. Available online: https://www.oerlikon.com/ecoma/files/Oerlikon-AM-Factsheet_II.pdf (accessed on 20 February 2020)

[Oerlikon, 2019] MetcoClad 718 Material Product Data Sheet, Oerlikon Metco: Pfäffikon, Switzerland, 2018

[Oh, 2019] S. Oh, H. Ki, *Deep learning model for predicting hardness distribution in laser heat treatment of AISI H13 tool steel*, Appl. Therm. Eng. 153 (2019) 583–595.

[Okuma, 2019a] *MU-5000V Laser EX*, Okuma, Available online: https://www.okuma.eu/products/by-technology/laser-hardening-laser-metal-deposition/mu-v-laser-ex-series/mu-5000v-laser-ex/ (accessed on 20 February 2020)

[Okuma, 2019b] *Multus U3000 Laser EX*, Okuma. Available online: https://www.okuma.eu/products/by-technology/laser-hardening-laser-metal-deposition/multus-u-laser-ex-series/multus-u3000-laser-ex/ (accessed on 20 February 2020)

[Optech, 2018] *Laser Market Data*, Optech. Available online: http://www.optech-consulting.com/html/laser_market_data1.html (accessed on 20 February 2020)

[Oyelola, 2018] O. Oyelola, P. Crawforth, R. M'Saoubi, A.T. Clare, *On the machinability of directed energy deposited Ti6Al4V*, Addit. Manuf., 19, 39–50, 2018.

[Paar, 2007] U. Paar, I. Valls, *Werkzeugstähle und Strategie für die Warmumformung und Hartbeschneiden*, in: Erlangener Workshop Warmblechumformung, Bamberg, Meisenbach, 73–92, 2007.

[Padmanabham, 2018] G. Padmanabham, R. Bathe, *Laser Materials Processing for Industrial Applications*, Proc. Natl. Acad. Sci., India Sect. A: Phys. Sci., 88, 359-374, 2018.

[Parker, 1961] W.J. Parker, R.J. Jenkins, C.P. Butler, G.L. Abbott, *Flash Method of Determining Thermal Diffusivity, Heat Capacity, and Thermal Conductivity*, J. Appl. Phys., 32, 1679–1684, 1961.

[Patra Karmakar, 2019] D. Patra Karmakar, M. Gopinath, A.K. Nath, *Effect of tempering on laser remelted AISI H13 tool steel*, Surf. Coatings Technol., 361, 136-149, 2019.

[Pinkerton, 2004] A.J. Pinkerton, L. Li, *The significance of deposition point standoff variations in multiple-layer coaxial laser cladding (coaxial cladding standoff effects),* Int. J. Mach. Tools Manuf., 44, 573–584, 2004.

[Pinkerton, 2016] A.J. Pinkerton, *Lasers in Additive Manufacturing*, Opt. Laser Technol., 78, 25-32, 2016.

[Poprawe, 2011] R. Poprawe, Tailored Light 2: Laser Application Technology, Springer-Verlag Berlin Heidelberg, 2011.

[Pou, 2018] J. Pou, F. Lusquiños, R. Comesaña, M. Boutinguiza, *Production of Biomaterial Coatings by Laser-Assisted Processes*, In: Advances in Laser Materials Processing, Editor(s): J. Lawrence, Woodhead Publishing, 381-412, 2018.

[Priarone, 2017] P.C. Priarone, G. Ingarao, *Towards criteria for sustainable process selection: On the modelling of pure subtractive versus additive/subtractive integrated manufacturing approaches*, J. Clean. Prod., 144, 57-68, 2017.

[PR Newswire, 2018] *3D Systems and GF Machining Solutions Announce DMP Factory 500—Integrating the Best of Additive and Subtractive to Transform Manufacturing*, PR Newswire. Available online: https://www.prnewswire.com/news-releases/3d-systems-and-gf-machining-solutions-announce-dmp-factory-500---integrating-the-best-of-additive-and-subtractive-to-transform-manufacturing-300708474.html (accessed on 20 February 2020)

[Purtonen, 2014] T. Purtonen, A. Kalliosaari, A. Salminen, *Monitoring and adaptive control of laser processes*, Physcs. Proc., 56, 1218–1231, 2014.

[Ren, 2006] L. Ren, A.P. Padathu, J. Ruan, T. Sparks, F.W. Liou, *Three dimensional die repair using a hybrid manufacturing system*, Proceedings of the 17th Solid Freeform Fabrication Symposium, Austin, TX, USA, 51–59, 2006.

[Renderos, 2017] M. Renderos, A. Torregaray, M.E. Gutierrez-Orrantia, A. Lamikiz, N. Saintier, F. Girot, *Microstructure characterization of recycled IN718 powder and resulting laser clad material*, Mater. Charact., 134, 103-113, 2017.

[Rickli, 2014] J.L. Rickli, A.K. Dasgupta, G.P. Dinda, *A descriptive framework for additive remanufacturing systems*, Int. J. Rapid Manuf., 4, 199-218, 2014.

[Roberts, 1998] G. Roberts, G. Krauss, R. Kennedy, *Tool Steels,* 5th ed. ASM, International, 1998.

[Rofin, 2004] Introduction to Industrial Lasers Material Processing. Rofin-Sinar Laser, 2004.

[Ruiz, 2018] J.E. Ruiz, H. González, M. Cortina, J.I. Arrizubieta, A. Lamikiz, *IBR manufacturing by hybrid combination of laser metal deposition and machining process,* Proceedings of the 26th International Conference on Advanced Nanotechnology, Moscow, Russia, 4, 62-63, 2018.

[Salonitis, 2015] K. Salonitis, S.A. Zarban, *Redesign Optimization for Manufacturing Using Additive Layer Techniques*, Proc. CIRP, 36, 193–198, 2015.

[Sandmeyer, 2014] *Specification Sheet: Alloy 316/316L*, Sandmeyer Steel Company, 2014. Available online: https://www.sandmeyersteel.com/images/316-316l-317l-spec-sheet.pdf (accessed on 20 February 2020)

[Schieck, 2011] F. Schieck, C. Hochmuth, S. Polster, A. Mosel, *Modern tool design for component grading incorporating simulation models, efficient tool cooling concepts and tool coating systems*, CIRP J. Manuf. Sci. Technol., 4, 189–199, 2011.

[Schuh, 2017] G. Schuh, M. Salmen, T. Kuhlmann, J. Wiese, *Highly Iterative Product Development Within The Tool and Die Making Industry*, Proc. CIRP, 61, 576-581, 2017.

[Schuler Group, 2017] Hot Stamping with PCH FLEX, Schuler Group.

[Sciaky, 2017] Available online: http://www.sciaky.com/ (accessed on 20 February 2020)

[Scott, 2016] C. Scott, *Mitsui Seiki USA to Introduce the Vertex 55X-H, a New Hybrid CNC Machine and 3D Printer*, 3DPrint, 2016. Available online: https://3dprint.com/141841/mitsui-seiki-cnc-3d-printer/ (accessed on 20 February 2020)

[Shamsaei, 2015] N. Shamsaei, A. Yadollahi, L. Bian, S.M. Thompson, *An overview of Direct Laser Deposition for additive manufacturing; Part II: Mechanical behavior, process parameter optimization and control*, Addit. Manuf., 8, 12–35, 2015.

[Shan, 2013] Z.D. Shan, Y.S. Ye, M.L. Zhang, B.Y. Wang, *Hot-stamping die-cooling system for vehicle door beams*, Int. J. Precis. Eng. Manuf., 14, 1251-1255, 2013.

[Shapiro, 2009] A.B. Shapiro, *Using LS-Dyna for Hot Stamping*, 7th Eur. LS-DYNA Conf., 2009.

[Shinde, 2017] M.S. Shinde, K.M. Ashtankar, *Additive manufacturing-assisted conformal cooling channels in mold manufacturing processes*, Adv. Mech. Eng., 9, 1–14, 2017.

[Shokrani, 2019] A. Shokrani, I. Al-Samarrai, S.T. Newman, *Hybrid cryogenic MQL for improving tool life in machining of Ti-6Al-4V titanium alloy*, J. Manuf. Process., 43, 229–243, 2019.

[Siemens, 2015] *Additive & Hybrid Manufacturing*, Siemens PLM. Available online: https://community.plm.automation.siemens.com/t5/News-NX-Manufacturing/Additive-amp-Hybrid-Manufacturing-The-Future-of-3D-Printing-is/ba-p/309426 (accessed on 20 February 2020)

[Siemens, 2018a] *Quality Inspection for 3D Printing*, Siemens PLM. Available online: https://www.plm.automation.siemens.com/global/en/products/manufacturing-planning/quality-inspection-3d-printing.html (accessed on 20 February 2020)

[Siemens, 2018b] *NX for Manufacturing*, Siemens PLM. Available online: http://www.plm.automation.siemens.com/en_us/products/nx/for-manufacturing/cam/hybrid-additive-manufacturing.shtml (accessed on 20 February 2020)

[Siemens, 2018c] *NX CAM Hybrid Manufacturing*, Siemens PLM Software. Available online: https://www.flickr.com/photos/31274959@N08/albums/72157653490811501/with/18100938796/ (accessed on 20 February 2020)

[Skarzynski, 2018] J. Skarzynski, *Tech Tuesday—Is a Powder Stream Additive Process Right for You?,* Techsolve, 2018. Available online: https://www.techsolve.org/blog/manufacturing-blog/tech-tuesday-powder-stream-additive-process-right-you-check-out-these-4-key (accessed on 20 February 2020)

[Sodick, 2019a] *OPM 250L*, Sodick. Available online: https://www.sodick.com/products/metal-3d-printing/opm250l (accessed on 20 February 2020)

[Sodick, 2019b] *OPM 350L*, Sodick. Available online: https://www.sodick.org/products/additive-manufacturing/opm350l.html (accessed on 20 February 2020)

[Soshi, 2017] M. Soshi, J. Ring, C. Young, Y. Oda, M. Mori, *Innovative grid molding and cooling using an additive and subtractive hybrid CNC machine tool*, CIRP Ann., 66, 401–404, 2017.

[Srivastava, 2003] A. Srivastava, V. Joshi, R. Shivpuri, R. Bhattacharya, S. Dixit, *A multilayer coating architecture to reduce heat checking of die surfaces*, Surface and Coatings Technology, 163–164, 631-636, 2003.

[Stavropoulos, 2018] P. Stavropoulos, P. Foteinopoulos, A. Papacharalampopoulos, H. Bikas, *Addressing the challenges for the industrial application of additive manufacturing: Towards a hybrid solution,* Int. J. Lightw. Mater. Manuf., 1, 157–168, 2018.

[Steen, 2003] W.M. Steen, K.W. Watkins, *Laser Material Processing*, Springer, New York, 2003.

[Steen, 2010] W.M. Steen, J. Mazumder, *Background to laser design and general applications*, In: Laser Material Processing, Springer Science & Business Media, 11-78, 2010.

[Steinbeiss, 2007] H. Steinbeiss, H. So, T. Micheltisch, H. Hoffmann, *Method for Optimizing the Cooling Design of Hot Stamping Tools*, Prod. Eng., 1, 149-155, 2007.

[Strategies Unlimited, 2017] The Worldwide Market for Lasers: Market Review and Forecast 2018.

[Taha, 2014] Z. Taha, A.R. Yusoff, M.F.M Sharif, M.A.H. Saharudin, M.F. Zamri, *Comparison of Cooling Performance between High Thermal Conductivity Steel (HTCS 150) and Hot Work Tool Steel (SKD 61) Insert for Experimental Tool Using Finite Element Analysis*, Advanced Materials Research, 903, 163-168, 2014.

[Tapia, 2014] G. Tapia, A. Elwany, *A review on process monitoring and control in metal- based additive manufacturing*, J. Manuf. Sci. Eng., 136(6), 2014.

[TCT Magazine, 2015] *World's First Hybrid Grinding and Additive Manufacturing Machine Unveiled*, TCT Magazine, 2015. Available online: https://www.tctmagazine.com/3d-printing-news/worlds-first-hybrid-grinding-andadditive-manufacturing-machine/ (accessed on 20 February 2020)

[Thomas, 2011] G. Thomas, R. Isaacs, *Basic principles of lasers*, Anaesthesia & Intensive Care Medicine, 12(12), 574-577, 2011.

[Thompson, 1999] S. Thompson, *Handbook of mold, tool and die repair welding*, William Andrew Publishing, 1999.

[Thompson, 2015] S.M. Thompson, L. Bian, N. Shamsaei, A. Yadollahi, *An overview of Direct Laser Deposition for additive manufacturing; Part I: transport phenomena, modeling and diagnostics*, Addit. Manuf., 8, 36-62, 2015.

[Torims, 2013] T. Torims, *The application of laser cladding to mechanical component repair, renovation and regeneration*, DAAAM International Scientific Book, DAAAM International, 2013.

[Townsend, 2018] A. Townsend, R. Racasan, R. Leach, N. Senin, A. Thompson, A. Ramsey, D. Bate, P. Woolliams, S. Brown, L. Blunt, *An interlaboratory comparison of X-ray computed tomography measurement for texture and dimensional characterisation of additively manufactured parts*, Addit. Manuf., 23, 422–432, 2018.

[Toyserkani, 2005] E. Toyserkani, A. Khajepour, S.F. Corbin, Laser Cladding, CRC Press, 2005.

[Transparency Market Research, 2018] *Hybrid Additive Manufacturing Machines – Global Industry Analysis, Size, Share, Growth, Trends and Forecast, 2018 – 2026*, Transparency Market Research. Available online: https://www.transparencymarketresearch.com/hybrid-additive-manufacturing-machines-market.html (accessed on 20 February 2020).

[Trumpf, 2017] *2016/17 Annual Report*, Trumpf. Available online: https://www.trumpf.com/filestorage/TRUMPF_Master/Corporate/Annual_report/Current/TRUMPF_Annual-Report.pdf (accessed on 20 February 2020).

[Uddeholm, 2017] *Welding of Uddeholm Tool Steels*, Uddeholm, 2017. Available online: https://www.uddeholm.com/app/uploads/sites/45/2018/02/Uddeholm_welding_eng_1710_e7.pdf (accessed on 20 February 2020).

[Uddeholm, 2019] *Uddeholm Orvar Supreme Datasheet*, Uddeholm, 2019. Available online: http://www.uddeholm.com/files/PB_orvar_supreme_english.pdf (accessed on 20 February 2020).

[Valls, 2010] I. Valls, B. Casas, N. Rodríguez, U. Paar, *Benefits from using high thermal conductivity tool steels in the hot forming of steels*, La Metallurgia Italiana, Issue 11-12, 2010.

[Valls, 2017] I. Valls, A. Hamasaiid, A. Padré, *High Thermal Conductivity and High Wear Resistance Tool Steels for cost-effective Hot Stamping Tools,* Journal of Physics: Conference Series, 896, 2017.

[Valls, 2018] I. Valls, A. Hamasaiid, A. Padré, *New approaches to thermal tool performance, cooling and machining strategy: the strongly correlated triple that determines the cost effectiveness of the process*, IOP Conference Series Materials Science and Engineering 418(1), 2018.

[Venkatesh, 2017] G. Venkatesh, Y.R. Kumar, *Thermal Analysis for Conformal Cooling Channel*, Materials Today: Proceedings, 4, 2, 2592–2598, 2017.

[Vilar, 2014] R. Vilar, *Laser Powder Deposition*, In: Comprehensive Materials Processing, Editor(s): S. Hashmi, G. Ferreira Batalha, C.J. Van Tyne, B. Yilbas, Elsevier, 163-216, 2014.

[Vollmer, 2014] R. Vollmer, R. Kolleck, P. Schwemberger, *Herstellung oberflächennaher kühlkanalstrukturen für das Presshärten mittels Laserauftragschweißen,* Proceedings of the Tagungsband zum 9. Erlanger Workshop Warmblechumformung, Erlangen, Germany, 61–73, 2014.

[Volvo, 2017] *Volvo XC60 body structure*, Volvo, 2017. Available online: https://www.media.volvocars.com/image/low/205097/1_1/5 (accessed on 20 February 2020)

[Wally, 2019] Z.J. Wally, A.M. Haque, A. Feteira, F. Claeyssens, R. Goodall, G.C. Reilly, *Selective laser melting processed Ti6Al4V lattices with graded porosities for dental applications,* J. Mech. Behav. Biomed. Mater., 90, 20–29, 2019.

[Walter, 2018] J. Walter, A. Baumgärtel, M. Hustedt, R. Hebisch, S. Kaierle, *Inhalation exposure to hazardous substances during powder-bed processes,* Proc. CIRP, 74, 295–299, 2018.

[Wang, 2006] S.H. Wang, J.Y. Chen, L. Xue, *A study of the abrasive wear behaviour of laser-clad tool steel coatings*, Surf. Coatings Technol., 200(11), 3446–3458, 2006.

[Weisheit, 2001] A. Weisheit, G. Backes, R. Stromeyer, A. Gasser, K. Wissenbach, R. Poprawe, *Powder Injection: The Key to Reconditioning and Generating Components Using Laser Cladding,* Proceedings of the Materials Week, Munich, Germany, 1–4, 2001.

[WFL, 2019] *Additive Manufacturing,* WFL. Available online: https://www.wfl.at/en/technologies/additive-manufacturing (accessed on 20/02/2020)

[Wilson, 2014] J.M. Wilson, C. Piya, Y.C. Shin, F. Zhao, K. Ramani, *Remanufacturing of turbine blades by laser direct deposition with its energy and environmental impact analysis*, J. Clean. Prod., 80, 170-178, 2014.

[Wohlers, 2017] Wohlers Report 2017

[Wohlers, 2018] Wohlers Report 2018

[Woods, 2009] S. Woods, *Understanding Materials Processing Lasers*, Laser Systems, 2009. Available online: https://onlinelibrary.wiley.com/doi/pdf/10.1002/latj.200990070 (accessed on 20/02/2020)

[Wu, 2018] B. Wu, Z. Pan, D. Ding, D. Cuiuri, H. Li, J. Xu, J. Norrish, *A review of the wire arc additive manufacturing of metals: properties, defects and quality improvement*, Journal of Manufacturing Processes, 35, 127-139, 2018.

[Xue, 2004] L. Xue, A. Theriault, M.U. Islam, M. Jones, H.P. Wang, *Laser consolidation of TI-6AL-4V alloy to build functional net-shape airfoils with embedded cooling channels,* Proceedings of ICALEO, 2004.

[Yamazaki, 2016] T. Yamazaki, *Development of A Hybrid Multi-tasking Machine Tool: Integration of Additive Manufacturing Technology with CNC Machining*, Proc. CIRP, 42, 81–86, 2016.

[Yan, 2018] L. Yan, Y. Zhang, J.W. Newkirk, F. Liou, E. Thomas, A. Baker, *Investigation of machining coolant residue cleaning methods for Ti6Al4V part fabrication through hybrid manufacturing process*, Manuf. Lett., 16, 10–13, 2018.

[Yang Chua, 2017] Z. Yang Chua, I.H. Ahn, S.K. Moon, *Process Monitoring and Inspection Systems in Metal Additive Manufacturing: Status and Applications,* Int. J. Precis. Eng. Manuf.-Green Technol., 4, 235–245, 2017.

[Zadi-Maad, 2018] A. Zadi-Maad, R. Rohib, A. Irawan, *Additive manufacturing for steels: a review*, IOP Conference Series: Materials Science and Engineering, 285(1), 2018.

[Zekovic, 2007] S. Zekovic, R. Dwivedi, R. Kovacevic, *Numerical simulation and experimental investigation of gas–powder flow from radially symmetrical nozzles in laser-based direct metal deposition*, Int. J. Mach. Tools Manuf., 47, 112–123, 2007.

[Zelinski, 2015] P. Zelinski, *Panel Discusses Promise and Challenges of Both Additive and Hybrid Machines*, Additive Manufacturing Magazine, 2015. Available online: https://www.additivemanufacturing.media/blog/post/panel-discusses-promise-and-challenges-of-both-additive-and-hybrid-machines- (accessed on 20 February 2020)

[Zelinski, 2016] P. Zelinski, *Integrating Additive without Inhibiting Machining,* Additive Manufacturing Magazine, 2016. Available online: https://www.additivemanufacturing.media/blog/post/integrating-

additive-without-inhibiting-machining (accessed on 20 February 2020)

[Zelinski, 2018] P. Zelinski, *Okuma Engineer Offers Safety Tips for Hybrid Machine Tools*, Additive Manufacturing Magazine, 2018. Available online: https://www.additivemanufacturing.media/blog/post/okuma-engineer-offers-safety-tips-for-hybrid-machine-tools (accessed on 20 February 2020)

[Zhang, 2016] X. Zhang, Q. Yan, S. Lang, M. Xia, C. Ge, *Texture evolution and basic thermal-mechanical properties of pure tungsten under various rolling reductions*, J. Nucl. Mater., 468, 339–347, 2016.

[Zhang, 2018] R. Zhang, R. Dou, Z. Wen, X. Liu, *Effects of pressure and temperature on the effective thermal conductivity of oriented silicon steel iron core under atmospheric condition*, Int. J. Heat Mass Transf., 125, 780–787, 2018.

[Zhu, 2003] H.H. Zhu, L. Lu, J.Y.H. Fuh, *Development and characterisation of direct laser sintering Cu-based metal powder*, J. Mater. Process. Technol., 140, 314–317, 2003.

[Zhu, 2012] G. Zhu, D. Li, A. Zhang, G. Pi, Y. Tang, *The influence of laser and powder defocusing characteristics on the surface quality in laser direct metal deposition*, Opt. Laser Technol., 44, 349–356, 2012.

[Zhu, 2013] Z. Zhu, V.G. Dhokia, A. Nassehi, S.T. Newman, *A review of hybrid manufacturing processes - state of the art and future perspectives,* Int. J. Comput. Integr. Manuf., 26(7), 596–615, 2013.